

IMFUFA **tekst**

- I, OM OG MED MATEMATIK OG FYSIK

Exploring Treatment Strategies through Mathematical Modelling of Type 1 Diabetes – Updating and Expanding an Existing Model

Kenneth Hagde Mandrup Nielsen

marts 2011

nr. 477 - 2011

Roskilde University,
Department of Science, Systems and Models, IMFUFA
P.O. Box 260, DK - 4000 Roskilde
Tel: 4674 2263 Fax: 4674 3020



**Exploring Treatment Strategies through Mathematical Modelling of Type 1 Diabetes –
Updating and Expanding an Existing Model**

By: Kenneth Hagde Mandrup Nielsen

IMFUFA tekst nr. 477/ 2010

– 177 pages –

ISSN: 0106-6242

In this thesis we start out by dealing with a mathematical model of the onset of type 1 diabetes as proposed by Marée et al. (2006). It is a 5-dimensional model that uses ordinary differential equations (ODEs) to simulate the behavior of macrophages, activated macrophages, apoptotic β -cells, necrotic β -cells, and cytotoxic cytokines in neonate NOD- and Balb/c-mice. The purpose of Marée et al. (2006) is primarily to investigate the hypothesis that

impaired macrophage phagocytosis can mean the difference between health and type 1 diabetes (in mice).

Marée et al. (2006) base their hypothesis on previous work by Trudeau et al. (2003) and Marée et al. (2005). We start out by presenting an introduction to the biology behind the DuCa model and introduce some of the tentative treatment strategies as of today. With the groundwork in place we present, and discuss the foundations of, the model, which we have dubbed the DuCa model, and provide an analysis of a reduced version of the DuCa model, called the *intermediate model* (IM). The IM is based on the so-called Copenhagen model, made by Blasio et al. (1999).

After this gentle interlude we proceed to do a codimension 1 bifurcation analysis of the DuCa model. The analysis serves to determine the overall soundness of the model. Where by “soundness” we mean the lack of nonphysiological behavior within a reasonable range of key parameters.

The bifurcation analysis, and a thorough discussion of the adherent assumptions as well as simplifications, leads us to conclude that the DuCa model is sound.

Based on these findings we expand the DuCa model, guided by recent data and guidelines that should apply to all mathematical models as well as some criteria that pertain to this model in particular. The expansion consists of a compartment of healthy β -cells. By this expansion we add to the realism of the model and set up a model from which future researches can analyze how best to go about countering the chronic inflammation of the Islets of Langerhans that leads to T1D in 80 % of female NOD-mice. In our discussion of the expanded model we also provide some hints as to how one would go about implementing the effect of, in particular, one tentative drug, as well as point to additional features that need implementing (and how this could be done).

**Exploring Treatment Strategies for Type 1 Diabetes
through Mathematical Modelling**

Updating and Expanding an Existing Model

by

Kenneth Hagde Mandrup Nielsen

Supervisor

Johnny T. Ottesen

THESIS

for the degree of

MASTER OF SCIENCE

*NSM, IMFUFA
Roskilde University*

January 2010

Preface

This thesis took its beginning when Professor Johnny Ottesen introduced me to a number of articles all of which used mathematical modelling to look at diabetes. Amongst the articles I found that an article called “Onset of Type 1 Diabetes - A Dynamical Instability” (Blasio et al. (1999)) was the most interesting. At the same time Lars Hervig Jacobsen was looking to pick a subject for his bachelor thesis.

We got into contact with Professor, Dr. MD, Flemming Pociot, to discuss the aforementioned article, of which he is a coauthor, along with an article by Marée et al. (2006) called “Modelling the onset of Type 1 diabetes: can impaired macrophage phagocytosis make the difference between health and disease?” which we had found while searching for literature. The article by Marée et al. (2006) is a revised and expanded version of the model presented in Blasio et al. (1999). They modify the model from Blasio et al. (1999) to investigate another hypothesis than Blasio et al. (1999), but they also state that the model in Blasio et al. (1999) becomes physiologically unviable when estimated or experimentally obtained parameters are inserted in the model.

We decided to gain insight into the writings of Marée et al. (2006) to see if they were correct in their assertions and to see if the revised model was a good foundation from which we formulate our own model.

Acknowledgements

This thesis would not have existed in the form it is in today had it not been for a number of people. I would like to thank:

First of all my supervisor **Professor Johnny T. Ottesen** for all of his help with MATLAB, mathematical modelling, discussions about bifurcation diagrams, suggestions, his meticulous corrections, general inspiring interest and for establishing connection to the next person to whom I would like to extend my gratitude: Chief physician at Steno Diabetes Center **Dr. MD. Flemming Pociot** who was my external supervisor for the duration of my work.

At the outset of this thesis I knew as much about molecular biology as the common walrus knows about accounting, but thanks to Dr. Pociot’s willingness to meet with Lars Hervig Jacobsen and I, to discuss articles and answer questions of varying depth the language of biology soon became familiar. **B.Sc. Lars Hervig Jacobsen** who defied nature and weird looks from people in the computer lab at IMFUFA, Roskilde University, to be able to work 24-7 on his bachelors thesis. I collaborated with him during the first half of the thesis. It made the process much more enjoyable and without him a lot of the MATLAB-based results might not have existed in the form they are in today.

Approximately halfway through the process I was in the good fortune of receiving a grant from Mærsk. The grant was intended to allow one to go abroad for a semester, and thanks to the kindness of **Dr. Tom Archibald** and the mathematics department at the Simon Fraser University (SFU) in Vancouver, Canada, I was able to spend the fall-semester at SFU. This provided me with the privilege of having a meeting with **Dr. Diane T. Finegood** at her office on campus at SFU. There I was given the opportunity to discuss subjects from the article of Marée et al. (2006), which she coauthored, and ask questions of relevance in general. Dr. Finegood referred me to **Dr. MD Bruce Vercherer** of University of British Columbia (UBC), who provided me with answers to

questions that were outside Dr. Finegood's field of expertise. Dr. Vercherer's answers were very helpful, and he also suggested that I might visit UBC to discuss my questions further and present my work. Another person from UBC who has shown me kindness in accommodating my questions is **Dr. Leah Edelstein-Keshet**, who is another coauthor of the Marée et al. (2006) article. She answered some of my questions regarding the mathematical aspects of the DuCa model, and also invited me to visit UBC. Unfortunately *tempus fugit*, so I never got to see UBC. Furthermore I would like to thank **Dr. Ralf Wittenberg** of SFU for letting me pop by his office at random, and (I assume) inconvenient, hours of the day to ask questions of mathematical nature. He was also very kind in answering my email. Finally I would like to thank my girlfriend for putting up with my long hours of working and being no fun at all, graduate student Eric and Ph.D. student Marc from the IRMACS center at SFU for letting me share their cubical and last but not least the researches who agreed to let me use their graphs in my thesis.

Contents

Preface	ii
Acknowledgements	ii
Contents	v
List of Tables	viii
List of Figures	ix
1 Introduction	1
1.1 Thesis Statement	3
1.2 Method	3
1.3 Introductory Remarks	4
1.4 Thesis Structure	5
2 Type 1 Diabetes and Its Etiology	7
2.1 Prediction and Detection Using Autoantigens	8
2.2 The Immune Cells	9
2.3 Summary and Discussion	10
3 Prospects for Therapy – A Mini Review	13
3.1 Treatment Strategies	13
3.2 Glucagon-Like Peptide 1	14
3.3 Gastrin	15
3.4 Dendritic Cells	15
3.5 Antigen Treatment Merits Caution	16
4 Mathematical Modelling	17
5 The DuCa Model	19
5.1 Background for the DuCa Model	19
5.2 Purpose of Marée et al. (2006)	20
5.3 The DuCa Model – An Appetiser	21
An introduction to compartment models	21
5.4 The DuCa Model – Compartment Model and Equation System	23
5.5 Discussion of the Compartment Model	28
5.6 Our Compartment Model	29
5.7 Discussion of Marée et al. (2006)’s Model Assumptions	32
The role of naturally occurring apoptosis	33

Significance of the Apoptotic Wave	33
Michaelis-Menten versus a Hill function	34
Implication of secretion of cytokines upon B_a phagocytosis	35
Activation by phagocytosis of necrotic β -cells	36
5.8 Discussion of Parameters	37
Reversible or irreversible activation?	38
The DuCa model with turnover of M_a	41
6 The Intermediated Model	45
Model observations	47
6.1 Fixed Points of the IM Model	48
Stability of the fixed points	50
Downfall of the IM	53
Phase plane analysis	54
A brief note on linearizing	59
6.2 The IM Including Crowding-Terms	60
6.3 Recapitulation of The Analysis of the IM	63
7 A Brief Introduction to Bifurcation Analysis and Numerical Methods	65
7.1 Generic Bifurcations	65
7.2 The Hopf bifurcation	66
7.3 Biological Relevance of Bifurcation Analysis	69
7.4 Choice of Bifurcation Parameters	69
7.5 Locating the Fixed Points	70
Evaluation of stability of the fixed points and detection of bifurcations	71
8 Bifurcation Diagrams and Analysis	73
8.1 Codimension One Bifurcations	73
8.2 Using f_1 as the bifurcation parameter	74
Basic features of the NOD bifurcation diagram	74
Eigenvalues, manifolds and behavior of the fixed points on the NOD $_{f_1}$ -USB	75
Eigenvalues, manifolds and behavior of the fixed points on the NOD $_{f_1}$ -LUB	79
Combining the analysis of the NOD $_{f_1}$ -USB and LUB	81
Hidden features in figure 8.1	84
The Balb/c bifurcation diagram	87
8.3 Using f_2 as the bifurcation parameter	88
8.4 Reducing the DuCa-model	93
9 Discussion of the Bifurcation Analysis	97
9.1 Future Work	101
10 Conclusion 1	103
11 Expanding and Modifying the DuCa model	105
11.1 Including a Compartment of Healthy β -cells	105
Model criteria	105
11.2 First approximation to a governing equation – Model A	106
11.3 Modifying the governing equation – Model B	110

Model B – Balb/c-simulation	110
Model B – NOD-simulation	111
11.4 Adding β -cell growth – Model C	112
Model C – Balb/c-simulation	114
Model C – NOD-simulation	115
12 Discussion of the Expanded Model	117
12.1 Future Work	120
IL-1 induction of primary necrosis	120
Adding T cells	120
Adding treatment to Model C	121
13 Conclusion 2	123
Bibliography	125
A Mathematical Appendices	131
A.1 Existence and Uniqueness Theorem	131
A.2 The Implicit Function Theorem	132
A.3 The Hartman-Grobman Theorem	132
A.4 Michaelis-Menten Kinetics	133
A.5 Newton-Raphson Method	134
A.6 Dimensionless Form of the Intermediate Model Including Crowding Terms	136
A.7 Fixed Point for the IM Including Crowding Terms	137
B Additional Figures	139
B.1 Eigenvalue-Plots Used to Evaluate Stability of the Fixed Points Shown in Figure 8.1	139
B.2 Eigenvalue-Plots Used to Evaluate Stability of the Fixed Points Shown in Figure 8.11	142
B.3 Eigenvalue-Plots Used to Evaluate Stability of the Fixed Points Shown in Figure 8.12	146
B.4 Eigenvalue-Plots used to Evaluate Stability of the Fixed Points Shown in Figure 8.15	149
B.5 Eigenvalue-plots Used to Evaluate Stability of the Fixed Points Shown in Figure 8.18	152
B.6 Stable Spirals for f_1 near the Bifurcation Point	155
C matlab Code	157
C.1 Code for the Bifurcation Diagrams in Chapter 8	157
C.2 Code for the Newton-Raphson Method	167
Code for Approximation of the Jacobian	168
C.3 The Function-File for Model C	170
Simulation Code for Model C	171
Index	173

List of Tables

5.1	summarizes the model-parameters and their values	27
5.2	different parameter values as found in the literature	38
5.3	gives a comparison of the values as they are estimated in the most likely reversible and irreversible models in Marée et al. (2007).	39
8.1	Overview of the eigenvalues of the DuCa model, with NOD parameters and f_1 as the bifurcation parameter near the NOD_{f_1} -USB.	80
8.2	Overview of the eigenvalues of the DuCa model, with NOD parameters and f_1 as the bifurcation parameter near the NOD_{f_1} -LUB.	81
8.3	Overview of the eigenvalues of the DuCa model, with NOD parameters and f_2 as the bifurcation parameter near the USB.	91
8.4	Overview of the eigenvalues of the DuCa model, with NOD parameters, and f_2 as the bifurcation parameter near the NOD_{f_2} -LUB.	92
12.1	Summary of the expanded models.	119

List of Figures

2.1	Relation between the number of autoantibodies in the blood and how likely the person is to develop diabetes	9
3.1	Dependence of treatment strategy on β -cell mass	13
5.1	shows an example of a generic compartment model	22
5.2	shows the compartment system as given by Marée et al. (2006)	24
5.3	dynamics of the Balb/c-mouse and NOD-mouse.	28
5.4	the non-necrotic part of our modified compartment model	30
5.5	the necrotic part of our modified compartment model	31
5.6	shows the compartment system corresponding to equations 5.17 to 5.20	31
5.7	Simulations of the DuCa model with a Hill function instead of the Michaelis-Menten function	34
5.8	A plot based on the findings of Stoffels et al. (2004) that apoptotic as well as necrotic β -cells implies cytokine secretion	36
5.9	simulations of the DuCa model with activation due to necrotic cells	37
5.10	simulations of reversible and irreversible model with Balb/c phagocytosis parameters	39
5.11	simulations of the reversible and irreversible model with NOD phagocytosis parameters	40
5.12	shows simulations of the irreducible model with $k = 0$	42
5.13	shows a simulation made with MATLAB of the reversible model where a term of $-cM_a$ has been added to equation 5.7 to model turnover of active macrophages	42
5.14	In the figures simulations of the DuCa model with turnover of the active macrophages are presented	43
6.1	A compartment representation of the CPH model.	45
6.2	Shows the compartment system for the Intermediate Model	47
6.3	Sketch of the nullclines for the IM with $\frac{dM}{dt} = 0$	57
6.4	Sketch of the nullclines for the IM with $\frac{dM}{dt} = 0$	58
6.5	Sketch of the nullclines for the IM including crowding terms with QSS on M	62
7.1	A supercritical (I), a subcritical (II) and degenerate Hopf bifurcation (III).	68
8.1	Bifurcation diagram for the DuCa model using f_1 as the bifurcation parameter and NOD parameters	74
8.2	Plot of the real and imaginary parts of the eigenvalues on the NOD $_{f_1}$ -USB	76

8.3	Phase space plot of M , M_a and B_a , showing a stable spiral together with the corresponding time-plot	77
8.4	Time- and phase space plots of an unstable spiral.	78
8.5	Plots of the real and imaginary parts of the eigenvalues with respect to f_1 on the NOD_{f_1} -LUB	80
8.6	Simulation of the DuCa model setting $f_1 = 2.7 \times 10^{-5}$ and $f_2 = 1 \times 10^{-5}$.	82
8.7	An illustrative figure of the flow in phase space after the Hopf bifurcation has occurred. The point named “optimal initial condition” would flow along the unstable manifold of the NOD_{f_1} -LUB to the USB.	84
8.8	The difference between chronic inflammation or not comes down to one active macrophage.	85
8.9	The UUB added to figure 8.1	86
8.10	The flow of M_a represented on a circle.	87
8.11	Bifurcation diagram for the DuCa model using f_1 as the bifurcation parameter and Balb/c parameters	88
8.12	Bifurcation diagram for the DuCa model using f_2 as the bifurcation parameter, and NOD parameters	89
8.13	Overview of the eigenvalues with f_2 as the bifurcation parameter with f_1 as in NOD-mice.	90
8.14	The real and imaginary parts of the eigenvalues of the fixed point along the NOD_{f_2} -LUB.	91
8.15	Bifurcation diagram for the DuCa model using f_2 as the bifurcation parameter, and Balb/c parameters	92
8.16	Simulation of the DuCa model setting $f_1 = 2 \times 10^{-5}$ and $f_2 = 2.54 \times 10^{-5}$	93
8.17	Simulations of the DuCa versus the reduced DuCa model	94
8.18	Bifurcation diagram for the three dimensional version of the full model using NOD parameters	95
11.1	Behavior of the concentrations for Balb/c- and NOD-mice with the inclusion of a compartment of healthy β -cells; Model A.	108
11.2	Behavior of the concentrations for Balb/c-mice with the inclusion of a compartment of healthy β -cells; Model B.	110
11.3	Behavior of the concentrations for NOD-mice with the inclusion of a compartment of healthy β -cells; Model B.	111
11.4	Behavior of the concentrations for Balb/c-mice based on Model C.	115
11.5	Behavior of the concentrations for NOD-mice based on Model C.	115
B.1	Plot of the eigenvalues for the Jacobian evaluated in fixed points in the upper inflamed region.	139
B.2	Plot of the eigenvalues for the Jacobian evaluated in fixed points in the lower inflamed region.	140
B.3	Plot of the eigenvalues for the Jacobian evaluated in the healthy rest state.	140
B.4	A classical diagram of the imaginary part versus real part of the eigenvalues for the Jacobian evaluated in fixed points in the upper inflamed region.	141
B.5	Plot of the eigenvalues for the Jacobian evaluated in fixed points in the upper inflamed region.	142

B.6	Plot of the eigenvalues for the Jacobian evaluated in fixed points in the lower inflamed region.	143
B.7	Plot of the eigenvalues for the Jacobian evaluated in the healthy rest state.	143
B.8	Plot of the eigenvalues for the Jacobian evaluated in the fixed points along the dotted (black) line seen in figure 8.11.	144
B.9	Plot of the eigenvalues for the Jacobian evaluated in the fixed points along the dashed-dotted (magenta) line seen in figure 8.11.	144
B.10	A classical diagram of the imaginary part versus real part of the eigenvalues for the Jacobian evaluated in fixed points in the upper inflamed region. . .	145
B.11	Plot of the eigenvalues for the Jacobian evaluated in fixed points in the upper inflamed region.	146
B.12	Plot of the eigenvalues for the Jacobian evaluated in fixed points in the lower inflamed region.	147
B.13	Plot of the eigenvalues for the Jacobian evaluated in the healthy rest state.	147
B.14	A classical diagram of the imaginary part versus real part of the eigenvalues for the Jacobian evaluated in fixed points in the upper inflamed region. . .	148
B.15	Plot of the eigenvalues for the Jacobian evaluated in fixed points in the upper inflamed region.	149
B.16	Plot of the eigenvalues for the Jacobian evaluated in fixed points in the lower inflamed region.	150
B.17	Plot of the eigenvalues for the Jacobian evaluated in the healthy rest state.	150
B.18	A classical diagram of the imaginary part versus real part of the eigenvalues for the Jacobian evaluated in fixed points in the upper inflamed region. . .	151
B.19	Plot of the eigenvalues for the Jacobian evaluated in fixed points in the upper inflamed region (setting $f_2 = 1 \times 10^{-5}$).	152
B.20	Plot of the eigenvalues for the Jacobian evaluated in fixed points in the lower inflamed region (setting $f_2 = 1 \times 10^{-5}$).	153
B.21	Plot of the eigenvalues for the Jacobian evaluated in the healthy rest state (setting $f_2 = 1 \times 10^{-5}$).	153
B.22	A classical diagram of the imaginary part versus real part of the eigenvalues for the Jacobian evaluated in fixed points in the upper inflamed region (setting $f_2 = 1 \times 10^{-5}$).	154
B.23	Stable spirals for $f_1 = 2.56 \times 10^{-5}$, and $f_1 = 2.566 \times 10^{-5}$	155
B.24	Stable spirals for $f_1 = 2.5661 \times 10^{-5}$, and $f_1 = 2.5662 \times 10^{-5}$	155
B.25	Stable spirals for $f_1 = 2.5663 \times 10^{-5}$, and $f_1 = 2.566305 \times 10^{-5}$	156

1 Introduction

Insulin dependent diabetes mellitus (IDDM) or Type 1 Diabetes (T1D) is an autoimmune disease that, in brief, is characterized by an unnatural depletion of the pancreatic β -cells, which implies a drop in the production of insulin. Insulin is needed to regulate the blood sugar level upon ingestion of nutrients¹, or else hyperglycemia, i.e. elevated blood sugar, occurs.

It is known that patients with T1D are genetically predisposed for the disease, but environmental factors are needed to facilitate the events leading to overt diabetes (Pociot (2009)) – often the symptoms become apparent only in late adolescence or adulthood (Wang et al., 2006, p.80). It affects about 0.5% of the population in the developed countries, and 5-15% of those diagnosed with Type 2 Diabetes (T2D) are believed to have T1D – not T2D (Mathis et al. (2001)). Without daily subcutaneous injections of insulin the disease is fatal (Lo and Clare-Salzler, 2006, p.17).

Despite intensive research, the exact etiology (the cause of the disease) remains illusive, though progress has been made.

In 2004 Wild et al. (2004) made an assessment of how the prevalence of diabetes (T1D and T2D) will evolve between the year 2000 and 2030, and their projections are dim! Diabetes is mostly a problem in the western world today, but as more and more developing countries switch from manual to knowledge-based sedentary labor as their primary source of income, the number of people with diabetes in these countries is expected to soar, and the total number of people in the world with diabetes will increase from 171 million in 2000 to 366 million by the year 2030 (Wild et al., 2004, p.1047).

Dire forecasts such as these together with the fact that the life expectancy of diabetics is reduced² (Manuel and Schultz (2004)) emphasizes the need for an actual cure of diabetes – the best case scenario would be the possibility of pre-natal screening for genes known to induce diabetes, so precautionary measures could be taken. But this is still a utopian scenario, so until the advent of such times, the best cause of action is research in post-natal treatments; see chapter 3.

Since the first bolus of insulin was administered to a human, on January 11. 1922 (Rosenfeld, 2002, p.2277)³, it has been the foremost applied treatment for diabetes.

At the infancy of insulin-treatment the insulin was often bovine, porcine or canine in origin, furthermore it was impure, which meant that albeit it was better than no treatment, allergic reactions could ensue upon injection (Rosenfeld (2002)). This prompted the need for better purification methods as well as research aimed at making analogs to human insulin.

¹ For a more thorough description of the mechanisms behind T1D see chapter 2

² Insulin can be administered to cure the symptoms of diabetes throughout the entire life of a patient, but diabetes is associated with sequela, see e.g. Franco et al. (2007).

³ The first successful administration was, however, not until January 23 (Rosenfeld, 2002, p.2278).

In the following decades research along these lines became the top priority, with not too much attention given to alternatives. Though La Barre, as early as 1930, saw the potential in using an *incretin*⁴ substance, the influential gastrointestinal physiologist Andrew C. Ivy “disproved” the applicability of the incretin concept (Creutzfeldt, 2005, p.89), and it was not until 1964 that the incretin concept had a renaissance, and was recognized as a promising course of research.

An incretin has to fulfill three criteria (taken from (Creutzfeldt, 2005, p.90))

1. The hormone must be released from gut endocrine cells after ingestion of nutrients, especially of glucose
2. The circulating hormone must stimulate insulin secretion in a concentration which is easily achieved after ingestion of a nutrient
3. The hormone releases insulin only at elevated glucose levels (glucose dependence)

One such hormone that was discovered in the mid-eighties is Glucagon-Like Peptide 1 (GLP-1)(Nauck (1998); Creutzfeldt (2005)), which we will touch upon in section 3.2. GLP-1 is still subject to extensive research (e.g. Nauck (1998); Siegel et al. (1999); Farilla et al. (2003); Egan et al. (2003); Urusova et al. (2004); Suarez-Pinzon et al. (2008) to name a few), and will also be given special attention in this thesis.

We were introduced to mathematical modelling of diabetes through the pioneering article by Blasio et al. (1999), who proposed the so-called Copenhagen (CPH) model (see section 6), and are recognized as the first to utilize the language of mathematics to qualitatively investigate the mechanisms thought to prompt T1D.⁵ We found the idea of using mathematical modelling to identify key players in the etiology enthralling, and started perusing through the literature baring mathematical modelling and T1D (or IDDM) in mind, while we at the same time started stocking up on the biological knowledge needed.

As a bit of a surprise we were not overwhelmed by articles that matched our criteria, but we did come across a couple of articles. One of great interest was by Wang et al. (2006) in which they extend the CPH model to investigate the age-at-onset of T1D, another was by Marée et al. (2006) where they investigate the role of a specific type of immune cell in the development of T1D. Almost in extension of this article is the one by Mahaffy and Edelstein-Keshet (2007), where the aim is to model the cyclic pattern of behavior that the same type of immune-cell exhibits, later in the course of the disease. We also came across an older article by Finegood et al. (1995) where they present a (simple) mathematical model of the β -cell dynamics in the growing rat pancreas.

Though all of these articles had interesting approaches and aims we decided in the end to base our continued work on an article by Athansius F. M. Marée, Richard Kublik, Diane T. Finegood, and Leah Edelstein-Keshet⁶ called “*Modelling the onset of Type 1 Diabetes: can impaired macrophage phagocytosis make the difference between health and disease?*” We chose this article over the others because it deals with a hypothesis regarding the onset of T1D, which was consistent with our primary objective, namely

⁴ An incretin substance is a substance extracted from the upper gut mucosa, that induces hypoglycemia (Creutzfeldt, 2005, p.88), i.e. lowers the blood-sugar level and counters hyperglycemia.

⁵ Later we have learned that other diabetes models existed beforehand, but they typically model the interaction between insulin, glucose and β -cell mass.

⁶ Leah Edelstein-Keshet is a mathematician at the University of British Columbia, while the others are biologists.

modelling of the onset. Furthermore they are inspired by the CPH model; see section 6.

1.1 Thesis Statement

The purpose of this thesis is twofold. First of all we want to perform a thorough analysis of the DuCa model to decide if it is a sound model for the early stage of T1D. Secondly we seek to expand the DuCa model to make it more realistic.

Before we state the questions, we will answer on our path to obtain the first purpose, we must first clarify what we mean by a “sound model.” We will define a sound model as one in which

altering significant parameters within a physiologically reasonable interval does *not* induce behavior that is irreconcilable with the underlying physiology.

By a “physiologically reasonable interval” we mean, e.g., within the limit of the standard deviation. We must also explain what we deem “irreconcilable with the underlying physiology.” An obvious example of this is if we observe that one or more of the concentrations in the DuCa model diverge when we tweak a parameter. Another example is if the concentrations become negative.

Through the analysis of the DuCa model the following questions can be answered

- I Are the parameter values given in Marée et al. (2006) reasonable?
- II Do bifurcations occur when a suitable parameter is varied within a physiologically reasonable range?
- III Is the model sound?

When we have analyzed the DuCa model and answered questions I-III we will pursue our second (and most important) goal, which is to try and expand the model. In doing so three questions are natural to ask

- i can we add a natural expansion to the DuCa model?

If the answer to this is yes then the next course of action is to determine if

- ii the expansion induces a more realistic behavior

If this is the case, then we will ask ourselves

- iii does the (natural) expansion agree with experimental data?

By “natural” we basically mean one that is based on the underlying physiology and will not cause nonnatural behavior when added to the DuCa model. By “more realistic” we mean compared to the behavior of the DuCa model by itself. Notice that being unable to induce a more realistic behavior implies failing at agreeing with experimental data, while the opposite is not the case.

1.2 Method

The first question (I) will be answered through literature studies, the second (II) will be answered based on a bifurcation analysis, while the answer to the third (III) hinges on the answer of the former two and a general analysis and discussion of the assumptions and simplifications that are made with the DuCa model.

There are several scenarios that can unfold as we try to answer questions I-III. For example: if we find that bifurcations occur abundantly, and also within physiologically realistic parameter spans, then we must look to the literature to see if such behavior has any foundation in reality before we can answer question III. If we do not find any data to back such behavior then of course the answer to question III is: No! However let us assume that we find that the answer to I is yes, and further assume that no bifurcations occur within such parameter spans, and the literature tells us that this is as it should be. Then of course we have learned that the DuCa model is a sound model, but should such a point come, then we can ask ourselves a new question. Namely: how should the parameter composition be before unnatural behavior is achieved? Perhaps we can relate the answer to this question to the biology or imagine that it assist in a cure. This last piece of text goes to illustrate that the questions (I-III) that at first seem to be simple “yes” or “no” questions are the first layer of several followup questions.

In regards to question i the answer to this question is very much connected to the way we define “natural expansion.” If we find that we cannot contribute with a natural expansion based on the physiology that is available to us from the DuCa model, then we may have to add additional biological features to the mixture in hope of adding an expansion – notice that we may take several stabs at constructing an expansion, for we may have overlooked something at first or oversimplified things. The answer to question ii comes down to whether an expansion entails a behavior that is in qualitative agreement with what we expect based on the literature. If we get past i and find that we must answer “No” to ii, then we will go back to question i to see if we could have done something differently. If we get to question iii, then the answer simply depends on data. Note that we may want to contest some data, especially if we find contradicting conclusions and answers in the literature.

1.3 Introductory Remarks

The biology of the pancreas is immensely rich, and could easily fill all of the pages in this thesis, therefore it will be treated in an introductory fashion only. This facilitates the overview, and when biological words and concepts appear that have not merited a prior introduction, then these will be explained in a footnote.

We find that it is often tedious and not very illuminating to read through a long theoretical chapter that is often more or less a rewording of an existing textbook. Therefore relevant mathematical subjects will be covered along the way as they appear naturally. This way of presenting the theoretical machinery allows the reader to see it in action immediately, rather than waiting 20 pages. Though we have strived to refrain from regurgitating what others have written, some examples are so generic that it is impossible to be completely novel. By meshing theory with application the reader, who is in the know, is unfortunately deprived of the possibility of skipping the theory entirely, but we have found it to be the most instructive way to introduce the theory.

1.4 Thesis Structure

Due to the dichotomy between the questions numbered I to III and those numbered i to iii we have more or less split the thesis into two according pieces. This implies two discussions and two conclusions – one of each based on the analysis of the DuCa model and one of each based on the expanded DuCa model. The first part ends with the conclusion given in chapter 10. After that three chapters follow.

The contents of this thesis is such that in Chapter 2, called **Type 1 Diabetes and Its Etiology** we provide a basic introduction to the biology that is needed to understand and work with the DuCa model. Chapter 3, called **Prospects for Therapy – A Mini Review**, sheds light on what kind of therapeutic measures are suitable at different stages of the disease, and also looks at some of the compounds that are of interest today. In Chapter 4, called **Mathematical Modelling**, we turn away from the biology for a moment to discuss how mathematical modelling can contribute in biology and other natural sciences. Chapter 5 introduces **the DuCa model**, along with an analysis and a discussion of the parameters, assumptions and simplifications that belong to the model. Chapter 6 is retained for the more basic model which the DuCa model is based on. This basic model is called **the Intermediate Model**. In regards to the intermediate model we reproduce and unfold an analysis done in Marée et al. (2006). Furthermore we discuss key elements and features of the DuCa model; e.g. parameters and model assumptions. Chapter 7 is called **A Brief Introduction to Bifurcation Analysis and Numerical Methods** and is aimed at readers who are somewhat new to the field of applied mathematics. It is also the chapter where we choose our bifurcation parameters, present the method we have used to estimate fixed points, and touch upon why bifurcation analysis can be interesting to biology or physiology. After this mathematical groundwork we bring it all into play in Chapter 8 where we perform the bifurcation analysis. Thus we have dubbed Chapter 8 **Bifurcation Diagrams and Analysis**. Chapter 9 rounds off the first part of this thesis, by summarizing the findings of the bifurcation analysis and discussing the implications of these findings, after which follows the conclusion of the first part in chapter 10. In Chapter 11 the focus is on expanding the DuCa model, analyzing the implications of the expansion, and investigating which effects a potential treatment should have on the healthy β -cells to reverse a negative spiral. In chapter 11 we provide the final discussion before bring our conclusion of part 2 in chapter 13.

The appendices are divided into three categories. In the first everything relating to mathematics is gathered. The second contains some figures that either serve as documentation or they corroborate points put forth in the analysis. Finally the third appendix contains MATLAB code. At the very end of the thesis is an index which should ease the job of finding a given subject or if one forgot what an important word meant, then there is a good chance that it is listed in the index.

This thesis has been done in two rounds so to speak. Initially I worked with Lars Hervig Jacobsen. The goal for Lars was to finish his thesis for the degree of bachelor of science.

Lars had more experience with MATLAB, and I had more knowledge of the mathematics that is used in nonlinear dynamics. Thus we formed a partnership where the workload was split more or less 50-50 – he could draw on my insight into the mathematics, while I learned from his knowledge of MATLAB. Eventually we broke off the partnership,

because I had to make preparations for staying in Canada during the fall-semester, and Lars had to defend his thesis before the beginning of said semester, which he did on August the 31. 2009.

Since then I have added new parts (chapters 11 and 12, the subsection on activation by necrotic β -cells in section 5.7 and appendices A.1, A.2, A.3 and B.6) cut out and/or replaced other parts (e.g. the bifurcation analysis of the DuCa model (section 7) has been totally redone as well as the following discussion in chapter 9) and reworked virtually the whole thesis. Nevertheless I have chosen to keep my writing in a “we-form” as opposed to an “I-form” to honor the initial collaboration between Lars and I.

The reader may wonder why so much time and space has been devoted to the analysis of the DuCa model instead of the expanded model. My answer is that: when you write a project or a thesis such as this, where you work within a time-limit, it is often the case that the most interesting work is done toward the end, thus leaving little time to incorporate and analyze discoveries that arise from said work. I have also included all the model-variations of the expanded model to illustrate how the final model came about; i.e. another insight into the work process.

2 Type 1 Diabetes and Its Etiology

The pancreas consists of an exocrine gland and an endocrine gland, of which only the endocrine gland is of any concern to us. The endocrine part consists of between 5×10^5 - 1×10^6 *islets of Langerhans*, which in turn are constituted by different cell types. The cells of the pancreas we are interested in are the β -cells. They make up around 75% of the total number of cells in the islets of Langerhans which comes to about 500-1000 β -cells per islet Verchere (2009).

Postcibal¹ the β -cells are stimulated to secrete insulin, to maintain homeostasis of the blood glucose level (Seeley et al., 2008, p.632-639). Much has been unveiled in the field of autoimmune diabetes during the past 20 years. These advances owe a great deal to what in the field of medicine is known simply as *models*. These are essentially animal models, i.e. an animal in which the development of diabetes resembles, or can be made to resemble, that of the human development. From here on we call these models *bio-models* so as not to confuse them with mathematical models. One such bio-model that is particularly suitable, and also the most extensively used in T1D-research, is the diabetes prone NOD mouse. This is because the development of diabetes in NOD-mice resembles the human development in some key aspects (Höglund et al. (1999))(Cantor and Haskins, 2006, p.381), such as presence of autoantibodies in the pancreas and autoreactive T cells (Anderson and Bluestone (2005)).

The use of bio-models has led to the consensus of today which is that: T1D arises when β -cells fall prey to an autoimmune response (Höglund et al. (1999), Green and Flavell (1999), Yoon and Yun (2001), Notkins and Åke Lernmark (2001), Beyan et al. (2002), Cantor and Haskins (2006) to name a few). This depletion leads to a lack of endogenous insulin, which has a detrimental impact on the homeostasis of blood glucose, and inevitably results in constant hyperglycemia, leaving the subject dependent on exogenous administered insulin. Clinical symptoms of T1D, in humans, become apparent when 60-90% of the β -cells have been depleted (Notkins and Åke Lernmark, 2001, p.1247)(Seeley et al., 2008, p.636). In the NOD-mouse strain about 80% of female and 20% of male NOD-mice develop overt hyperglycemia, this happens at 30 weeks of age (Sreenan et al., 1999, p.989).

The autoimmune response induces β -cell death either by *apoptosis* or *necrosis*. Apoptosis is commonly described as “programmed cell death”. It entails an organized shutting-down of the cell (like the regulated shutting-down of a computer), where the cell shrinks, and no or little cell-debris is spilled (Steer et al., 2006, p.254-257). The result of this “quiet” death is that no inflammation ensues. Necrosis on the other hand is associated with inflammation, and entails loss of cell-membrane integrity which implies spillage of cell-debris (Steer et al., 2006, p.254).

¹ After ingestion of nutrients.

This much is understood and well documented today, but the exact etiology of T1D in humans as well as NOD-mice is still a Nobel Prize away. In the following we shed light on mechanisms, at a cellular level, that recent research has identified as crucial to the development of diabetes.² Some of the findings are still a matter of debate, and to the uninitiated it sometimes seems as though the ones who are “right” are the ones who are most respected or are the most cited; e.g. Andrew C. Ivy’s rejection of the incretin concept. We try to explain things without venturing too deep into the field of advanced cellular biology – when it is necessary to use technical terms, these will be accompanied by an explanatory footnote.

2.1 Prediction and Detection Using Autoantigens

Just as the old saying goes: there is no smoke without a fire, so there are no autoantibodies without diabetes.³ This may be an overstatement but there is some truth to it, since 70-80 % of newly diagnosed patients have autoantibodies to the autoantigen⁴ known as *glutamic acid decarboxylase* (GAD), approximately the same number are positive for antibodies to another autoantigen called *tyrosine phosphatase* (IA-2) (Wong and Jr., 1999, p.643)(Notkins and Åke Lernmark, 2001, p.1249), the remaining cases that are not associated with antibodies for these two autoantigens can be ascribed to insulin autoantibodies, and to a lesser extent autoantigens that are less frequent (Notkins and Åke Lernmark, 2001, p.1248-1249). In total over 90 % of newly diagnosed T1D patients are positive for autoantibodies (Pociot (2009)).

Insulin has been shown to be an autoantigen for the pathogenic T cells⁵ CD4⁺ and CD8⁺ (Wong and Jr., 1999, p.645) while GAD is an autoantigen to CD4⁺ but not CD8⁺ in NOD-mice (Wong and Jr., 1999, p.644). Though the exact interaction between autoantigens and immune cells is not fully understood (Yoon and Yun (2001)), there are results that indicate a clear connection between GAD as well as insulin and diabetes in NOD-mice (Yoon and Yun, 2001, p.202). Furthermore Notkins and Åke Lernmark (2001) report of the presence of autoantibodies in humans long before the onset of diabetes (Notkins and Åke Lernmark, 2001, p.1249), and further lists a number of articles (e.g. Leslie et al. (1999)) that provide results that indicate how the presence of one or more autoantibodies in a healthy person can be used to assess how likely said person is to develop diabetes. This relation between autoantibodies and the risk of developing diabetes is shown in figure 2.1. The y -axis represents the risk of developing

² Though scientific evidence has been gathered that indicates that environmental factors also play a part (Notkins and Åke Lernmark, 2001, p.1250)(Gianani and Eisenbarth, 2005, p.233)(Onengut-Gumuscu and Concannon, 2006, p.634)(Yu and Eisenbarth (2006)) we omit these results, because they are of no importance to the aim of this project.

³ Antibodies are proteins that can attach themselves to *antigens* (see next footnote) and cause them to self-destruct (Seeley et al., 2008, p.661). Autoantibodies have the same function, but for autoantigens.

⁴ An antigen can be a virus, a bacteria or even drugs just to name a few; i.e. substances that cause the immune system to react. An autoantigen, sometimes called a self-antigen, is an antigen produced by the body itself (Seeley et al., 2008, p.798).

⁵ When an immature T cell is presented with an antigen it matures into either a helper T cell, also called a CD4, or a cytotoxic T cell, also called a CD8. The respective cells are called so because they “express” CD4 and CD8 (Seeley et al., 2008, p.802), for the same reason they are sometimes called CD4⁺ and CD8⁺ T cells.

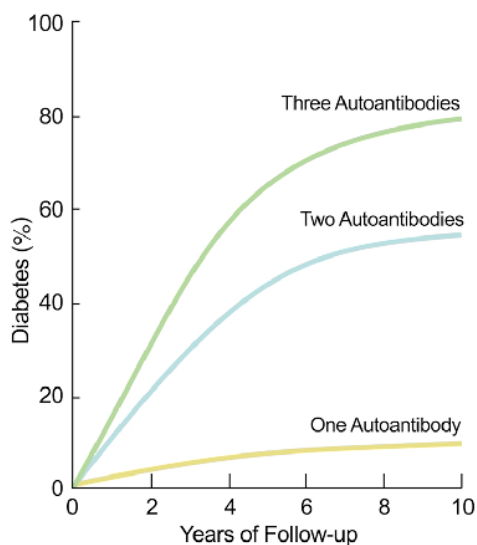


Figure 2.1 Relation between the number of autoantibodies in the blood and how likely the person is to develop diabetes in the following ten years. The figure is based on data obtained from longitudinal studies on first-degree relatives (i.e. parents, siblings or children) of T1D patients (Notkins and Åke Lernmark, 2001, p.1249). If tested positive for three autoantibodies, then there is an 80% risk of developing T1D during the next 10 years. The figure is borrowed with permission from Notkins and Åke Lernmark (2001)

diabetes in percentages. The x -axis represents the years that have transpired since the detection of autoantibodies. The figure is based on studies of first-degree relatives of individuals with T1D (Notkins and Åke Lernmark, 2001, p.1249). The detection of three autoantibodies means that after 10 years the person has an 80% risk of developing diabetes.

Now that we have touched upon the autoantigens, and their role in the autoimmune process let us turn to the cells that are implicated in mediating the autoimmunity.

2.2 The Immune Cells

Most⁶ of the articles published on T1D today focus on dendritic cells (DC), macrophages, T cells and B cells. The B cells (not to be confused with β -cells), macrophages and DC's are so-called *antigen presenting cells* (APC). APCs “swallow” antigens in a process called *phagocytosis*⁷, where they are processed, i.e. broken down into smaller fragments. After the antigens have been processed the APCs present them to receptors of T cells (and other cells) via proteins on their surface.

The most illusive problem in the etiology of T1D is where *in vivo* the T cells are stimulated to initiate an immune response towards the islets of Langerhans (Höglund et al., 1999, p.331). At the early stages of insulinitis macrophages and DCs have been found to infiltrate the islets of Langerhans (Yoon and Yun, 2001, p.203). So one possibility is that when the macrophages and DCs encounter antigens in the islets, they travel to the pancreatic lymph nodes where they present these antigens to mature as well as immature T cells. The immature T cells become mature, and the mature cells start

⁶ The following is based on (Seeley et al., 2008, p.792-816) when not stated otherwise.

⁷ In the phagocytosis the APC literally ingests the antigen as opposed to, say, drink it.

to divide. The findings of Höglund et al. (1999) corroborates that the T cells are first stimulated in the lymph nodes. Other results favor the hypothesis⁸ that activation of intralysosomal macrophages initiates sustained β -cell death through macrophage-derived pro-inflammatory cytokines⁹ (Steer et al., 2006, p.263) – T cells become a key-factor in the β -cell destruction at 4-5 weeks of age (Trudeau et al., 2003, p.219).

When the T cells divide they excrete cytokines of which interleukin-2 (IL-2) is especially important. IL-2 is one of several cytokines that have been found to precipitate T1D due to their cytotoxic¹⁰ effect on β -cells. Two other important cytotoxic cytokines are interleukin-1 (IL-1), and interferon- γ (IFN- γ), which are macrophage-derived.

Besides the role as an APC, and more importantly, according to Marée et al. (2006) and Steer et al. (2006), macrophages also secrete cytokines themselves (Marée et al. (2006), (Steer et al., 2006, p.253)) when they phagocytize apoptotic and necrotic β -cells. Recent results indicate that (some of the) cytokines secreted upon phagocytosis of necrotic cells are cytotoxic, and thus further the death of β -cells by necrosis (Steer et al., 2006, p.257) and apoptosis. But at the same time it has been found that β -cell regeneration takes place in the midst of the inflammation (Akirav et al., 2008, p.2883). One could speculate that this is due to some benign cytokines, but this is *only* speculation. While dwelling on cytokines we will briefly introduce one discrepancy between the NOD bio-model and humans, which, according to Steer et al. (2006) and Eizirik and Darville (2001), is that in humans cytokines only induce β -cell apoptosis (for reasons we will not get into here), whereas they induce apoptosis as well as necrosis in the NOD mouse (and other bio-models) (Steer et al., 2006, p.263) (Eizirik and Darville, 2001, p.65). This illustrates that one should take care not to overextend the conclusions drawn from the NOD-mouse model, and other bio-models, to apply to humans as well. Sparre et al. (2005) provide arguments based of the genetic makeup of the NOD-mouse as to why one must proceed cautiously when making conclusions based on these mice (Sparre et al., 2005, p.443).

2.3 Summary and Discussion

We have learned that macrophages/dendritic cells, T cells and cytokines excreted from these cells constitute a deadly combination, that ultimately leads to β -cell apoptosis or necrosis (Yoon and Yun (2001)). It is debateable which are the most important. Eizirik and Mandrup-Poulsen (2001) report that CD8⁺ are the most important T cells for the initiation of the immune process that leads to sustained apoptosis, but CD8⁺ cells alone cannot lead to diabetes. NOD macrophages are unable to present antigens and are as such not important as APCs in the NOD bio-model of T1D, this implies that DC's and B cells are the important APCs in this bio-model (Eizirik and Mandrup-Poulsen, 2001, p.2117). They also find that the cytotoxicity of the cytokines depends on the period in the life of the NOD-mouse at which they are released (Eizirik and Mandrup-Poulsen, 2001, p.2119).

Despite all the recent advances one remaining mystery still needs to be solved: what

⁸ This is also the hypothesis that Marée et al. (2006) utilize in their mathematical model, though they also recognize the significance of T cells.

⁹ A cytokine is a protein that stimulates cell proliferation and differentiation, but they can also be harmful to other cells.

¹⁰ Cytotoxic means harmful to cells.

triggers the autoimmune response that leads to T1D?¹¹

One way of getting closer to a definitive answer to this could be through using a bio-model that was more akin to a human. Though bio-models have proven to be priceless assets in diabetes research it is important not to forget that they are *models*, and despite certain similarities the results obtained from these can not be directly interpreted in the frame of human physiology. Hopefully medical instruments will be so fine-tuned in the future that human pancreatic biopsies, that are too hazardous today (Notkins and Åke Lernmark (2001)), can be performed with great benefit for the research society and so also diabetes patients.

One could speculate that there are several subtypes of autoimmune diabetes, each associated by a specific trigger/event. In chapter 3 we will see how tentative treatments are sometimes, but not always, successful. An explanation for this fact could be that a treatment needs to be paired up with the right subtype of autoimmune diabetes.

¹¹ This is not only the case with T1D, but with a wide range of autoimmune diseases (Christen and von Herrath (2004)), of which T1D is one of the most common (Cantor and Haskins (2006)).

3 Prospects for Therapy – A Mini Review

As more information about the etiology of diabetes has become available, several possible means of preventing/curing it have surfaced. In this chapter we give a brief account of some of these.

3.1 Treatment Strategies

Depending on the progression of the disease different therapeutical approaches are relevant (Greenbaum and Harrison (2008)), though some of them are not confined to one stage. Figure 3.1 gives a qualitative indication of how the amount of β -cells left is related to treatment strategy, how prediction becomes more and more accurate with time while prevention of T1D becomes less and less possible.

Firstly and most ideally every infant should be genetically screened to test for genes

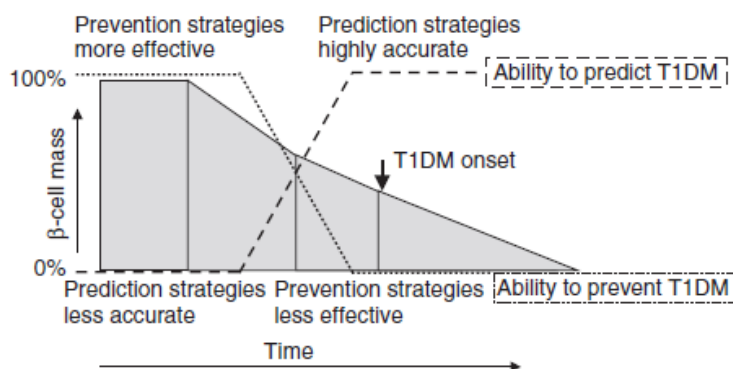


Figure 3.1 shows how different treatment strategies apply as β -cell mass is reduced over time. On the y -axis we have β -cell mass and along the x -axis we have time. As time passes the ability to prevent T1D becomes smaller and smaller. Figure was borrowed, with permission, from Staeva-Vieira et al. (2008)

that are linked with T1D. This would permit for precautionary measures such as diet changes or antigen-based therapy. The only problem with this is that these genes need still be identified.

Secondly, when autoimmunity is observed, antigen therapy is still an option, but also direct administration of regulatory cells (e.g. macrophages) has been suggested. At this stage the aim of the treatment is to prevent β -cell destruction.

Unless the autoimmunity is treated it will inevitably lead to β -cell destruction, the

third stage of T1D, at which point antigen therapy loses its applicability. Regeneration, neogenesis and proliferation of β -cells are defining aspects of potential treatment strategies.

Total depletion of β -cells delineates the fourth stage. Future possible courses of action at this stage is to insert “immune-blind” β -cells and use intermittent immunotherapy, i.e. stopping the autoimmune process.

Besides this brief introduction to the different strategies applicable to different stages of the disease the following sections are reserved solely for strategies directed at autoimmunity and β -cell destruction. We choose to do so because these are the most realistic stages to aim at today, and they are the most relevant stages of the model of Marée et al. (2006). Furthermore GLP-1 will be commented on most extensively simply because articles on GLP-1 were most abundant.

Though different promising ideas for therapy have been proposed since the mid-eighties, it is necessary to be cautious (Marée et al. (2006)) – the final section of this chapter is reserved for a brief note on this.

3.2 Glucagon-Like Peptide 1

GLP-1 is an incretin peptide, i.e. it meets the criteria given in the introduction. GLP-1 was interesting for T2D-patients from the point of its discovery (Nauck (1998)), because it

- enhances glucose-stimulated postcibal insulin secretion,
- inhibits glucagon release and
- inhibits gastric emptying, and food intake (Brubaker and Drucker (2004)),

while it was not until the beginning of the 1990’s, that results emerged that suggested that GLP-1 also had an effect in patients with T1D (Nauck, 1998, p.125). Since then an abundance of articles on GLP-1 has appeared – and continue to appear. A search for GLP-1 and diabetes on the scholar version of google as of June 2009 returns 14300 results. Accordingly we are not able to give a full overview, and have chosen to confine ourselves to some recent results.

Suarez-Pinzon et al. (2008) found that a combination of GLP-1 and gastrin (we will return to gastrin in section 3.3) restored normoglycemia in NOD-mice through an increase in β -cell mass and downregulation of the autoimmune response (Suarez-Pinzon et al., 2008, p.3281), while GLP-1 or gastrin alone did not induce such an effect. The downregulation of the autoimmune response arises when the cytokines change their expression from cytotoxic to benign, thus sparing the β -cells from further cytokine-induced apoptosis. Beside this intermittence of autoimmunity Suarez-Pinzon et al. (2008) also observed an increase in β -cell replication of duct cells, but not from the pancreatic β -cells (Suarez-Pinzon et al., 2008, p.3284). The results of Suarez-Pinzon et al. (2008) suggests that combination therapy with GLP-1 and gastrin can be used at the third stage of T1D.

Besides these positive results obtained by the combination of GLP-1 and gastrin, Urusova et al. (2004) gives a summary of recent data that shows that GLP-1 on its own has an anti-apoptotic effect on β -cells. Urusova et al. (2004) also reports that GLP-1 regulates the differentiation of progenitor cells as well as induces β -cell prolif-

eration *in situ* Urusova et al. (2004). The findings reported Urusova et al. (2004) are corroborated in Brubaker and Drucker (2004).

Though we have several other articles on GLP-1 we stop here, and present a summary of GLP-1-related positive effects that could be included in a mathematical model:

- Regulates differentiation of pancreatic progenitor cells (Urusova et al., 2004, p.27)
- It causes β -cell proliferation in the islets (Urusova et al., 2004, p.28)
- Protects β -cells from apoptosis (Urusova et al., 2004, p.30-31)
- Increases replication of duct cells (Suarez-Pinzon et al. (2008))
- Has an intermittent effect on the autoimmune response (Suarez-Pinzon et al. (2008))

We would like to reiterate that the results of Suarez-Pinzon et al. (2008) are for GLP-1 *and* gastrin, while those of Urusova et al. (2004) and Brubaker and Drucker (2004) are for GLP-1 alone. In the following section we will turn our attention to gastrin.

3.3 Gastrin

Rooman and Bouwens (2004) tested the effects of gastrin and epidermal growth factor (EGF), as well as gastrin only and EGF only on (C57Bl6/J¹) alloxan² treated mice. They also treated healthy specimens, that were not to be given alloxan, with the combination to see if it had any effect on these.

On the first day the mice that were not chosen as control specimens were given intravenous injections of alloxan. The mice that were treated with gastrin and EGF all became normoglycemic after eight days of treatment, and normoglycemia persisted until 6 weeks after administration of alloxan, at which point the mice were terminated. The mice that were treated with gastrin only or EGF only were unsuccessful in reaching normoglycemia (Rooman and Bouwens, 2004, p.261). Rooman and Bouwens (2004) speculates that duct cells are responsible for regeneration in the pancreas (Rooman and Bouwens, 2004, p.264). In the mice that were given gastrin only neogenesis of β -cells was observed.

Again we see that the desired effects depend on a combination of gastrin and another drug – in this case epidermal growth factor.

3.4 Dendritic Cells

Dendritic cells (DC) may play a crucial part in the initiation T1D, but they also have a part to play in regards of possible therapeutic advances. Immature DCs are responsible for keeping the immune system from initiating autoimmune attacks, by making T cells tolerant to autoantigens.³ However under certain (pathological) circumstances the DC's travel to the lymph nodes where they activate the immune system, thus initiating an

¹ The C57Bl6 mouse is the most commonly used laboratory mouse. The "J" in C57BL6/J indicates that it is an C57Bl6 mouse that has been (genetically) altered (Pociot (2009)).

² Alloxan is a medicament used to induce experimental diabetes (Szkudelskii (2001)).

³ Autoantigens are recognized by the adaptive immune system – if the immune system recognizes the autoantigens as foreign antigens, then an autoimmune response may occur leading to cell destruction (Seeley et al., 2008, p.798-801).

autoimmune response focused on the pancreatic β -cells, see e.g. Ludewig et al. (1998) or Haase et al. (2004). Dendritic cells have also been linked to predisposition for T1D (Skarsvik et al. (2004)).

Some of the first experiments using transfer of dendritic cells as therapy were carried out approximately at the same time as GLP-1 came into the spotlight (Clare-Salzler et al. (1992)). But where GLP-1, and especially GLP-1 together with gastrin, showed potential as a stage-3 drug, successful therapy using DC has been carried out primarily at early stages of islet destruction (Lo and Clare-Salzler, 2006, p.421), though preliminary results of Lo and Clare-Salzler (2006) indicate that treatment using DC's can be initiated at any time before onset of T1D.

3.5 Antigen Treatment Merits Caution

In the previous sections we have only encountered cases where antigen therapy yielded positive results. However not all results are so optimistic. Blanas et al. (1996) urges caution in administering antigen therapy to human patients, as it can precipitate rather than arrest the onset of T1D (and other autoimmune diseases). Häenninen (2000) report similar results, and ascribes the continued autoimmune response to cytotoxic T cells. In Marée et al. (2006)(b) (not to be confused with Marée et al. (2006) which contains the model we will analyze in this work) they have taken the consequence of these seemingly contradictory results and made a mathematical model that shows that the difference between failure or success of antigen therapy hinges on marginal deviations in dose or peptide affinity.

4 Mathematical Modelling

The language of mathematics is widely used to describe a myriad of naturally occurring phenomena. This is partly due to the fact that mathematical modelling along with stability analysis allows for a qualitative description/understanding of systems in which one or more of the components are not sufficiently or accurately determined, as it is particularly the case in the medical sciences, where it is next to impossible to obtain data for many *in vivo* parameters, e.g. rate constants. It can also help estimate parameters based on which dynamical behavior is expected from a given system, or it can aide in the understanding of which parameters are the most significant for the behavior – given of course that the model is accurate enough, but more about this in the next paragraph. The construction of mathematical models is not something that is based on a set of well-defined rules or prescriptions, and one must always keep in mind what the purpose of the model is; Do we (think we) know all the parameters and just want to make long-term simulations? Are there stochastic processes involved, so we are content with results within a confidence interval? Is the model made with the single purpose of estimating parameters or do we just want to mimic a certain behavior regardless of quantitative agreement with nature? To each purpose different *a priori* guidelines for constructing a mathematical model comes to mind. In terms of mathematical modelling in the biosciences we find these to be:

1. A reliable model should be based on an observable *structure*, by *structure* we mean the underlying physiological/physical/biochemical etc. system which is of interest.
2. The model should be rid of non-natural behavior, e.g. concentrations should not be able to reach infinity or assume negative values.
3. The model must exhibit the measured/expected behavior within a given range of known parameter-values.

The first guideline should secure that the model is not taken out of the thin air. The second and third guidelines serve to validate the model's foundation in reality.¹

In this study we will concern ourselves with modelling of type 1 diabetes. To the uninitiated this may sound as a well-defined and isolated task, but the workings of the pancreas like most physiological systems is astonishingly complex. Thus the mathematical description of such systems becomes a difficult balancing act between including relevant factors and not making the model impossible to work with. Including every single mechanism involved in the onset of T1D would very likely obscure rather than elucidate which are the important components in the system dynamics. Therefore it is often advisable to seek a parsimonious model. Or as Murray (2002) puts it (Murray, 2002, p.175)

¹ Notice that question i (cf. section 1.1) deals with the second guideline.

The complexity of biological and biochemical processes is such that the development of a simplifying model is often essential in trying to understand the phenomenon under consideration. [...] Frequently the first model to be studied may itself be a model of a more realistic, but still to complicated, biochemical model.

It is however important to stress that one should not oversimplify a system when trying to model it – modelling the dynamics of hares versus foxes makes no sense if you remove either one of them!

But how then can mathematical modelling contribute to research in the etiology of T1D? Luckily it is possible to obtain data from bio-models such as the diabetes prone NOD mouse and the Balb/c mouse; cf. section 2. These data can be used as a reference, both quantitatively and qualitatively to see if a mathematical model that is based on a certain hypothesis matches this hypothesis. Thus the bio-models allows for testing of different hypothesis in a (to humans) non-invasive manor. This means that the mathematical models can be refined (based on biological reasoning), and hopefully at some point be so in tune with the data, that we can learn something from it that can be of assistance in the understanding of the human development of T1D.

This symbiosis between data and mathematical modelling is exemplified in the next chapter where we will introduce the model of Marée et al. (2006). They use mathematical modelling to test the hypothesis that it is first of all macrophages that are the most important immune cells affiliated with the onset of T1D, and secondly that it is a defect in the macrophages of NOD mice that is responsible for the spontaneous outbreak of insulinitis in this rodent. This means that they do not include T or B cells, or DCs for that matter – in agreement with Murray (2002).

In section 5.7 we will present and look closer at some of Marée et al. (2006)'s simplifications and assumptions.

5 The DuCa Model

In the following we give an account of the background of the full model of Marée et al. (2006), which we have coined *the DuCa model* since it is a Dutch-Canadian collaboration. We will also present the compartment system and the system of differential equations as they have presented it in their article. While doing so we will comment or clarify when we find it necessary. Afterwards, in sections 5.5 and 5.7, we discuss and give a critical appraisal of the DuCa model and the assumptions/simplifications made with it.

5.1 Background for the DuCa Model

The model proposed by Marée et al. (2006) is partly based on an earlier work by Marée et al. (2005) and findings by Trudeau et al. (2000).

In Marée et al. (2005) they conclude that Balb/c macrophages are generally more efficient at phagocytizing apoptotic β -cells than NOD macrophages. Furthermore they found that the Balb/c macrophages undergo an *activation step* after they have engulfed their first apoptotic β -cell. After the activation step, their phagocytosis rate increases; see table 5.1. In NOD-mice no activation step was observed, i.e. the NOD macrophages do not become more efficient at phagocytizing after engulfment of an apoptotic β -cell. Trudeau et al. (2000) found that a wave of apoptosis¹ occurs in the pancreatic β -cells in neonatal mice and other rodents as well. These findings led the scientific community to hypothesize that the reason why T1D is more prevalent in NOD-mice (relative to Balb/c-mice) is due to the poor phagocytosis rate of their macrophages (e.g. Trudeau et al. (2000), Mathis et al. (2001)).

The greater phagocytosis rate in Balb/c-mice implies that the macrophages are able to accommodate the increased amount of apoptotic β -cells during the apoptotic wave, whereas this is not the case in NOD-mice. Here some of the apoptotic β -cells are left uncleared long enough for the cells to become necrotic.²

When an activated macrophage engulfs a necrotic β -cell it secretes cytokines of which some are cytotoxic to β -cells (Stoffels et al. (2004)). Thus more β -cells undergo apoptosis, yielding a higher concentration of apoptotic β -cells to be phagocytized. The NOD macrophages are already incapable of clearing the cells that entered the system during the apoptotic wave, and so more cells become necrotic and the cycle continues. In other words a feedback loop is initiated in the NOD-mice, which eventually leads to the decimation of the β -cell population. The more efficient phagocytosis of the Balb/c

¹ An apoptotic wave is when an elevated rate of cells undergo apoptosis over a short interval of time relative to the lifespan of the organism in which it takes place.

² This also happens in the Balb/c mice, but only during a brief period.

macrophages prevents the ignition of the feedback loop in these mice.

The following list summarizes the events that lead up to the sustained apoptosis of β -cells in NOD-mice.

1. An apoptotic wave occurs.
2. The resting macrophages become activated when they engulf an apoptotic β -cell.
3. The activated macrophages, being as (in)efficient as the inactivated macrophages are unable to clear all the apoptotic β -cells.
4. As some of the β -cells are left uncleared too long they enter necrosis.
5. The activated macrophages engulf necrotic β -cells as well as apoptotic β -cells. The phagocytosis of necrotic cells causes the active macrophages to secrete cytokines.
6. Some of the cytokines are cytotoxic to β -cells, thus causing more β -cells to undergo apoptosis.
7. As more β -cells undergo apoptosis the NOD macrophages will be more and more overburdened thus more β -cells will become necrotic, which amplifies the detrimental feedback mechanism.

This should not be understood as though these things happen in a consecutive order, rather they take place more or less concurrently. For example the instance the apoptotic wave starts macrophages begin to become activated, a concentration of necrotic cells arise and so also a concentration of cytokines etc.

To give a proper critique of the DuCa model we must now what the purpose of it is. This leads us to our next section.

5.2 Purpose of Marée et al. (2006)

The purpose of Marée et al. (2006) is to answer the following questions (Marée et al., 2006, p.1269)

- Can the difference in macrophage phagocytosis function in NOD versus Balb/c mice (alone, or in combination with other factors) account for the distinct fates of these two strains, i.e. possible initiation of autoimmunity in NOD but not in Balb/c mice?
- Can the wave of β -cell death associated with normal development in all mice be a triggering stimulus that initiates the inflammation in NOD mice?

using a mathematical model that retains the most important features of the preface of T1D, i.e. continued β -cell destruction, based on a *less is more* concept (Marée et al., 2006, p.1269).

They do not want to construct a mathematical model that incorporates every detail involved in the onset of T1D, in agreement with our thoughts on mathematical modelling; cf. chapter 4.

One example of their parsimonious approach is their handling of cytokines (and other harmful factors). In chapter 2 we learned that several cytokines play a role in the etiology of T1D (Blasio et al. (1999)), but Marée et al. (2006) lump all of these together in one compartment (Marée et al., 2006, p.1276).

Marée et al. (2006) emphasizes that this mathematical model is based on the NOD

and Balb/c bio-models, and they make no claims as to its applicability to the human physiology.

The novel features in the DuCa model are comprised of the incorporation of an apoptotic wave and necrotic β -cells.

5.3 The DuCa Model – An Appetiser

The DuCa model is not presented in a mathematical frame³ however Marée et al. (2006) notes in an almost Fermatian⁴ way on the fact that their model holds interesting dynamics by stating (Marée et al., 2006, p.1280):

Extended bifurcation analysis ... points to other interesting dynamics, including cycle dynamics within certain parameter ranges. This will be the subject of a mathematical treatment elsewhere.

The co-author Leah Edelstein-Keshet has informed us that no such analysis has been performed because “[they] got busy with other projects” (Edelstein-Keshet (2009)). The aim of this chapter is to embark on such an analysis.

Firstly we give a presentation to the DuCa model. The DuCa model contains five coupled nonlinear differential equations. After the introduction to the DuCa model we will analyze a few less complicated, or intermediate models, that contain only three equations and are based on the CPH model. This gives the reader the opportunity to appreciate what the simplifications made with the intermediate models entail and contemplate the soundness of said simplifications. It should be noted that Marée et al. (2006) themselves analyze, what we have called, *The Intermediate Model (IM)*, and since it is *comme il faut* to reproduce the results of others in the natural sciences, when using their work as a basis, we reproduce and extend the analysis performed in the article of Marée et al. (2006) in order to confirm the results they obtained in section 6. Marée et al. (2006) presents a so-called compartment model as a visual representation of their full system. Therefore we would like to present the principles behind compartment models as they are widely used in mathematical modelling of biological and physiological systems.

An introduction to compartment models

In figure 5.1 a simple example of a basic compartment model with three compartments is shown. Species **A**, **B** and **C** are some generic molecules/compounds/reactants/cells/etc. of interest to a given model – in order not to make the rest of the text in this tutorial too cumbersome let us say molecules. The concentration of species **A** is governed by k_1 and k_2 times the concentration itself. k_1 is the *inflow*, which is a measure of how much, or how many, of species **A** that, possibly on average, flows into the first compart-

³ The article is from Philosophical Transactions of The Royal Society, and so not written with a strictly mathematical audience in mind.

⁴ Fermat was a mathematician who lived in the seventeenth century. He is most famous for leaving a note in the margin of his example of Arithmetica stating that $a^n + b^n = c^n$, where $(a, b, c, n) \in \mathbb{N}$ has no solution for $n > 2$, and that he had found a wonderful proof for this, though the margin was too little to contain it. A formal proof was not given until 1995.

ment over some given period, e.g. a day. k_2 is the corresponding efflux rate, or when multiplied by the concentration the expression is the outflow, from the first compartment, and is simultaneously the influx of the second compartment and so forth with k_3 and k_4 . Every k_i is a positive *rate constant*, since they indicate the rate at which the different molecules “are made” or turned into the type of molecule residing in the next compartment – this process is assumed to be constant (as a first approximation), hence rate constant (Murray, 2002, p.176). The rate constants k_2 , k_3 and k_4 have the dimension time^{-1} , thus one of these rate constants times a molecular concentration implies a flow of said molecule with dimensions molecules per volume per time – notice that the dimensions of k_1 necessarily must differ from the other k 's, since it will not be multiplied by a concentration. Therefore the dimension of k_1 is molecules per volume per time.

Molecules in the same compartment are all alike, with emphasis on “all”, i.e. a molecule that has just entered the compartment cannot be singled out among the others.

It is important to notice that the arrows signify an actual flow of molecules from one compartment to the next – the importance should become clear in a little while, as this is not the case for all arrows in the compartment diagram made by Marée et al. (2006) for the DuCa model.

Models such as the one in figure 5.1 can (often) be deconstructed into a set of biochemical reaction equations as given in equations 5.1 to 5.4



By noting that an influx implies a positive contribution of molecules, and an efflux implies a negative contribution, we can construct the corresponding differential equations

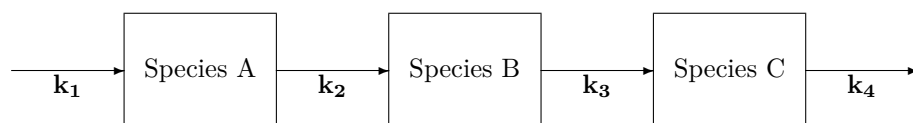


Figure 5.1 shows an example of a generic compartment model.

for the change in the concentration of $\mathbf{A}, \mathbf{B}, \mathbf{C}$ (Othmer (2006)):

$$\begin{aligned}\frac{d\mathbf{a}}{dt} &= k_1 - k_2\mathbf{a} \\ \frac{d\mathbf{b}}{dt} &= k_2\mathbf{a} - k_3\mathbf{b} \\ \frac{d\mathbf{c}}{dt} &= k_3\mathbf{b} - k_4\mathbf{c} \\ \frac{d\mathbf{p}}{dt} &= k_4\mathbf{c}\end{aligned}\tag{5.5}$$

where we have assumed that we have an inexhaustible source and sink, and lower-case letters denotes concentrations.

Using a compartment description of a system has the benefit that it provides an easy overview of the molecular flow in the system, and thereby it facilitates a visual understanding of how the differential equations interact.

Now that we have presented some fundamentals regarding compartment models we present a slightly modified version of Marée et al. (2006)'s compartment model; see figure 5.2. In the original compartment diagram in Marée et al. (2006), the arrow pointing from the compartment of macrophages toward the compartment of active macrophages was associated with a rate constant called g . But in the Marée et al. (2006) article they write that $g = f_1$ several times so we have decided only to use f_1 to avoid confusion – this is our modification. Besides this figure 5.2 is a replication of the original compartment diagram as presented on page 1277 in Marée et al. (2006).

5.4 The DuCa Model – Compartment Model and Equation System

As we have just learned the fully drawn arrows should signify an actual flow of molecules from one compartment to another; e.g. resting macrophages become activated, and leave the macrophage compartment, only to enter the compartment of activated macrophages (at rate f_1); figure 5.2. But as we will soon learn from equations 5.6 to 5.10 the fully drawn arrow from the M_a compartment to the cytokine compartment does not obey this rule. The interpretation of the stippled arrows is also a little abstruse. On one hand the stippled arrows seem to indicate that a stimuli is mediated to the appropriate receptors/cells thus facilitating an increase/decrease in the molecular concentration at hand; e.g. the activated macrophages do not themselves flow into the surrounding tissue and reenter the macrophage compartment – rather they *recruit* macrophages by signaling, signified by b . On the other hand the secretion of cytokines, at rate α , is evidently not a signaling process, but Marée et al. (2006) also identify it by a stippled arrow that meets the fully drawn arrow from the M_a -compartment which we mentioned just before. We will get back to these sources of confusion in section 5.5, where we will present a modified compartment model that we have constructed ourselves.

Just as there was a correspondence between figure 5.1 and equations 5.5 so Marée et al.

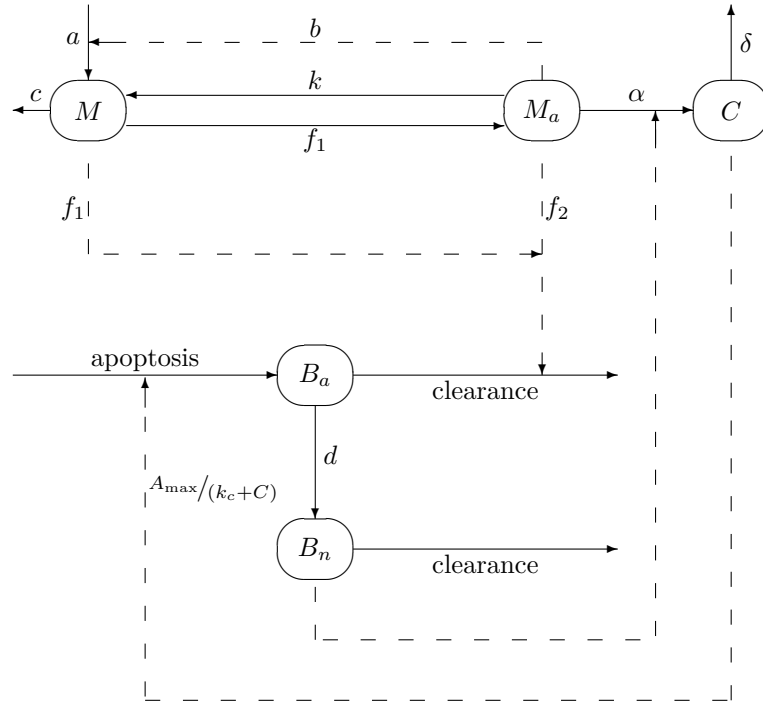


Figure 5.2 shows the compartment system as given by Marée et al. (2006). M , M_a , B_a , C and B_n are the concentrations of macrophages, activated macrophages, apoptotic β -cells, cytokines and necrotic β -cells respectively, and $A_{\max}/(k_c + C)$ is a Michaelis-Menten saturation function of the concentration of cytokines; cf. appendix A.4 for an introduction to Michaelis-Menten kinetics. An explanation and values of a , b , c , d , f_1 , f_2 , k_c , A_{\max} , α , δ is given in table 5.1.

(2006) set up a set of nonlinear coupled differential equations as follows (cf. figure 5.2)

$$\frac{dM}{dt} = a + (k + b)M_a - cM - f_1MB_a - e_1M(M + M_a) \quad (5.6)$$

$$\frac{dM_a}{dt} = f_1MB_a - kM_a - e_2M_a(M + M_a) \quad (5.7)$$

$$\frac{dB_a}{dt} = W(t) + \frac{A_{\max}C}{k_c + C} - f_1MB_a - f_2M_aB_a - dB_a \quad (5.8)$$

$$\frac{dB_n}{dt} = dB_a - f_1MB_n - f_2M_aB_n \quad (5.9)$$

$$\frac{dC}{dt} = \alpha B_n M_a - \delta C \quad (5.10)$$

with initial conditions $(M, M_a, B_a, B_n, C) = (4.77 \times 10^5, 0, 0, 0, 0)$.⁵ The equations should be interpreted thusly:

Equation 5.6: the rate of change in the concentration of macrophages, M , is made up of a gain from the influx, a , the deactivation rate of the active macrophages times the concentration of active macrophages, kM_a , and the recruitment rate times the concentration of active macrophages, bM_a , and a loss constituted by the efflux, c , times M , the activation rate of resting macrophages, f_1 , times M times the concentration of apoptotic β -cells, B_a , and lastly the crowding rate, e_1 , times $M(M + M_a)$.

Equation 5.7: the rate of change of the concentration of active macrophages, M_a , is made up of a gain from f_1 times MB_a and a loss or efflux due to the deactivation rate, k times M_a , and the crowding rate, e_2 , times $M_a(M + M_a)$.

Equation 5.8: the rate of change in the concentration of apoptotic β -cells, B_a , is governed by the phagocytosis rates, f_1 and f_2 , times MB_a and M_aB_a respectively and the nonspecific decay rate, d , times B_a . These make up the negative contributions while the apoptotic wave (not shown in the figure), $W(t)$, and the Michaelis-Menten saturation function of cytokines, $(A_{\max}C)/(k_c + C)$, where A_{\max} is the maximal rate of apoptosis that the cytokines can induce, and k_c is the Michaelis constant, constitute the positive contributions.

Equation 5.9: the rate of change of the necrotic β -cells, B_n , is influenced by a positive contribution from dB_a , and negative contributions from f_1 and f_2 times MB_n and M_aB_n respectively.

Equation 5.10: the rate of change in the cytokine concentration, C , depends on the decay rate, δ , times C and the secretion rate by active macrophages, α times M_aB_n .

The meaning and units of the different parameters are given in table 5.1. At a first glance the equations almost seem to be in accordance with what we learned when we looked at generic compartments in subsection 5.3. But soon we see that something is amiss. We will return to these matters in section 5.5. For now let us return to the DuCa model, or rather the equations that comprise it.

To unfold equations 5.6 to 5.10 a little more and to give ourselves the opportunity to think thoroughly about every term on the right hand side in said equations we present a comprehensive list of how we understand each term:

- a is daily inflow of resting macrophages from the surrounding tissue
- kM_a is the deactivation rate of activated macrophages times the concentration of activated macrophages, i.e. the dimensions are cells $\text{ml}^{-1}\text{d}^{-1}$, where “d” in this case is days, not to be confused with the parameter d . This term represents the flow of deactivated macrophages from the M_a -compartment into the M -compartment
- bM_a is a measure of the extra influx of resting macrophages due to signalling to the surrounding tissue by active macrophages.
- cM is daily efflux of resting macrophages, i.e. the outflow of resting macrophages to the surrounding tissue.
- f_1MB_a in equation 5.6 represents the outflow of resting macrophages that have become activated upon clearance of an apoptotic β -cell, hence B_a is included in

⁵ For a statement of the existence and uniqueness theorem, and its application to the DuCa model cf. appendix A.1.

the expression. This is also why f_1MB_a appears in equation 5.8 as a loss and in equation 5.7 as a positive inflow.

- $e_1M(M + M_a)$ and $e_2M_a(M + M_a)$ are effluxes that model the effect of crowding. More precisely they model the competition for space (Strogatz, 2000, p.156) between macrophages and active macrophages. The specific expressions are classical for two-species competition (Edelstein-Keshet (2009)), e.g. the Lotka-Volterra model of competition (Strogatz, 2000, p.155-159). They serve as inhibitory terms, that become significant only when the concentration of M and/or M_a becomes large. In other words they ensure a limit to the growth of M and M_a – as the concentrations M and M_a grow the $e_1M(M + M_a)$ and $e_2M_a(M + M_a)$ terms become more and more significant, thus limiting the growth, while when M and M_a are small the terms are insignificant. In the original parameter-table given in Marée et al. (2006) the units of e_1 and e_2 were $\text{cell}^{-1}\text{d}^{-1}$, but naturally this implies a dimensional-discrepancy in the model, so we have altered these units in table 5.1.
- $W(t)$ is the apoptotic wave. In the DuCa model it is modeled by a Gaussian function given by $4 \times 10^7 \exp(-((t - 9)/3)^2)$ $\text{cells ml}^{-1} \text{d}^{-1}$ because the wave peaks after 9 days and 4×10^7 enter apoptosis overall due the apoptotic wave.
- $\frac{A_{max}C}{k_c+C}$ describes the rate of cytokine induced apoptosis. $\frac{A_{max}}{k_c+C}$ is a Michaelis-Menten saturation function of C which in other words means that the cytokine induced apoptosis is saturated. Other functions could have been chosen, e.g. a general Hill function which is a function of the form $\frac{A_{max}C^r}{k_c^r+C^r}$ where $r > 0$ is not generally an integer (Murray, 2002, p.200), and the higher the r the quicker the saturation effect, but Marée et al. (2006) assumes the saturation to follow a Michaelis-Menten function (Marée et al., 2006, p.1276) (notice that a Michaelis-Menten function is just a Hill function with $r = 1$). In section 5.7 we will take a look at what happens if Hill functions are used instead.
- $f_2M_aB_a$ is the amount of B_a cleared by M_a at rate f_2 , thus $f_2M_aB_a$ appears as a loss in equation 5.8, but not in 5.7, since this does not imply any contribution to the M_a -concentration (the active macrophages remain active, and therefore do not leave the M_a -compartment).
- dB_a is the amount of apoptotic β -cells that become necrotic per day.
- f_1MB_n is the amount of B_n cleared by M at rate f_1 – Marée et al. (2006) assumes that only clearance of apoptotic β -cells induces activation, thus the resting macrophages do not leave their compartment (we will return to this assumption in section 5.7).
- $f_2M_aB_n$ is the amount of B_n cleared by M_a at rate f_2 . As with the apoptotic cells, the active macrophages remain activated during the process of phagocytosis.
- $\alpha B_n M_a$ is the amount of cytokines that are secreted by M_a upon phagocytosis of B_n – once again the active macrophages do not leave their compartment due to this, therefore this does not influence the rate of change of M_a .
- δC gives a measure of how many cytokines turnover a day without inducing apoptosis.

As a macrophage engulfs an apoptotic β -cell it becomes activated, moves from the compartment of resting macrophages, and into the compartment of activated macrophages, yielding a positive contribution to this compartment. This can be seen in equation 5.6 and 5.7 where $f_1 M B_a$ is an efflux in equation 5.6 and reappears as the positive input in equation 5.7 – remember that the macrophage engulfs the apoptotic β -cell i.e. “it carries it with it” to the active macrophages compartment. We must remark that in reality the macrophage does not move into a specific part of the tissue once it has engulfed a β -cell, but rather into another state.

Now that we have introduced the compartment model, the equations and the para-

Parameter	Meaning	Balb/c	NOD	Units
a	Normal macrophage influx	5	–	$\times 10^4$ cells ml ⁻¹ d ⁻¹
b	Recruitment rate of M by M_a	0.09	–	d ⁻¹
c	Macrophage egress rate	0.1	–	d ⁻¹
d	B_a non-specific decay rate	0.5	–	d ⁻¹
k	M_a deactivation rate	0.4	–	d ⁻¹
l	B_a apoptosis induced per M_a	0.41	–	d ⁻¹
f_1	Basal phagocytosis rate per M	2	1	$\times 10^{-5}$ ml cell ⁻¹ d ⁻¹
f_2	Activated phagocytosis rate per M_a	5	1	$\times 10^{-5}$ ml cell ⁻¹ d ⁻¹
$e_1 = e_2$	Anti-crowding rates	1	–	$\times 10^{-8}$ ml cell ⁻¹ d ⁻¹
A_{max}	Maximal cytokine-induced β -cell apoptosis rate	2	–	$\times 10^7$ cells ml ⁻¹ d ⁻¹
k_c	Cytokine concentration for half-maximal apoptosis rate	1.0	–	nM
α	Cytokine secretion rate by M_a due to B_n	5	–	$\times 10^{-9}$ nM cell ⁻² d ⁻¹
δ	Cytokine turnover rate	25	–	d ⁻¹
k_b	$\delta/\alpha k_c$	5	–	$\times 10^{10}$ cell ²

Table 5.1 summarizes the model-parameters and their values – d⁻¹ is days to the power of minus one, or “per day”. If not stated otherwise the parameters for NOD-mice are the same as for Balb/c-mice. The rate constant l is not included in the DuCa model but appears in the intermediate model in section 6. k_b is not in the DuCa model either, but it appears in section 7 in equation 8.5. The table is a combination of the table on p. 1271 and p. 1278 in Marée et al. (2006)

eters it is time to take a look at how the two systems (NOD and Balb/c) evolve over time.

In figure 5.3 MATLAB-simulations of the systems with parameters as given in table 5.1 are shown. The concentrations in figure 5.3 are logarithmic.

On the left we see that the Balb/c-mouse is rid of everything but resting macrophages after 50 days.⁶ This is not the case for the NOD-mouse. Here all concentrations become constant, and greater than 0. This is in itself not a problem as long as they settle at a very low concentration (save for the resting macrophages). The concentration of apoptotic β -cells stabilizes at approximately 12 after 50 days. Thus after day 50 e^{12} β -cells per ml become apoptotic. This is not a huge number, but if we add to this the number of β -cells that were depleted before the first 50 days it starts adding up. We must also remember that around 4-5 weeks of age, T cells will start infiltrating the islets, and add to the destruction. The most important consequence of the constant concentration is that the β -cells will keep on becoming apoptotic.

⁶ Remember that the concentrations are logarithmic, so a concentration of 0 is not really a concentration of 0, rather it is a concentration of 1.

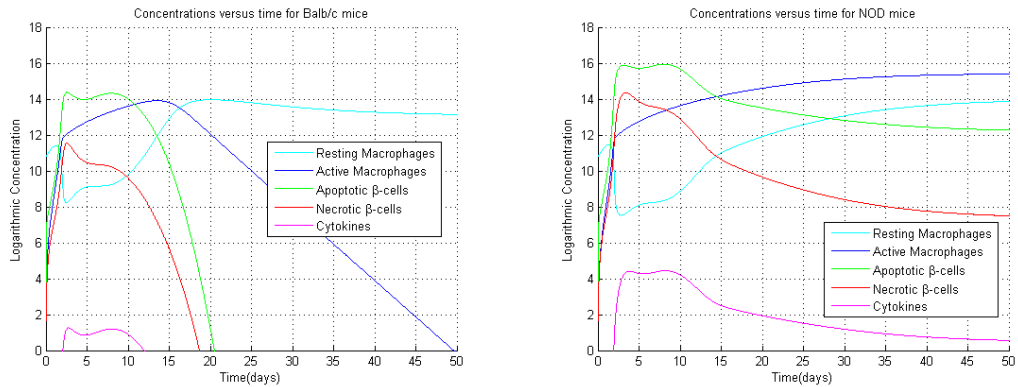


Figure 5.3 To the left: dynamics of the Balb/c-mouse. To the right: dynamics of the NOD-mouse. Based on parameters found in Marée et al. (2006), see table 5.1, and initial conditions that correspond to a healthy rest state, i.e. $(M, M_a, B_a, B_n, C) = (4.77 \times 10^5, 0, 0, 0, 0)$. The apoptotic wave and the effect of it is seen as the peak at 9 days on the curves describing B_a -, B_n - and C -concentrations. We see that inflammation persists in the NOD-mouse, whereas nearly all apoptotic β -cells are removed before 21 days have transpired in Balb/c-mice.

5.5 Discussion of the Compartment Model

As we pointed out in the above section there are some discrepancies between equations 5.6-5.10 and figure 5.2, compared to how the equations in 5.5 corresponded to the compartment system in figure 5.1. Not least the use of stippled arrows makes a transformation from the compartment-system to a set of conventional reaction-kinetic equations ambiguous.

Here we will make these matters more precise, devise some stringent rules for when it is appropriate to use stippled arrows, or when the use of such arrows can be circumvented, and when full-drawn arrows should be used. Ultimately we want to present a compartment model that is in accordance with our rules and has a clearer correspondence with the equations.

Firstly let us compare figure 5.2 to equations 5.6 to 5.10, and start with the most blatant mismatches.

First of all the crowding terms are nowhere to be seen, secondly the apoptotic wave is not shown, this could be because it is a short-lived event, but still it would at least merit an explanatory remark why it is not there. Thirdly the stippled arrows identified by f_1 and f_2 meet. While we do understand the meaning of this, and granted the article is not written with compartment diagram-puritans in mind, it is still not a clear way of setting up a compartment diagram – after the two arrows have merged it is impossible to tell which of f_1 and f_2 we should assign to the arrow that continues after the merging.

If we follow the aforementioned stippled arrows we get to the first of the two “clearance” arrows. These arrows are not (directly) associated with any rate constant, as they should be. Lastly there is the fully drawn arrow from the M_a compartment to the cytokine compartment. This would normally imply that the active macrophages

migrate to the cytokine compartment, i.e. become cytokines. This is naturally not the case, so this is another issue we must address in the next section, where we present our own version of compartment model.

5.6 Our Compartment Model

Now that we have touched upon what we perceive as inconsistencies in the original model (figure 5.2), we will devise our own compartment model. But before we present our version, we will specify how we use the fully drawn and stippled arrows, since ambiguous use of the arrows was one of the major problems in the original model.

- Fully Drawn Arrow: is to be used only when there is an actual flow of molecules. This means that if a fully drawn arrow points into a compartment, then the differential equation that describes the rate of change in concentration of the molecule in that compartment will contain a term that constitutes an inflow; e.g. a in equation 5.6 or f_1MB_a in equation 5.7. If a fully drawn arrow points out of a compartment, then the corresponding differential equation must contain a term that signifies this outflow; e.g. $-dB_a$ in equation 5.8.
- Stippled Arrow: if a stippled arrow points into a compartment, it yields a positive contribution in the corresponding differential equation, but without causing an identical loss in the differential equation associated with the compartment the arrow came from; e.g. $\alpha M_a B_n$ in equation 5.10 and $A_{\max}C/(k_c+C)$ in equation 5.8.

Now that these definitions are in place let us look at our compartment models. Yes, we wrote *models* in plural, because we have found it necessary to divide the model into two figures. We have split the model into a part that contains M , M_a and B_a compartments which we call the non-necrotic part, and a part that contains M , M_a , B_n and C compartments, which we call the necrotic or B_n -part. Had we not done so arrows would be crossing each other, which does not facilitate the transparency of the model. In figure 5.4 we have the non-necrotic part of our modified compartment model. While figure 5.5 is the B_n -part of the compartment model. The compartment diagrams are made in agreement with our definitions of full-drawn, and stippled arrows.

One feature of figure 5.4 that may seem a bit confusing is the stippled arrow that leaves the M_a compartment to coincide with the fully drawn arrow leaving the B_a compartment. This is done so because the apoptotic β -cells are phagocytized by the active macrophages, which implies that the β -cells leave their compartment, hence a full-drawn arrow. The active macrophages on the other hand do not leave their compartment during phagocytosis (they remain activated), and they do not go to the B_a compartment either, hence the stippled arrow from the M_a compartment points to the fully drawn arrow.

Another feature that needs to be commented on is the stippled arrow that coincides with the apoptosis arrow to the left of the B_a compartment. This arrow denotes the cytokine induced apoptosis which appears as gain in equation 5.8. In figure 5.5 the same arrow leaves the cytokine compartment. Another arrow that transcends the figures is the arrow that represents the non-specific decay of β -cells – those that become necrotic. This arrow enters the B_n compartment in figure 5.5, and thus entails a loss in equation 5.8 and a gain in equation 5.9.

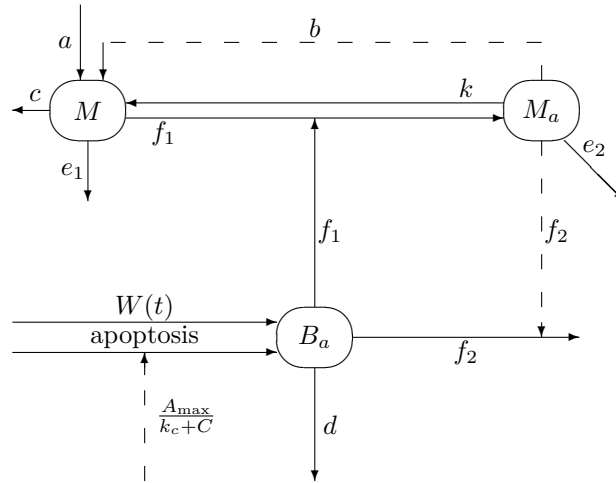


Figure 5.4 shows the non-necrotic part of our modified compartment model. M , M_a , and B_a are the concentrations of macrophages, activated macrophages and apoptotic β -cells respectively. An explanation of $a, b, c, d, e_1, e_2, f_1, f_2, A_{\max}, k_c$ is given in table 5.1.

Besides standardizing the use of arrows we have also included the apoptotic wave, and the crowding terms to make a compartment model that, albeit divided into two figures, agrees with the governing equations.

Initially we wanted to rid the model of stippled arrows all together, in order to be able to make a translation from the compartment model to a set of reaction equations, and from there to the set of governing equations.

It is not impossible to get rid of the stippled arrows, but it requires extra compartments, that contain intermediate combinations of, say, active macrophages that have engulfed necrotic β -cells, and also we must introduce some extra parameters. In figure 5.6 we have picked out a part of the original compartment model and added a compartment containing active macrophages that have engulfed one or more necrotic β -cells. The macrophages will either secrete a cytokine, at rate k_4 , or merely clear the necrotic β -cell, at rate k_5 , without releasing any cytotoxic compounds – either way the active macrophage will return to its compartment, at rate k_3 . If k_1 and k_2 are equal it means that one macrophage engulfs one necrotic β -cell – if this engulfment is similar to the engulfment of apoptotic β -cells, this need not be the case⁷ (Marée et al. (2005)).

Upon engulfment the macrophage will either consume the β -cell quietly, at rate k_5 , or it will secrete a cytokine, at rate k_4 . We will not concern ourselves with the fate of the cytokines in this example.

When we decompose the compartment system in figure 5.6 into mass action kinetic

⁷ In Marée et al. (2005) they observed that an activated macrophage could contain up to 7 apoptotic β -cells (that were at different levels of phagocytosis), and this did not appear to be an upper bound (Marée et al., 2005, p.542).

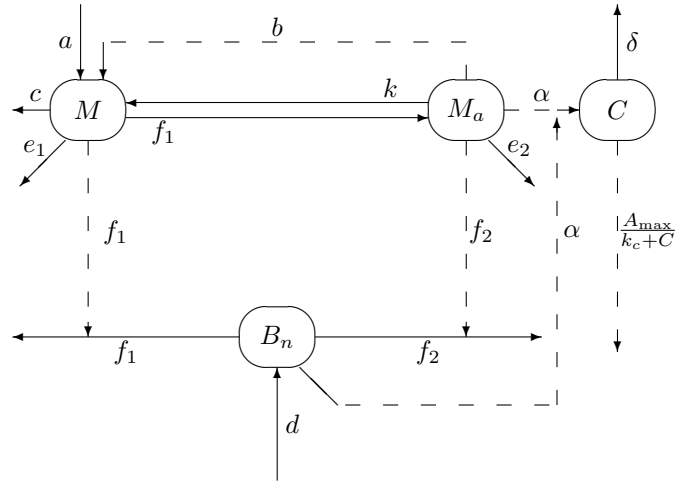


Figure 5.5 shows the necrotic part of our modified compartment model. M , M_a , C and B_n are the concentrations of macrophages, activated macrophages, cytokines and necrotic β -cells respectively. An explanation of $a, b, c, d, e_1, e_2, f_1, f_2, \alpha, \delta, A_{\max}, k_c$ is given in table 5.1.

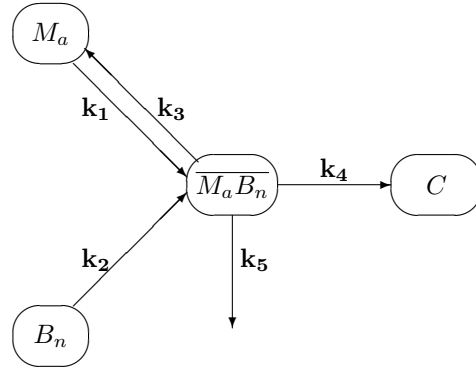


Figure 5.6 shows the compartment system corresponding to equations 5.17 to 5.20. The active macrophages enter the $\overline{M_a B_n}$ -compartment at rate k_1 . The necrotic β -cells enter the same compartment at rate k_2 . The necrotic β -cell can either be broken down quietly, at rate k_5 or yield a cytokine, at rate k_4 . After digestion of the necrotic β -cell, the active macrophage returns to the compartment containing these, at rate k_3 , i.e. k_3 is a digestion rate.

equations we get

$$M_a + B_n \xrightarrow{k_1} \overline{M_a B_n} \quad (5.11)$$

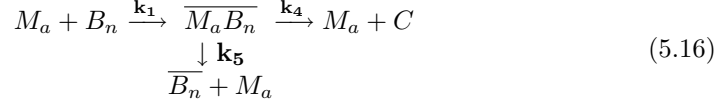
$$\overline{M_a B_n} \xrightarrow{k_3} M_a \quad (5.12)$$

$$\overline{M_a B_n} \xrightarrow{k_4} C + M_a \quad (5.13)$$

$$\overline{M_a B_n} \xrightarrow{k_5} \overline{B_n} + M_a \quad (5.14)$$

$$(5.15)$$

Where $\overline{B_n}$ are necrotic cells that have been cleared quietly. Assuming that $k_1 = k_2$, and noticing that quiet clearance or secretion of a cytokine implies that the macrophage returns to the M_a -compartment, we require $k_3 = k_4 + k_5$. Thus these equations can be encompassed in a simple reaction equation as



equation 5.16 corresponds to the following set of differential equations

$$\frac{dM_a}{dt} = k_3 \overline{M_a B_n} - k_1 M_a B_n \quad (5.17)$$

$$\frac{dB_n}{dt} = -k_1 M_a B_n \quad (5.18)$$

$$\frac{d\overline{M_a B_n}}{dt} = k_1 M_a B_n - k_3 \overline{M_a B_n} \quad (5.19)$$

$$\frac{dC}{dt} = k_4 \overline{M_a B_n} \quad (5.20)$$

$$\frac{d\overline{B_n}}{dt} = k_5 \overline{M_a B_n} \quad (5.21)$$

Where we have used $k_1 = k_2$. If we assume that the $\overline{M_a B_n}$ -compartment is at a steady state we get an expression for the concentration of the $\overline{M_a B_n}$ complex in terms of the concentration of M_a and B_n thusly

$$\overline{M_a B_n} = \frac{k_1}{k_3} M_a B_n \quad (5.22)$$

Substituting equation 5.22 into equation 5.17 we get

$$\frac{dM_a}{dt} = k_3 \frac{k_1}{k_3} M_a B_n - k_1 M_a B_n \quad (5.23)$$

If we want to add the compartments in figure 5.6 into the full system, then we must add the right hand side of equation 5.23 to equation 5.7, but this comes to zero. Thus we obtain

$$\frac{dM_a}{dt} = f_1 M B_a - k M_a - e_2 M_a (M + M_a) \quad (5.24)$$

for the rate of change in M_a , which is of course identical to equation 5.7. Thus we have shown how we can avoid using stippled arrows, by introducing intermediate complexes. We could just as well have made an extra compartment that contained $\overline{M B_a}$, $\overline{M B_n}$ or $\overline{M_a B_a}$.

5.7 Discussion of Marée et al. (2006)'s Model Assumptions

To facilitate the overview we present a list of elements in the model that are either not included or we find merits more discussion.

- They do not include the constant apoptosis which occurs naturally regardless of pathophysiological conditions.
- The apoptotic wave
- They choose a Michaelis-Menten function because they want to
avoid unrealistically high [cytokine induced] damage during the neonatal apoptotic wave
- Only engulfment of necrotic β -cells by active macrophages yields cytotoxic cytokines.
- Clearance of necrotic β -cells does not imply any activation of the resting macrophages.
- It is assumed that macrophages are equally efficient at clearing apoptotic and necrotic β -cells.

The role of naturally occurring apoptosis

Apoptosis of β -cells is not exclusively reserved for pathophysiological cases, but also takes place in healthy individuals (Bouwens and Rooman (2005)). This assumption will be dealt with in section 11.1 where it arises as a natural part of an expansion of the DuCa model.

Significance of the Apoptotic Wave

In this short subsection we will discuss the apoptotic wave based on varying data from the literature. We will also determine how the wave should behave if chronic inflammation was not to occur in NOD-mice. It may be that modulating the apoptotic wave is not a viable means of countering the ignition of the chronic inflammation, but this is not for us as mathematicians to decide.

That an apoptotic wave occurs in neonates seems to be out of discussion when we look at recent literature (e.g. Trudeau et al. (2000), Steer et al. (2006), and Ablamunits et al. (2007)). Unfortunately we have not had access to the data, so we find it hard to criticize the expression that Marée et al. (2006) use for the wave. We can however look at how different peak-days influence the effect of the wave.

Marée et al. (2006) model the neonatal apoptotic wave by $4 \times 10^7 \exp(-((t-9)/3)^2)$ cells $\text{ml}^{-1} \text{d}^{-1}$, which implies that the wave peaks at 9 days of age. Other results points to that the wave peaks between 14 and 17 days of age (Steer et al., 2006, p.262)(Ablamunits et al., 2007, p.19). Here we will first determine how low a peak-value the apoptotic wave must have as not to be the cause of chronic inflammation under the assumption of the 9'th day being the peak day, and thereafter under the assumption of 14 to 17 days. We will use the basic mathematical form of the wave as given by Marée et al. (2006) to investigate these matters.⁸ I.e. we will change the peak value, and the number of days after birth at which the wave peaks. In the original term (given above) the number of days, at peak, is the number subtracted from time, t , as can be found by differentiating the expression.

Simulations of the DuCa model with NOD parameters (not shown) reveal that the

⁸ Other forms could have been used, but we will not go into these matters here.

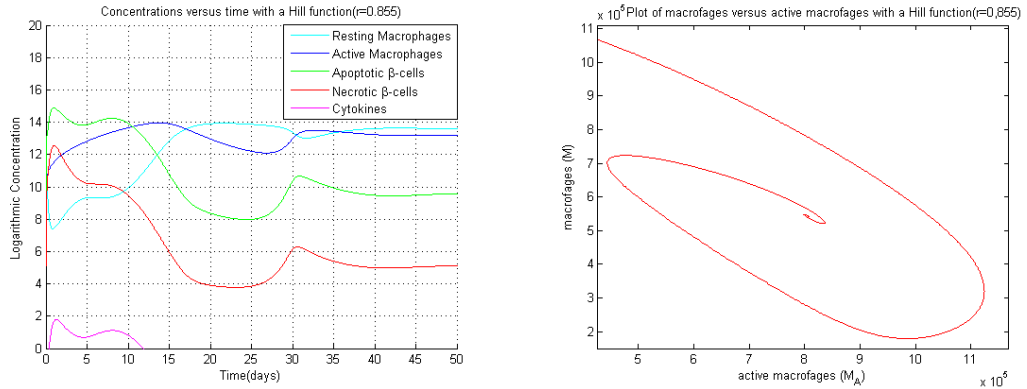


Figure 5.7 Shows simulations of the DuCa model with a Hill function instead of the Michaelis-Menten function. The Hill-coefficient is $r = 0.855$, and Balb/c phagocytosis parameters as stated in table 5.1 are used, as are initial conditions that correspond to a healthy rest state, i.e. $(M, M_a, B_a, B_n, C) = (4.77 \times 10^5, 0, 0, 0, 0)$.

apoptotic wave must have a peak value of less than $2834 \text{ cells ml}^{-1}$ entering apoptosis, if inflammation is to be non-persistent, when 9 days designates the peak of the wave. That is the wave should be modelled by $2.834 \times 10^3 \exp(-((t-9)/3)^2) \text{ cells ml}^{-1}$. When the peak-day was increased to 14 the peak value increased to 2840, which was also the value for 15 days – it only makes sense to work with whole cells. For 16 and 17 days the peak value was $2841 \text{ cells ml}^{-1}$.

The conclusion from this quick study of the relation between peak value and peak day shows that when we compare the minuscule increase in the number of β -cells that can undergo apoptosis at the peak, without causing chronic inflammation, to the peak value given by Marée et al. (2006), it seems futile to use delaying the peak day of the apoptotic wave as a way of preventing inflammation. Therefore we also find that it is reasonable to use the wave as modelled by Marée et al. (2006), with a peak at 9 days, but we could just as well have used 14 or 17 days.

Michaelis-Menten versus a Hill function

Our second discussion point regards the usage of the Michaelis-Menten function. As we mentioned in section 5.4 Hill functions can also be used to model saturation behavior. We have made simulations of the DuCa model with a Hill function given by $\frac{A_{\max} C^r}{k_c^r + C^r}$ instead of the Michaelis-Menten function; figure 5.7. For $r \geq 0.86$ the behavior is qualitatively the same as for the Michaelis-Menten function, but for a Hill-coefficient of $r < 0.8564$ some interesting things start to happen. Simulations done in MATLAB with Balb/c parameters reveals a stable spiral that tends to a point that is consistent with a state of constant inflammation, albeit the inflammation is not as severe as the one experienced by the NOD-mice in figure 5.3; cf. figure 5.7 right subplot. The spiral is seen as the transient period of damped oscillations in the left subplot. However before we start to make hasty conclusions about the soundness of the DuCa model based on figure 5.7 we must specify that Hill functions are often used to model systems in which a

phenomenon called *cooperativity* occurs. Cooperativity describes the phenomenon that an enzyme can become more (or less) prone to bind with substrates after binding with one substrate (Murray, 2002, p.197). If the enzyme becomes more prone to bind, then we speak of positive cooperativity, if the enzyme remains as prone to bind as before binding to the substrate, then it is neutral cooperativity (Michaelis-Menten), and finally if it becomes less prone to bind we call it negative cooperativity (Murray, 2002, p.201). The Hill-coefficient reveals if we are dealing with negative, neutral or positive cooperativity.

Marée et al. (2006) do not want to model cooperativity, they just want the cytokine induced apoptosis to be saturated, therefore we find that the use of a Michaelis-Menten function is a sound assumption.

Implication of secretion of cytokines upon B_a phagocytosis

In Stoffels et al. (2004) they find that NOD macrophages produce cytotoxic cytokines upon encountering necrotic as well as apoptotic cells, while Brouckaert et al. (2004) holds that phagocytosis of neither apoptotic nor necrotic cells generates proinflammatory cytokines (Brouckaert et al., 2004, p.1089). The results of Brouckaert et al. (2004) indicates that phagocytosis of necrotic cells is less efficient than phagocytosis of apoptotic cells – it may be so because the macrophages are better “tuned in” to the apoptotic cells (Pociot (2009)). This is at variance with the assumption of Marée et al. (2006). Brouckaert et al. (2004) does not dispute the fact that cytokines are observed together with necrotic cells, but speculates that it is the necrotic cells themselves, rather than the macrophages, that release cytokines, and speculates further that the inflammatory effect is enhanced because the macrophages spend too much time engulfing the necrotic cells, leaving more apoptotic cells to enter secondary necrosis (Brouckaert et al., 2004, p.1099) thus proliferating the cytokines. Of course one could adjust the model to fit these different result, but we must note that the macrophages studied in Brouckaert et al. (2004) are of the so-called L929sA-type. The L929sA-type macrophage is associated with cancer cells (Pociot (2009)), which obfuscates our ability to draw direct parallels to NOD-macrophages.

Turning back to the results of Stoffels et al. (2004) and assuming that they are correct in their findings, and further more assuming that the rate of secretion of cytokines based on engulfment of apoptotic β -cells is equal to that from phagocytosis of necrotic cells, then equation 5.10 is transformed to

$$\frac{dC}{dt} = \alpha B_n M_a + \alpha B_a M_a - \delta C \quad (5.25)$$

This seemingly minor adjustment (remember that the secretion rate, α was a mere 5×10^{-9} nM cell⁻²d⁻¹) has a dramatic effect on the dynamics of the Balb/c mice, for now the concentrations M_a, B_a, B_n, C do not go to zero, rendering the Balb/c mouse in the same dire state as the NOD-mouse; see figure 5.8. This is of course at variance with experimental observations. Thus if Stoffels et al. (2004) are correct, then the hypothesis of Marée et al. (2006), that the onset of T1D in NOD, but not in Balb/c, mice is a consequence of phagocytosis rate cannot hold. Something else must be involved. One possibility is that the NOD-macrophages themselves have a predisposition for secreting

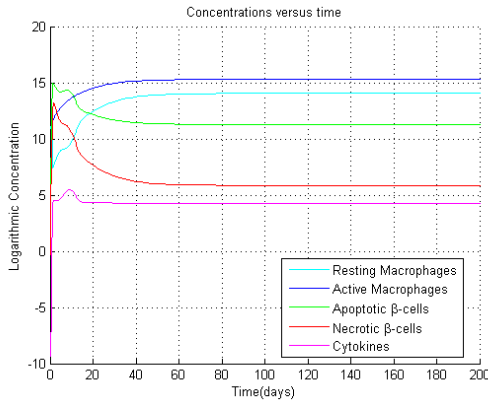


Figure 5.8 A plot based on the findings of Stoffels et al. (2004) that apoptotic as well as necrotic β -cells implies cytokine secretion. The implications of this in terms of the model of Marée et al. (2006) is that the Balb/c-mouse becomes diabetic as well.

cytotoxic cytokines that the Balb/c macrophages do not have or that the NOD- β -cells become necrotic faster than the Balb/c- β -cells; i.e. d is higher in NOD-mice. We have, however, not been able to find any publications that report this. A totally other possibility is that the cytokines secreted upon ingestion of an apoptotic β -cell is not cytotoxic. As we learned in section 2.2 not all cytokines are cytotoxic, some stimulate differentiation and stimulation, in agreement with the observation of Sreenan et al. (1999) of increased β -cell proliferation before onset of T1D in NOD-mice (Sreenan et al., 1999, p.992), i.e. during the preceding inflammation.

All things aside it is interesting that Marée et al. (2006) partially base their hypothesis on the Stoffels et al. (2004) article, without mentioning that according to Stoffels et al. (2004) phagocytosis of apoptotic cells also leads to release of cytokines.

Activation by phagocytosis of necrotic β -cells

A curious thing is that the resting macrophages do not become activated via phagocytosis of necrotic β -cells. If we assume that the activation rate due to phagocytosis of necrotic cells is equal to that due to apoptotic cells we could include activation due to phagocytosis of necrotic cells by introducing a $-f_1MB_n$ -term in equation 5.6, and a $+f_1MB_n$ -term in equation 5.7. In figure 5.9 we have done simulations with these additional terms, for NOD and Balb/c parameters. To the right we have Balb/c behavior, on the left we have the NOD behavior. When we compare figure 5.9 to 5.3, we see that assuming that resting macrophages become activated through phagocytosis of necrotic cells imposes some noticeable differences during the initial face, but apart from that there is no difference.

If we look at the graphs for the Balb/c parameters, the most obvious difference is that the cytokines hardly make an appearance (when we use a logarithmic concentration). At the same time, the apoptotic and necrotic cells have a significantly smaller max concentration. This is naturally because initially there is a higher concentration of active macrophages compared to simulations of the DuCa model without activation from necrotic cells. With activation due to necrotic cells, the concentration of active macrophages grows rapidly until it reaches a logarithmic concentration of approxi-

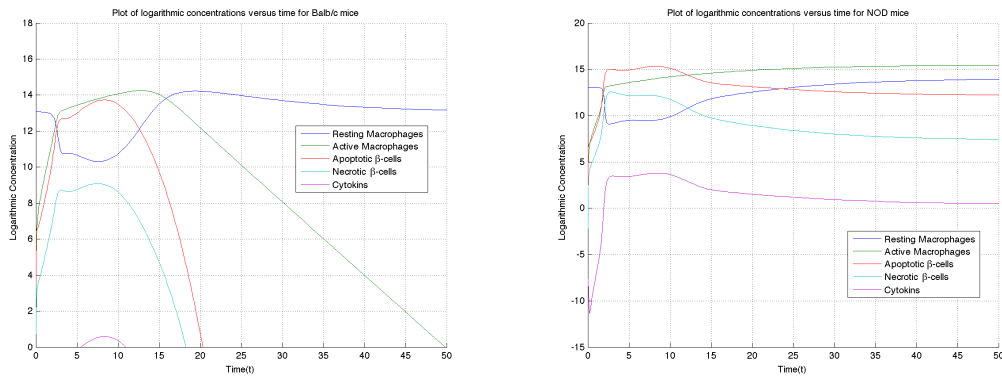


Figure 5.9 shows simulations of the DuCa model with activation due to necrotic cells. Initial conditions correspond to a healthy rest state, i.e. $(M, M_a, B_a, B_n, C) = (4.77 \times 10^5, 0, 0, 0, 0)$.

mately 13, at which point the growth decreases. Without this activation, cf. figure 5.3, the growth starts to decrease at 12. Thus with the additional activation more resting macrophages become activated within the same time interval as without additional activation. This implies that more apoptotic β -cells are phagocytized during the same amount of time as before, thus less are left to become necrotic, which in turn implies fewer necrotic cells, and thereby less cells to facilitate the detrimental cycle.

When we turn the graphs that are made based on NOD parameters, we see that there is very little, if any, difference between the original DuCa model, and the one with activation from necrotic cells – the concentration of apoptotic β -cells does not go to zero. This is not very surprising, since there is no difference in the phagocytosis rate between activated and resting macrophages in the NOD mouse.

Thus the moral of the tale is that when there is a difference between the phagocytosis rate of a resting and an activated macrophage, it does make a slight difference in the initial behavior to include activation due to necrotic cells.

5.8 Discussion of Parameters

Some parameter values are notoriously hard to measure, and therefore they are often associated with estimates, or they may be known to lie within a given range. The parameters in table 5.1 are no different. In table 5.2 we have gathered values from different articles. It is interesting to see how much some of the values differ. An obvious example is the difference in the efflux rate, c . Marée et al. (2006) report that Furth and den Dulk (1984) find the turnover rate of resting macrophages to be in the range $(0.07 - 0.25) \text{ d}^{-1}$, and based on this they estimate $c \approx 0.1 \text{ d}^{-1}$ (Marée et al., 2006, p.1275). We have, however, not been able to locate this range in the article of Furth and den Dulk (1984), and have based our value stated in table 5.2 on the value that Furth and den Dulk (1984) report at the very end of their discussion (and in their abstract), where they state that (Furth and den Dulk, 1984, p.1282)

The mean turnover time calculated with the value for the efflux of spleen

Parameter	Range/Estimate	Units	Source
b	(0.03,0.05)	d^{-1}	Wigginton and Kirschner (2001)
c	0.011	d^{-1}	Wigginton and Kirschner (2001)*
	0.17	d^{-1}	Furth and den Dulk (1984)
$f_{1,Balb/c}$	$2.57 \pm 0.07 \times 10^{-5}$	$ml \times cell^{-1} \times d^{-1}$	Marée et al. (2005)
$f_{1,Balb/c}$	$1.29 \pm 0.04 \times 10^{-5}$	$ml \times cell^{-1} \times d^{-1}$	Marée et al. (2007)†
$f_{1,Balb/c}$	2.0×10^{-5}	$ml \times cell^{-1} \times d^{-1}$	Marée et al. (2006)
$f_{1,NOD}$	1.10×10^{-5}	$ml \times cell^{-1} \times d^{-1}$	Marée et al. (2005)
$f_{1,NOD}$	0.50×10^{-5}	$ml \times cell^{-1} \times d^{-1}$	Marée et al. (2007)†
$f_{1,NOD}$	1.00×10^{-5}	$ml \times cell^{-1} \times d^{-1}$	Marée et al. (2006)
$f_{2,Balb/c}$	$5.11 \pm 0.24 \times 10^{-5}$	$ml \times cell^{-1} \times d^{-1}$	Marée et al. (2005)
$f_{2,Balb/c}$	$5.66 \pm 0.34 \times 10^{-5}$	$ml \times cell^{-1} \times d^{-1}$	Marée et al. (2007)†
$f_{2,Balb/c}$	5.00×10^{-5}	$ml \times cell^{-1} \times d^{-1}$	Marée et al. (2006)
$f_{2,NOD}$	$1.02 \pm 0.01 \times 10^{-5}$	$ml \times cell^{-1} \times d^{-1}$	Marée et al. (2007)†
$f_{2,NOD}$	1.00×10^{-5}	$ml \times cell^{-1} \times d^{-1}$	Marée et al. (2006)
k	(0.3,2.0)	d^{-1}	Wigginton and Kirschner (2001)*

Table 5.2 Different parameter values as found in the literature, and in the different articles of Marée et al. An asterisk denotes that the value is an estimate. The † illustrates that this is the most extreme value found in Marée et al. (2007) for the given rate constant; see subsection 5.8 for details. We have included the phagocytosis rates from Marée et al. (2006) for the sake of comparison.

macrophages is 6.0 d

from which we obtain $c = 0.16\bar{6} d^{-1} = 0.17 d^{-1}$. This value differs by a factor of ten relative to the value found in Wigginton and Kirschner (2001).

Another interesting point concerns the phagocytosis rates, which we will take a closer look at in the next subsection.

Reversible or irreversible activation?

The NOD phagocytosis rates stated in table 5.1 are based on the Marée et al. (2005) article. In this article they investigate various hypothetical phagocytosis models to determine which one fits data obtained by *in vitro* assays on NOD and Balb/c macrophages best – they determine this based on a statistical method called the *Akaike Information Criterion*.⁹

They find that a model called *the basic model* fits the behavior of NOD-mice best (Marée et al., 2005, p.546). The basic model assumes that there is no activation step after engulfment of the first apoptotic cell (Marée et al., 2005, p.536), i.e. the macrophages do not increase their phagocytic ability. This agrees with the assumption that $f_1 = f_2$ for NOD-mice in the DuCa model, though f_1 can be calculated to be $1.10 \times 10^{-5} ml cell^{-1} d^{-1}$ from the Marée et al. (2005) article and not merely 1 as in table 5.1.

For Balb/c-mice a model called *Variant I* yields the best fit (Marée et al., 2005, p.546). This model assumes an activation step, and a deactivation step that follows after digestion of engulfed apoptotic bodies (Marée et al., 2005, p.537). Though the f_1 and f_2 values found in Marée et al. (2005) are a little higher than those given in table 5.1, see

⁹ In short the Akaike Information Criterion (AIC) is a way of identifying the optimal and most parsimonious model from a set of model candidates when doing data analysis (Bozdogan, 1987, p.346). Put another way: the AIC yields the best fit based on a notion of keeping the number of parameters to a minimum.

Parameter/mouse strain	Value	Dimensions	Model type
$f_{1,NOD}$	0.50×10^{-5}	$\text{ml cell}^{-1}\text{d}^{-1}$	Reversible
$f_{2,NOD}$	$0.97 \pm 0.01 \times 10^{-5}$	$\text{ml cell}^{-1}\text{d}^{-1}$	Reversible
$f_{1,NOD}$	0.50×10^{-5}	$\text{ml cell}^{-1}\text{d}^{-1}$	Irreversible
$f_{2,NOD}$	$1.02 \pm 0.01 \times 10^{-5}$	$\text{ml cell}^{-1}\text{d}^{-1}$	Irreversible
$f_{1,Balb/c}$	$1.31 \pm 0.05 \times 10^{-5}$	$\text{ml cell}^{-1}\text{d}^{-1}$	Reversible
$f_{2,Balb/c}$	$5.18 \pm 0.30 \times 10^{-5}$	$\text{ml cell}^{-1}\text{d}^{-1}$	Reversible
$f_{1,Balb/c}$	$1.29 \pm 0.04 \times 10^{-5}$	$\text{ml cell}^{-1}\text{d}^{-1}$	Irreversible
$f_{2,Balb/c}$	$5.66 \pm 0.34 \times 10^{-5}$	$\text{ml cell}^{-1}\text{d}^{-1}$	Irreversible

Table 5.3 gives a comparison of the values as they are estimated in the most likely reversible and irreversible models in Marée et al. (2007).

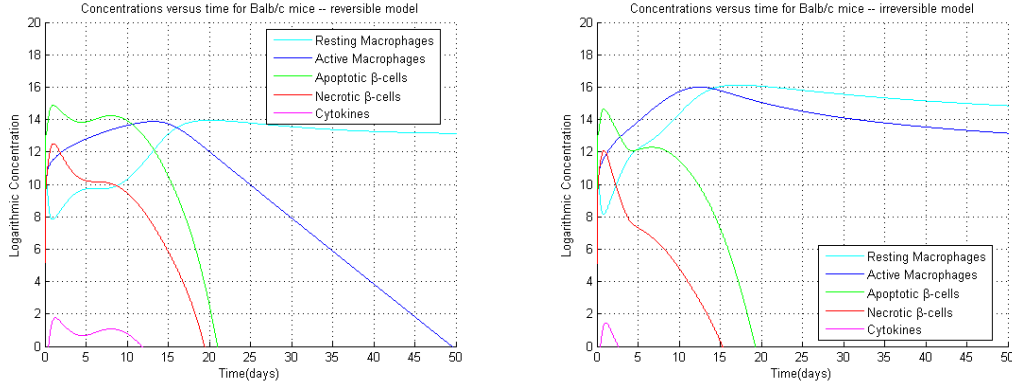


Figure 5.10 shows simulations with Balb/c phagocytosis parameters from table 5.3, and initial conditions that correspond to a healthy rest state, i.e. $(M, M_a, B_a, B_n, C) = (4.77 \times 10^5, 0, 0, 0, 0)$. On the left we have the reversible model which is tantamount to the DuCa model. On the right is the irreversible model, i.e. with $k = 0$.

table 5.2 for comparison, this model still agrees with the DuCa model, and the solution curves do not change noticeably from those presented in figure 5.3. So besides some minor discrepancies between phagocytosis rates things seem to be in order. The interesting part reveals itself when the later work done in the Marée et al. (2007) article is taken into account. In this article they find that model variants with a deactivation step (called reversible) and without deactivation steps, i.e. with $k = 0$ (called irreversible), are statistically indistinguishable (Marée et al., 2007, p.162). Furthermore they find that the basic model, which was used to estimate the NOD phagocytosis rates, is less likely than models with an activation step. This of course entails that $f_1 \neq f_2$ for NOD-mice. In table 5.3 we have calculated the phagocytosis rates for the reversible and irreversible models, based on the estimates given in Marée et al. (2007). In figure 5.10 simulations of the reversible and the irreversible model ($k = 0$) with Balb/c phagocytosis rates are presented. An obvious difference is how the concentration of active macrophages evolves over time. The figure where we have used parameters from the reversible model is almost interchangeable with the Balb/c behavior of the parameters from table 5.1; though the solution curves for how the concentrations of cytokines and apoptotic and necrotic β -cells evolve over time take on a slightly different form after

the apoptotic wave, they all reach a (logarithmic) concentration of 0 within the same amount of time as in figure 5.3. For the irreversible model it is another case. Here we see the effects of setting $k = 0$. When we compare the behavior of the irreversible model with figure 5.3 (the one showing Balb/c behavior) we see that it has a drastic influence on the concentration of active macrophages. In the case of the irreversible model, there is no natural efflux of the active macrophages, so it is the crowding term only that provides a limitation to the growth of the concentration of active macrophages, which as we can see in the righthand figure in figure 5.10 implies a much lengthier decline in M_a concentration. This is in contrast with the behavior we should expect from the concentration of active macrophages in Balb/c-mice (Marée et al., 2006, p.1279), where it should tend to zero after the apoptotic wave has taken its toll. Thus if the DuCa model is essentially correct, then the irreversible model cannot qualify as a model of phagocytosis (statistically indistinguishable from the reversible model or not), and if the irreversible model is to be taken as a good approximation of macrophage phagocytosis in Balb/c-mice, then the DuCa model needs to be revised. Besides these observations we must remember that the irreversible and the reversible model were statistically indistinguishable – a conclusion that is based on measurements without any connection to the DuCa model. Figure 5.11 shows how the different concentrations evolve in the

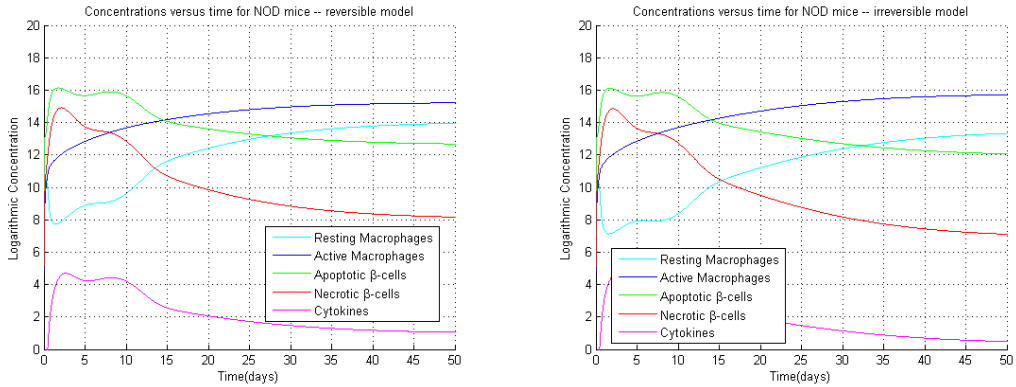


Figure 5.11 shows simulations with NOD phagocytosis parameters from table 5.3. On the left we have the reversible model, i.e. the DuCa model. To the right is the irreversible model, i.e. with $k = 0$. The two figures are qualitatively indistinguishable.

reversible and the irreversible model with NOD phagocytosis rates. Relative to the differences we observed for Balb/c rates, there is not much to speak of for the NOD rates, except that the concentrations of apoptotic and necrotic β -cells and cytokines stabilize at a higher concentration in the reversible model, while the resting and active macrophages stabilize at a lower concentration. In biological terms this means that the β -cells will be depleted faster in this scenario.

When we compare figure 5.11 to the NOD behavior in figure 5.3, we see that qualitatively there is no difference in how the concentrations evolve – following an initial period of oscillations the course is set for the demise of the population of β -cells.

One very important thing to notice is that the phagocytosis rates presented in table 5.2 are based on *in vitro* experiments. This is naturally a much more artificial environment

than an *in vivo* environment. This means that a lot of processes that occur *in vivo* have been removed from the equation, so to speak. It may be that the only way of obtaining good estimates of the phagocytosis rates is via such *in vitro* studies, but it implies that we cannot readily assume that the *in vivo* phagocytosis rates are exactly the same.

Another thing that is interesting when we are speaking about phagocytosis rates, is the fact that there is a major difference in the percentage of NOD-mice that develop T1D, when one looks at female versus male specimens.

If Marée et al. (2006) are correct, i.e. if the difference between developing T1D or not is predominantly a matter of macrophage phagocytosis rates, then this must mean that there is a difference in these rates between male and female NOD-mice. Though we are not capable of inferring any direct relation between the phagocytic differences in male and female mice and their bodily attributes (such as weight) or other things that may have an impact on their immune system or pancreas, such as living circumstances (e.g. the female mice give birth which may have an impact on their immune system), it would be very interesting if anyone had the expertise to make such an inference, as this could take the model to a new level. This would mean that the model could be used as a specimen-specific model, i.e. by adjusting the rate constants according to some rule that relates phagocytosis rates to the attributes of the specimen at hand the model should yield a behavior that is specific for the specimen at hand.

The DuCa model with turnover of M_a

In the figures we have presented above we have blindly used the DuCa equations, though we have set $k = 0$ for the simulations of the irreversible model, and changed the phagocytosis rates. Now we would like to present some simulations we have done with a seemingly minor alteration that addresses the fact that active macrophages in reality also succumb to turnover (Blasio et al., 1999, p.1680), with a turnover rate that is equal to the turnover/efflux rate of resting macrophages (Wigginton and Kirschner, 2001, p.1963). This means implementing a term of $-cM_a$ in equation 5.7.

When we use the original model parameters, given in table 5.1, this alteration does not change the behavior of the NOD nor the Balb/c concentrations. But when we introduce it in the reversible as well as the irreversible model with matching parameters something interesting happens to the behavior of the Balb/c concentrations. In figure 5.12 we have the log-concentration versus time plot on the left and a phase space plot of M versus M_a on the right. Introducing the turnover of active macrophages in the irreversible model entails the occurrence of a stable spiral. Obviously this is at variance with the dynamics we would expect from Balb/c-mice.

For the reversible model the change in behavior is less interesting (there is no spiral), but as we can see in figure 5.13 the behavior differs essentially from the behavior we saw in figure 5.3, in the key aspect that once again inflammation persists, though the concentration of cytokines is removed. As we mentioned earlier the original DuCa model with parameters given in table 5.1 retained its behavior after we added the turnover of active macrophages. However as we learned that the reversible model with matching Balb/c phagocytosis parameters also exhibited persistent apoptosis of β -cells (when we added the turnover of active macrophages), we found it interesting to investigate how much the Balb/c phagocytosis rates should deviate from their original values, $f_1 = 2 \times 10^{-5}$, $f_2 = 5 \times 10^{-5} \text{ml cell}^{-1} \text{d}^{-1}$, before the DuCa model with M_a -efflux

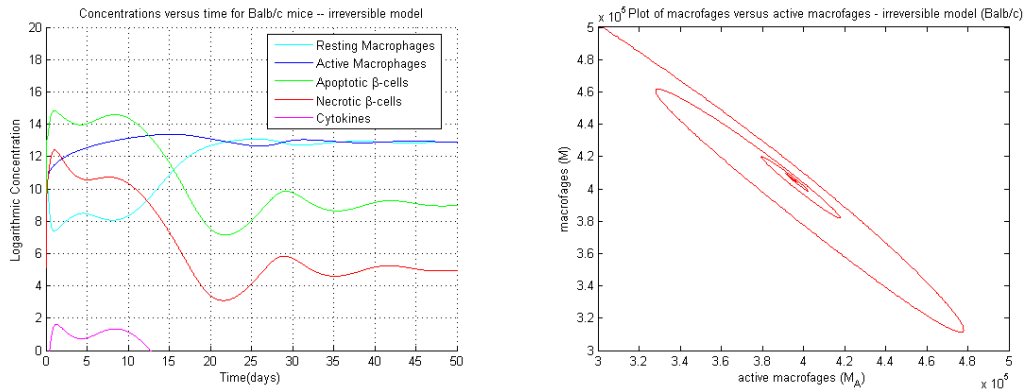


Figure 5.12 shows simulations of the irreducible model made with MATLAB where $k = 0$, $f_1 = 1.29 \times 10^{-5} \text{ml cell}^{-1} \text{d}^{-1}$, $f_2 = 5.66 \times 10^{-5} \text{ml cell}^{-1} \text{d}^{-1}$, and the term $-cM_a$ has been added in equation 5.7 to model turnover of active macrophages. The initial values are that of a healthy rest state. On the left we have the log-concentration versus time plots of the concentrations. On the right is a phase space plot of M versus M_a .

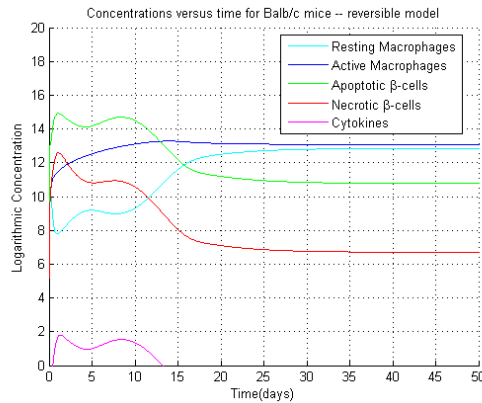


Figure 5.13 shows a simulation made with MATLAB of the reversible model where a term $-cM_a$ has been added to equation 5.7 to model turnover of active macrophages. The simulation is done with $f_1 = 1.31 \times 10^{-5} \text{ml cell}^{-1} \text{d}^{-1}$, $f_2 = 5.18 \times 10^{-5} \text{ml cell}^{-1} \text{d}^{-1}$ and initial conditions that simulate a healthy rest state.

fails to exhibit Balb/c dynamics as observed in experiments. In figure 5.14 we see the solution curves of the respective concentrations in a log-concentration versus time plot, and a phase space portrait of the resting versus active macrophages. The phase space portrait shows that a so-called *limit cycle* exists for $(f_1, f_2) = (1.88, 5)$ in the DuCa model with M_a -efflux.

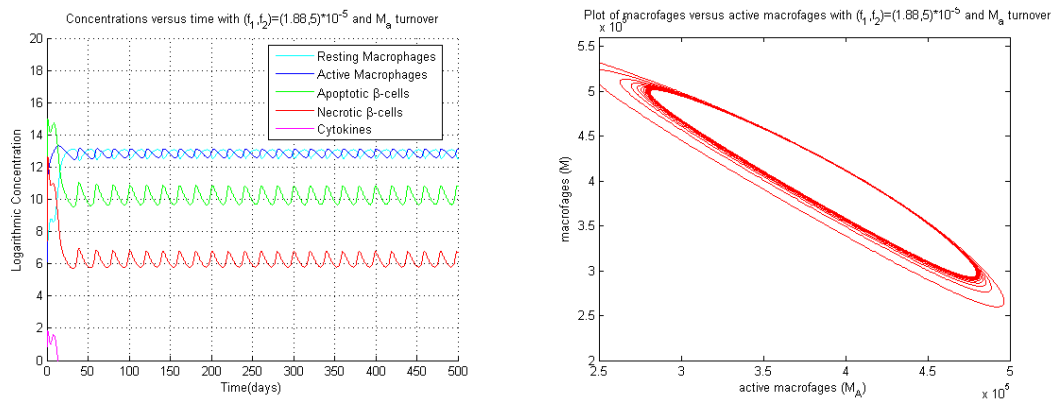


Figure 5.14 In the figures simulations of the DuCa model with turnover of the active macrophages are presented. To the right we see sustained oscillations in the concentrations of macrophages, active macrophages, apoptotic and necrotic β -cells, and to the left we have a phase space plot of macrophage versus active macrophage concentration. The phase space portrait reveals the existence of a limit cycle, which by further numerical inspection turns out to be semi-stable.

6 The Intermediated Model

The following section will give some insight into the origin of the DuCa model presented in the beginning of section 5. Before Marée et al. (2006) present the DuCa model they take a look at the (reduced) CPH model;¹ see figure 6.1 and equations 6.1–6.3. The (reduced) CPH model describes how the concentration of macrophages (M), active macrophages (M_a), and β -cell antigens (A), depend on each other.

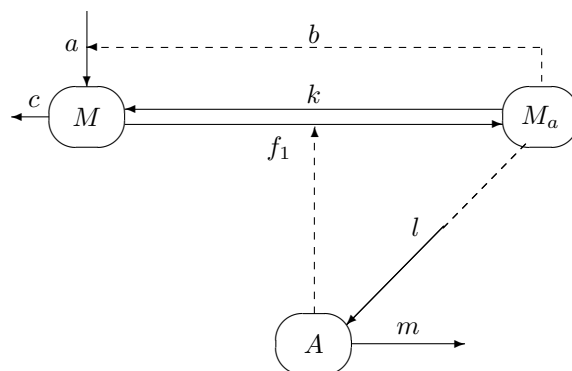


Figure 6.1 A compartment representation of the CPH model. a denotes inflow of macrophages, b is cytokine induced macrophage-inflow, c is the efflux of macrophages, f_1 is the activation rate of macrophages due to antigens, k is the deactivation rate of active macrophages, l is cytokine induced damage that furthers the production of antigens, and lastly m is the decay rate of antigens (Blasio et al., 1999, p.1680). The figure is a reworked version of the figure found on page 1680 in Blasio et al. (1999).

¹ For the full version of the CPH model we refer to Blasio et al. (1999).

The differential equations that correspond to the compartment system in figure 6.1 are

$$\frac{dM}{dt} = a + (b + k)M_a - cM - f_1MA \quad (6.1)$$

$$\frac{dM_a}{dt} = f_1MA - kM_a \quad (6.2)$$

$$\frac{dA}{dt} = lM_a - mA \quad (6.3)$$

The purpose of the CPH model was not to give a quantitative prediction of how the onset of T1D comes about, rather it was to illustrate that T1D is caused by multiple factors coming together in a synergetic way, and to show that the difference between onset and not onset depends on a threshold that incorporates these factors, i.e. the onset of T1D implies crossing a “threshold surface” that is spanned in the parameter space, of the model. This threshold was found through stability analysis and defined as f_0 (Blasio et al., 1999, p.1684)

$$f_0 \equiv \frac{f_1l}{ck} \quad (6.4)$$

Where the system is guaranteed to be stable for $f_0 < 1$. Marée et al. (2006) wants to illustrate that chronic inflammation can not occur for biologically reasonable parameter values in the CPH model, and thus the CPH model needs revision if it is to be used as a quantitative model. Therefore the DuCa model can be seen as an extension of the CPH model that has been modified to investigate a different hypothesis.

In this section we are going to take a look at what we have dubbed the *Intermediated Model* (IM). This model bridges the gap between the CPH model and the DuCa model. The IM can be seen as a slightly modified CPH model and as a rudimentary version of the DuCa model. Marée et al. (2006) does not, however, tell the story of how to revise the IM model to transform it into the DuCa model. This implies that even though the DuCa model originates from the IM there is no straight line between the imperfections of the CPH model/IM model and the modifications done on the IM to reach the DuCa model. However the extension of the CPH model is quite straightforward since Marée et al. (2006) aims to investigate whether the effectiveness in phagocytosis can make the difference between a diabetic and a non-diabetic mice. As stated in section 5.1 this hypothesis is rooted in an observed difference in phagocytosis rates for Balb/c and NOD-mice, seen in the basal phagocytosis rate of the resting macrophages, but also in their ability to undergo an activation step, when the first apoptotic cell is engulfed. To investigate the effect of these differences they implement the clearance of apoptotic β -cells done by the resting and activated macrophages into the CPH model, by including the terms f_1MB_a and $f_2M_aB_a$. This modification addresses another peculiar aspect of the CPH model since there was no clearance of the antigens due to macrophage engulfment, but only a nonspecific decay. This seems odd since one should expect that upon engulfment of a protein, there is one less to activate the remaining resting macrophages. This leads us to the next modification, albeit of a more conceptual matter. Instead of monitoring the antigens – i.e. small protein fractions of the β -cells that underwent apoptosis, they look at the clearance of an apoptotic β -cell as a whole. These changes lead to the system of differential equations seen in 6.5 - 6.7, and the corresponding compartment can be seen in figure 6.2.

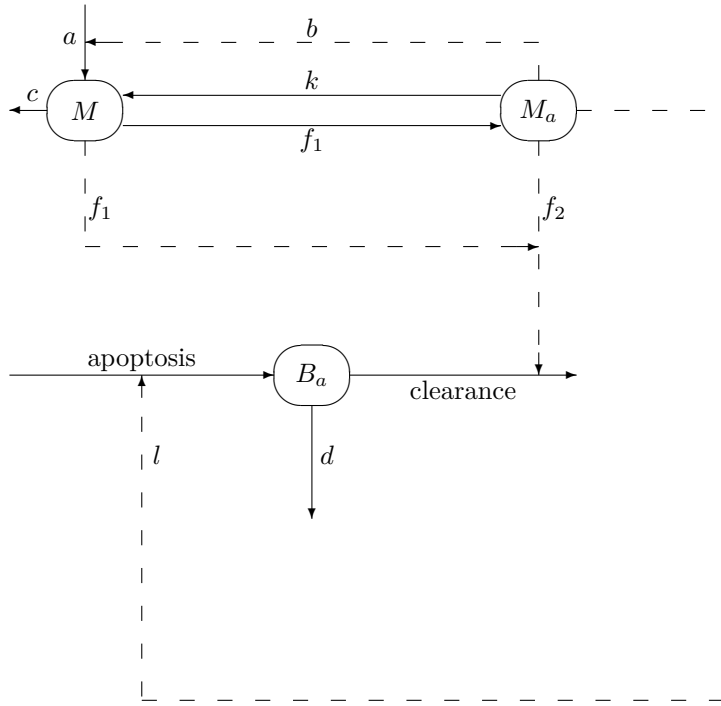


Figure 6.2 The figure shows the compartment system for the IM, as given by Marée et al. (2006). M , M_a , and B_a are the concentrations of macrophages, activated macrophages, and apoptotic β -cells respectively. An explanation of a, b, c, d, f_1, f_2 is given in table 5.1. Adopted with minor changes from (Marée et al., 2006, p.1270)

$$\frac{dM}{dt} = a + (k + b)M_a - cM - f_1MB_a \quad (6.5)$$

$$\frac{dM_a}{dt} = f_1MB_a - kM_a \quad (6.6)$$

$$\frac{dB_a}{dt} = lM_a - f_1MB_a - f_2M_aB_a - dB_a \quad (6.7)$$

Notice if we set $f_1MB_a = 0$, $f_2M_aB_a = 0$ and $B_a = A$ the system of equations reduces to the CPH model seen in 6.1,6.2 and 6.3. This is also presented in Marée et al. (2006) under the alias “the basic model”, and it undergoes an analysis which we will review and unfold. But first we will state what to expect from the behavior of the model from a physiological point of view.

Model observations

The biological frame plays a twofold role in the modelling process. It sets the limit for the dynamics the model should exhibit (e.g. no negative concentrations), but at the same time it works as a guideline for what kind of dynamics that, at least, should be

expected. So on that basis it is possible, before digging deeper into a mathematical analysis, to give an outline of what kind of dynamics that is expected from the IM model.

First of all it must allow for the existence of a stable healthy rest state, for both NOD as well as Balb/c-mice. That is, a stable steady state where no apoptotic β -cells are present, and hence no activated macrophages and therefore just a constant density of resting macrophages in the tissue, given by the fraction between influx and efflux, (a/c), of macrophages. This is a necessity since no unprovoked inflammation occurs, and when inflammation does occur it is given that Balb/c-mice, and (in the real world) even some NOD-mice², return to the healthy state, so it has to be stable. This is a consequence of the observation that not all NOD-mice develop T1D, as we stated in chapter 2. Furthermore the model should hold the possibility for NOD-mice to acquire a chronic inflammation, initiating the removal of pancreatic β -cells. This implies the existence of, at least one, nontrivial fixed point, or a (at least in theory) stable limit-cycle in the positive region, \mathbb{R}_+^3 . Information about the stability of this fixed point requires further mathematical treatment.

6.1 Fixed Points of the IM Model

We now turn to the analysis of the IM which, once again, should be pointed out to be an unfolding of what is already presented in Marée et al. (2006). From a modelling point of view we are only concerned about what happens in the nonnegative region since this is the only physiologically valid domain. Therefore we are only going to look for fixed points in the nonnegative region. An equilibrium, or a fixed point of a system, say $\dot{\mathbf{x}} = f(\mathbf{x})$, where the dot denotes the derivative with respect to time, satisfies $\dot{\mathbf{x}} = \mathbf{0}$, so for the IM we have

$$0 = \frac{dM}{dt} = a + (k + b)M_a - cM - f_1MB_a \quad (6.8)$$

$$0 = \frac{dM_a}{dt} = f_1MB_a - kM_a \quad (6.9)$$

$$0 = \frac{dB_a}{dt} = lM_a - f_1MB_a - f_2M_aB_a - dB_a \quad (6.10)$$

Note that as in the full model all the parameters are positive. Looking at the healthy rest state by setting $(M_a, B_a) = (0, 0)$ and solving equation 6.8 with respect to M yields $M = a/c$. So the healthy rest state is at

$$(M, M_a, B_a) = (a/c, 0, 0) \quad (6.11)$$

This is furthermore a good approximation for the healthy rest state of the system where crowding terms are included provided that $e_1 \ll c^2/a$; cf. appendix A.7). Now, turning

² When we run simulations of the DuCa model using NOD parameters, naturally, we will never witness that the concentrations return to the healthy rest state; cf. chapter 2. We model one mouse at a time so to speak, thus if we use NOD parameters the concentrations will stabilize at the pathological concentrations.

to the nontrivial fixed point where $M, M_a, B_a > 0$ ³ This can be found by first solving equation 6.9 with respect to M to obtain

$$M = \frac{kM_a}{f_1 B_a} \text{ for } B_a \neq 0 \quad (6.12)$$

Then by adding equation 6.8 and 6.9 together and rearranging, it is possible to find another expression for M

$$0 = \frac{dM}{dt} + \frac{dM_a}{dt} = a + bM_a - cM \quad (6.13)$$

$$M = \frac{a + bM_a}{c} \quad (6.14)$$

Now setting equation 6.12 equal to 6.14 and solving with respect to B_a we get

$$\frac{kM_a}{f_1 B_a} = \frac{a + bM_a}{c} \Leftrightarrow B_a = \frac{kcM_a}{f_1(a + bM_a)} \quad (6.15)$$

Note by plugging this expression for B_a into equation 6.12 gives us equation 6.14, where it is evident that the stable rest state appears when setting $M_a = 0$. To obtain another expression for B_a we add equation 6.9 and equation 6.10

$$0 = \frac{dM_a}{dt} + \frac{dB_a}{dt} = (l - k)M_a - (f_2 M_a + d)B_a \quad (6.16)$$

$$B_a = \frac{(l - k)M_a}{f_2 M_a + d} \quad (6.17)$$

Equation 6.15 and 6.17 leads to an expression that solely depends on M_a

$$\frac{kc}{f_1(a + bM_a)} = \frac{(l - k)}{f_2 M_a + d}, \quad l \neq k \quad (6.18)$$

Which through some algebraic steps can be rearranged to

$$M_a = \frac{kdc - af_1(l - k)}{bf_1(l - k) - kcf_2}, \quad bf_1(l - k) \neq kcf_2 \quad (6.19)$$

By plugging this into equation 6.14 and equation 6.17, the nontrivial fixed point expressed by the parameters finally emerges

$$(M, M_a, B_a) = \left(\frac{k(db - af_2)}{f_1 b(l - k) - k f_2 c}, \frac{kdc - af_1(l - k)}{bf_1(l - k) - kcf_2}, \frac{kdc - af_1(l - k)}{f_1(db - af_2)} \right) \quad (6.20)$$

It should be emphasized that these equations are valid only for $M, M_a, B_a > 0$.

³ Note that for the system of differential equations given in equations 6.8 to 6.10 to be satisfied, either all the variables are positive or both M_a and B_a are zero as in the case for the trivial fixed point.

Stability of the fixed points

The classification of the stability of the fixed points is done by linearizing the system of differential equations about each fixed point, i.e. calculating and evaluating the Jacobian matrix in each fixed point (Strogatz, 2000, p.150-154). Then the eigenvalues of the Jacobian matrix given as the solutions to the equation $Det(J - \lambda I) = 0$, i.e. the characteristic polynomial, can be used to classify the stability of each individual fixed point.

The Jacobian matrix for the IM is

$$J = \begin{pmatrix} -c - f_1 M B_a & k + b & -f_1 M \\ f_1 B_a & -k & f_1 M \\ f_1 B_a & l - f_2 M B_a & -f_1 M - f_2 M_a - d \end{pmatrix} \quad (6.21)$$

And when evaluated in the healthy rest state $(M, M_a, B_a) = (a/c, 0, 0)$ we get

$$J = \begin{pmatrix} -c & k + b & -\frac{f_1 a}{c} \\ 0 & -k & \frac{f_1 a}{c} \\ 0 & l & -\frac{f_1 a}{c} - d \end{pmatrix} \quad (6.22)$$

Thus the characteristic polynomial is found from

$$0 = Det(J - \lambda I) = \begin{vmatrix} -c - \lambda & k + b & -\frac{f_1 a}{c} \\ 0 & -k - \lambda & \frac{f_1 a}{c} \\ 0 & l & -\frac{f_1 a}{c} - d - \lambda \end{vmatrix} \quad (6.23)$$

Expanding the determinant by the first column we get

$$0 = (-c - \lambda) \begin{vmatrix} -k - \lambda & \frac{f_1 a}{c} \\ l & -\frac{f_1 a}{c} - d - \lambda \end{vmatrix} \quad (6.24)$$

We can see that the eigenvalue in the parentheses will always remain negative, since $-c - \lambda = 0 \Leftrightarrow \lambda = -c$. However for the healthy rest state to be stable the eigenvalues must have negative real parts. The general solution for the eigenvalues of the 2×2 matrix in equation 6.24 can be written as

$$\lambda_{1,2} = \frac{1}{2} \left((Tr(J_{(2 \times 2)})) \pm \sqrt{Tr^2(J_{(2 \times 2)}) - 4Det(J_{(2 \times 2)})} \right) \quad (6.25)$$

Now since $Det = \lambda_1 \lambda_2$ and $Tr = \lambda_1 + \lambda_2$ it is evident that in order for all the eigenvalues to be negative the determinant must be larger than zero, $Det > 0$, and the trace must be less than zero, $Tr < 0$, and vice versa for positive eigenvalues, where

$$Tr(J_{(2 \times 2)}) = -k - \frac{f_1 a}{c} - d < 0 \quad (6.26)$$

$$Det(J_{(2 \times 2)}) = \frac{k f_1 a}{c} + kd - \frac{l f_1 a}{c} \quad (6.27)$$

The parameters are all positive so the trace is negative. The determinant however is positive only when $(k f_1 a)/c + kd > (l f_1 a)/c$, which is rearranged in the following way

$$\frac{a}{d} < \frac{ck}{f_1(l - k)} \quad (6.28)$$

The parameters have to obey the constraint in equation 6.28, for the model to have a stable healthy rest state. To elaborate a little: the inflow of resting macrophages divided by the turnover of β -cells must be less than the turnover of the resting macrophages times the deactivation rate of the activated macrophages, divided by the phagocytosis/activation rate of resting macrophages times the result of subtracting the deactivation rate of activated macrophages from the cytokine induced damage. We see that the threshold is not dependent on the phagocytosis rate of activated macrophages, f_2 , or the recruitment rate, b . This means that we can essentially set these to e.g. zero, and the system will still tend to the stable healthy rest state.

To link the threshold in equation 6.28 to the threshold value in the CPH model, cf. equation 6.4, we rewrite 6.28 to obtain

$$\frac{a}{d} \left(\frac{f_1 l}{ck} - \frac{f_1}{c} \right) < 1 \quad (6.29)$$

from this we get

$$\frac{a}{d} \left(f_0 - \frac{f_1}{c} \right) < 1 \quad (6.30)$$

or

$$f_0 < \frac{d}{a} + \frac{f_1}{c} \quad (6.31)$$

So with the modifications added by Marée et al. (2006) this is the new constraint that f_0 must obey if the solutions of the IM are to converge to the healthy rest state for $t \rightarrow \infty$.

It is possible to give the nontrivial fixed point the same treatment, by evaluating the Jacobian in the point given in equation 6.20. This however leads to expressions for the trace and determinant which are difficult to analyze analytically. Therefore we make use of a different approach inspired by Marée et al. (2006). It is given that $M_a > 0$ for the nontrivial fixed point so it follows from equation 6.19 that

$$\frac{kdc + af_1k - af_1l}{bf_1l - bf_1k - ckf_2} > 0 \quad (6.32)$$

This is satisfied when the numerator and denominator have the same sign. All the parameters are positive, so this leaves two options. For reasons soon to be explained the following restrictions are chosen

$$kdc + af_1k > af_1l \quad (6.33)$$

and

$$bf_1l > bf_1k + ckf_2 \quad (6.34)$$

From equation 6.33 it follows that

$$kdc > af_1(l - k) \Leftrightarrow \frac{a}{d} < \frac{ck}{f_1(l - k)} \quad (6.35)$$

Which can be recognized as the constraint that guarantees the existence of the stable healthy rest state. This would not have been satisfied had we chosen the opposite

restriction in equation 6.33, so the choice of restrictions is justified. Equation 6.34 can be rearranged in a similar fashion to

$$bf_1(l - k) > ckf_2 \Leftrightarrow \frac{ck}{f_1(l - k)} < \frac{b}{f_2} \quad (6.36)$$

This is the constraint for the existence of a nontrivial fixed point in addition to the trivial stable fixed point, that corresponds to no chronic inflammation. By combining equation 6.35 and 6.36 it follows that

$$\frac{a}{d} < \frac{ck}{f_1(l - k)} < \frac{b}{f_2} \quad (6.37)$$

Thus when the parameters satisfy equation 6.37 a nontrivial stable fixed point will coexist with the trivial (stable) fixed point. In other words the restriction on the parameters, given in equation 6.37, must be satisfied if we are to observe NOD-mice dynamics, i.e. chronic inflammation. For the Balb/c-mice, however, all inflammation must be nonpermanent, thus leaving the healthy stable fixed point as the only one present. If we look at equation 6.37 this implies that for the Balb/c-mice, the right-most inequality must not be satisfied, i.e. the parameters of the Balb/c-mice must fulfill

$$\frac{a}{d} < \frac{ck}{f_1(l - k)} \quad (6.38)$$

and

$$\frac{b}{f_2} < \frac{ck}{f_1(l - k)} \quad (6.39)$$

Notice that the inequality sign is reversed when compared to equation 6.37. Equation 6.39 implies the non-existence of a stable fixed point besides the trivial one.

It is noteworthy, that the transition between Balb/c and NOD dynamics can be done simply by tweaking f_2 , i.e. the activated phagocytosis rate, in accordance with the hypothesis that impaired phagocytosis by the macrophages can make the difference between health and disease.

We now arrive at the challenge of evaluating the stability of the nontrivial fixed point. A glimpse at the Jacobian matrix in equation 6.21 together with the fixed points in equation 6.20 reveals that the expression for the characteristic polynomial, trace and determinant are going to be hard to analyze analytically, due to the mere size of them. So to approach this practically we define the parameters to be equal to some arbitrary values, let us say: $a = 0.04, f_1 = 0.8, k = 0.3$ and $c = b = l = d = f_2 = 1$, that satisfy the constraints given in equation 6.37

$$\frac{0.04}{1} < \frac{1 \cdot 0.3}{0.8(1 - 0.3)} < \frac{1}{1} \quad (6.40)$$

$$0.04 < 0.536 < 1 \quad (6.41)$$

The Jacobian matrix evaluated in the point $(M, M_a, B_a) = (1.11, 1.07, 0.36)$ is

$$0 = \text{Det}(J - \lambda I) = \begin{pmatrix} -1.32 - \lambda & 1.3 & -0.89 \\ 0.29 & -0.3 - \lambda & 0.886 \\ 0.29 & 0.6 & -2.95 - \lambda \end{pmatrix} \quad (6.42)$$

The characteristic polynomial is given by

$$0 = \text{Det}(J - \lambda I) = \lambda^3 - \text{Tr}(J)\lambda^2 + (pm_1 + pm_2 + pm_3)\lambda - \text{Det}(J) \quad (6.43)$$

where pm_i designates the principal minors.⁴ These are calculated to be $pm_1 = 0.02$, $pm_2 = 0.36$ and $pm_3 = 4.16$ while the trace and determinant are obtained to be $\text{Tr}(J) = -4.57$ and $\text{Det}(J) = 0.74$. The conditions for $\text{Re}(\lambda) < 0$, and thus a stable fixed point, are given by the Routh-Hurwitz criteria; $\text{Tr}(J) < 0$, $\text{Det}(J) < 0$ and $\text{Det}(J) - \text{Tr}(J)(pm_1 + pm_2 + pm_3) < 0$ (Murray, 2002, p.508). This is not satisfied since $\text{Det}(J) = 0.74 > 0$. The fixed point is therefore unstable for the chosen parameter values. We cannot, however, accept this as a general statement at this point, since there might be other parameter values that satisfy the constraints but do not yield the same type of stability for the fixed point. In the next section we, among other things, strive to give a more general stability analysis of the nontrivial fixed point, albeit through a more qualitative approach using phase plane analysis.

Downfall of the IM

So far we have discussed what kind of behavior that at least should be expected from the IM based upon the observational knowledge of how the inflammatory response progresses in NOD and Balb/c-mice. This led to the conclusion that a stable healthy steady state must exist for both NOD and Balb/c-mice, since Balb/c-mice are prone to return to the healthy rest state, and also some NOD-mice return to a noninflammatory state. In addition the model should also hold the possibility for a state of chronic inflammation for the NOD-mice, which implies the existence of a physiologically valid nontrivial stable fixed point. The fixed points of the IM have been located, their stability evaluated and through this the constraints given in equation 6.37, 6.38 and 6.39 were derived. These constraints clearly state how the relation between the parameters must be for the model to exhibit either NOD or Balb/c behavior. The question is now: will these constraints be satisfied when using the parameter-estimates shown in table 5.1, in section 5.4? To be able to answer this the estimated parameters for Balb/c-mice are substituted into the constraints that satisfy Balb/c dynamics. First equation 6.38 (the question mark indicates that we are checking if the given inequality holds)

$$\frac{5 \times 10^4}{0.5} \stackrel{?}{<} \frac{0.1 \times 0.4}{2 \times 10^{-5}(0.41 - 0.4)} \quad (6.44)$$

$$1 \times 10^5 < 2 \times 10^5 \quad (6.45)$$

And then equation 6.39

$$\frac{0.09}{5 \times 10^{-5}} \stackrel{?}{<} \frac{0.1 \times 0.4}{2 \times 10^{-5}(0.41 - 0.4)} \quad (6.46)$$

$$1.8 \times 10^3 < 2 \times 10^5 \quad (6.47)$$

⁴ The principal minors are the determinants that are obtained from the 2×2 matrix we get when we remove the first column together with the first row, the second column with the second row, and the third column with the third row – the determinant of each of these matrices is called a principal minor.

We see that Balb/c-parameters satisfy both conditions. To see if this is also the case when using NOD parameters these are substituted into equation 6.37

$$\frac{1 \times 10^{-5}}{0.5} \stackrel{?}{<} \frac{0.1 \times 0.4}{1 \times 10^{-5}(0.41 - 0.4)} \stackrel{?}{<} \frac{0.09}{5 \times 10^{-5}} \quad (6.48)$$

$$1 \times 10^5 < 4 \times 10^5 \not< 9 \times 10^3 \quad (6.49)$$

We see that NOD parameters satisfy the conditions for a stable healthy rest state, but *not* the constraints for a nontrivial fixed point. That is, for both the estimated NOD and Balb/c parameters the IM will exhibit Balb/c dynamics – in both cases the inflammation will be nonpermanent. Based on this Marée et al. (2006) conclude that the CPH model is quantitatively incorrect (Marée et al., 2006, p.1280), and as a solution suggest adding necrotic β -cells and cytokines.

Phase plane analysis

Before we turn to the analysis of the DuCa model we will resort to a phase plane analysis of the IM. We have found this to be, a very useful tool to achieve a conceptual understanding of – what we believe to be – the kind of dynamics that Marée et al. (2006) aimed for, when modifying the CPH model. There is but one problem. In the end of last section we saw that the estimated NOD parameters do not satisfy the constraints for a nontrivial fixed point. This means that the use of the estimated NOD parameters do not bring the system to exhibit NOD dynamics. So for the purpose of providing qualitative illustrations we choose to use some arbitrary positive parameter values. Thus in the following assume that the parameters are chosen so that we have a set of NOD parameters that satisfy the constraints for NOD dynamics, and a set of Balb/c parameters that satisfy the constraints for Balb/c dynamics.

A phase plane analysis implies looking at *nullclines*, and how the flow behaves around these. To specify what nullclines are, assume that we have a system $\dot{x} = f(x, y)$, $\dot{y} = g(x, y)$, where \dot{x} means dx/dt . Then the nullclines of this system are the curves given by $\dot{x} = 0$ and $\dot{y} = 0$. I.e. the nullclines define where the flow is horizontal or vertical (Lynch, 2004, p.186), and an intersection between nullclines defines a steady state also called a fixed point. The IM consists of three equations, and a phase *plane* analysis is as the name hints a two-dimensional undertaking. However because we are only interested in the nullclines, when we do the analysis, this does not pose a problem.⁵ We simply pick one of the equations 6.5, 6.6 or 6.7 and equate it to zero – let us choose 6.5, so we set $dM/dt = 0$. Then we isolate M in this equation to obtain

$$M = \frac{a + (k + b)M_a}{c + f_1 B_a} \quad (6.50)$$

⁵ We do not have to restrict ourselves to the plane! We could do a phase space analysis, but since we are interested in the nullclines we can do a phase plane analysis.

and substitute the expression for M into the two other equations.⁶ So we get

$$\frac{dM_a}{dt} = f_1 \left(\frac{a + (k+b)M_a}{c + f_1 B_a} \right) B_a - kM_a \quad (6.51)$$

$$\frac{dB_a}{dt} = lM_a - f_1 \left(\frac{a + (k+b)M_a}{c + f_1 B_a} \right) B_a - f_2 M_a B_a - dB_a \quad (6.52)$$

Linearizing and evaluating the Jacobian Matrix of this reduced system at $M_a = B_a = 0$ yields

$$J = \begin{pmatrix} -k & \frac{f_1 a}{c} \\ l & -\frac{f_1 a}{c} - d \end{pmatrix}$$

Which is similar to the 2×2 matrix shown in equation 6.24, thus the stability behavior and criteria for the healthy rest state is the same for the two dimensional system as the three dimensional system.

The nullclines are found analytically by setting $dM_a/dt = 0$ and $dB_a/dt = 0$ in equation 6.51 and 6.52 and then solving with respect to M_a (or B_a)

$$M_a \text{ nullcline} : M_a = \frac{B_a f_1 a}{ck - B_a b f_1} \quad (6.53)$$

$$B_a \text{ nullcline} : M_a = -\frac{dc + af_1 + f_1 dB_a}{f_2 c + f_1(b+k) - lf_1 + f_1 f_2 B_a - \frac{lc}{B_a}} \quad (6.54)$$

As it turns out, the nullcline for M_a is fairly easy to analyze whereas the nullcline for B_a is a little more tricky.

They both approach the point $(B_a, M_a) = (0, 0)$. To convince oneself of this in the case of the B_a -nullcline, let $B_a \rightarrow 0$. Then the term $lc/B_a \rightarrow \infty$. Thus the entire fraction will approach zero as $B_a \rightarrow 0$. Now, by differentiating the two expressions for the nullclines (equations 6.53 and 6.54) we get the slope of the M_a nullcline:

$$\frac{dM_a}{dB_a} = \frac{af_1}{ck - bf_1 B_a} + \frac{abf_1^2 B_a}{(ck - bf_1 B_a)^2} \quad (6.55)$$

and the slope of the B_a nullcline:

$$\begin{aligned} \frac{dM_a}{dB_a} &= \frac{(cdB_a + af_1 B_a + df_1 B_a^2)(f_1(b+k) + cf_2 - f_1 l + 2f_1 f_2 B_a)}{(f_1 B_a(b+k) - cl + cf_2 B_a - f_1 f_2 B_a^2)^2} \\ &\quad - \frac{(cd + af_1 + 2df_1 B_a)(f_1 B_a(b+k) - cl + cf_2 B_a - f_1 f_2 B_a^2)}{(f_1 B_a(b+k) - cl + cf_2 B_a - f_1 f_2 B_a^2)^2} \end{aligned} \quad (6.56)$$

By setting $B_a = 0$, the initial slope is found to be af_1/ck for the M_a -nullcline and $(dc+af_1)/lc$ for the B_a -nullcline. Remember that we are working with arbitrary (positive)

⁶ Here we are lucky enough that we are able to separate B_a from the other variables, which is not always the case. The *implicit function theorem*, see e.g. (Abraham et al., 1988, p.121), always tells us if such a separation is possible (in a given interval), and can be applied, if it is not apparent if it is possible to isolate one variable from the others.

parameters so let us assume the initial slope of the M_a -nullcline is less than the initial slope of the B_a nullcline. That is

$$\frac{af_1}{ck} < \frac{dc + af_1}{lc} \quad (6.57)$$

This can be rearranged to the familiar expression

$$\frac{a}{d} < \frac{ck}{f_1(l-k)} \quad (6.58)$$

The constraints for a stable healthy rest state reappears, which means that in order for the model to show a physiological realistic behavior (see chapter 6) the relation between the initial slopes must in fact be as stated in equation 6.57. Another feature of the nullclines is that they both exhibit asymptotic behavior. This occurs when the denominator in the expression of the nullclines tend towards zero which happens at

M_a nullcline asymptote:

$$B_{a(Asymp1)} = \frac{ck}{bf_1} \quad (6.59)$$

B_a nullcline asymptote:

$$B_{a(Asymp2)} = \frac{-(f_1(b+k-l) + f_2c) + \sqrt{(f_1(b+k-l) + f_2c)^2 + 4f_1f_2cl}}{2f_1f_2} \quad (6.60)$$

Where the term on the right hand side is the positive root $f_1f_2B_a^2 + (f_1(b+k-l) + f_2c)B_a - cl$ Assuming that $B_{a(Asymp1)} < B_{a(Asymp2)}$ together with the initial slope-relation (slope of M_a -nullcline must be less than slope of B_a -nullcline) leads to an intersection of the nullclines and hence a nontrivial fixed point;⁷ cf. figure 6.3. This configuration implies the healthy rest state to be stable and the direction of the slope field is easily determined and indicated by a few arrows. Once the direction of the slope field is in place it is evident that the nontrivial fixed point at the intersection of the nullclines is a saddle point, which corresponds to what we found numerically to be the case for the IM without setting $dM/dt = 0$; cf. the subsection titled ‘‘Stability of the fixed points.’’ However for the IM with $dM/dt = 0$ we can claim it as a general statement. That is, as long as the parameters fits the constraints given in equation 6.37 the nontrivial fixed point must be a saddle. It is interesting to note that the stable manifold of the saddle point comprises a separatrix that when exceeded results in a escalating inflammation or, in the case of points below, a damped inflammation. So the saddle point separates the healthy regime from the inflamed regime. It should also be noted that the extensiveness of the inflammation is independent of the size of the apoptotic wave that is implemented in the IM to trigger the inflammation as long as it pushes the system above the given separatrix! In that case the densities of the macrophages and apoptotic β -cells will tend towards infinity.

Now let us consider the phase plane where parameters that satisfy Balb/c dynamics

⁷ Under the assumption that the nullclines are otherwise well behaved; i.e. continuous between 0 and the asymptotes.

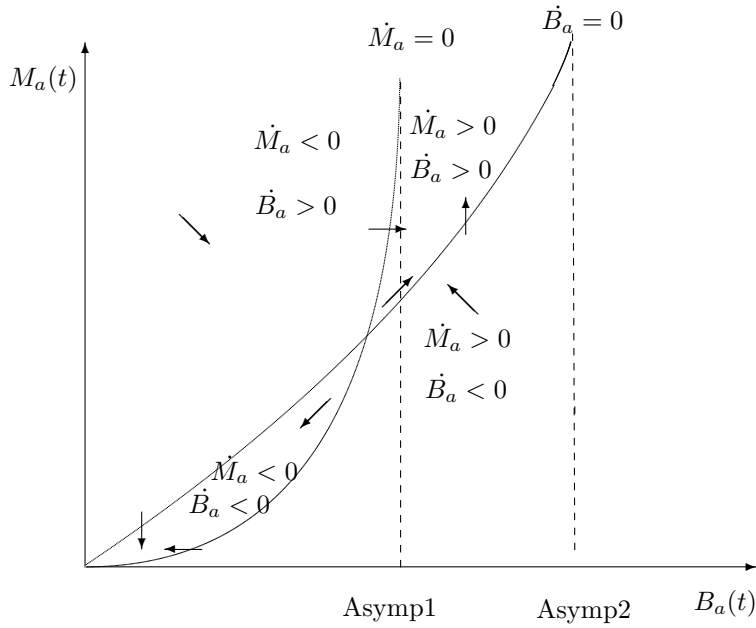


Figure 6.3 Sketch of the nullclines and some representative arrows that indicate the flow for the IM with $\frac{dM}{dt} = 0$. For the healthy rest state, $(B_a, M_a) = (0, 0)$, to be stable the initial slope of the M_a -nullcline must be less than the initial slope of the B_a -nullcline. Then by assuming that the nullcline of M_a reaches its asymptotic point before the nullcline of B_a introduces a nontrivial fixed point at the intersection of the nullclines characteristic for the NOD dynamics. By the knowledge of the stability of the healthy rest state it is a simple matter to determine the direction of the slope field. This reveals that the nontrivial fixed point must be a saddle.

are used. We have already concluded that the initial slope of the M_a nullcline must be less than the initial slope of the B_a nullcline for the healthy rest state to be stable. Thus this must still be the case when using Balb/c parameters. However unlike the NOD configuration there should be no nontrivial fixed point which implies that $B_{a(Asymp1)} > B_{a(Asymp2)}$ so no intersection of the nullclines occur. This leads to the nullclines and slope field as seen on the sketch in figure 6.4. Here it is evident that any stimulated inflammation will be nonpermanent.

Before we continue with the next subsection we would like to make a brief remark.

Usually at the point where one is conducting a phase plane analysis the model under scrutiny has been recast in a dimensionless form, since this eases the job of deciding if some terms in the model can be disregarded, if some of the parameters are (relatively) significantly smaller than others or some parameters hold a greater impact on the behavior of the dynamic. This is often helpful if some or none of the parameters are

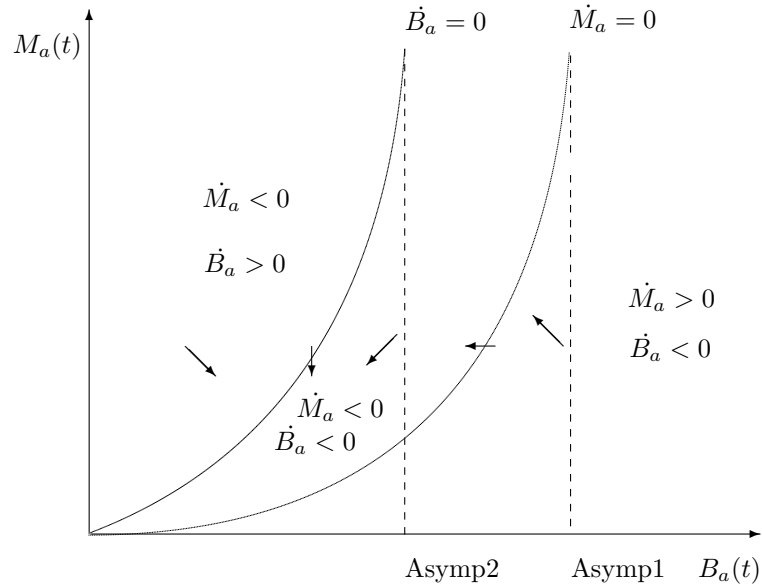


Figure 6.4 Sketch of the nullclines and some representative arrows that indicate the flow for the IM with $dM/dt = 0$. For the healthy rest state, $(B_a, M_a) = (0, 0)$, to be stable the initial slope of the M_a -nullcline must be less than the initial slope of the B_a -nullcline. Then by assuming that the nullcline of B_a reaches its asymptotic point before the nullcline of M_a leaves the stable healthy rest state to be the only existing physiological relevant fixed point. This means that any stimulated inflammation will be nonpermanent.

unknown, and it also reduces the number of parameters to keep track of. Per automation we also nondimensionalized the IM (including crowding terms) – cf. appendix A.6 – but since we are in the rare situation of having estimates of all the parameters, we have chosen not to work with the nondimensional version.

A brief note on linearizing

Some newcomers to the field of mathematical modelling may think that we oversimplified things by linearizing the system when we analyzed the stability of the fixed points because we casually threw away the higher order nonlinear terms without making any remarks about these. So what gave us the right to do so?

Hartman-Grobman's theorem⁸ informally states that the flow of a nonlinear system is topologically equivalent to that of a linear system in the neighborhood of a steady state solution, provided that the eigenvalues of the Jacobian of the linear system are not purely imaginary or take on zero value.⁹ The equivalence here being a homeomorphism, i.e. a continuous deformation with a continuous inverse, that preserves the sense of time (Guckenheimer and Holmes (2002)). More so the eigenspaces attributable to the eigenvectors, of the linearized system, where the eigenvalues are subject to the behavior given above, are tangent to the invariant manifolds of the fixed points of the nonlinear system (Guckenheimer and Holmes (2002)) – provided that the fixed points are hyperbolic. This last statement is the essence of the theorem known as *The Stable Manifold Theorem for a Fixed Point*; see e.g. Guckenheimer and Holmes (2002) page 13. When we are in three or less dimensions this fact should lend a helping hand to the intuitive understanding of the situation.

Let us recapitulate in (pseudo) laymen terms: when the eigenvalues of the Jacobian does not take on zero or purely imaginary values, the behavior obtained from the linear system is in qualitative agreement with that of the nonlinear system.

One could hope that as long as we knew all the eigenvalues we could precisely determine what kind of behavior is in play, and in fact it is so when we are in \mathbb{R}^2 . But when we enter \mathbb{R}^3 and higher dimensions there are no theorems such as e.g. the Poincaré-Bendixson theorem, that yield guarantees about the dynamical behavior, when we are dealing with systems that evolve in more than two dimensions (Strogatz (2000)) – the Poincaré-Bendixson theorem states that given a trajectory confined to a compact subset of the plane, \mathbb{R}^2 , that does not contain any fixed points, then said trajectory will either approach a closed orbit, or it is itself a closed orbit (Strogatz, 2000, p.203). When dealing with systems that evolve in \mathbb{R}^3 and above a plethora of dynamics, including chaos, can arise.¹⁰

Now that we have elaborated a little on the relationship between a nonlinear system and the linearized version thereof we will return to the analysis of the intermediate model for that story is not completely over.

⁸ For a formal statement of the Theorem cf. appendix A.3.

⁹ Note that we are not given any promises regarding the size of said neighborhood.

¹⁰ Actually we would find it boring if there was no more to the study of systems of differential equations than determining the eigenvalues.

6.2 The IM Including Crowding-Terms

Marée et al. (2006) extends the IM by including the terms $e_1M(M+M_a)$ and $e_2M_a(M+M_a)$ to simulate the outflow of resting and activated macrophages due to overcrowding in the compartment. This addition is made to counter the unlimited growth that is possible in the CPH model (Marée et al., 2006, p.1270) and also in the IM without the crowding terms as we can see in figure 6.3. To get an idea of the effect of the crowding terms we now include them in the IM.

The system of differential equations for the IM including crowding terms is

$$\frac{dM}{dt} = a + (k + b)M_a - cM - f_1MB_a - e_1M(M + M_a) \quad (6.61)$$

$$\frac{dM_a}{dt} = f_1MB_a - kM_a - e_2M_a(M + M_a) \quad (6.62)$$

$$\frac{dB_a}{dt} = lM_a - f_1MB_a - f_2M_aB_a - dB_a \quad (6.63)$$

As a first observation the crowding terms are included such that they decrease the rate of change for M and M_a quadratically. To get a feel for what difference the crowding terms have on the flow we will, again, make use of a phase plane analysis, and as before we set $dM/dt = 0$, so we have

$$0 = -e_1M^2 - (e_1M_a + c + f_1B_a)M + a + (k + b)M_a \quad (6.64)$$

This means that M is found as the positive root of the second degree polynomial in equation 6.64, i.e. M is

$$M = \frac{-(e_1M_a + c + f_1B_a) + \sqrt{(e_1M_a + c + f_1B_a)^2 + 4e_1(a + (k + b)M_a)}}{2e_1} \quad (6.65)$$

The negative root is disregarded since it leads to a negative concentration of resting macrophages which makes no sense from a physiological point of view. To proceed from here one should insert the expression for M into equation 6.62 and 6.63 and then the nullclines are found by setting $dM_a/dt = 0$, and $dB_a/dt = 0$ and then solving for M_a . However these are difficult to solve analytically, because of the the nonlinear crowding terms. Therefore it is necessary to engage in a more subtle argument.

Let us assume that the parameters are chosen such that the system exhibits NOD dynamics, and let us imagine that the nontrivial fixed point is relatively close to the stable healthy rest state, and finally let the crowding parameters e_1 and e_2 be relatively small (we are still working with arbitrary parameters), so that the crowding terms are negligible near the nontrivial fixed point. Under these assumptions the phase plane would look similar to what is seen in figure 6.3 up to the nontrivial fixed point. However beyond the nontrivial fixed point the concentrations of M_a and B_a have grown to a size where the crowding terms cannot be neglected. Now, since the expression for dM_a/dt (equation 6.62) is directly affected by the inclusion of the crowding terms – a crowding term appears in the expression – and implicitly through the revised expression for M (equation 6.65). The expression for dB_a/dt (equation 6.63) on the other hand is only affected implicitly; through the expression for M . The first question that needs to be answered is then: what is the relative difference between the expression for M derived

from the IM without crowding terms (equations 6.50 and the expression for M derived from the IM including crowding terms (equation 6.65)? Let us approach this matter in an intuitive fashion by looking at the nullsurface of equation 6.61 (setting $dM/dt = 0$).

$$0 = a + (k + b)M_a - cM - f_1MB_a - e_1M(M + M_a) \quad (6.66)$$

Then from a given point (M, M_a, B_a) on the nullsurface we increase M_a and B_a by a small amount $|\delta M_a|$ and $|\delta B_a|$. From this we see that M has to increase less, relative to the equation without the crowding terms, to maintain the equilibrium. If this argument seems strange, picture the system as a leaky bucket, where the volume of water is kept constant by pouring water into it. That is, the inflow of water from the top of the bucket is the same as the outflow through the holes in the bottom of the bucket. Then suddenly some additional holes appear in the bottom but the equilibrium remains. This means that the outflow have more outlets to be distributed among and therefore less flow through every single outlet. However, in the case above we defined the change of M_a and B_a so only M was allowed to vary. This leads to the crucial observation that for a given concentration of M_a and B_a , the concentration of M can be considered to be “less” relative to if the crowding terms were excluded.

Continuing in the same direction we now take a look at the nullclines¹¹ of M_a

$$0 = f_1MB_a - kM_a - e_2M_a(M + M_a) \quad (6.67)$$

This time let M_a increase with at small amount $|\delta M_a|$. Then because of the inclusion of the quadratic crowding terms causing a greater efflux and the relatively smaller M , there must be a greater increase of B_a relatively to the equation without the crowding terms. In other words, $\frac{dM_a}{dB_a}$ must be less in the case where the crowding terms are included compared to when they are not. This is interesting since it reveals that the slope of the M_a -nullcline must decrease when the crowding terms are no longer negligible. To complete the analysis let us turn to the nullcline of B_a

$$0 = lM_a - f_1MB_a - f_2M_aB_a - dB_a \quad (6.68)$$

As mentioned the only difference here in respect to the model without the crowding terms is the decrease of M . This implies that if we increase B_a by a small amount $|\delta B_a|$ then M_a must increase less, relative to the case where the crowding terms are excluded. Thus the slope of the nullcline $\frac{dM_a}{dB_a}$ is again gradually reduced when the crowding terms are no longer negligible, so that the asymptotic behavior fails to happen. However the reduction is less for the nullcline of B_a compared to the nullcline of M_a such that an inevitable third intersection of the nullclines takes place; cf. figure 6.5. From the slopefield we see that the fixed point is stable, which makes it an upper bound for the inflammation as claimed by Marée et al. (2006). Note that when the system is stimulated above the separatrix the concentrations of the macrophages and apoptotic β -cells will tend towards the concentrations that represent the coordinate of the upper stable fixed point.

¹¹ We now consider them as nullclines instead of nullsurfaces since M is considered to be a constant of a size that is less than if the crowding terms were excluded.

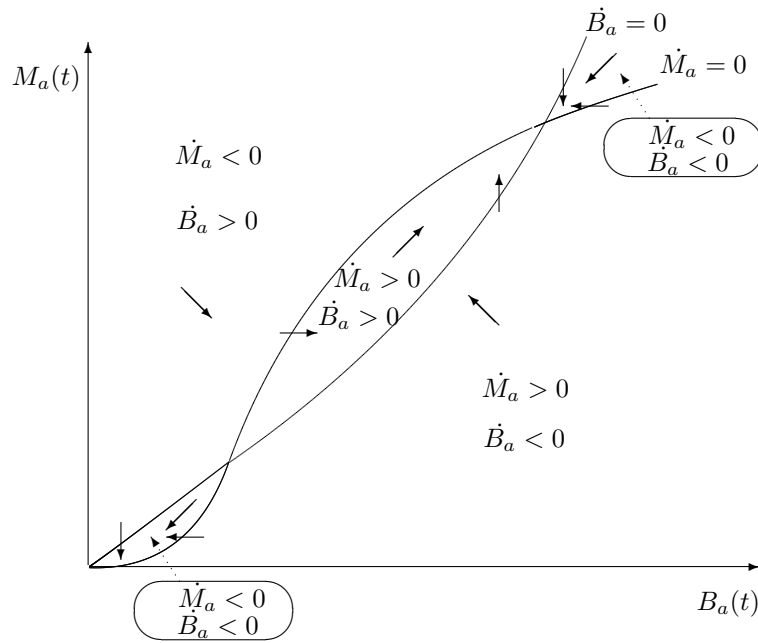


Figure 6.5 Sketch of the nullclines and arrows that indicate the flow for the IM including crowding terms with $\frac{dM}{dt} = 0$. It is assumed that the inclusion of crowding terms only have a minuscule effect on the position of the saddle point compared to figure 6.3, in the limit case close to the healthy rest state. Beyond the saddle point the crowding terms start to effect the behavior of the nullclines. Through analysis we have found that the crowding terms gradually reduce the slope of the nullclines, albeit more effectively for the nullcline of M_a . Thereby the asymptotic behavior fails to happen and instead the continuity and the relation between the slope of the nullclines causes a third intersection to take place. This additional nontrivial fixed point is stable and works as an upper bound for the inflammation.

6.3 Recapitulation of The Analysis of the IM

On the basis of the analysis of the IM we have reached an understanding of what kind of dynamics that the people of Marée et al. (2006) were looking for when modifying the CPH model and at the same time gained insight into the problems they were facing in this process. To summarize: the CPH model was extended to the IM for the purpose of testing the hypothesis that impaired phagocytosis makes the difference between health and disease. For the hypothesis to be confirmed the model should be able to exhibit two kinds of dynamics by changing the values of the parameters f_1 and f_2 . The two types of dynamics were dubbed Balb/c and NOD dynamics respectively and refers to the classification of the mice that are prone to develop T1D (NOD-mice) and those who are not (Balb/c-mice). In the case where the estimated Balb/c phagocytosis rates were applied, the model was expected to show Balb/c dynamics. This implies the existence of a healthy rest state, where there is no activated macrophages and no apoptotic β -cells, as the only fixed point in the physiological relevant region of the phase space. This fixed point should furthermore be stable such that any stimulated inflammation will be nonpermanent. When using the estimated phagocytosis rates for NOD-mice the model was expected to exhibit NOD dynamics which is more eventful than the former. Here the possibility for a permanent and nonpermanent inflammation should be open, since not all NOD-mice develop T1D. In addition the chronic inflammation should be bounded such that the concentration of neither the activated macrophages nor the apoptotic β -cells tends towards infinity. These expectations are reached when, besides the stable healthy rest state, there is a saddle point that together with its stable manifold comprises a separatrix. Below the separatrix the inflammation is damped, i.e. nonpermanent, whereas, if the separatrix is traversed, the inflammation will escalate. The escalating inflammation needs to be bounded, so a third fixed point must exist that has to be stable.

These are the two types of dynamics that the model should be able to exhibit when using the estimated Balb/c and NOD parameters. However as discussed in section 6.1 this is not the case, since the IM also exhibits Balb/c dynamics when applying the estimated NOD parameters. By this realization the people of Marée et al. (2006) suggest to implement the role of necrosis in the model. We will proceed by embarking on an analysis of this model, i.e. the DuCa model, in the following sections.

7 A Brief Introduction to Bifurcation Analysis and Numerical Methods

A natural question to ask one self when working with models of physiological phenomena is how sensitive the model is to changes in parameter values. This is interesting from a purely mathematical point of view, because an analysis of how the stability depends on one or several parameter values is a *bifurcation analysis*. A bifurcation analysis also provides insight into the behavior of the mathematical model, which of course should reflect the biology it models. Thus the bifurcation analysis is also interesting from the modelling/biological perspective.

In this chapter we provide the reader with an introduction to (local) bifurcations in general, and proceed on to choose bifurcation parameters and appertaining intervals. After this we briefly describe how we have found, and determined the stability of, the eigenvalues. All of these pieces are combined into bifurcation diagrams in chapter 8 where we also perform an analysis of the DuCa model.

But first let us introduce the concept of *bifurcation*, and shed some light on its significance in modelling of biological system in general and the DuCa model in particular.

7.1 Generic Bifurcations

Assume that we have a one-parameter system of differential equations, $\mathbf{f}(\mathbf{x}, r)$, where $r \in \mathbb{R}$ is the parameter, and $\mathbf{f}(\mathbf{x}) := \dot{\mathbf{x}} \in \mathbb{R}^n$, where the dot denotes d/dt . We want to find out what happens to the behavior for different values of r .

Case 1 is: different values of r shifts the location of the equilibria, but does not change their stability or create new ones. Like changing $p \in \mathbb{R}^+ \setminus 0$ in $g(x) = x^2 - p$ will change the roots for g , but not the number of solutions. In this case the flows corresponding to different r 's are topologically equivalent.

Case 2 is: different values of r *does* induce a change in the flow, i.e. change in stability of, or creation of, equilibria. In this case there is no longer a topological equivalence between the flows that arise for the different r values, and we say that a bifurcation has occurred. It may be easier to think of a bifurcation as a sudden change in the qualitative behavior of the solutions to a system of differential equations.¹

Thus a bifurcation analysis is the investigation of how the qualitative behavior of a system depends on a parameter.

When a bifurcation occurs upon shifting only one parameter, the bifurcation is sometimes called a *codimension one* bifurcation. Similarly if two parameters must be varied

¹ Here system is used in the general sense, so one differential equation alone can be a system.

to induce a bifurcation, we speak of a codimension two bifurcation, and so forth up to n parameters.

An instructive one-dimensional example is:

$$\dot{x} = r + x^2 \quad (7.1)$$

For $r < 0$ there are two fixed points ($x^* = \pm\sqrt{-r}$). One is stable and one is unstable, as one can see by plotting \dot{x} in a $\dot{x}x$ -coordinate system. For $r \rightarrow 0$ the two fixed points will approach each other. Finally at $r = 0$ they will coalesce to become a half-stable point or a saddle-point, i.e. a point that is attracting from one side and repelling from the other – the flow is in one direction. Immediately after r becomes positive the fixed points (on the real line) no longer exist. They have *annihilated*; a bifurcation has occurred. $r^* = 0$ is called the bifurcation point or bifurcation value, and r is in this case called the *bifurcation parameter*. More specifically the bifurcation value is defined as a value r^* for which the flow of the system in equation 7.1 is not structurally stable (Guckenheimer and Holmes, 2002, p.119).

This was an example of a so-called saddle-node bifurcation, which is one of the generic or archetypical local bifurcations. The other generic one-dimensional bifurcations are (Guckenheimer and Holmes, 2002, p.145-148)

The transcritical bifurcation this one arises from the system $\dot{x} = rx - x^2$. When r is negative there are two fixed points – one stable (at the origin) and one unstable (at r). For $r = 0$ there is only one half-stable fixed point (at the origin), and for $r > 0$ there is once again two fixed points, but now the the fixed point at the origin is unstable, while $x^* = r$ is stable – an exchange of stability has occurred.

The pitchfork bifurcation this one comes in two categories, a subcritical (arises from $\dot{x} = rx + x^3$), and a supercritical (arises from $\dot{x} = rx - x^3$). These two are qualitatively different, but what they have in common is that one fixed point branches into three fixed points as r crosses 0.

There is one additional bifurcation that can be categorized as generic, namely the *Andronov-Hopf* bifurcation or more commonly simply the Hopf bifurcation. This bifurcation type merits a little more explanation, so we have endowed it with its own section. Introducing the Hopf bifurcation also allows us to give a brief description of how some of the more interesting behaviors a system can exhibit come about, i.e. why complex eigenvalues entail spirals or closed orbits.

7.2 The Hopf bifurcation

The Hopf bifurcation differs from the other bifurcations in that it cannot occur in one-dimensional systems, so let us start by supposing that we have a system of autonomous nonlinear differential equations that depend on a bifurcation parameter $r \in \mathbb{R}$, and that we have linearized the system around a fixed point, i.e. we have disposed of the higher order nonlinear terms. The linear system can be written in the form

$$\dot{\mathbf{x}} = \mathbf{A}\mathbf{x} \quad (7.2)$$

with initial condition $\mathbf{x}(0) = \mathbf{x}_0$, and \mathbf{A} is the Jacobian. Now suppose that we find the corresponding characteristic polynomial from which we obtain the eigenvalues. Then

the general solution to equation 7.2 is given by

$$\mathbf{x}(t) = \sum_{i=1}^n c_i e^{\lambda_i t} \mathbf{v}_i \quad (7.3)$$

where c_i are constants that are found by invoking the initial condition, $\lambda_i \in \mathbb{C}$ are the eigenvalues, t is time, and \mathbf{v}_i are the corresponding eigenvectors, which are found by solving $(\mathbf{A} - \lambda \mathbf{I})\mathbf{v} = 0$ (Braun, 1993, p.333-334).²

If we take a step back now, and think about how our solution curves should behave if we wanted to observe spirals or closed orbits in phase space, the solution curves should exhibit some kind of oscillatory motion – the motion may be dampened, growing or sustained, either way yields one of the mentioned dynamics. One obvious way such motions could arise is if (some of) the eigenvalues are complex, i.e. we have at least one pair of eigenvalues on the the form

$$\lambda_{1,2} = \alpha \pm i\beta \quad (7.4)$$

By remembering Euler's formula – $e^{(\alpha \pm \beta i)t} = e^{\alpha t}(\cos(\beta t) \pm i \sin(\beta t))$ – we see why complex eigenvalues imply oscillations. The term $e^{\alpha t}$ is the amplitude of the motion, and it determines the qualitative behavior of the oscillations: for $\alpha < 0$ the oscillations are damped, and vice versa for $\alpha > 0$. If the oscillations are damped, then we have stable spirals (in phase space), while growing oscillations are a trait of unstable spirals. But what happens at $\alpha = 0$? Assume that 7.4 can be rewritten as $\lambda(r)_{1,2} = \alpha(r) \pm i\beta(r)$, so that these two eigenvalues of our system, 7.2, are smooth functions of the bifurcation parameter r . Now suppose that we vary r continuously, then at some value of r , denoted by r^* , the real part of the eigenvalues is zero. This is naturally the instance where the value of the real part changes sign. Actually we will also require that

$$\left(\frac{d\operatorname{Re}(\lambda(r))}{dr} \right)_{r=r^*} \neq 0 \quad (7.5)$$

so that the eigenvalue cross the complex axis with non-zero velocity. When these criteria³ are fulfilled a Hopf bifurcation occurs at $r = r^*$. The Hopf bifurcation comes in three very different variations (Allen, 2007, p.202), but before we present these we must introduce a phenomenon that is an inherent feature of many real-life, and nonlinear, systems (Strogatz, 2000, p.196-197). This phenomenon is the *limit cycle*. Limit cycles are closed solution curves that can be 1. stable: all nearby trajectories will approach the cycle for $t \rightarrow \infty$, 2. unstable: all nearby trajectories will approach the cycle as $t \rightarrow -\infty$, and finally 3. semi-stable: the cycle is attracting from some directions, and repelling in other (Strogatz, 2000, p.196-197). Limit cycles differ from periodic solutions of linear systems in that they are not regular ellipses, and that (in stable limit cycles) any disturbance will die out over time contrary to the periodic solution curve, $\mathbf{x}(t)$, which, if perturbed by $\varepsilon > 0$, becomes a new solution, $\mathbf{x}_\varepsilon(t)$.

Now we are ready to present the three types of Hopf bifurcations (cf. figure 7.2), which are

² We have assumed that the algebraic and geometric multiplicity is equal.

³ Actually we need a bit more. Confer Guckenheimer and Holmes (2002) for a thorough introduction.

- I The supercritical Hopf bifurcation. Stable spirals exist for $r < r^*$ as $\alpha(r) < 0$, up until $r = r^*$ where $\alpha(r) = 0$. At the bifurcation point, $r = r^*$, the spiral is still stable but very weakly so (Strogatz, 2000, p.250). For $r > r^*$ the spirals are unstable, with stable limit cycles surrounding them, i.e. $\alpha(r) > 0$.
- II The subcritical Hopf bifurcation. For $r < r^*$ we have $\alpha(r) < 0$ thus stable spirals coexists with unstable limit cycles. As $r \rightarrow r^*$ the radius of the unstable limit cycles decrease. Ultimately, at $r = r^*$, the limit cycle engulfs the fixed point that was the focus of the stable spiral, and for $r > r^*$ the fixed point is unstable, thus making the spirals unstable.
- III The degenerate Hopf bifurcation. This type of Hopf bifurcation is characterized by stable spirals for $r < r^*$, and unstable spirals for $r > r^*$, while at $r = r^*$ infinitely many neutrally stable concentric closed orbits encircle the fixed point that is the focus of the spirals.

Figure 7.2 provides an example in \mathbb{R}^2 of the three bifurcation types. The limit cycles

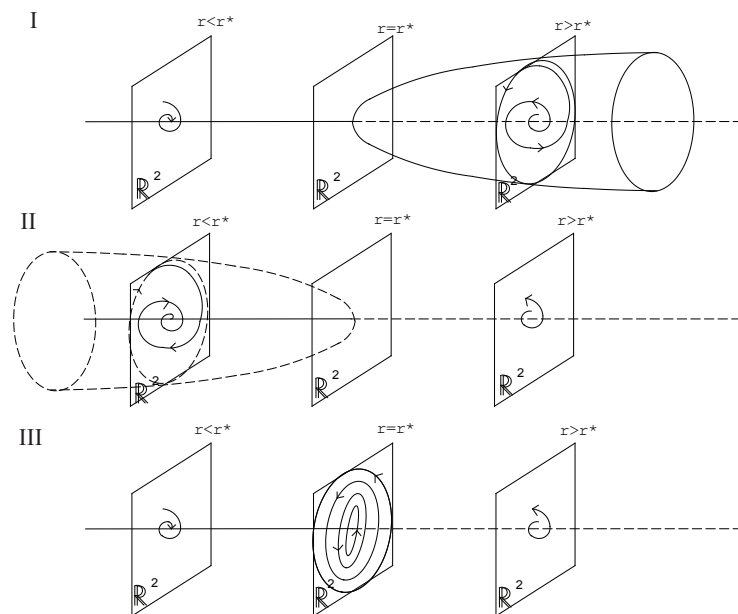


Figure 7.1 A supercritical (I), a subcritical (II) and degenerate Hopf bifurcation (III). From Zeeman (1990) with minor modifications. The dashed lines denote unstable fixed points or limit cycles.

that arise from the supercritical version (I) are easiest identified by means of computer-generated phase plots. The unstable limit cycle that exists before the bifurcation point in the subcritical case (II) can in theory be found by reversing the time when one does simulations of the system of interest. This is tantamount to multiplying the right-hand-side of the differential equations in question by minus one. At the instance where the

focus of the stable spiral in case II changes stability, from attracting to repelling, the flow will make a sudden jump, possibly to another stable fixed point, another limit cycle or it may even diverge. This extreme change in behavior is known as hysteresis. Hysteresis also implies that we cannot make the system return to the behavior before the bifurcation point by simply turning the bifurcation parameter back to before the bifurcation value (Strogatz, 2000, p.252). In other words the behavior is irreversible in regards to changes in the bifurcation parameter.

7.3 Biological Relevance of Bifurcation Analysis

Now returning to the biological relevance of bifurcation analysis. What biological conclusions can we draw from a model that exhibits bifurcations? The answer is, naturally, that this depends on what the model is supposed to model! If we have data that suggests that our biological system goes from having, say, one to two stable states as a given parameter value is changed, then it is natural that our mathematical model exhibits a bifurcation. But if the stable states in the mathematical model appear at a parameter value that is completely irreconcilable with the *actual* value, then we must reassess the model. On the other hand if some behavior, that is biologically reasonable, is observed in a mathematical model, then one can use this to make predictions/conclusions about the biological system.

In our case it is particularly interesting to see if the qualitative behavior of the system changes close to, or maybe within the span of uncertainties associated with the parameter values; cf. sections 5.8 and 5.8. Should the qualitative behavior change within, or close to, the parameter range of a given parameter then the model is parameter sensitive. This does not necessarily indicate that the model is ill-conceived, e.g. not all NOD mice develop diabetes, so these mice may have a slightly different parameter composition.

7.4 Choice of Bifurcation Parameters

The DuCa model contains 12 parameters which makes it a daunting task to conduct a thorough investigation. This amount of parameters also opens up the possibility of co-dimension 12 bifurcations⁴, which is way beyond the scope of this work. Thus we must limit our analysis to a few important parameters. We have gone with f_1 and f_2 for two reasons:

1. Wang et al. (2006) (see section 1) remark that an analogue of our phagocytosis rates is the most important for the stability in their model
2. The other, and perhaps most important, reason is that the model was originally intended to investigate whether the difference in the values of f_1 and f_2 alone, could lead to different dynamics of the system – permanent or nonpermanent inflammation

Now that we have chosen our bifurcation parameters we must decide what intervals we want f_1 and f_2 to take values in. Of course the whole negative range of \mathbb{R} is out

⁴ The amount of parameters could naturally be brought down by nondimensionalizing the system, but even after this 9 dimensionless groups remain, which are still too many.

of the question, and so is very large positive values. To determine these intervals we must naturally look at the magnitude of the parameters. We have already discussed the values and uncertainties of f_1 and f_2 ; cf. section 5.8. So just as a reminder the resting and activated macrophage phagocytosis rates were found to be the same for NOD-mice, $f_1 = f_2 = 1 \times 10^{-5}$.⁵ While for Balb/c-mice the resting phagocytosis rate was estimated to be $f_1 = 2 \times 10^{-5}$, whereas the phagocytosis rate of the activated macrophages was $f_2 = 5 \times 10^{-5}$. These estimated values are associated with uncertainties in the area of 10-20%. The scale (10^{-5}) defines the magnitude of our interval, and the uncertainties tell us what parameter range to investigate as a minimum. This minimum range is very small, and since we are interested in the bigger picture we have decided to let f_1 take values in interval from 0 to 4×10^{-5} while f_2 is in the interval from 0 to 10×10^{-5} . Naturally we need fixed points to conduct a bifurcation analysis. How we came about these is the subject of the next section.

7.5 Locating the Fixed Points

The application of the Newton-Raphson method has proven fruitful for finding fixed points. The Newton-Raphson method is a numerical method that, through iterations, computes the zeros of a vector-valued function \mathbf{x} , based on the following equation

$$\mathbf{x}^{k+1} = \mathbf{x}^k - (\mathbf{J}(\mathbf{f}(\mathbf{x})))^{-1} \mathbf{f}(\mathbf{x}^k) \quad (7.6)$$

where \mathbf{x}^k and \mathbf{x}^{k+1} are the approximations of the zero, \mathbf{x}^* , after k and $k+1$ iterations respectively, $(\mathbf{J}(\mathbf{f}(\mathbf{x})))^{-1}$ is the inverted Jacobian⁶, and $\mathbf{f}(\mathbf{x}) = \dot{\mathbf{x}}$. The iteration continues until $\|\mathbf{x}^{k+1} - \mathbf{x}^k\| = \|\Delta \mathbf{x}\| < \varepsilon$ where ε is a user defined error-tolerance on the estimated value of \mathbf{x}^* compared to the analytical value. The partial derivatives of the Jacobian matrix $\mathbf{J}(\mathbf{f}(\mathbf{x}))$ are approximated as the finite difference.⁷

The procedure of Newton-Raphson requires one to make a guess on the initial conditions from where to start the iteration. This determines what fixed point the function converges to – if it converges at all! However, to begin with, it is not in anyway evident what initial conditions to use when searching for nontrivial fixed points, so this tends to be a process of trial and error based on an “educated guess”, that is based on simulations of the DuCa model. Despite this guideline, there is no guarantee that we see the “full picture” when less than five fixed points are found – there may be non-relevant fixed points located outside 1. quadrant, but undetected fixed points in the 1. quadrant may also exist. The procedure is easiest in the case where the first fixed point for a given value of the bifurcation parameter is found, and the position of the fixed point changes very little for small changes of the bifurcation parameter. Then it is possible to use the coordinates of the located fixed point as an initial guess, when searching for fixed points at values of the bifurcation parameter close to the initial value.

The stability of the fixed points has been determined by computing the eigenvalues, of the Jacobian, in each point. Plots of the eigenvalues with respect to f_1 and f_2 can be seen in appendices B.1 to B.5.

⁵ From here on we will drop the dimensions for the sake of convenience.

⁶ We have tacitly assumed that the Jacobian has a non-zero determinant.

⁷ For a derivation of the Newton-Raphson method and a more detailed description of the procedure applied see appendix A.5.

Evaluation of stability of the fixed points and detection of bifurcations

The method we have used for detection of bifurcations is to look for fixed points and evaluating their stability for different values of the chosen bifurcation parameter.⁸ E.g. when we have looked for Hopf bifurcations we have made use of their defining characteristic, i.e. two complex eigenvalues that cross the imaginary axis. Using these traits of the Hopf bifurcation we use the numerical estimates of the fixed points found by the Newton-Raphson method. This eases the job of evaluating the Jacobian in each fixed point since this is already done, albeit as an approximation, by the Newton-Raphson method.

The eigenvalues of the Jacobian were computed in order to plot the real and imaginary part of the eigenvalues as a function of the bifurcation parameter. Furthermore a plot of the imaginary part as a function of the real part will be shown. This is the “traditional” way of presenting the behavior of eigenvalues during a Hopf bifurcation.

⁸ It should be mentioned that this approach limits us to the detection of only local bifurcations since global bifurcations involve large regions of the phase space, and therefore cannot be detected solely by looking at the stability of local fixed points (Lynch, 2004, p.330-333).

8 Bifurcation Diagrams and Analysis

Bifurcation diagrams provide a nice overview of how the stable and unstable solutions change as a bifurcation parameter changes. We have used MATLAB to produce our bifurcation diagrams for the DuCa model.¹ Please note that we have not included the apoptotic wave in the simulations behind these bifurcation diagrams since we are interested in investigating other regions besides those the apoptotic wave pushes the system into. We are aware that the apoptotic wave is the initiator of inflammation so in lieu of the wave as a catalyst we apply appropriate initial conditions to stimulate the system.

The bifurcation diagrams are plotted with the fixed points of the activated macrophages M_a^* as a function of the phagocytosis rate constants; f_1 or f_2 (e.g figure 8.1). From a mathematical point of view we could have chosen any of the variables M, M_a, B_a, B_n, C to be the dependent variable in the bifurcation diagram. However from a medical point of view the presence of activated macrophages – which implies an activated immune system – is a more direct measure of inflammation in the DuCa model, and thus the development of T1D.

8.1 Codimension One Bifurcations

In the next two sections we deal with codimension one bifurcations based on f_1 first and f_2 second. One thing this analysis can tell us is: given that f_2 (or f_1), is kept at a given value. Can we make the flow in NOD-mice approach the healthy stable rest state? And if so: what should the value of f_1 (or f_2) be before this happens? Such an event will imply some kind of bifurcation, so in other words, this analysis can provide us with (an approximation of) such a bifurcation value of f_1 , respectively f_2 .

The bifurcation diagrams based on NOD values will be given the most extensive scrutiny. Dealing with the Balb/c bifurcation diagram to the same extent as these would not yield any fundamentally new knowledge – had there been some interesting behavior associated with the Balb/c diagram, then we would naturally have presented this, but the behavior is qualitatively similar to the bifurcation diagrams based on NOD parameters. Furthermore, from a physiological point of view, it is most interesting to find out if we can induce a healthy state in NOD-mice by simply tweaking the phagocytosis rates, or the amount of active macrophages.²

The bifurcation analysis is primarily done on the full DuCa model, but in section 8.4 we also look at a bifurcation diagram (figure 8.18) that is based on a reduced three

¹ A template of the MATLAB code for the bifurcation diagrams can be found in appendix C.1.

² As mathematicians doing mathematical modelling of biological systems we are allowed to dream up solutions to problems, unaffected by the applicability of said solutions to the real world – though we are not inimical to solutions that are readily applicable.

dimensional version of it, suggested by Marée et al. (2006), to see if making the QSS assumptions

$$\frac{dB_n}{dt} = 0 \quad (8.1)$$

$$\frac{dC}{dt} = 0 \quad (8.2)$$

has any influence on the behavior of the detected fixed points. This is interesting to determine, because it is, *ceteris paribus*, easier to analyze a three dimensional rather than a 5 dimensional system.

8.2 Using f_1 as the bifurcation parameter

Figure 8.1 is the bifurcation diagram of the DuCa model with NOD parameters, using f_1 as the bifurcation parameter (seen on the x-axis), and M_a as the variable (seen on the y-axis). Let us start by dealing with the obvious features, and then get into more subtle things after that.

Basic features of the NOD bifurcation diagram

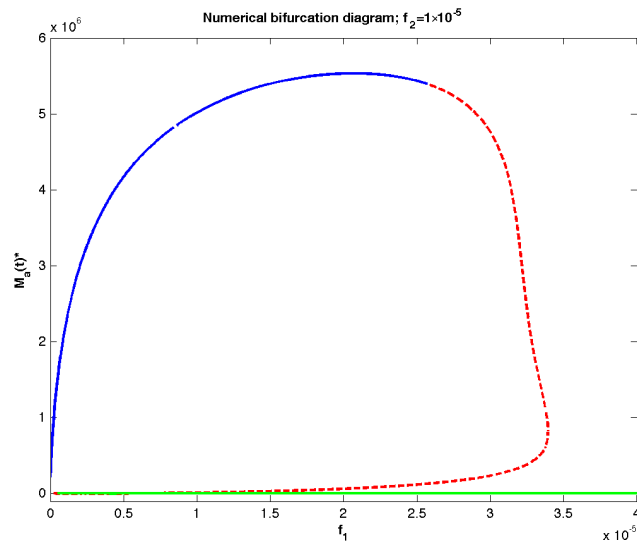


Figure 8.1 Bifurcation diagram for the DuCa model using f_1 as the bifurcation parameter and NOD parameters; cf. appendix B.1 for auxiliary figures. The solid and dashed lines illustrate fixed points that have only negative and mixed, i.e. positive and negative, eigenvalues respectively. The system is bistable up to $f_1^* \approx 2.57 \times 10^{-5}$. The NOD_{f_1} -LUB separates the two stable domains. For $f_1 > 2.57 \times 10^{-5}$ only the HRS remains stable.

First of all, we notice two kinds of curves: there are dashed, and then there are fully drawn curves. Dashed curves are associated with fixed points whose eigenvalues are not purely negative, while a fully drawn curve signifies fixed points that have strictly negative eigenvalues (or complex eigenvalues with negative real parts). At some point ($f_1 \approx 2.57 \times 10^{-5}$) the fully drawn curve that is increasing from the origin becomes dashed, and then proceeds to meet with the dashed curve from beneath it. The curve that starts out being fully drawn will be referred to as the *NOD $_{f_1}$ upper stable branch*, *NOD $_{f_1}$ -USB*³ for “short”. The lower dashed line will be referred to as the *NOD $_{f_1}$ lower unstable branch*, or *NOD $_{f_1}$ -LUB* (both of these names turn out to be somewhat of a couple of misnomers, but it eases the matter of explaining what is going on). Near the x-axis, or rather through $M_a = 0$ is another curve, which is colored green, this one is also fully drawn and is referred to as the *healthy rest state* (HRS). The HRS is the situation where no inflammation is present, hence healthy rest state – the HRS is the same in all the bifurcation diagrams, so we will not give it a prefix. Just as a reminder we state that each branch is actually a line of fixed points.

Figure 8.1 tells us that for $f_1 \in (0 : 2.57) \times 10^{-5}$ the system is bistable⁴ with at least three stability branches in all.⁵

The most interesting branches are the *NOD $_{f_1}$ -USB* and the *NOD $_{f_1}$ -LUB* – the HRS remains stable for all values of f_1 , i.e. the eigenvalues associated with it are negative for all $f_1 \in \mathbb{R}^+$.

Along the *NOD $_{f_1}$ -USB* the concentration of active macrophages increases as f_1 is increased. This is naturally because f_1 is also the activation rate of resting macrophages. The concentration ceases to increase at $f_1 \approx 2.067 \times 10^{-5}$, the curve flattens, and then slowly decreases (which may be because the amount of apoptotic β -cells stabilizes at a lower concentration, due to the initial faster phagocytosis). As f_1 is increased beyond $\approx 2.57 \times 10^{-5}$ the fixed points on the *NOD $_{f_1}$ -USB* become unstable, and the HRS is the only stable state that remains. The point where the transition occurs is the point where the eigenvalues shown in the bottom left subplot of figure 8.2 have zero real value, i.e. it is a Hopf bifurcation point. After the *NOD $_{f_1}$ -USB* has become unstable it descends until it coalesces with the *NOD $_{f_1}$ -LUB*. This happens at $f_1 \approx 3.45 \times 10^{-5}$ where they annihilate each other in what, to some extent, resembles a saddle-node bifurcation.

From the look of figure 8.1 it does not seem as though there is anything interesting going on with the *NOD $_{f_1}$ -LUB*, but in a moment when we look closer at the eigenvalues associated with it, we will learn that this is not true.

Eigenvalues, manifolds and behavior of the fixed points on the *NOD $_{f_1}$ -USB*

The *NOD $_{f_1}$ -USB* has five distinct, real, and negative, eigenvalues until $f_1 \approx 3.4 \times 10^{-7}$. Here two large and negative eigenvalues become complex conjugates. This implies that we should observe spirals, but because the real part of the eigenvalues is large (com-

³ It may be a cumbersome acronym, but it is necessary to avoid confusion when we get to the other bifurcation diagrams

⁴ Notice that the phagocytosis rate for resting macrophages in NOD-mice, $f_1 = 1 \times 10^{-5}$, lies well within the bistable region on both NOD-based bifurcation diagrams (figure 8.1 and 8.12). This accounts for the development of a chronic inflammation for NOD-mice, because the apoptotic wave stimulates the system to exceed the unstable fixed points along the *NOD $_{f_1}$ -LUB*.

⁵ Please be aware that other fixed points can exist, as we pointed out in section 7.5.

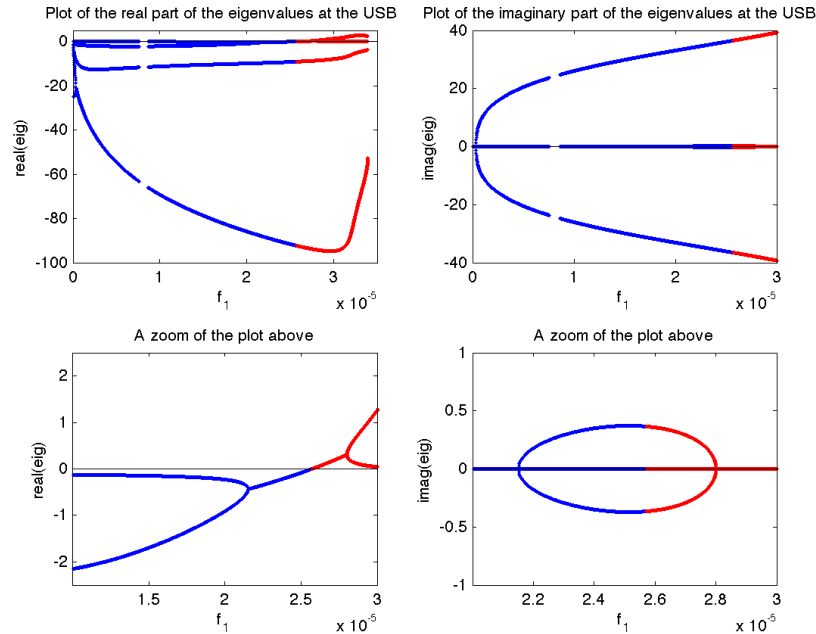


Figure 8.2 The figure is divided into four subplots that shows the real and imaginary parts of the eigenvalues plotted with respect to f_1 . We see that for two of the complex eigenvalues the real part of the eigenvalues goes from being negative to positive with nonzero speed (seen from the slope of the curve), at $f_1^* \approx 2.57 \times 10^{-5}$.

pared to the rest of the eigenvalues) and negative, these spirals approach the stable fixed points very quickly, without much actual spiraling.⁶ Or put another way, the motion is very damped.

After the advent of these complex eigenvalues nothing happens qualitatively before we get near $f_1 \approx 2.15 \times 10^{-5}$, here two more of the eigenvalues become complex. In the bottom left subplot of figure 8.2, which shows eigenvalue plots based on initial values that are near the NOD_{f_1} -USB, we see the two real eigenvalues coalesce at this approximate point, thus spawning the additional set of complex eigenvalues.

At this point we have a stable situation with a 5-dimensional stable manifold, that has two oscillatory directions. This second pair of complex eigenvalues should, naturally, also imply the existence of stable spirals, up until the real part of the eigenvalues becomes positive. Indeed we do find stable spirals when the real part is negative. One such spiral is depicted in figure 8.3, where the spiral is portrayed in MM_aB_a -phase space – $f_1 = 2.570039 \times 10^{-5}$ and $f_2 = 1 \times 10^{-5}$ have been used. In appendix B.6 we have gathered a series of figures that show how the spiral evolves as f_1 is increased, while f_2 is kept at 1×10^{-5} . As long as we have stable spirals we still have a stable

⁶ The existence of stable spirals has been revealed by plots done in MATLAB. However portraying the spirals requires one to zoom in extensively on the area around the stable fixed points, and do not make very illustrative figures, therefore we have left them out.

5-dimensional manifold, but this is about to change.

The real parts become positive at some point just after f_1 has exceeded 2.570039×10^{-5} ,

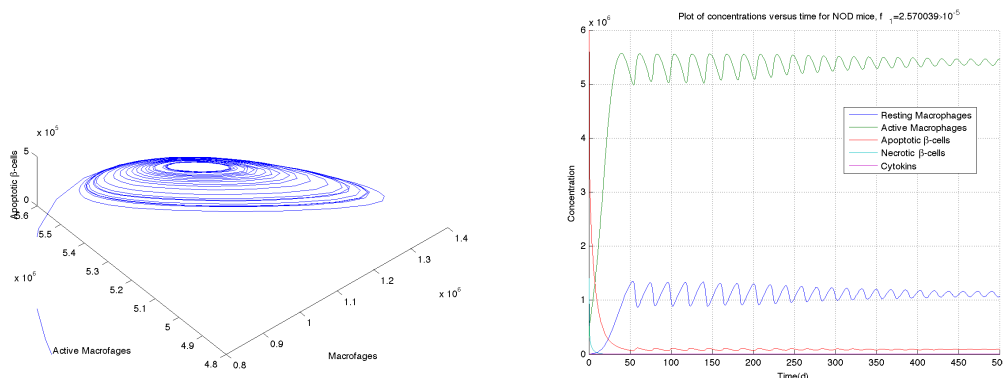


Figure 8.3 On the left we have a 3D phase space plot of M , M_a and B_a with $f_1 = 2.570039 \times 10^{-5}$. The initial conditions are $(M, M_a, B_a, B_n, C) = (4.77 \times 10^5, 0.001, 4 \times 10^7, 0.001, 0.001)$. This confirms the presence of stable spirals before the bifurcation point. To the right we have a plot of the concentrations as functions of time, made by using the ode15s-solver in MATLAB with the same initial conditions. NOD parameters are used except for $f_1 = 2.570039 \times 10^{-5}$. The dynamic of the system displays damped oscillations, constituting the spiral seen in the 3D plot in the figure to the right.

when unstable spirals are found; cf. figure 8.4 for an example. Looking at the bottom left subplot of figure 8.2 we see that $\text{Re}(\lambda)/df_1 > 0$ when the real part of the complex eigenvalues becomes positive – the imaginary parts of these eigenvalues are shown in the bottom right subplot. Thus a Hopf bifurcation occurs at the point where the real part of the eigenvalues intersects the f_1 -axis transversally.⁷ The Hopf bifurcation theorem tells us that one or more limit cycles should exist before, or after, the bifurcation point (depending on the type of Hopf bifurcation). We tried to locate the limit cycles numerically. However we only observed a stable spiral (cf. figures 8.3, 8.8 and appendix B.6), while very close to- and after the bifurcation point the spiral changes to an unstable spiral that terminates at the HRS; cf. figure 8.4. We have not been able to detect any stable nor unstable limit cycles near or at the bifurcation point.⁸ This does not however imply that they do not exist. The Hopf bifurcation theorem is an existence theorem and so does not provide us with any exact interval around the bifurcation point in which to look. In reality the interval could be an epsilon to each side of the bifurcation point, where epsilon is arbitrarily small but positive.

Upon closer inspection we discovered that there is more going on near the Hopf bifurcation, than figure 8.1 reveals. We will return to this when we have concerned ourselves with the NOD $_{f_1}$ -LUB. At that time we will also comment on the criticality of the Hopf

⁷ The system fulfills the remaining conditions of the Hopf bifurcation theorem; cf. section 7.2 and Guckenheimer and Holmes (2002).

⁸ The method applied for searching for unstable limit cycles uses the principle that a point in phase space will tend towards the unstable fixed point as $t \rightarrow -\infty$, by reversing (i.e. changing the sign of) dM/dt , dM_a/dt , dB_a/dt , dB_n/dt and dC/dt .

bifurcation.

After the Hopf bifurcation we find unstable spirals that tend to the HRS, as figure 8.4 shows. To produce the simulations in figure 8.4 we needed initial values that were

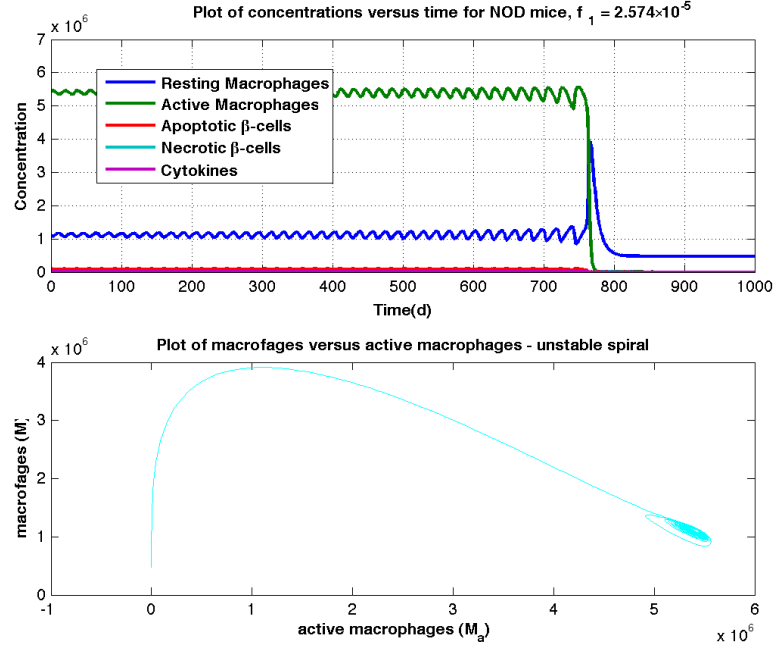


Figure 8.4 The upper figure shows the, initially oscillating, solution curves. The oscillations suddenly die out after $t \approx 775$, and the solution curves all tend to zero except for the curve describing the concentration of resting macrophages. The lower figure shows the unstable spiral just after the Hopf bifurcation has occurred. The initial conditions are $(M, M_a, B_a, B_n, C) = (1.06 \times 10^6, 5.45 \times 10^6, 9 \times 10^4, 550, 0.6)$.

close to the unstable fixed point for $f_1 = 2.574 \times 10^{-5}$. We used $(M, M_a, B_a, B_n, C) = (1.06 \times 10^6, 5.45 \times 10^6, 9 \times 10^4, 550, 0.6)$. because these were the approximate values that the concentrations stabilized at when we did simulations with $f_1 = 2.570039$; i.e. the fixed point that was the focus of the stable spiral shown in figure 8.3. This was done based on the intuitive notion that even though several branches can potentially arise from the bifurcation point, each of these is continuous, i.e. they will not be too far away from the unstable focus, and as we can see in figure 8.4 it worked.

The upper subplot in figure 8.4 shows the solution curves, while the lower subplot presents the unstable spiral in MM_a -phase space. We see that the oscillations endure a shift in behavior at $t \approx 775$ days. After this amount of time the oscillations that appeared to be sustained and growing converge to the HRS.⁹ In terms of the flow we can understand this behavior by noting that as $t \rightarrow \infty$ the flow (that does not lie

⁹ We have done simulations where f_1 was even closer to the bifurcation value – to narrow the bifurcation value down – in which the oscillations continued to grow to $t \approx 100000$.

directly on the manifold) diverges more and more from the unstable manifold of the NOD_{f_1} -USB, and it is eventually attracted to the stable manifold of the HRS.

The fixed points on the NOD_{f_1} -USB for f_1 values bigger than the Hopf bifurcation value have a three-dimensional stable, W^s , and a two-dimensional unstable manifold, W^u , associated with them. The biological significance of these findings is that if we could somehow increase f_1 beyond the Hopf bifurcation value of f_1 , while keeping f_2 at 1×10^{-5} , the NOD mice would be able to overcome the initial, otherwise pathological, inflammation of the pancreatic β -cells, rendering it healthy.

Looking at the bottom left subplot of figure 8.2, we see that shortly after the real part of the complex eigenvalues has become positive, these eigenvalues return to being strictly real and positive. As this happens we have two positive eigenvalues, one negative and two complex with negative real part. Thus the five-dimensional fixed points that exist for these values of f_1 , have a stable manifold, of dimension three, and an unstable manifold of dimension two, associated with them. We can add to the analysis of these points by looking at the magnitude of the eigenvalues. In the bottom left subplot of figure 8.2 we see that, after the two eigenvalues have become real, one of the positive eigenvalues is close to zero, thus the points are weakly repelling in the direction of the corresponding eigenvector. The fixed points are a little more repelling in the direction of the eigenvector associated with the other positive eigenvalue.

The remaining eigenvalues are negative. The eigenvalues that became complex at $f_1 \approx 3.4 \times 10^{-7}$ have large negative real part, see top left subplot in figure 8.2, thus the fixed points are “very attracting” from these eigendirections, i.e. the flow will tend fast to the fixed points from these directions. The last negative eigenvalue is comparable in magnitude to the largest of the positive eigenvalues, and will not attract the flow quite as fast as the two complex eigenvalues. This basically means that, suppose we have some initial values, at a given f_1 , that yield a flow that starts near the fast attracting eigendirection. Then this flow will quickly approach the slow attracting eigendirection as to become tangent to this direction – far away from the fixed point when we are near the attracting eigendirections, the fixed point looks like a stable fixed point. As the flow nears the fixed point the fixed point will become more and more repelling, so the flow will start to diverge from the attracting direction, and for $t \rightarrow \infty$ it will tend to the unstable manifold, W^u , spanned by the two positive eigenvectors. Of course if we started near the unstable manifold we would simply be repelled from the fixed point.

Table 8.1 summarizes the behavior along the NOD_{f_1} -USB at different intervals of f_1 .

Eigenvalues, manifolds and behavior of the fixed points on the NOD_{f_1} -LUB

Returning to the NOD_{f_1} -LUB, cf. figure 8.5, we notice that the eigenvalues are almost as interesting as in the case of the NOD_{f_1} -USB. We also see why it was a misnomer to name this line of fixed points the lower *unstable* branch – only one eigenvalue is positive throughout the investigated interval, as compared to the NOD_{f_1} -USB which has two positive eigenvalues after the Hopf bifurcation. The figure is unfortunately a little smothered in the area close to the x-axis, but for the NOD_{f_1} -LUB the most interesting behavior comes from the two eigenvalues that become complex at $f_1 \approx 1.165 \times 10^{-5}$. The complex eigenvalues have negative real parts, so in theory if we chose the initial values just right, so the solution curve would be exactly on the stable manifold, we should actually be able to observe a stable spiral that would converge to the NOD_{f_1} -LUB as

NOD $_{f_1}$ -USB					
$f_1 \in$	$(0; 3.4 \times 10^{-2})$	$(3.4 \times 10^{-2}; 2.15)$	$(2.15; 2.57)$	$(2.57; 2.8)$	$(2.8; 3.45)$
Nr. $\lambda \in \mathbb{R}^+$	0	0	0	0	2
Nr. $\lambda \in \mathbb{R}^-$	5	3	1	1	1
Nr. $\lambda \in \mathbb{C}(Re(\lambda))$	0	2(-)	4(-)	2(-), 2(+)	2(-)
Fixed pt.	S	S	SS	USS	SP
Dim(W^s)	5	5	5	3	3
Dim(W^u)	0	0	0	2	2

Table 8.1 Gives an overview of the eigenvalues, and the behavior of the fixed points on the NOD $_{f_1}$ -USB. By $\mathbb{C}(Re(\lambda))$ we mean the sign of the real part of the complex eigenvalues. “S” stands for stable, “SS” stands for stable spiral, “USS” stands for unstable spiral, and “SP” stands for saddle-point. Dim(W^s) is the dimension of the stable manifold, and Dim(W^u) is the dimension of the unstable manifold. All intervals are in the order of 10^{-5} , and all values are approximate.

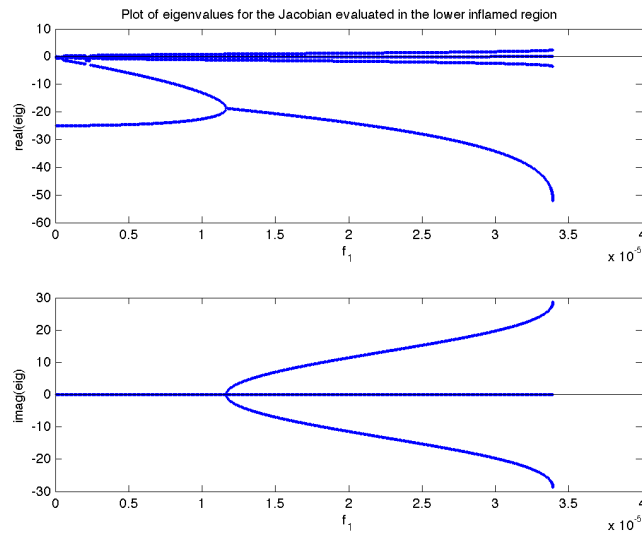


Figure 8.5 In the upper figure we see (real) values of the eigenvalues of the NOD $_{f_1}$ -LUB. At $f_1 \approx 1.165 \times 10^{-5}$ two of the eigenvalues become complex, and stay complex up until $f_1 = 3.45 \times 10^{-5}$ where the NOD $_{f_1}$ -LUB coalesces with the NOD $_{f_1}$ -USB (that consists of saddle-points at this point); cf. figure 8.1. The values of the complex part of these two eigenvalues are plotted in the lower figure. The complex eigenvalues retain negative real parts through the entire interval.

NOD $_{f_1}$ -LUB		
$f_1 \in$	(0;1.165)	(1.165; 3.45)
Nr. $\lambda \in \mathbb{R}^+$	1	1
Nr. $\lambda \in \mathbb{R}^-$	4	2
Nr. $\lambda \in \mathbb{C}(Re(\lambda))$	0	2(-)
Fixed pt.	SP	SP
Dim(W^s)	4	4
Dim(W^u)	1	1

Table 8.2 Gives an overview of the eigenvalues, and thus the behavior of the DuCa model with NOD parameters on the NOD $_{f_1}$ -LUB; cf table 8.1 for an explanation of $\mathbb{C}(Re(\lambda))$ and “SP”. Dim(W^s) is the dimension of the stable manifold, and Dim(W^u) is the dimension of the unstable manifold. All intervals are in the order of 10^{-5} , and all values are approximate.

$t \rightarrow \infty$ (Strogatz, 2000, p.128-134). This is because the stable manifold (as well as the unstable manifold) is invariant. We must be aware that any slight deviation from the stable manifold would make the flow tend to the unstable one-dimensional manifold, thus making the flow tend to the NOD $_{f_1}$ -USB or the HRS. The behavior along the NOD $_{f_1}$ -LUB is summarized in table 8.2.

Now that we have dealt with the NOD $_{f_1}$ -USB and the NOD $_{f_1}$ -LUB separately let us touch upon some of the more interesting mathematical aspects of the bifurcation diagram (figure 8.1), as a whole.

Combining the analysis of the NOD $_{f_1}$ -USB and LUB

The first thing that came to mind was that, when f_1 takes on values in the interval where the system is bistable, the flow seems similar to the flow displayed by the intermediate model (IM) including crowding terms in figure 6.5; cf. section 6.2. That is, a stable healthy rest state and a stable nontrivial fixed point, that serves as an upper bound for the inflammation. This comparison with the IM seemed even more justified as the NOD $_{f_1}$ -LUB consists of saddle-points, just as the “middle” fixed point is in figure 6.5. Unfortunately a discovery, that will be introduced soon, ruined what looked like an interesting turn of events, but at the same entailed some interesting consequences for the health of NOD-mice that will be elaborated on in the discussion.

In general, when we look at the bifurcation diagram, before the Hopf bifurcation occurs, it resembles that of a saddle-node bifurcation; cf. e.g. page 150 of Guckenheimer and Holmes (2002) or (Strogatz, 2000, p.242-243). We must not let the fact that there are three lines of fixed points (that we see) fool us. $M_a = 0$ remains stable for all f_1 , and all of the interesting (change in) behavior revolves around the NOD $_{f_1}$ -USB and the NOD $_{f_1}$ -LUB.

After the Hopf bifurcation both the NOD $_{f_1}$ -USB and NOD $_{f_1}$ -LUB are unstable. This is very interesting, since usually one should, at least locally, be able to reduce any bifurcation to one of the generic, or archetypical, types we encountered in section 7.1. But the bifurcation from two stable points and one unstable in the middle to two unstable fixed points with one stable fixed point, that is *not* between them is hard to reconcile with any of the generic (1-dimensional) bifurcation types. However we must remember

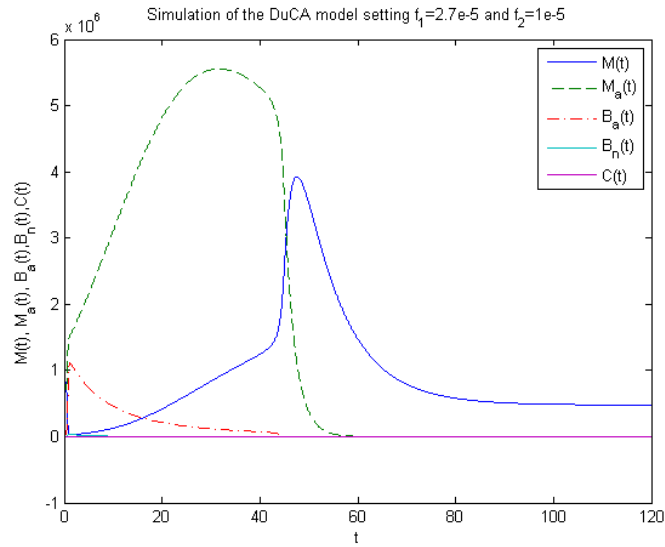


Figure 8.6 Simulation of the DuCA model setting $f_1 = 2.7 \times 10^{-5}$ and $f_2 = 1 \times 10^{-5}$, corresponding to the region where all the nontrivial fixed points are unstable (see figure 8.1). We see that the activated macrophages exhibit a burst of growth from their initial conditions. This large inflammatory response eventually goes down towards the HRS.

that, at any given f_1 , we only see a one-dimensional slice of something that happens in five dimensions, and that we are only doing a codimension one analysis, so what we are witnessing may be something that is actually a codimension two (or higher) bifurcation.

By doing simulations using values of f_1 , and initial values of M_a , in the region with two unstable nontrivial fixed points, we have observed that the concentration of activated macrophages exhibits a growth burst from its initial conditions, cf. figure 8.6, until it peaks after which it returns to the HRS. Some might have expected that we would see a continuously growing concentration because we are above the repelling NOD_{f_1} -LUB, but when we think about this in terms of the biological system the behavior is not surprising. When the system suddenly contains a large number of activated macrophages, it does not matter if they have a slow phagocytosis rate, i.e. $f_2 = 1 \times 10^{-5}$, since they have strength in numbers, adding to this is the fact that the resting macrophages have a high phagocytosis rate – it is after all this rate we increase to induce bifurcations. This means that the concentration of apoptotic β -cells is quickly depleted to the point of extinction, and when there are no apoptotic β -cells around the resting macrophages can no longer become activated. Hence we observe a drop in the concentration of active macrophages.

We can also think about it mathematically. After the Hopf bifurcation the NOD_{f_1} -USB has three negative eigenvalues. Which implies that it is attracting from these eigendirections – this could explain the growth towards a higher concentration that occurs initially. But when the flow nears the fixed points on the NOD_{f_1} -USB it will be repelled from them after which it (the flow) will go toward the only stable fixed point

that is left, i.e. the HRS. We could also look at the equation that describes the rate of change in the concentration of activated macrophages; cf. equation 5.8. There we see the damping term given by $-e_2 M_a (M + M_a)$ which becomes dominating when M_a becomes high – this prevents the concentration from diverging.

As mentioned there is a theoretical possibility that other branches of fixed points could exist in-between the NOD_{f_1} -USB and the NOD_{f_1} -LUB though the flow seems to speak against it. Even so, we have done many simulations with different initial values for M_a , and different values of f_1 in the area that is bordered by the unstable NOD_{f_1} -USB and the NOD_{f_1} -LUB, and every single one of them exhibit a behavior that is in qualitative agreement with figure 8.6, so we find it to be unlikely that there are any additional fixed points in this area.

The fact that we find it unlikely that any stable fixed points exist in the area mentioned above, and the behavior seen in figure 8.6 led us to wonder what else could be going under in the area under scrutiny. We suspect that so-called *heteroclinic orbits* – that is an orbit, that connects one saddle-point with another saddle-point – inhabits this domain. Heteroclinic orbits arise when the stable manifold of a saddle-point intersects the unstable manifold of another saddle-point (Guckenheimer and Holmes, 2002, p.22). The behavior of the concentration of active macrophages shown in figure 8.6 corroborates the existence of such orbits. Let us assume that there are indeed heteroclinic orbits connecting the fixed points on the NOD_{f_1} -LUB to those on the unstable part of the NOD_{f_1} -USB, and let us further assume that we could start our flow directly on the unstable manifold of the fixed points on the NOD_{f_1} -LUB then for $t \rightarrow \infty$ the flow would approach the unstable fixed points on the NOD_{f_1} -USB. This is because the unstable manifold is invariant, so the flow cannot leave it when it has started there. We have tried to illustrate this in figure 8.7. The figure represents a slice of the 5-dimensional phase space.¹⁰ The stable fixed point, HRS, is represented by the full dot while the saddle-points, NOD_{f_1} -LUB and NOD_{f_1} -USB, are represented as black circles with white interior. There is a heteroclinic orbit from the NOD_{f_1} -LUB to the NOD_{f_1} -USB, along with some representative manifolds, and arrows designating the flow. On the orbit is a point that represents an optimal starting condition; i.e the point represents a set of initial conditions that would let us establish the existence of heteroclinic orbits graphically. But since we are not able to determine the unstable manifold analytically it is next to impossible to start precisely on the unstable manifold of the NOD_{f_1} -LUB, therefore the flow initially tends to the unstable fixed points on the NOD_{f_1} -USB, and then becomes repelled from them¹¹ the nearer it comes, and is led down to the HRS along the unstable manifold of the NOD_{f_1} -USB, which is depicted by the dashed line. We have made the line dashed to illustrate that its path may not be in the 2-dimensional plane.

The existence of heteroclinic orbits would be very interesting for one reason in particular: the existence of heteroclinic orbits opens up for the possibility of a global bifurcation (Guckenheimer and Holmes, 2002, p.290). Furthermore heteroclinic orbits would act as a constant reminder that the flow is *not* 1-dimensional

¹⁰ Please be aware that this figure is for illustrative purposes only, and does not represent an exact slice of the phase space! I.e. the figure only gives a qualitative gist of how the flow might behave.

¹¹ To avoid confusion we would like to restate, that for each f_1 there is only one fixed point on the USB!

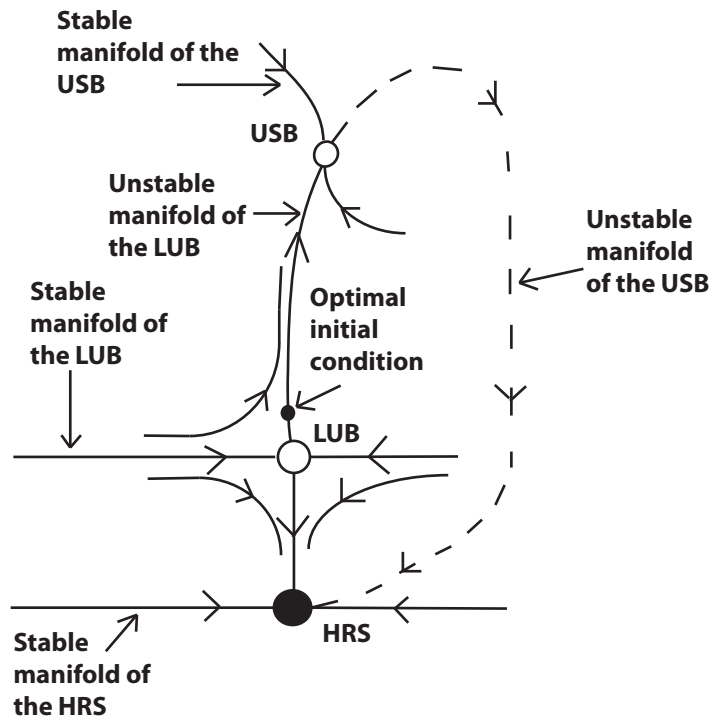


Figure 8.7 An illustrative figure of the flow in phase space after the Hopf bifurcation has occurred. The point named “optimal initial condition” would flow along the unstable manifold of the NOD_{f_1} -LUB to the USB.

After the saddle-node bifurcation where the two nontrivial unstable fixed points collide, and annihilate, only the HRS remains.

Hidden features in figure 8.1

We promised earlier in this section that we would return to the events surrounding the Hopf bifurcation. We intend to do this now. For we discovered that there is actually more to the story than figure 8.1 reveals! The discovery came about when we wanted to determine if the stable part of the NOD_{f_1} -USB was attracting for arbitrarily large initial values of M_a . We also wanted to make sure that there was no pathological behavior when we used initial values that were lower than the concentration at the NOD_{f_1} -USB. In short: we wanted some insight into the basin of attraction of the (stable part of the) NOD_{f_1} -USB in terms of M_a .

We found that initial values for M_a that are beneath the stable concentration induced the behavior we had expected. This is not the interesting part, the interesting part comes from initial value of M_a that is slightly above the stable concentration, combined with an f_1 that is close to the Hopf bifurcation point. Here we found that the phase

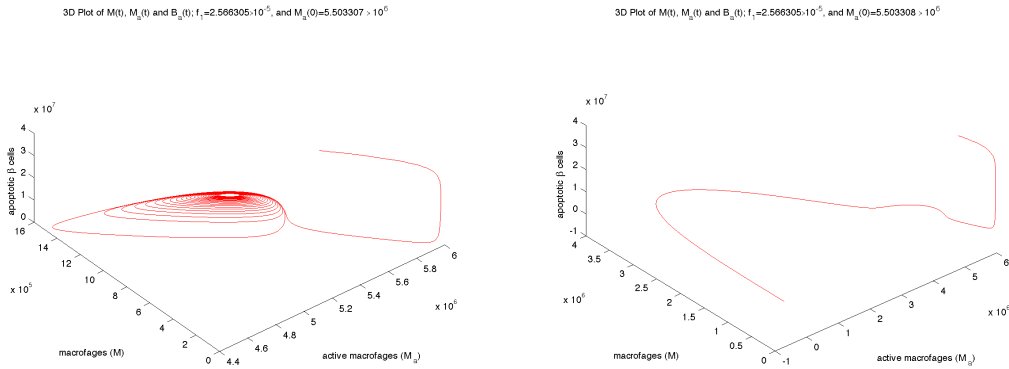


Figure 8.8 To the left we see a stable spiral, that settles down to the NOD_{f_1} -USB. The simulation is based the initial values $(M, M_a, B_a, B_n, C) = (4.77 \times 10^5, 5.503307 \times 10^5, 4 \times 10^7, 0.001, 0.001)$ and $f_1 = 2.566305 \times 10^{-5}$. To the right the initial value for M_a has been changed to 5.503308×10^5 , which makes the flow go to the HRS.

space curve does not exhibit stable spirals, rather it converges to the healthy rest state; cf. figure 8.8.

This observation spawned an investigation of how large an initial value M_a should have at a given f_1 if we wanted the flow to go to the HRS. The investigation was done simply by choosing a value for f_1 , e.g. $f_1 = 0.5 \times 10^{-5}$, and then determining the approximate initial value of M_a that would make the flow go to the HRS rather than the NOD_{f_1} -USB. The value was approximated, in a very pedestrian way, by choosing a very high initial value, e.g. $M_a = 25 \times 10^6$ for $f_1 = 0.5 \times 10^{-5}$, that would make the flow go to the HRS. Then we would know that the demarcation value of M_a would be somewhere between this value, and the value associated with the NOD_{f_1} -USB for that given f_1 . Then it was merely a matter of making guesses that were closer and closer to the concentration at the NOD_{f_1} -USB, and run simulations in MATLAB, until at some point the flow would converge to the NOD_{f_1} -USB again. When the demarcation value of M_a had been approximated to a satisfactory amount of decimals for one value of f_1 , the procedure was repeated for a new value of f_1 up to the value of f_1 at which the flow undergoes a Hopf bifurcation. Initially we thought that what we had found was a new line of unstable fixed points hence we called it the upper unstable branch (UUB). However we cannot be certain of this. The line we call UUB may be a separatrix since it separates two regions of phase space in which the flow behaves qualitatively different. Nonetheless we will keep the name in the following.

We discovered that for smaller and smaller f_1 's we need to make the initial value of M_a larger and larger – which is not a big surprise when we think about it biologically. For f_1 close to the bifurcation value the UUB is very near to the NOD_{f_1} -USB. We found that the concentration needed to make the flow tend to the HRS decreases approximately exponentially with f_1 .

In figure 8.9 we have modified the original bifurcation diagram, figure 8.1, to include

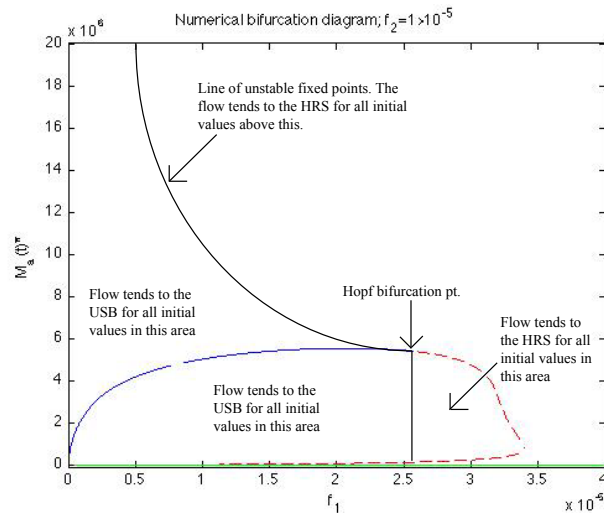


Figure 8.9 Shows a modified version of figure 8.1, where we have added a curve that approximates the UUB. We have also added legends to facilitate the overview.

a curve that approximates the UUB.¹² We have also added text to explain how the flow behaves for different initial M_a -concentrations. We see that the UUB and the NOD_{f_1} -USB ultimately coincide. This appears in the eigenvalues of the NOD_{f_1} -USB approximately with the advent of positive eigenvalues. We dare not state that it is exactly when the eigenvalues become positive. If the UUB is in fact a line of unstable fixed points then the collision between the NOD_{f_1} -USB and the UUB is basically a (presumably degenerate) sub-critical pitchfork bifurcation – an unstable and a stable fixed point coalesce to produce one unstable fixed point.

We have speculated if the UUB constitutes a section of the unstable limit cycle that

¹² Notice that though we used MATLAB to approximate the demarcation values, the UUB-curve shown in figure 8.9 is not made with MATLAB it was drawn using Adobe Illustrator CS3.

should surround the stable spirals that arise at $f_1 \approx 2.15 \times 10^{-5}$, but we have not been able to verify this through simulations. When we discovered the UUB we realized that

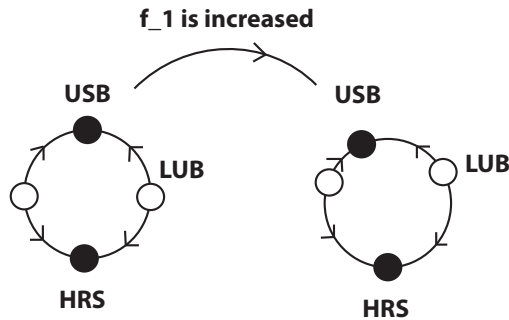


Figure 8.10 The flow of M_a represented on a circle with two stable and two unstable fixed points. The fixed point without a label is the UUB. As f_1 increases the NOD_{f_1} -USB and the UUB draw closer together (depicted on the right circle).

the flow in terms of M_a , can be envisioned as the flow on a circle with four fixed points. Two stable and two unstable. We have depicted this in figure 8.10. From the left circle to the right f_1 is increased. Increasing f_1 further would make the NOD_{f_1} -USB and the UUB meet, to become a saddle-point, that is repelling in the direction of the HRS, and attracting from the side of the NOD_{f_1} -LUB.

A final thing that should be mentioned about figure 8.1 is that it tells us that the system is irreversible with respect to changes in f_1 . In other words hysteresis occurs. This happens as f_1 exceeds a threshold value that is identical to the Hopf bifurcation value. This suggests that we have a subcritical Hopf bifurcation (Strogatz, 2000, p.252). However, if we want to make sure that this is indeed the case we must bring our system to normal-form and find the adhering coefficients. This is a substantial undertaking for a 5-dimensional system which we have not ventured, though it is not impossible; cf. e.g. Yu (1997).

The Balb/c bifurcation diagram

Now let us turn to the bifurcation diagram in which $f_2 = 5 \times 10^{-5}$. This bifurcation diagram differs from figure 8.1 (as well as those to come) by having two additional unstable curves of fixed points, illustrated by the dotted line (black) and the dashed-dotted line (magenta). Figures B.8 and B.9 in appendix B.2 provide the eigenvalue

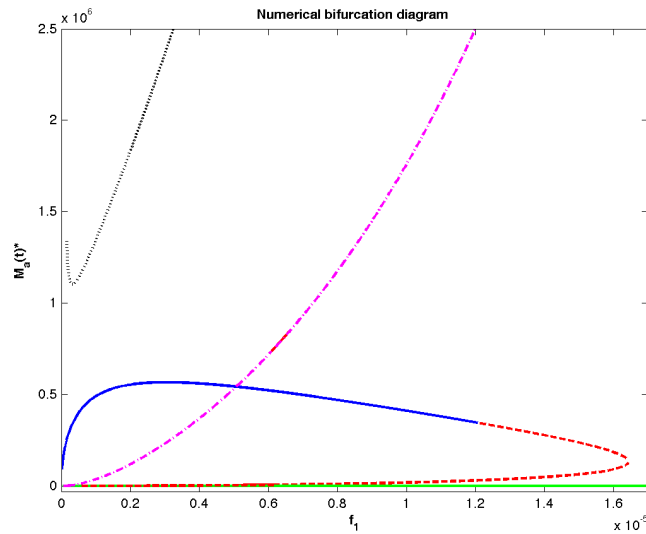


Figure 8.11 Bifurcation diagram for the DuCa model using f_1 as the bifurcation parameter and Balb/c parameters. The solid and dashed lines represent stable and unstable fixed points respectively. The system is bistable in the range $(0; 1.206 \times 10^{-5})$ with the Balb/ c_{f_1} -LUB separating the region where the flow will approach the Balb/ c_{f_1} -USB and the region where it will tend to the HRS. For $f_1 > 1.206 \times 10^{-5}$ only the healthy rest state remains stable.

diagrams for the black and magenta lines respectively. The fixed points illustrated by the dotted line exist only for negative values of M , B_a and B_n and C . For the fixed points illustrated by the dashed-dotted line it is mostly M and B_a that have negative values. In other words these curves are physiological irrelevant, but we have included them nonetheless to illustrate that (in this one case) we have succeeded in finding more than three solutions, with MATLAB. Please be aware that the curves do not intersect the Balb/ c_{f_1} -USB – it seems so because we are projecting something that occurs in a 6-dimensional space (the five concentrations and f_1) onto the $M_a f_1$ -plane. What it does tell us is that there are two different fixed points associated to the value of M_a where the magenta curve crosses the Balb/ c_{f_1} -USB – one where all the concentrations are positive and f_1 is approximately 0.5×10^{-5} , and one where M_a , B_n and C are positive while M and B_a are negative.

According to Marée et al. (2006) f_1 lies in the monostable region ($f_1 = 2 \times 10^{-5}$ for Balb/c-mice), in agreement with the nonpermanent inflammation observed in Balb/c-mice.

8.3 Using f_2 as the bifurcation parameter

Figure 8.12 shows the bifurcation diagram for $f_1 = 1 \times 10^{-5}$, and f_2 as the bifurcation parameter. First of all we remark that f_2 is estimated to be within the bistable region ($f_2 = 1 \times 10^{-5}$ for NOD-mice), so it agrees with the fact that a chronic inflammation

for NOD-mice is reached, when the apoptotic wave stimulates the system to exceed the threshold concentration that corresponds to unstable fixed points. We notice that the

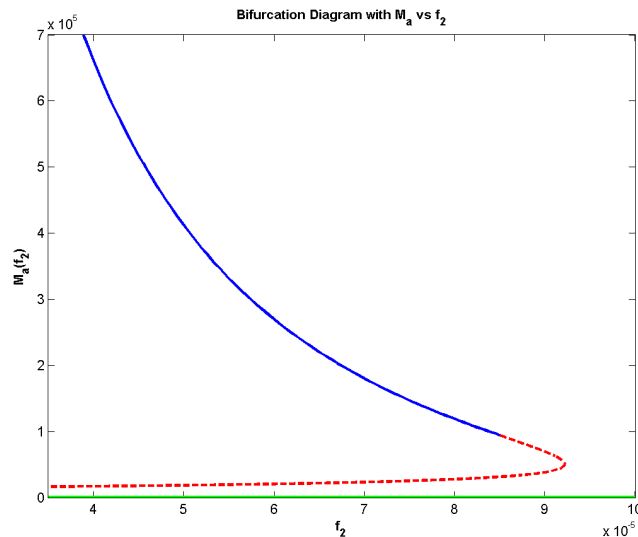


Figure 8.12 Bifurcation diagram for the DuCa model using f_2 as the bifurcation parameter and NOD parameters. The solid and dashed lines illustrate stable and unstable fixed points respectively. The x-axis has been chosen such that the change in stability is apparent – leaving out the monotonic part for $f_2 < 4 \times 10^{-5}$. The system is bistable in the (approximate) range $[0; 8.5 \times 10^{-5}]$ with a “line” of unstable fixed points to separate the two regions. For $f_2 > 8.5 \times 10^{-5}$ only the healthy rest state remains stable.

behavior has some similarities as well as differences from its f_1 -counterpart in figure 8.1. Let us start with the resemblances.

Again we start out by having three stability branches; two stable and one unstable – $M_a = 0$ being one of the stable branches. These change into two unstable and one stable (at $f_2 \approx 8.5 \times 10^{-5}$), and eventually the two unstable branches coalesce in a saddle-node bifurcation (at $f_2 \approx 9.25 \times 10^{-5}$) after which only the healthy rest state remains. Finally both figures exhibit hysteresis. These are the superficial similarities we can gather from a quick glance at figure 8.12.

The dissimilarities are easily spotted. First of all, the nontrivial line of stable fixed points decreases as f_2 is increased, and changes stability at a much lower M_a -value than was observed when we used f_1 as the bifurcation parameter. If we return to the biological setting for a moment then this makes excellent sense. The active macrophages still come from the pool of resting macrophages. Now, since f_2 is the phagocytosis rate of the active macrophages, turning up f_2 means that a fewer amount of active macrophages are needed to handle the same amount of apoptotic β -cells, but during the initial apoptotic wave a significant recruitment of active macrophages from the resting pool will still take place. This together with the enhanced phagocytic ability implies that the apoptotic β -cells will be decimated quickly, thus leading to a drop in the number of

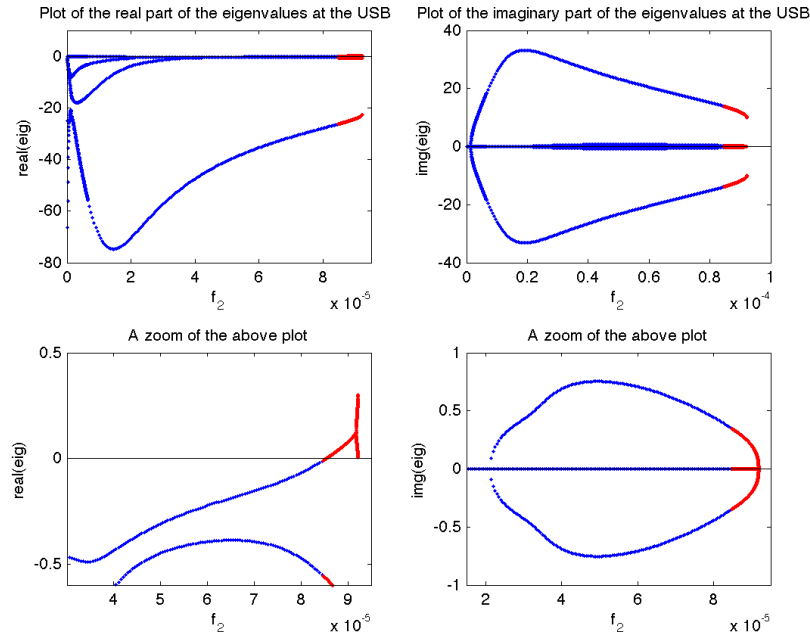


Figure 8.13 Gives an overview of how the real and imaginary parts of the eigenvalues behave on the NOD_{f_2} -USB as f_2 is increased.

resting macrophages that become activated. However due to the slow initial activation of the resting macrophages and the, though increased, insufficient phagocytic ability of the activated macrophages, the population of apoptotic β -cells, and hence necrotic β -cells, have already established themselves due to the cytokine-induced β -cell death, though the populations become stable at a lower concentration than for $f_2 = 1 \times 10^{-5}$. Ultimately as f_2 attains a certain value the increased phagocytic ability of the activated macrophages becomes sufficient to compensate for the slow activation.

Looking at figure 8.13, which provides the behavior of the real and imaginary parts of the eigenvalues along the upper stable branch of the f_2 -bifurcation diagram, NOD_{f_2} -USB, we find similarities additional to the superficial ones. Again two real eigenvalues coalesce with the emergence of two complex eigenvalues, that maintain a negative real part throughout the entire interval, for the fixed points along the upper stable branch; seen on the upper left subplot.¹³ And again an additional pair of complex eigenvalues arise. A pair that ultimately cross the imaginary axis to become eigenvalues with positive real parts. Thus a Hopf bifurcation also occurs when we use f_2 as the bifurcation parameter. The behavior of the eigenvalues, the type of fixed point, and the dimension of the stable unstable manifolds for f_2 in different intervals is given in table 8.3.

The lower unstable branch of the f_2 -bifurcation diagram (NOD_{f_2} -LUB) also displays

¹³ This may be impossible to make out from the subplot, but the real part of the eigenvalues is the one that start at approximately minus 20 which is also the approximate final value of the real part.

$f_2 \in$	$(0; 1.4 \times 10^{-1})$	$(1.4 \times 10^{-1}; 2.15)$	$(2.15; 8.544)$	$(8.544; 9.184)$	$(9.184; 9.2205)$
Nr. $\lambda \in \mathbb{R}^+$	0	0	0	0	2
Nr. $\lambda \in \mathbb{R}^-$	5	3	1	1	1
Nr. $\lambda \in \mathbb{C}(Re(\lambda))$	0	2(-)	4(-)	2(-), 2(+)	2(-)
Fixed pt.	S	SS	SS	SP	SP
Dim(W^s)	5	5	5	3	3
Dim(W^u)	0	0	0	2	2

Table 8.3 Gives an overview of the eigenvalues, and the behavior of the fixed points on the NOD_{f_2} -USB. “S” stands for stable, “SS” stands for stable spiral, and “SP” stands for saddle-point. $\text{Dim}(W^s)$ is the dimension of the stable manifold, and $\text{Dim}(W^u)$ is the dimension of the unstable manifold. All intervals are in the order of 10^{-5} , and all values are approximate.

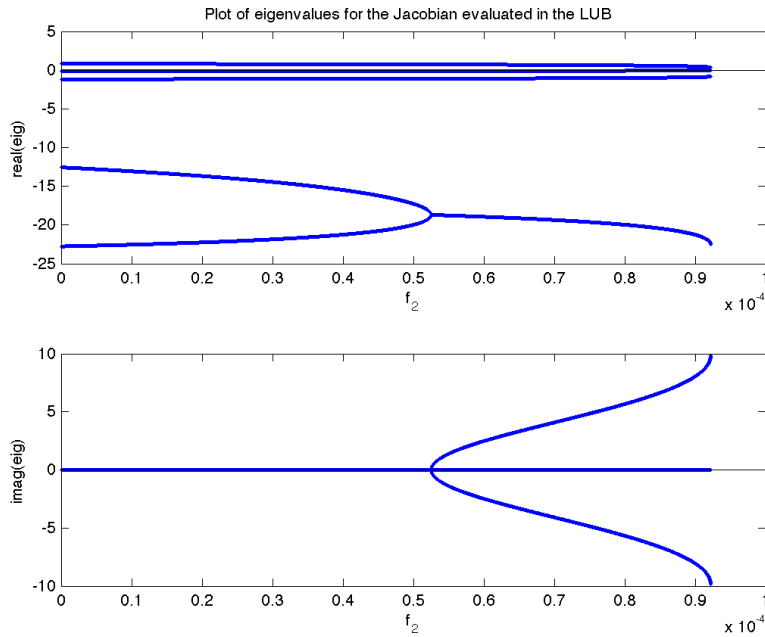


Figure 8.14 The real (upper subplot) and imaginary (lower subplot) parts of the eigenvalues of the fixed point along the NOD_{f_2} -LUB.

features similar to the NOD_{f_1} -LUB. The behavior of the eigenvalues is less erratic for the eigenvalues along the NOD_{f_2} -LUB, than along the NOD_{f_2} -USB, as we see when we compare table 8.4 to table 8.3. The bifurcation diagram for f_2 with Balb/c parameters is given in figure 8.15. We clearly see that for the value of f_2 that Balb/c-mice have inflammation is non-persistent, in agreement with what we would expect. The way the concentration of active macrophages decreases along the Balb/c f_2 -USB makes it look similar to figure 8.12, but we see that the shift between a stable and an unstable USB comes at a much lower f_2 -value when we use the Balb/c-value for f_1 .

As we did in the case of the NOD-mice we have also searched for additional fixed

NOD $_{f_2}$ -LUB		
$f_2 \in$	(0;5.255)	(5.255; 9.2205)
Nr. $\lambda \in \mathbb{R}^+$	1	1
Nr. $\lambda \in \mathbb{R}^-$	4	2
Nr. $\lambda \in \mathbb{C}(Re(\lambda))$	0	2(-)
Fixed pt.	SP	SP
Dim(W^s)	4	4
Dim(W^u)	1	1

Table 8.4 Gives an overview of the eigenvalues, and the behavior of the fixed points on the NOD $_{f_2}$ -LUB. “S” stands for stable, “SS” stands for stable spiral, “USS” stands for unstable spiral, and “SP” stands for saddle-point. Dim(W^s) is the dimension of the stable manifold, and Dim(W^u) is the dimension of the unstable manifold. All intervals are in the order of 10^{-5} , and all values are approximate.

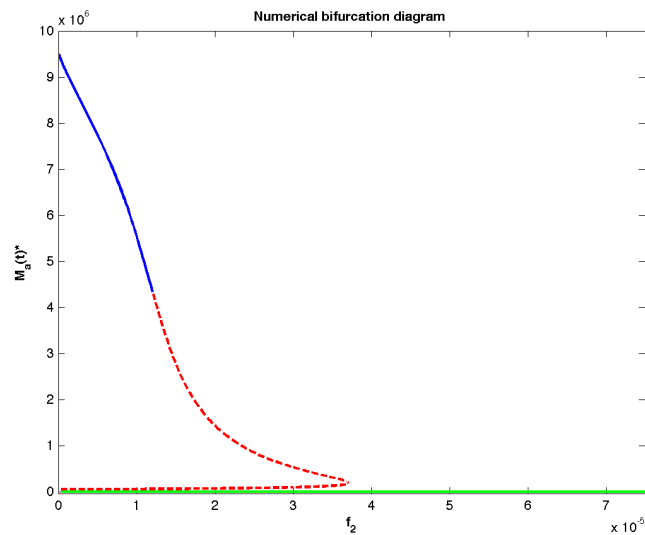


Figure 8.15 Bifurcation diagram for the DuCa model using f_2 as the bifurcation parameter and Balb/c parameters. The solid and dashed lines illustrate stable and unstable fixed points respectively. The system is bistable in the (approximate) range $(0; 1.21 \times 10^{-5})$ where the Balb/c $_{f_2}$ -LUB separates the two regions. For $f_1 > 1.21 \times 10^{-5}$ only the HRS remains stable. f_2 is estimated to be within the monostable region ($f_2 = 5 \times 10^{-5}$ for Balb/c-mice) so the diagram agrees with the nonpermanent inflammation observed for Balb/c-mice.

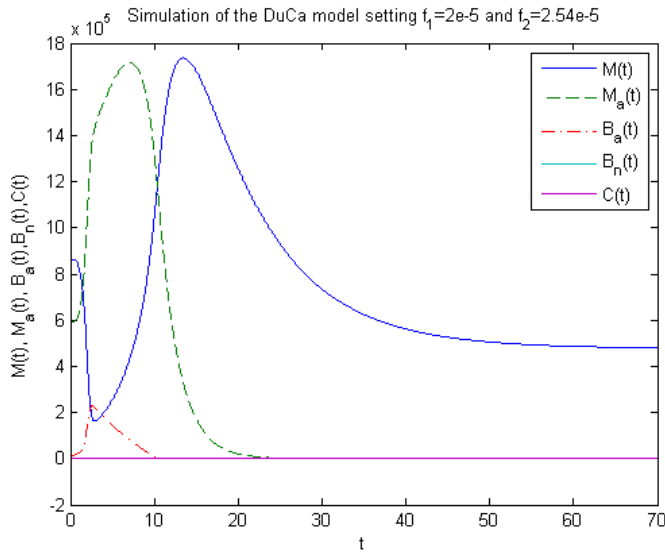


Figure 8.16 Simulation of the DuCa model setting $f_1 = 2 \times 10^{-5}$ and $f_2 = 2.54 \times 10^{-5}$, corresponding to the region where all the nontrivial fixed points are unstable; cf. figure 8.15. It can be seen that the activated macrophages exhibit a burst of growth from their initial conditions. This large inflammatory response eventually goes down towards the stable healthy rest state.

points in the region where the B_{alb}/c_{f_2} -USB is also unstable. Figure 8.16 shows one of these simulations. We see that the behavior is similar to the behavior we witnessed in figure 8.6.

8.4 Reducing the DuCa-model

Marée et al. (2006) suggests using a QSS assumption on dB_n/dt and dC/dt . Setting $dC/dt = 0$ leads to the following expression for the cytokines

$$C_{(QSS)} = \frac{\alpha}{\delta} B_n M_a \quad (8.3)$$

And the QSS on dB_n/dt leads to the expression for B_n

$$B_{n(QSS)} = \frac{dB_a}{f_1 M + f_2 M_a} \quad (8.4)$$

By plugging equation 8.3 and 8.4 into the equation for dB_a/dt reduces the number of equations to three

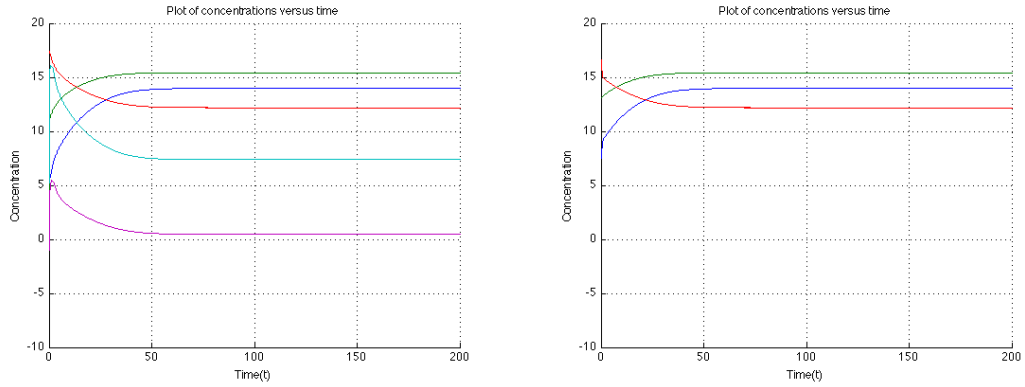


Figure 8.17 On the left we have the original five dimensional DuCa model, on the right the reduced three dimensional DuCa model. We see that despite some minor initial differences the curves are interchangeable.

$$\frac{dM}{dt} = a + (k + b)M_a - cM - f_1MB_a - e_1M(M + M_a) \quad (8.5)$$

$$\frac{dM_a}{dt} = f_1MB_a - kM_a - e_2M_a(M + M_a) \quad (8.6)$$

$$\frac{dB_a}{dt} = W(t) + \frac{A_{max}dB_aM_a}{k_b(f_1M + f_2M_a)} - f_1MB_a - f_2M_aB_a - dB_a \quad (8.7)$$

Figure 8.18 shows a bifurcation diagram of this reduced model with f_1 as the bifurcation parameter. The similarities with figure 8.1 are striking, but this may not come as a surprise since the positions of the fixed points are expected to be the same because the QSS assumption of course holds in the fixed points. The real test is to see if the solution curves of M , M_a and B_a change under this assumption. As we can see in figure 8.17 there is not much difference, if any.

But how else could we justify making a QSS assumption. The answer lies in the eigenvalues of the full system versus those of the reduced system. Let us digress to the example where we looked at the general solution to 7.2; given by equation 7.3.

For the sake of argument let us assume that we have a two-dimensional system, and that both the eigenvalues are negative and not too different in magnitude. We know that in reality another component play a part in the behavior of system. Thus in reality we need an extra equation, which describes this extra component. At the same time we are aware that this makes the stability analysis more cumbersome. Thus we would like to know if it would be reasonable to make a QSS assumption on the extra equation, so we would be back in 2D land. To figure this out we add the extra equation, and take a look at the corresponding characteristic polynomial for the now three-dimensional system. If the new eigenvalue is significantly more negative than the others, then the solution curve associated with this eigenvalue will stabilize much faster than the two others. In fact the solution curve associated with this very negative eigenvalue will tend to the stable manifold spanned by the eigenvectors of the two other eigenvalues as an

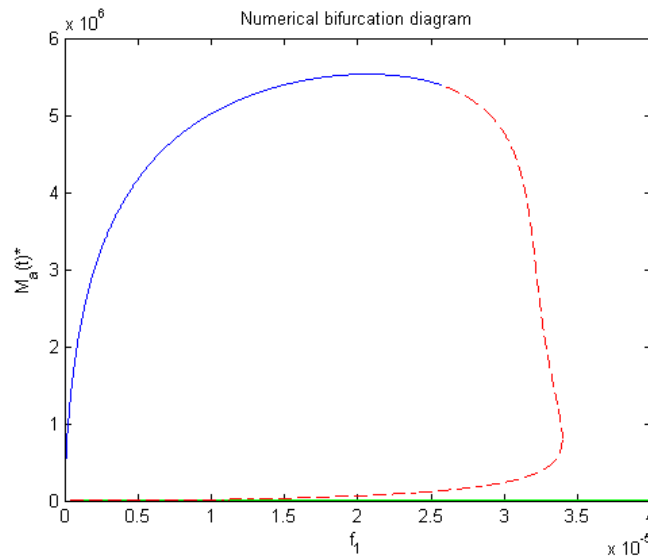


Figure 8.18 Bifurcation diagram for the three dimensional version of the full model using NOD parameters (see table 5.1). The diagram shows the fixed points of M_a when using f_1 as the bifurcation parameter. The solid and dashed lines illustrates stable and unstable fixed points respectively. We see that the system is bistable in the approximate range $(0 - 2.57 \times 10^{-5})$ with a “line” of unstable fixed points to separate the two regions. For $f_1 > 2.57 \times 10^{-5}$ only the healthy rest state remains stable.

exponential function raised to the power of the eigenvalue. This means that adding the extra equation does not contribute any new information about the system after a given amount of time (which depends on the magnitude of the eigenvalue) has transpired. By then the dynamics of the system will be governed by the two other eigenvalues. Thus when this is the case we can justify applying a QSS to the equation that describes the rate of change of the variable we introduced lastly.

In our case this is exactly the case, though the story is reversed. We started out with 5 equations in the DuCa model, and wanted to know if three would suffice; using QSS assumptions on the last two.

Furthermore the value of the remaining fixed points do not change significantly which again indicates that the QSS assumptions are sound approximations.

The stability analysis of the fixed points reveals that the behavior of the eigenvalues are less complicated than in the five dimensional case; cf. figures B.18-B.22 in appendix B.5. The unstable fixed points in the LUB are now rid of complex eigenvalues, while the set of large, negative and complex eigenvalues that were associated with USB have also gone. The LUB still serves as a separatrix that divides the region of nonpermanent inflammation from the region of chronic inflammation. The Hopf bifurcation still happens as the stable nontrivial fixed points become unstable and the saddle-node bifurcation is also present.

Now that we have learned that the behavior of the reduced DuCa model is very much

like the full DuCa model a natural question comes to mind: why did we devote so much of our time to analyzing the full DuCa model rather than the reduced 3-dimensional version? The answer is that in order to compare the reduced DuCa model to the full DuCa model we needed to produce bifurcation diagrams for the full DuCa model. These were immensely time-consuming to produce, especially due to the trial-and-error approach we used to make initial guesses when using the Newton-Raphson method. Another question one might ask is: why did we not use the reduced model to perform an analytical analysis based on f.x. the Routh-Hurwitz criteria? We actually tried to do this, but the Michaelis-Menten term in the reduced DuCa model makes it extremely hard to obtain anything that will provide new information.

9 Discussion of the Bifurcation Analysis

In chapter 8.1 we presented bifurcation diagrams and some diagrams showing how the eigenvalues behaved with increasing f_1 and f_2 in the NOD-bifurcation diagrams. In this chapter we will give a summary of our analysis, discuss our findings, relate them to the underlying biological system and comment on question I-III of the thesis statement. Finally we will touch upon subjects for future work.

By conducting a bifurcation analysis we obtained information about how much f_1 and f_2 needed to be tweaked to induce bifurcations. Both the NOD- and Balb/c-diagrams revealed the existence of (what inspection of the eigenvalues revealed to be) a Hopf-bifurcation, which indirect results, e.g. hysteresis, suggest is sub-critical. In addition all figures also contained a bifurcation that consisted of two branches of saddle-points amalgamating, as well as the possibility of bistability – the Hopf-bifurcation point serves as the demarcation point between bi- and mono stability.

When using NOD parameters the chosen bifurcation parameter, f_1 or f_2 , lies within the parameter span where the model shows bistability: a stable healthy rest state (the HRS) and a stable upper nontrivial fixed point (the USB) that is associated with the chronic inflammation that is observed in NOD-mice; cf. figure 8.1 and 8.12. Between these is an unstable nontrivial fixed point (the LUB). This configuration accounts for the NOD behavior, i.e. they develop a chronic inflammation because the unstable fixed point is exceeded during the apoptotic wave, thus making the flow tend to the USB.

The phagocytosis rates Marée et al. (2006) have used in the DuCa model come from several experiments. We discussed this in section 5.8 where we also provided different values of f_1 and f_2 as given in the different articles of Marée et al.; cf. table 5.2. The different values along with their standard errors are important in determining if any qualitative change occurs for physiologically realistic parameter-values. The standard error for f_1 was $< 0.005 \times 10^{-5}$ (not included in table 5.2), and the most extreme f_2 -value we could come across was 1.02×10^{-5} in NOD-mice. This value was associated with a standard error of 0.01×10^{-5} . When we compare these values to the f_1 - and f_2 -values at which the Hopf-bifurcations, $\sim 2.57 \times 10^{-5}$ and $\sim 8.5 \times 10^{-5}$ respectively, take place we find that no NOD-mouse that have phagocytosis rates in the intervals given in table 5.2 will escape chronic inflammation following the apoptotic wave.

We know that not all NOD-mice become diabetic. But how can that be if the standard errors do not permit any NOD-mouse to supersede the Hopf-bifurcation value? For one thing the macrophages used in the various experiments of Marée et al. were from female mice – we learned in chapter 2 that 80 % of the female mice develop T1D against only 20 % of the male mice. In addition O'Brien et al. (2002) find that macrophages from male NOD-mice have a higher phagocytic capacity during the first 2 weeks of life (O'Brien et al., 2002, p.2483). At week 3 the phagocytic ability of the female NOD-mice is leading, but at this point the apoptotic wave has already set things in motion, and

the inflammation is irreversible. Besides these results the experiments that were used to obtain the phagocytosis rates were *in vitro* experiments, how this exactly affects the macrophages we do not know. It would be interesting to obtain f_1 - and f_2 -values from male NOD-mice to see if their mean value is above the Hopf-bifurcation value.

Hence when we compare the phagocytosis rates to the values at which the Hopf-bifurcations occur, we find that based on the parameter values from (female) NOD-mice the DuCa-model is sound in the sense that no bifurcations occur within a physiologically reasonable range.

So far we have used the NOD-bifurcation diagrams to discuss if bifurcations occur in f_1 - and f_2 -intervals that are close to the estimated f_1 - and f_2 -values, and found that this is not the case. Now, let us see what extra information we can gather from the diagrams. For instance, from a medical point of view, it would be interesting to know which of the phagocytosis rates it is most opportune to manipulate with stopping the inflammation in mind. Comparing figure 8.1 to 8.12 we conclude that, if we can only adjust one of the phagocytosis rates in the NOD bio-model, enhancing f_1 is most efficient. By this we mean that f_1 needs “only” be changed to little more than 2.57×10^{-5} to arrest and reverse any inflammation, whereas f_2 must exceed a staggering 8.544×10^{-5} to induce the same effect. Furthermore, due to the irreversibility, we would only need to enhance the phagocytic ability of the resting macrophages until they had phagocytized enough apoptotic β -cells, as to make the concentration of activated macrophages drop beneath the NOD $_{f_1}$ -LUB.

While we are in the area of inferring treatment strategies from the bifurcation diagram, we saw in figure 8.9 that there was more to figure 8.1 than had revealed itself from our method of producing bifurcation-diagrams. What did not reveal itself was the so-called upper unstable branch, or the UUB. The existence of the UUB (be it an unstable fixed point or a separatrix) opens up for a completely novel approach to curing T1D (in NOD-mice).¹ The mathematical analysis tells us, that if the inflammation has reached a chronic/stable stage, then by adding an extra amount of activated macrophages to the inflamed islets we can exceed the UUB thus making the flow tend to the HRS. The specific amount will depend on f_1 . Thus if we are not able to make f_1 exceed the Hopf-bifurcation value, we can (hypothetically) add active macrophages, to achieve a positive outcome, where by positive we mean that the chronic inflammation ceases. On this basis we would like to establish an approximative relation between f_1 and the UUB. Let M_a^+ denote the UUB-curve in figure 8.9, $f_{1,h}$ be the f_1 -value at which the Hopf-bifurcation occurs and $M_{a,h}$ be the M_a -concentration at the Hopf-bifurcation, then we find that

$$M_a^+(f_{1,h}) \approx M_{a,h} \quad (9.1)$$

Furthermore we hypothesize that

$$M_a^+(0) = M_{a,0}^+ \quad (9.2)$$

where $M_{a,0}^+$ is the M_a -value that is needed to make the flow tend to the HRS if we set $f_1 = 0$. We remind the reader that based on calculations done with MATLAB, we found that the UUB decreases approximately exponentially for $f_1 < f_{1,h}$. Thus we guess that

¹ The approach is novel in as much as we have not come across it in our literature studies.

there is an exponential relation between f_1 and the concentration of active macrophages that must be exceeded to induce a non-inflammatory state. We propose

$$M_a^+(f_1) \approx M_{a,h} + (M_{a,0}^+ - M_{a,h}) \times \exp(-h(f_1)) \quad (9.3)$$

For $h(f_1)$ we require

$$\lim_{f_1 \rightarrow f_{1,h}} h(f_1) = \infty, \quad \lim_{f_1 \rightarrow 0} h(f_1) = 0 \quad (9.4)$$

A suitable candidate is

$$M_a^+(f_1) \approx M_{a,h} + (M_{a,0}^+ - M_{a,h}) \times \exp\left(-\left(\frac{pf_{1,h}}{f_{1,h} - f_1} - p\right)\right) \quad (9.5)$$

where $p \in \mathbb{R}^+ \setminus 0$ and $f_1 \in [0; f_{1,h}]$. The slope of the $M_a^+(f_1)$ -curve is determined by which values we use for p .² Based on equation 9.5 we can estimate the concentration that must be added to an NOD-mouse to overcome chronic inflammation; at least in theory. We find the concentration to be $\Delta M_a := M_a^+(f_1) - M(f_1)$. Looking at figure 8.9 we find that at $f_1 = 1 \times 10^{-5}$ we have $M_a^+ \approx 10 \times 10^6$ cells ml⁻¹ and $M_a \approx 5 \times 10^6$ cells ml⁻¹, so at the estimated NOD-value of f_1 we need to add at least 5×10^6 cells ml⁻¹, or double the concentration of activated macrophages, to stop the inflammation. However if we were able to turn the value of f_1 up to, say, 1.5×10^{-5} , then we find $\Delta M_a \approx 1 \times 10^6$ cells ml⁻¹; i.e. a fifth of what was needed at the estimated f_1 -value for NOD-mice.

There are two problems with the expression given in equation 9.5; . First have assumed that $M_{a,0}^+$ is finite, secondly, even though this may be the case, there is still the matter of fitting all the cells into the volume available. If the former is the case, then our mathematical relation between M_a^+ and f_1 is wrong, and the M_a^+ -curve would in this case better be approximated by a hyperbola. However in reality NOD-mice are never born with a phagocytosis rate of 0, so we can more or less disregard this problem, and accept equation 9.5 as a reasonable approximation for the cases where f_1 is not unreasonably small. This allows us to address the second problem. From Poulter and Turk (1975) we obtain an estimate of the volume of a macrophage to be $1450 \mu\text{m}^3$ (Poulter and Turk, 1975, p.198) which converts to 1.45×10^{-9} ml. Hence based on the result of Poulter and Turk (1975) there is room for 689655172 macrophages within 1 ml. So, depending on the volume of the other cells, we will not rule out adding supplementary activated macrophages as a viable mean of inducing health in NOD-mice with chronic islet inflammation; especially if it can be combined with some way of enhancing the phagocytic ability of the macrophages. However it is up to readers with a medical background to check it experimentally.

Please be aware that we under no circumstances claim that the expression for $M_a^+(f_1)$ given in equation 9.5 is canonical. We could just as well have chosen a function of the form

$$M_a^+(f_1) = M_{a,h} + (M_{a,0}^+ - M_{a,h}) \times \exp(-kf_1) \quad (9.6)$$

where k is a constant much greater than 1.

This much we learned from the NOD-bifurcation diagrams. Now let us look at what information can be extracted from the Balb/c-diagrams.

² By using MATLAB to better approximate the UUB-curve at several values of f_1 we could fit equation 9.5 to these data points to obtain to a value for p ; i.e. be more meticulous with the method we used to estimate the UUB in the first place.

The bifurcation diagrams compiled from Balb/c parameters (figures 8.11 and 8.15) reveal that, for the estimated Balb/c-values of f_1 and f_2 , there is only one fixed point, namely the HRS. In essence the macrophages of the Balb/c-mice should be able to overcome any apoptotic wave! This may seem like ludicrous since we could just imagine a wave that would wipe out all of the β -cells thus inducing a very severe case of T1D. However we must remember that such a wave would (probably) never occur, and we should always judge a model based on what it is intended to model, hence, not based on some extreme event that is science-fiction rather than science.

If we are to learn anything from the Balb/c-diagrams, it must be how low the two phagocytosis rates should be (from birth) if chronic inflammation were to appear in Balb/c-mice. Again the phagocytosis rates of the resting macrophages is the one that needs to be modified the least to induce this detrimental change. The difference between chronic inflammation or not appears at $f_1 \approx 1.2 \times 10^{-5}$ when f_2 is kept at 5×10^{-5} .³

An interesting question to raise is: suppose we were mad scientists, and we had found a way of engineering the phagocytosis rates to be higher or lower at birth as we saw fit. Would it then be easier to induce NOD-like behavior in a Balb/c-mouse or could we sooner save an NOD-mouse from the dire future of it's unengineered peers? The bifurcation diagram that reveals the smallest margin between NOD and Balb/c behavior is the one compiled using the Balb/c-value of f_2 with f_1 as the bifurcation parameter (figure 8.11). Here the Hopf bifurcation takes place at $f_1 = 1.21 \times 10^{-5}$ which is 0.79×10^{-5} from the estimated value of $f_1 = 2 \times 10^{-5}$. If we take f_1 -values from other articles into account we find that we are close to loosing our job as mad scientists. In the 2007 article of Marée et al. (Marée et al. (2007)) they give estimates $f_1 = 1.31 \pm 0.05 \times 10^{-5}$ and $f_1 = 1.29 \pm 0.04 \times 10^{-5}$ for their reversible and irreversible models respectively; cf. table 5.3 and the subsection titled "Reversible or irreversible activation?" in section 5.8. Even with these intervals of deviation we are still a little above the bifurcation value, but we must remember that the deviations of ± 0.05 and ± 0.04 are based on several measurements, so it is not entirely impossible that some of the Balb/c-macrophages had a phagocytosis rate that was ≤ 1.21 .⁴ Furthermore there is an uncertainty associated with the step size of f_1 or f_2 when locating the bifurcation value which could shift the result either way.

All in all the DuCa model corresponds well its underlying biological system and it fully works on the premises that were made with it, and it also provides an answer to the hypothesis that it was constructed to investigate. An answer that does not change if the phagocytosis rates are changed within a sensible range. Naturally you can always criticize the choice of assumptions and/or simplifications in a mathematical model, but, without repeating our thoughts from chapter 4 we will state that, fact of the matter is that these are necessary means if you want to be able to model anything.

³ Interestingly enough this is very close to the value at which chronic inflammation occurs upon tweaking f_2 .

⁴ This is also in agreement with the fact that some Balb/c mice develop diabetes.

9.1 Future Work

One thing we unfortunately did not finish in time, and which therefore has been left out, is a codimension two analysis. The purpose of the codimension two analysis was to understand what happens to the stability as f_1 and f_2 are varied simultaneously. From a medical point of view this is interesting because: from figure 8.1 and the adhering eigenvalue plots we know that at the Hopf-bifurcation value of f_1 ($f_{1,h}$) the inflammation becomes non-persistent in the NOD-mouse. Now suppose that biologically we are able to induce an increase in f_1 but we are unable to achieve $f_{1,h}$. Then it would be interesting to know how much f_2 should be changed before we obtain the same effect as if f_1 had been changed to $f_{1,h}$. We should also be able to achieve a (at least in theory) continuous set of points (f_1, f_2) , i.e. a curve, that defines the transition from multistability to only one stable point, namely the healthy rest state.

Needless to say the codimension two analysis is interesting in its own right from a mathematical point of view. However the bifurcation that happens, in all the bifurcation diagrams, as the USB and the LUB amalgamate would be particularly interesting.⁵

More effort could also be put into trying to bring, if not the 5-dimensional DuCa model then, the 3-dimensional DuCa model (not to be confused with the intermediate model) into normal form in order to determine if the Hopf-bifurcation is indeed sub-critical. A couple of articles exist in online form where they provide Mathematica code, albeit a code that is 10 years old, that can put up to 7-dimensional systems into normal form. Furthermore a thorough inspection of the area in the $M_a f_1$ -plane that is bordered by $f_1 = f_{1,h}$, the LUB and the unstable part of the USB would be interesting – but probably time-consuming. Special attention should be devoted to establishing whether or not heteroclinic orbits exist. This is interesting mathematically due to their implications for the global flow.

Before we round off this first section of the thesis we would like to comment on the availability of usable data, which we found was scarce – or we may just be inexperienced in finding. We found it hard to procure usable data to which we could compare the simulations of Marée et al. (2006).⁶ Access to data would also better modelling of, e.g., the apoptotic wave. How a different expression for the apoptotic wave would influence the DuCa model we cannot precisely determine, but we suspect that it will not make much difference in this model, since it is an “all-or-nothing model.” Either the mouse develops T1D or it does not, all it takes is the right composition of parameters and some initial spark that drives the concentration of apoptotic β -cells up, and thus increases the concentration of activated macrophages above the NOD $_{f_1}$ -LUB. However for “patient-specific” model we hypothesize that a better model of the apoptotic wave will be important.

⁵ Should anyone perform this analysis in the future, please let us know.

⁶ This is also a problem when it comes to the expanded model which will be presented in chapter 11.

10 Conclusion 1

For convenience we restate the research questions that we stated in the thesis statement. The questions are

- I Are the parameter values given in Marée et al. (2006) reasonable?
- II Do bifurcations occur when a suitable parameter is varied within a physiologically reasonable range?
- III Is the model sound?

As for question I we discussed the different parameter values in section 5.8, and we find that, the parameters are indeed reasonable.

Question II was treated in the discussion in the previous chapter and we find that we cannot give an exact answer; it depends on how much of an error is associated with the bifurcation-values and which of the phagocytosis rates we choose to stick to. If we answer based on the estimated values from Marée et al. (2006) then the answer is: No, bifurcations do not occur within such a range. However if we choose a Balb/c- f_1 value from one of the other articles, then the answer is: probably some (Balb/c-)mice have phagocytosis rates that lead to T1D, but it is a small portion.

Overall we find that the answer to the third question is: Yes. Indeed some of the assumptions could have used a little more explanation and discussion and we could force unnatural behavior out of the model. But this merited modifications that were unnatural e.g. a Hill coefficient less than 1. So overall we find that the model is sound.

11 Expanding and Modifying the DuCa model

Thus far we have given a thorough description, analysis and critique of the DuCa model. In this next section we will expand the DuCa model in two steps. First by including a compartment of healthy β -cell, and second, by incorporating some recent findings. Instead of just presenting the last model as though it was the first we came up with, we have chosen to include them all as this constitutes a more accurate reflection of the modelling-process.

11.1 Including a Compartment of Healthy β -cells

A natural extension of the DuCa model would be a compartment constituting healthy β -cells, with according changes in the system of differential equations. Including such a compartment also addresses one of the major discrepancies between the progression of diabetes in NOD-mice and how the DuCa model behaves. Remember that in the DuCa model, the reservoir for apoptotic β -cells is *de facto* infinite, but in the NOD-mice there will eventually be no more β -cells left, if no prophylactic measures are taken – the same is in essence true for Balb/c-mice given that they could live long enough.

An equation describing the change in concentration in β -cells should naturally reflect the “real-life” behavior associated with the population of β -cells, so before we try to construct such an equation, let us first define some criteria an expanded model must fulfill and next discuss how we should go about putting together the additional equation based on these criteria.

Model criteria

A mathematical model’s ability to fit data is a necessary but not sufficient gauge for the model’s applicability and soundness. Thus we need a bit more to validate the model(s) to come.

As stated in chapter 4 there must be a correspondence between the physiological system we aim to model and the mathematical model we construct. In our case this correspondence consists of four key-features that our expanded model(s) must live up to (besides the three guidelines stated in chapter 4)

- I In the NOD-mice the β -cells should not be removed at the time where T cells come into play – there must be room for T cells to play an active part in the depletion of β -cells though this will not be included in this thesis.

- II When the amount of β -cells do tend to 0, due to persistent inflammation or natural apoptosis, after a while so must the concentrations of cytokines, apoptotic- and necrotic β -cells as well as the active macrophages.
- III The concentration of β -cells in NOD-mice must die out quicker than in Balb/c-mice.
- IV In the Balc/c-mice, the depletion of β -cells must be due to natural apoptosis only, after the neonatal phase.

I is based on the fact that macrophages, cytokines and apoptotic-, necrotic- and healthy β -cells are not the only cell/protein-types that are involved in the pathogenesis of T1D, as T cells also play a significant part. In NOD-mice they enter the scene after about 4-5 weeks (Trudeau et al., 2003, p.219), and symptoms of T1D become apparent at about 30 weeks of age (Sreenan et al., 1999, p.989). II is a result of the causal relationship between the components of the model – if there are no apoptotic β -cells then resting macrophages cannot become activated, and no apoptotic β -cells can become necrotic – there will be some residual apoptotic cells after the healthy β -cells are gone, so to be very precise it is not until these cells have been phagocytized that all concentrations will tend to zero (except for the resting macrophages). Thus once the deleterious process of β -cells has been completed, the NOD-mice, too, will tend to what we called the HRS in the bifurcation analysis, i.e. $(M, M_a, B_a, B_n, C) = (a/c, 0, 0, 0, 0)$, but in this case it will obviously not be a sign of health, quite the contrary. III serves as a necessary, though not sufficient, condition for the validity of the model. IV is explained below. Because T cells become significant at 4-5 weeks of age, the expanded models, presented below, become more or less unrealistic at the same time; they will not include T cells. However, including several weeks more than 5 in our simulations (and in the adhering figures) makes us more able to determine if the models comply with the criteria.

11.2 First approximation to a governing equation – Model A

At the neonatal stage the behavior of the β -cell mass in NOD-mice is a little more complex than a simple depletion from day one. The pancreas is still undergoing remodeling (Steer et al., 2006, p.262), e.g. the apoptotic wave. But even after these early events and after the perpetual inflammation has begun, data exists that suggests that the inflammation itself stimulates β -cell regeneration (Akirav et al., 2008, p.2883). This could be because some of the cytokines produced in the inflammatory process are anti-inflammatory or benign growth factors (Souza et al. (2008)). This has been disputed by others, whose data indicates a more linear decline in the β -cell population after insulinitis has been established (Akirav et al., 2008, p.2883). However a decrease in the β -cell population is not reserved for those destined to become diabetic. Everybody would be become diabetic at some point, given that they live long enough (Pociot (2009)), due to the natural occurring apoptosis. This is why we have the fourth criterion.

One thing that all parts can agree on is that the β -cells are being removed, so as a first approximation we will use a simple linearly decreasing model for the β -cell population. The equation for the β -cell population, at this stage, is given by

$$\frac{dB}{dt} = -x_1 \tag{11.1}$$

with the initial condition $B(0) = 1 \times 10^9 \text{ cells ml}^{-1}$.¹ Making the β -cell population decline linearly implies that the population will become negative, but it suffices as a first approximation. Notice that x_1 is the naturally occurring apoptosis. By “naturally occurring” we mean that it will go unaffected by factors that will tend to increase the overall apoptosis. Factors that contribute to the overall apoptosis will be added as terms on their own.

As a first approximation to the natural apoptosis we set $x_1 = 10^6 \text{ cells d}^{-1} \text{ ml}^{-1}$, i.e. a million cells terminate through apoptosis every day. This means that if no other factors bare influence on the population, the β -cells will be totally depleted after 1000 days, in comparison a normal laboratory mouse (e.g. Balb/c or C57BL/6J) has a median lifespan of 30 months (Blüher et al., 2003, p.573).

Another thing that has come to be generally accepted is that an apoptotic wave occurs at the neonatal stage in several bio-models (Rooman and Bouwens (2004)), including the NOD- and Balb/c-mouse. However we have to adjust the wave a little to fit into our program. We define

$$W_0(t) = \frac{W(t)}{B(0)} \quad (11.2)$$

to be the adjusted apoptotic wave – Marée et al. (2006) could not make use a wave that was dependent on the concentration of β -cells since they did not include such a concentration. Adding (or rather subtracting) the wave, as given in equation 11.2, we get

$$\frac{dB}{dt} = -x_1 - \frac{4 \times 10^7 \exp(-((t-9)/3)^2)}{B(0)} B = -x_1 - W_0(t)B \quad (11.3)$$

Besides this addition we must include the term that describes the death induced by cytokines. Again we need to recast it to fit our model. We redefine the cytokine induced apoptosis to be

$$\frac{A'_{\max} C}{k_c + C} B \quad (11.4)$$

where $A'_{\max} = A_{\max}/B(0)$. All in all the change in the concentration of healthy β -cells is given by

$$\frac{dB}{dt} = -x_1 - W_0(t)B - \frac{A'_{\max} C}{k_c + C} B \quad (11.5)$$

Adding this equation to the DuCa model (cf. equations 5.6-5.10), and adding the term x_1 to the equation describing the change in concentration of apoptotic β -cells, as well

¹ Here we have chosen the initial condition to be in the high end as readers, endowed with a good memory, may agree to; cf. chapter 2.

as substituting $W_0(t)B$ and $A'_{max}C/(k_c+C)B$ we get

$$\frac{dM}{dt} = a + (k + b)M_a - cM - f_1MB_a - e_1M(M + M_a) \quad (11.6)$$

$$\frac{dM_a}{dt} = f_1MB_a - kM_a - e_2M_a(M + M_a) \quad (11.7)$$

$$\frac{dB_a}{dt} = x_1 + W_0(t)B + \frac{A'_{max}C}{k_c + C}B - f_1MB_a - f_2M_aB_a - dB_a \quad (11.8)$$

$$\frac{dB_n}{dt} = dB_a - f_1MB_n - f_2M_aB_n \quad (11.9)$$

$$\frac{dC}{dt} = \alpha B_n M_a - \delta C \quad (11.10)$$

$$\frac{dB}{dt} = -x_1 - W_0(t)B - \frac{A'_{max}C}{k_c + C}B \quad (11.11)$$

with initial conditions $(M(0), M_a(0), B_a(0), B_n(0), C(0), B(0)) = (4.77 \times 10^5, 0, 0, 0, 0, 1 \times 10^9)$. For future reference we shall call this version of the expanded DuCa model, simply, Model A. Figure 11.1 shows simulations done in MATLAB of Model A – please notice

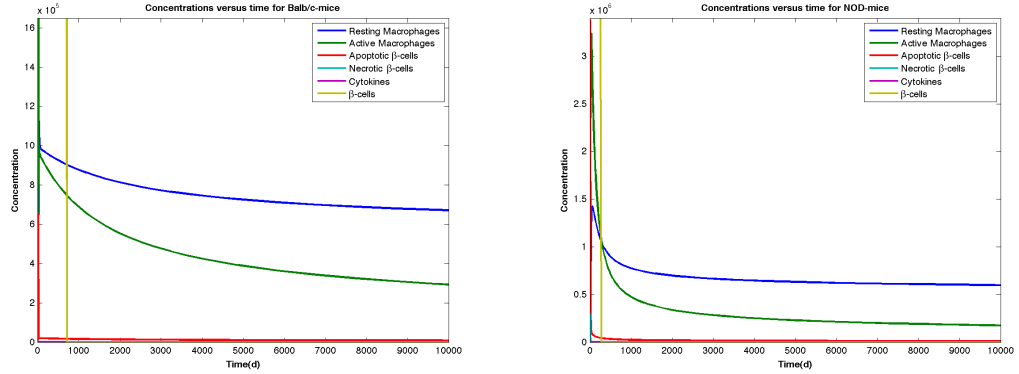


Figure 11.1 Simulation of Balb/c- and NOD-mice with the inclusion of a compartment of healthy β -cells, i.e. equations 11.6-11.11, where the natural apoptosis has been assumed to be constant. Left: the behavior of the concentrations in Balb/c-mice. Right: the behavior of the concentrations in NOD-mice. Initial values are $(M, M_a, B_a, B_n, C, B) = (4.77 \times 10^5, 0, 0, 0, 0, 1 \times 10^9)$.

the difference in scale on the y-axis. On the left we see how the concentrations behave in Balb/c-mice, while on the right we see the concentrations in NOD-mice. The first feature we should take notice of is how many days it takes before the healthy β -cells have all died out. In the Balb/c-mice the β -cells are gone after approximately 800 days, while it only takes about 200 days in an NOD-mouse, after which the concentration becomes negative. This is already a hint that Model A is not the most optimal candidate – the β -cells should *ceteris paribus* not be depleted at 800 days in a Balb/c-mouse, and there should still be some β -cells left in the NOD-mouse at the time when T1D becomes apparent. In addition to this Model A fails to live up to the second guideline

from chapter 4. Nevertheless, let us look at how the other concentrations behave, to see if we find anything instructive or other problems.

The Balb/c-behavior is different from before the compartment of healthy β -cells was added; cf. figure 5.3 for comparison. In particular the concentration of activated macrophages and apoptotic β -cells remains elevated.

The behavior of the concentrations in the NOD-mice has some similarities to the original DuCa model: there is a transient spike in B_n -concentration, the B_a -concentration peaks at ≈ 3.5 cells ml^{-1} . We also see that β -cells still remain at the point where T cells would start contributing to the deleterious process (had they been included in the model). However the β -cell concentration reaches a zero-concentration without the “aid” of T cells, so criterion I is not fulfilled.

Thus there are two immediate reasons why we should discard Model A: 1. the β -cells die out after too few days, 2. the M_a - and B_a -concentrations never tend to zero, which is in breach with criterion II. But we should have expected this! By adding the x_1 -term to equation 11.8 we supply a constant inflow of apoptotic β -cells, which never stops. This in turn provokes the activation of resting macrophages. However, no matter how we add a compartment of healthy β -cells (that undergo apoptosis) we will always observe prolonged elevation of B_a - and M_a -concentration in the Balb/c-mice (as well as in NOD-mice), when we compare it to the original DuCa model.

We should not be discouraged by this result, rather it is an indication that expanding the DuCa model with a compartment of healthy β -cells makes it more akin to what we would observe *in vivo*, since biological systems are seldom in equilibrium (Reynolds et al., 2006, p.224).² This leads us to an important lesson which Model A teaches us.

We must redefine what can be interpreted as healthy behavior, so we can use this as a gauge for the validity of future expanded models; i.e. we need an addendum to our four criteria, that describes how the different concentrations should behave in the Balb/c-mouse.

We are *not* in search of a stable healthy state as in the DuCa model, because, though the cellular concentrations, save for the resting macrophages, should eventually reach 0 as stated in the second criterion, this is no longer a sign of health.

We will define healthy behavior based on what is not healthy behavior. Non-healthy behavior is observed when the existence of necrotic β -cells and cytokines is not an artifact of the neonatal phase only.³ Thus if the concentration of necrotic β -cells and hence also cytokines tends to zero after the apoptotic wave has occurred and M_a and B_a tend to zero when $B \rightarrow 0$, we shall call it healthy behavior.

Model A also suffers the problem of the natural apoptosis being constant, which, as stated entails a non-physiological concentration of β -cells. Thus in the following we will strive to reconstruct the apoptosis-term so that: 1. the concentrations will obey criterion II, and 2. the concentration of healthy β -cells will not become negative due to the way we model the natural apoptosis.

² The healthy rest state of the original DuCa model $(M, M_a, B_a, B_n, C) = (a/c, 0, 0, 0, 0)$ is a highly idealized view of how the state of things are in the pancreas.

³ Notice that this may still be an oversimplification, but it will make due for our needs.

11.3 Modifying the governing equation – Model B

Based on the insights we obtained from Model A, we will now modify the apoptosis-term to obtain a more realistic behavior.

Verchere (2009) and Pociot (2009) reports that a rule of thumb is that approximately 0.1%, or 1 in 1000, β -cells become apoptotic per day in adult mice; i.e. the number of β -cells that become apoptotic at a given time, depends on how many are left.⁴ Thus we must adjust the governing equation accordingly. This is done simply by changing the term that describes the natural apoptosis from x_1 to x_2B in equation 11.8 and 11.11. The new constant, x_2 , has the dimension “per day” (d^{-1}) and a value of 0.001. We will refer to this model as Model B.

In figure 11.2 we present a simulation of the Balb/c- mouse based on Model B, while figure 11.3 shows the NOD-simulation.

Model B – Balb/c-simulation

We see that making the amount of β -cells, that enter natural apoptosis per day, dependent on the concentration of β -cells has improved the Balb/c-behavior in that the concentrations of apoptotic β -cells and activated macrophages tend toward zero as $t \rightarrow \infty$, and the concentration of β -cells also exhibits a more natural behavior. The Balb/c-simulation is in agreement with criteria II and IV, and if we compare the plots portraying the concentrations of healthy β -cells in figures 11.2 and 11.3 we see that the third criterion is also fulfilled.

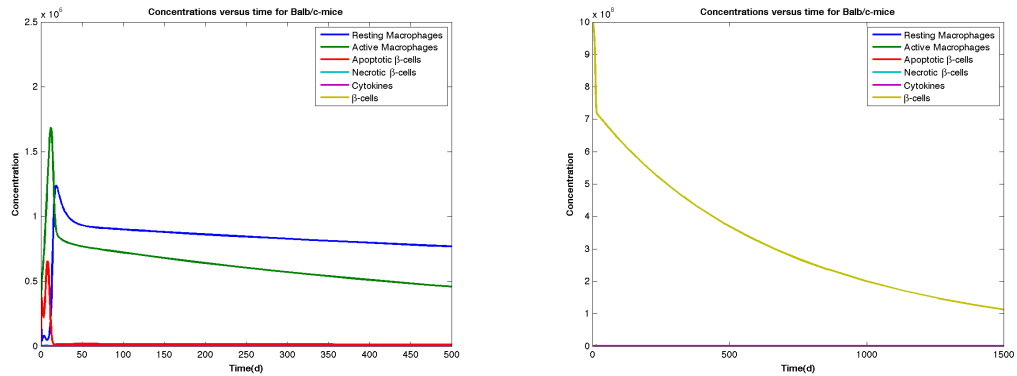


Figure 11.2 Behavior of the concentrations for Balb/c-mice with the inclusion of a compartment of healthy β -cells; based on Model B. Left: the concentrations of M, M_a, B_a, B_n, C . Right: the concentration of B . Initial values are $(M, M_a, B_a, B_n, C, B) = (4.77 \times 10^5, 0, 0, 0, 0, 1 \times 10^9)$

⁴ Teta et al. (2005) give an apoptosis rate of 0.0011 percent per day in one year old mice (Teta et al., 2005, p.2562).

Model B – NOD-simulation

Superficially speaking the NOD-simulation agrees with criteria I – there are still plenty of β -cells left when the T cells would start to take affect (not included in the model). We will discuss this further in chapter 12. Criteria II and III are also satisfied.

When we compare figure 11.2 and 11.3 we see that as a consequence of the increased

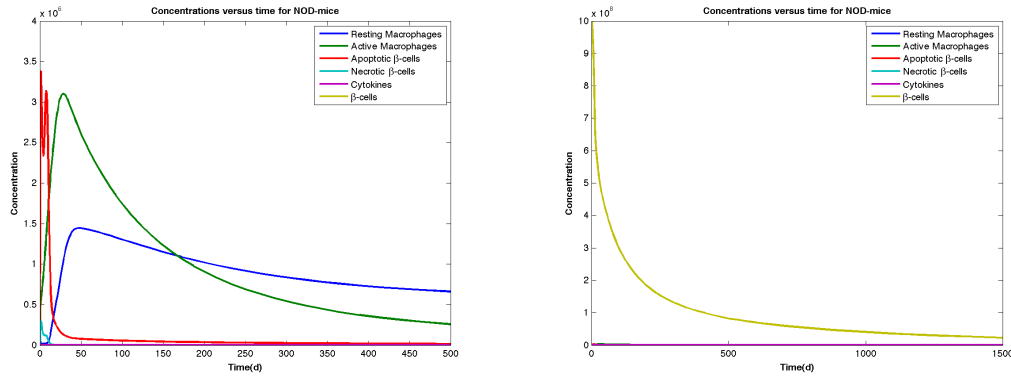


Figure 11.3 Behavior of the concentrations for NOD-mice with the inclusion of a compartment of healthy β -cells; based on Model B. Left: the concentrations of M, M_a, B_a, B_n, C . Right: the concentration of B . Initial values are $(M, M_a, B_a, B_n, C, B) = (4.77 \times 10^5, 0, 0, 0, 0, 1 \times 10^9)$

pathological β -cell apoptosis in NOD-mice the B_a -concentration has an initial peak at approximately 3.4×10^6 cells ml^{-1} compared to around 0.7×10^6 cells ml^{-1} in Balb/c-mice. This in turn implies that the NOD M_a -concentration reaches a significantly higher value than the Balb/c M_a -concentration. We also notice that the peak in M_a -concentration occurs earlier in Balb/c-mice because f_1 is higher in this type of mouse compared to NOD-mice. As stated the healthy β -cells in Balb/c-mice die out due, only, to natural apoptosis after the initial remodelling phase. This can be seen as the sudden change in the slope of the B -concentration curve in figure 11.2. The NOD β -cells do not experience this change in the slope and continue the steep slope that the initial phase has appointed for them. After 500 days the NOD B -concentration is less than 1×10^8 , compared to nearly four times that amount in Balb/c-mice. To get a sense of how well Model B does when compared to actual data, we would like to remind the reader that diabetes becomes overt at approximately 30 weeks of age in the NOD-mouse (Sreenan et al., 1999, p.989). In humans T1D becomes overt when about 60-90% of the β -cells are gone (Seeley et al., 2008, p.636). Assuming that it is the same for NOD-mice we find that the B -concentration should be 1×10^8 to 4×10^8 cells ml^{-1} at 30 weeks of age; cf. chapter 2. Looking at figure 11.3 we find that the concentration reaches 4×10^8 cells ml^{-1} after 80-100 days, and 1×10^8 just before 500 days. This speaks for the soundness of Model B, since $B(0)$ may vary from mouse to mouse and it is not unlikely that the apoptosis rate may do the same. We must also recall, that T cells play an important role after about 4-5 weeks in the development of T1D, and by the same token the depletion of β -cells. All in all it could seem as though Model B is a suitable model – at least for the NOD-mouse.

Now let us see how well Model B models the Balb/c-mouse. The Balb/c-simulation of Model B reveals that a B -concentration of 4×10^8 cells ml^{-1} is reached shortly before 500 days have transpired. This speaks against the soundness of Model B. $B = 1 \times 10^8$ is reached some time after 1500 days, which must be regarded as a Methuselan age for a mouse.

Thus on one hand Model B appears to fit the NOD-mouse. On the other the hand the Balb/c-mouse also becomes diabetic, when we adapt the assumption that removing 60% of the β -cells implies diabetes. But before we start making any final conclusions there is something we have left out in these first two models, namely the regeneration and replication of healthy β -cells that is concurrent with apoptosis – in young rodents at least. Adding a replication-term to the model may save the Balb/c-mouse from its ill-fated lab-colleague. The next subsection will deal with this aspect.

11.4 Adding β -cell growth – Model C

As we hinted earlier, there is experimental evidence that suggests that the β -cells do not simply die out linearly or according to an exponential law (Bouwens and Rooman (2005), Steer et al. (2006), Akirav et al. (2008), Saisho et al. (2008)), after the apoptotic wave has done its damage – even during the initial phase where the apoptotic wave occurs the β -cell mass may actually expand. In this subsection we add a growth- or replication term to equation 11.11. We will also do yet another modification of the apoptosis term.

Saisho et al. (2008) find the replication rate in islets of 1 month old rats to be 0.15% per hour, which can be calculated to be approximately 3.6% per day or 0.036d^{-1} . In order to obtain this estimate they use an assay where they add a growth-medium to their Langerhanian islets, which stimulates an increase in replication.⁵ Thus the value of 0.036d^{-1} should not be taken at face-value, nonetheless it is the only estimate of the replication rate in young rodents we have been able to find.

From the same article the apoptosis rate at 1 month of age can be calculated to approximately 0.018d^{-1} (Saisho et al., 2008, p.E90-E91). This differs from the apoptosis rate we used in Model A and B. One reason for this discrepancy could be the same as the reason why the replication rate estimated by Saisho et al. (2008) is inflated, i.e. we speculate that the growth-medium may attenuate the apoptosis rate. Another reason is that Saisho et al. (2008) use young rodents whereas the estimate given by Verchere (2009) and Pociot (2009) is for adult rodents.

Besides providing an estimate for the replication – and apoptosis – rate of young rodents, Saisho et al. (2008) also reports that in 10 week old rats replication is a rare phenomenon in agreement with the findings of Teta et al. (2005) who estimate the number of β -cells that undergo replication per day, in one year old mice of the so-called c57BL/6 \times 129Sv type, to be 1 in 1400, or $\approx 0.07\%$ per day (Teta et al., 2005, p.2561). Teta et al. (2005) further reports that the rate eventually drops to 0 (Teta et al., 2005, p.2563), and provide an estimate for the replication rate of 8 month old male and female Balb/c-mice, which they find to be $\approx 0.679\%$ per day for the males and $\approx 0.242\%$ per

⁵ The purpose of the article by Saisho et al. (2008) is not specifically to obtain a value for the replication rate, so this does not constitute tampering with the results.

day for the females. The average then becomes 0.461% per day, or a replication rate of 0.005 per day. The results of Saisho et al. (2008) were obtained from rats, which could lead one to speculate (as we did) that they are not applicable to a mathematical model that is based on mice, and as such could not be used in conjunction with the results of Teta et al. (2005). However Teta et al. (2005) comment on this issue in their discussion. They find it unlikely that results should differ (drastically) between rodent species (Teta et al., 2005, p.2565). Thus in the following we will make use of the results from Saisho et al. (2008) and Teta et al. (2005).

An important thing that the results of Saisho et al. (2008) can teach us, which has also been established by others (e.g. (Finewood et al. (1995))), is that the replication rate is not constant throughout the lifespan of a rat or other rodents (Saisho et al., 2008, p.E90) – this is true even without the growth medium-induced increase in replication rate. This provides an interesting extra feature of the dynamic of the β -cell population that we will attempt to incorporate in Model C.

If we assume that the replication rate decreases linearly from day 1 we get an equation for the replication rate that is approximately given by

$$r(t) = -1 \times 10^{-4}t + 0.0392 \quad (11.12)$$

Thus the replication rate at birth would be 0.0392 and the replication rate would reach zero after approximately 392 days. However, Saisho et al. (2008) reports that the replication is stable for at least 48 hours in 1 month old rat islets, which is incompatible with a linear decline. This prompted us to think about alternatives to the linear decline. Particularly the 48 hour stable period led us to speculate that maybe the replication rate declines slowly during the early period of life, and then decreases more or less rapidly as the rodent gets older, ultimately reaching a state where the replication rate again decreases slowly until it ultimately reaches 0. Based on this we propose using a time-dependent replication rate that is described by a logistic function.

A suitable candidate for the replication rate is

$$r(t) = \frac{r_0}{1 + \exp(p_1(t - t'_1))} \quad (11.13)$$

where r_0 is the replication rate at birth, t' is the time at which the replication rate has dropped to half its original value, and p_1 determines the steepness of the logistic curve as the replication rate decreases. Though we do not know the values of r_0 , p_1 and t' , we do know that $r(30) = 0.036\text{d}^{-1}$ and that $r(365) \approx 0.0007\text{d}^{-1}$. Based on these values we can obtain a relationship between t'_1 and r_0 , so we can see how different r_0 's influences the day where the replication rate has been halved compared to $t = 0$. Through some tedious calculations we find

$$t'_1 = \frac{365 \ln\left(\frac{r_0 - 0.036}{0.036}\right) - 30 \ln\left(\frac{r_0 - 0.0007}{0.0007}\right)}{\ln\left(\frac{0.0007(r_0 - 0.036)}{0.036(r_0 - 0.0007)}\right)} \quad (11.14)$$

Of course we can also determine a relation between p_1 and r_0 , as given in equation 11.15

$$p_1 = \frac{\ln\left(\frac{r_0 - 0.036}{0.036}\right)}{30 - t'_1} \quad (11.15)$$

where t'_1 is given by equation 11.14.

Because we have found different values for the apoptosis rate in young and adult animals, we hypothesize that the (natural) apoptosis rate might also decline with age. Again we choose a logistic function to describe the apoptosis rate as a function of time, but this time we do not want the rate to tend to zero as the animal ages. Instead we want it to reach the constant value given by Verchere (2009); 0.001d^{-1} . Thus we find

$$x_3(t) = \frac{x_{3,0}}{1 + \exp(p_2(t - t'_2))} + x_2 \quad (11.16)$$

As before we can relate p_2 and $x_{3,0}$ as well as t'_2 and $x_{3,0}$, as seen in equations 11.17 and 11.18.

$$t'_2 = \frac{365 \ln\left(\frac{x_{3,0}-0.018}{0.018}\right) - 30 \ln\left(\frac{x_{3,0}-0.001}{0.001}\right)}{\ln\left(\frac{0.001(x_{3,0}-0.018)}{0.018(x_{3,0}-0.001)}\right)} \quad (11.17)$$

$$p_2 = \frac{\ln\left(\frac{x_{3,0}-0.018}{0.018}\right)}{30 - t'_2} \quad (11.18)$$

t'_2 in equation 11.18 is given by 11.17.

By now we have altered the governing equations for the healthy and apoptotic β -cells so many times that we find it appropriate to restate them

$$\frac{dB_a}{dt} = x_3(t)B + W_0(t)B + \frac{A'_{max}C}{k_c + C}B - f_1MB_a - f_2M_aB_a - dB_a \quad (11.19)$$

$$\frac{dB}{dt} = -x_3(t)B - W_0(t)B - \frac{A'_{max}C}{k_c + C}B + r(t)B \quad (11.20)$$

The other equations remain as given in equation 11.6, 11.7, 11.9 and 11.10.

We could avoid the use of the non-autonomous apoptosis and replication terms by adding two additional differential equations to the system of equations (one describing the change in the apoptosis-rate and one describing the change in the replication-rate), and assume that $x_{3,0} \approx x_3(30)$ and $r(0) \approx r(30)$.

If we estimate $r_0 = 0.040\text{d}^{-1}$ we obtain $t'_1 \approx 148\text{d}$ and $p_1 \approx 0.019$. While by estimating $x_{3,0} = 0.022\text{d}^{-1}$ we get $t'_2 \approx 141\text{d}$ and $p_2 \approx 0.014$. Based on these estimates, and $x_2 = 0.001\text{d}^{-1}$, the simulations in figure 11.4 and 11.5 were produced.⁶ As with Model B we will compare Model C to the data that is available to us. However we will save the discussion of Model C for the next chapter.

Model C – Balb/c-simulation

Figure 11.4 shows that, after the β -cell population has endured the initial remodelling, it grows to a concentration of nearly 3.5×10^9 before it starts to decline. After 1500 days the concentration is still above 3×10^8 , and at 30 months the concentration is above what would be considered diabetic. The elevated number of β -cells, compared to

⁶ In appendix C.3 we have included the code that was used to do the simulations.

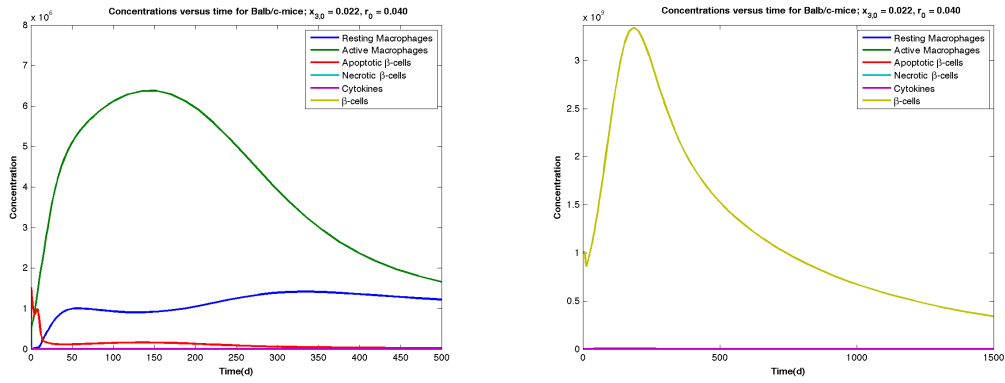


Figure 11.4 Simulations of Balb/c-concentrations based on Model C. Left: the concentrations of M, M_a, B_a, B_n, C . Right: the concentration of B . Initial values are $(M, M_a, B_a, B_n, C, B) = (4.77 \times 10^5, 0, 0, 0, 0, 1 \times 10^9)$

Model B, implies that the B_a -concentration is also elevated ($B_a(50) < B_a(150)$), this in turn results in an increased level in M_a -concentration ($M_a(150) \approx 6.5 \times 10^6$) thus yielding a reduction in M -concentration ($M(150) < M(50)$). After the B -concentration has peaked it declines due to natural apoptosis, which then leads to a drop in the other concentrations save for the M -concentration ($M(150) < M(50) < M(250)$).

Model C – NOD-simulation

Looking at figure 11.5 we find that the B -concentration reaches 4×10^8 cells ml⁻¹ after about 250 days, and, 1×10^8 just before 500 days. This tells us that in terms of

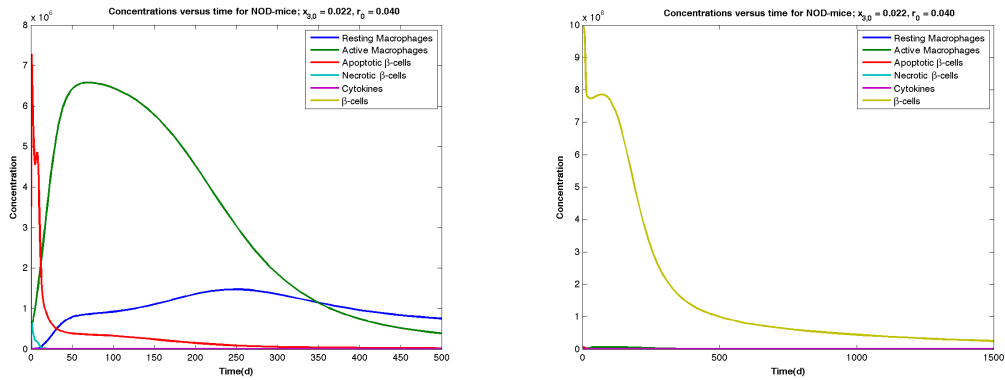


Figure 11.5 Simulations of NOD-concentrations based on Model C. Left: the concentrations of M, M_a, B_a, B_n, C . Right: the concentration of B . Initial values are $(M, M_a, B_a, B_n, C, B) = (4.77 \times 10^5, 0, 0, 0, 0, 1 \times 10^9)$

the healthy β -cells adding the replication-term shifts the number of days that transpire before we reach a B -concentration that is associated with overt T1D. Furthermore figure 11.5 shows that after the apoptotic wave has taken its toll, there is a brief increase in β -cell mass, before the concentration starts to diminish again. It is this difference between Model B and C that yields the different number of days that pass before diabetic conditions are reached. (If we imagine cutting out the part of the B -curve from where it starts to increase to after it has peaked and move the right-most part of the curve to the left, we get a sense of the influence of the effect of the short period of growth.)

Based on the models presented in this chapter we will proceed to our final discussion – this is why we have not treated Model C as thoroughly as the other models in this chapter. The discussion will provide a brief summary of what we have discovered in this chapter, a comparison of Model B and C and a discussion of how well Model C fits our criteria, our (limited) data, and the guidelines provided in chapter 4.

12 Discussion of the Expanded Model

Just as Marée et al. (2006) modified the qualitative Copenhagen model to obtain a model that was more quantitatively correct so we have modified the DuCa model to make it do better in terms of realistic properties, i.e. we changed it so that there is no longer an infinite supply of healthy β -cells.¹ In short we expanded the DuCa model based on the fact that the β -cell population is not infinite. This last step was taken in chapter 11 where we started out by stating some criteria that an expanded model should live up to. Then we made some basic assumptions about what influenced the concentration of β -cells based on recent literature, incorporated this into a differential equation that described the change in β -cell concentration, and altered the equation describing the change in concentration of apoptotic β -cells accordingly. MATLAB simulations were then done, and we analyzed the figures that were the product of these simulations. Based on the figures we were able to determine how well the different models complied with our criteria. In the following we will compare the model to the data given below, and compare Model B and Model C to each other.

Perhaps the most important step towards validating one's model(s) is to compare it to data. The only readily useable data we have is

- i The age at which symptoms of T1D becomes overt in the NOD-mouse – 30 weeks
- ii The number of β -cells that are left when symptoms of T1D present themselves (in NOD-mice) – 10-40 % of the initial β -cell mass
- iii The time at which T cells become significant in the depletion of β -cells in NOD-mice – 4-5 weeks
- iv The median lifespan of a laboratory mouse – 30 months

which is not an overwhelming amount of data. It is, however, some of the most important data that we could have hoped for, since it allows us to determine if our addition to the DuCa model behaves realistically, i.e. lets us answer questions ii and iii of the thesis statement; cf. section 1.1. Question i will be answered based on the simulations presented in the previous chapter.

Based on the simulations of the first expanded model, Model A, we found that it did not agree with model criteria I and II nor with the second guideline from chapter 4 (it exhibited nonphysiological behavior), and almost by implication it is at variance with the third guideline as well. We concluded that we needed to formulate an addendum, regarding what we would consider healthy behavior, to our criteria. This addendum had not previously occurred to us even though, looking back, it seems obvious.

A little wiser we proceeded to alter Model A slightly, so that we would avoid negative

¹ This should not be interpreted as though the DuCa model is irrelevant or wrong. It was not constructed to mimic Langerhansian Islets over long periods of time, only to analyze the hypothesis of Marée et al. (2006).

B -concentrations, the result of which was Model B. Based on the Balb/*c*-simulation of Model B (cf. figure 11.2) we found that the second and fourth criterion were fulfilled. When we compared figure 11.2 to figure 11.3 we found that Model B could also live up to the third criterion. But there was a problem with the B -concentration in the Balb/*c*-simulation. Though the concentration is declining due to natural apoptosis (criterion IV), we cannot neglect the fact that B reaches a level that is consistent with T1D during the lifetime of an average laboratory mouse (albeit the highest concentration of remaining β -cells that has been associated with T1D-symptoms). This discrepancy was avoided in Model C as will be discussed below.

The NOD-simulations revealed that Model B was able to meet the criteria that were specific to this type of mouse. However, the fulfillment of the first criterion is debateable. On one hand there are plenty of β -cells left at 4-5 weeks (where the T cells usually take effect). On the other hand a B -concentration that should result in overt T1D-symptoms is reached between 80 and 500 days of age ($B(\sim 80) \approx 0.4 \times B(0)$, $B(500) < 0.1 \times B(0)$) without the influence of T cells – symptoms become overt at ~ 210 days. So we must simply accept that criterion I is only partially fulfilled.

Though Model B was clearly a more suitable model than Model A we were not satisfied, and we wanted to add the feature of β -cell replication to the model. Furthermore we redid the apoptosis-term once more to make it more consistent with data found in the literature. Both the apoptosis and replication rates were made time-dependent, so that they would decrease over time; the replication rate ultimately reaching 0 while the apoptosis rate ultimately reached a rate of 0.1 % per day; cf. equation 11.13 and 11.16 respectively.

In Model C the B -concentration, in the Balb/*c*-mouse, reaches an unnaturally high value of 3.5×10^9 . This is a result of choosing $B(0) = 1 \times 10^9$, which is the concentration found in adult nondiabetic animals. In hindsight it would have been prudent of us to choose a smaller initial B -concentration. The choice of r_0 and $x_{3,0}$ also plays a part in how the concentrations behave, and as we pointed out, the replication rate was enhanced by the assay used by Saisho et al. (2008), while we speculate that the apoptosis rate was attenuated. One could try adjusting these values together with a lower $B(0)$ to get a more realistic Balb/*c*-behavior, and then compare the values that yield realistic behavior to values found in the (future) literature.

Compared to Model B there is a delay in the number of days that transpire after birth before the B -concentration in NOD-mice becomes less than 40 % of $B(0)$. This is not a cause for critique of Model C, rather it speaks in its favor. According to the first criterion the concentration of β -cells should be such that T cells are needed to induce diabetes by approximately 30 weeks of age. In terms of the B -concentration this means that with the inclusion of T cells, B should be between 0.1 – 0.4 times $B(0)$ at week 30. We speculate that by adding the effect of T cells the B -concentration should reach levels that are consistent with diabetes within 30 weeks.

Thus Model C provides a better NOD-model compared to Model B when it comes to the first criterion. As far as the second criterion goes it is hard to determine if Model B or Model C is more correct, since we have no data to judge from.

If we turn to the research questions we stated in section 1.1, we find that we can answer positively to i and ii based on both Model B and Model C. But what about iii? The only data that we can use to answer this question is how the level of β -cells should be (or rather not be) at 30 weeks of age in NOD-mice. Based on this we find that Model

Question	Model A	Model B	Model C
i	÷	✓	✓
ii	÷	✓	✓
iii	÷	÷	✓
Guideline			
1	✓	✓	✓
2	÷	✓	✓
3	-	-	-
Criteria			
I	÷	÷/✓	✓
II	÷	✓	✓
III	✓	✓	✓
IV	✓	✓	✓
Data			
i+ii	÷	÷	✓
iii	÷	÷	✓

Table 12.1 The “-” indicates that we have not had the time to analyze how the expanded models respond when we vary significant parameters. Under “Data” it only made sense to compare our simulations to point ii and iii.

C does agree with the experimental data.

To sum up all of the results we have obtained and conclusions we have drawn through our work with the expanded model we give table 12.1. It provides an overview of how the different models did compared to the questions from the thesis statement, the guidelines, our criteria and the data. It is divided into three categories: 1, a question-category, 2, a guideline-category, and 3, a data-category. A ÷ underneath e.g. Model A and to the right of e.g. question i, indicates that Model A did not provide for a natural extension of the DuCa model. Similarly a check mark under e.g. Model B and to the right of question ii signifies that Model B yielded more realistic behavior, than the DuCa model. In the guideline category all the spots to the right of guideline number 3 are marked with a dash. This is to show that we have not analyzed how the models behave when we tweak significant parameters.

The data-category merits a little more explanation. The best way is to provide an example of how it should be interpreted. Let us look at the third data point, which tells us that T cells become significant in the depletion of healthy β -cells, in NOD-mice, at approximately 4-5 weeks of age. Under Model A there is a ÷-sign to the right of this point. This signifies that Model A is unfit to incorporate T cells – it would only serve to kill off the β -cells even quicker. From the NOD-simulations of Model C we saw that diabetic B -concentrations were not reached at 30 weeks, leaving room for T cells to have an effect. Thus there is a check mark underneath Model C. We should also make clear what is to be understood by i+ii in the data-category. This comes from the fact that i and ii are intertwined (the NOD-mice show signs of diabetes at 30 weeks of age when 60-90 % of the β -cells are gone), but when we listed the data we found it more convenient to split them in two. In table 12.1 they are taken together, and a check mark signifies that at 30 weeks there is more than 40 % of the initial β -cell mass left

in the NOD-mouse (seen from the simulations).

12.1 Future Work

Had we had more time we would have rerun our simulations with a smaller initial β -cell concentration, and tried several combinations of $x_{3,0}$ and r_0 . A smaller initial concentration of β -cells should bring down the concentration of active macrophages which reaches very high values in Model C. This was especially the case in the Balb/c-mouse, due to the higher f_1 -value. Though we do not have any data that tell us what M_a -concentrations are realistic (except that we have a number for the maximum number that can fit within a milliliter), we still thought about how we could keep the M_a -concentration down if those displayed in the simulations are unrealistic.

One natural way to control the supply of activated macrophages (besides the crowding term), would be to take a step back and limit the supply of resting macrophages. This could be achieved by adding an additional compartment of resting macrophages, that would play the part of the surrounding tissue, from where the inflow of resting macrophages (given by a and b in the equation describing the change in M -concentration) comes from.

IL-1 induction of primary necrosis

When we researched the literature to get information on how the concentration of β -cells should behave, we came across some interesting articles. The article that is most interesting in the light of the DuCa model is an article by Steer et al. (2006). They find that the cytokine interleukin-1, when secreted by macrophages in the pancreatic islets, induces necrosis in the islet β -cells. In other words: some of the β -cells, become necrotic “straight away”, i.e. without first enduring apoptosis. Some of the other cytokines that are released induce death by apoptosis.² We must remark that the findings of Steer et al. (2006) are based on Sprague Dawley rats, which is another animal model that is widely used in diabetes research. Whereas the model of Marée et al. (2006) is based on results obtained from experiments performed on NOD- and Balb/c-mice.

One could investigate how this influences the model by letting a fraction of the β -cells that would usually go to the compartment of apoptotic β -cells go directly to the compartment of necrotic β -cells. This would be most interesting in terms of simulations with Balb/c parameters, since it would imply a larger concentration of cytokines.

Adding T cells

As we pointed out earlier T cells play a vital role in the development of T1D, and they would make an interesting addition to Model C as far as NOD-simulations go. Those interested in pursuing this idea should read the interesting article by Mahaffy and Edelstein-Keshet (2007).

² This article is from the same year as the article by Marée et al. (2006), so it is possible that they have not been aware of the results.

Adding treatment to Model C

Our initial goal was to modify the DuCa model as presented in chapter 11 and then proceed to analyze, mathematically, what would be the opportune way of reversing or arresting the deleterious process in NOD-mice. Based on the analysis we would determine if any of the treatment strategies presented in chapter 3 would fit the role laid out by the analysis. And if they could readily be implemented into the model. E.g. an easy way to implement a drug that reduces the rate of apoptosis (such as GLP-1) would be to modify the apoptosis term. But if we for a moment think in terms of humans, then the deleterious process does not become known until quite a large number of the β -cells are gone. So the term should be modified in such a way as not to take effect right from birth. Rather the term should take effect at a time that coincides with the time when the B -concentration is small enough such that symptoms become evident. A function that comes to mind is hyperbolic tangent – assuming that infusion of the drug becomes more or less steady after its first application. We could also conceive of wanting to add a drug such as that initiates β -cell regeneration, replication and/or differentiation. Again GLP-1 is a prime candidate as we learned in chapter 3. Here we could add an additional replication term is zero at $t = 0$ and then grows to whatever value we can justify based on data.

Regardless of the possible effects of such a drug, accessibility of supporting data is imperative. In years to come, we hope to see that relevant medical data in this field will become more readily available to all researchers interested in finding solutions to major health issues.

13 Conclusion 2

The primary objective of this thesis was to find out if

- i we could add a natural expansion to the DuCa model
- ii the expansion induced a more realistic behavior
- iii the (natural) expansion would agree with experimental data

Based on Model C we conclude that:

we were able to expand the DuCa model in a way that yielded more realistic simulations, and did not disagree with experimental data.

Furthermore we hypothesize that Model C can easily be modified/expanded to investigate different treatment strategies; as outlined in the discussion (chapter 12).

Bibliography

- Ablamunits, V., N. A. Sherry, J. A. Kushner, and K. C. Herold (2007). Autoimmunity and β cell regeneration in mouse and human type 1 diabetes. *Annals of the New York Academy of Sciences* 1103, 19–32.
- Abraham, R., J. Marsden, and T. Ratiu (1988). *Manifolds, Tensor Analysis, and Applications* (Second ed.). Springer.
- Akirav, E., J. A. Kushner, and K. C. Herold (2008). β -cell mass and type 1 diabetes – going, going, gone? *Diabetes* 57, 2883–2888.
- Allen, L. J. S. (2007). *An Introduction to Mathematical Biology*. Pearson Education.
- Anderson, M. S. and J. A. Bluestone (2005). The nod mouse: A model of immune dysregulation. *Annual Review of Immunology* 23, 447–485.
- Beyan, H., L. R. Buckley, N. Yousaf, M. Londei, and R. D. G. Leslie (2002). A role for innate immunity in type 1 diabetes? *Diabetes Metabolism Research and Reviews* 19, 89–100.
- Blanas, E., F. R. Carbone, J. Alison, J. F. Miller, and W. R. Heath (1996). Induction of autoimmune diabetes by oral administration of autoantigen. *Science* 274(5293), 1707–1709.
- Blasio, B. F. D., P. Bak, F. Pociot, A. E. Karlsen, and J. Nerup (1999). Onset of type 1 diabetes - a dynamical instability. *Perspectives in Diabetes* 48, 1677–1685.
- Blüher, M., B. B. Kahn, and C. R. Kahn (2003). Extended longevity in mice lacking the insulin receptor in adipose tissue. *Science* 299, 572–574.
- Bouwens, L. and I. Rooman (2005). Regulation of pancreatic beta-cell mass. *Physiological Reviews* 85, 1255–1270.
- Bozdogan, H. (1987). Model selection and akaike’s information criterion (aic): the general theory and its analytical extensions. *Psychometrika* 52(3), 345–370.
- Braun, M. (1993). *Differential Equations and Their Applications*. Springer.
- Brouckaert, G., M. Kalai, D. V. Krysko, X. Saelens, D. Vercaemmen, M. Ndlovu, G. Haegeman, K. D’Herde, and P. Vandenabeele (2004). Phagocytosis of necrotic cells by macrophages is phosphatidylserine dependent and does not induce inflammatory cytokine production. *The American Society for Cell Biology* 15, 1089–1100.
- Brubaker, P. L. and D. J. Drucker (2004). Minireview: Glucagon-like peptides regulate cell proliferation and apoptosis in the pancreas, gut, and central nervous system. *Endocrinology* 145.
- Cantor, J. and K. Haskins (2006). Interactions of macrophages and t cells in autoimmune diabetes. *Drug Discovery Today: Disease Mechanisms* 3(3), 381–385.

- Christen, U. and M. G. von Herrath (2004). Initiation of autoimmunity. *Current Opinion in Immunology* 16, 759–767.
- Clare-Salzier, M. J., J. Brooks, A. Chai, K. V. Herle, and C. Anderson (1992). Prevention of diabetes in nonobese diabetic mice by dendritic cell transfer. *The Journal of Clinical Investigation* 90.
- Crawford, J. D. (1991). Introduction to bifurcation theory. *Reviews of Modern Physics* 63.
- Creutzfeldt, W. (2005). The [pre-] history of the incretin concept. *Regulatory Peptides* 128, 87–91.
- Edelstein-Keshet, D. L. (2009). personal communication.
- Edelstein-Keshet, L. (1988). *MATHEMATICAL MODELS IN BIOLOGY*. McGraw-Hill, Inc.
- Egan, J. M., A. Bulotta, H. Hui, and R. Perfetti (2003). Glp-1 receptor agonists are growth and differentiation factors for pancreatic islet beta cells. *Diabetes Metab Res Rev* 19, 115–123.
- Eizirik, D. and T. Mandrup-Poulsen (2001). A choice of death – the signal-transduction of immune-mediated beta-cell apoptosis. *Diabetologia* 44, 2115–2133.
- Eizirik, D. L. and M. I. Darville (2001). β -cell apoptosis and defense mechanisms – lessons from type 1 diabetes. *Diabetes* 50, supplement 1, s64–s69.
- Eldén, L., L. Wittmeyer-Koch, and H. B. Nielsen (2004). *Introduction to Numerical Computation*. Studentlitteratur.
- Farilla, L., A. Bulotta, B. Hirshberg, S. L. Calzi, N. Khoury, H. Noushmehr, C. Bertolotto, U. D. Mario, D. M. Harlan, and R. Perfetti (2003). Glucagon-like peptide 1 inhibits cell apoptosis and improves glucose responsiveness of freshly isolated human islets. *Endocrinology* 144, 5149–5158.
- Finegood, D. T., L. Scaglia, and S. Bonner-Weir (1995). Dynamics of β -cell mass in the growing rat pancreas – estimation with a simple mathematical model. *Diabetes* 44, 249–255.
- Franco, O. H., E. W. Steyerberg, F. B. Hu, J. Mackenbach, and W. Nusselder (2007). Associations of diabetes mellitus with total life expectancy with and without cardiovascular disease. *Archives of International Medicine* 167, 1145–1151.
- Furth, R. V. and M. M. C. D. den Dulk (1984). Dual origin of mouse spleen macrophages. *Journal of Experimental Medicine* 160, 1273–1283.
- Gianani, R. and G. S. Eisenbarth (2005). The stages of type 1a diabetes: 2005. *Immunological Reviews* 204, 232–249.
- Green, E. A. and R. A. Flavell (1999). The initiation of autoimmune diabetes. *Current Opinion in Immunology* 11, 663–669.
- Greenbaum, C. J. and L. C. Harrison (2008). *Diabetes – Translating Research into Practice*, Chapter What are the Prospects for Preventing Autoimmune Diabetes?, pp. 99–122. Informa Health Care.
- Guckenheimer, J. and P. Holmes (2002). *Nonlinear Oscillations, Dynamical Systems, and Bifurcations of Vector Fields* (7 ed.). Springer.

- Haase, C., K. Skak, B. K. Michelsen, and H. Markholst (2004). Local activation of dendritic cells leads to insulinitis and development of insulin-dependent diabetes in transgenic mice expressing cd154 on the pancreatic β -cells. *Diabetes*, 2588–2595.
- Hänninen, A. (2000). Prevention of autoimmune type 1 diabetes via mucosal tolerance: Is mucosal autoantigen administration as safe and effective as it should? *Scandinavian Journal of Immunology* 52, 217–225.
- Höglund, P., J. Mintern, C. Waltzinger, W. Heath, C. Benoist, and D. Mathis (1999). Initiation of autoimmune diabetes by developmentally regulated presentation of islet cell antigens in the pancreatic lymph nodes. *Journal of Experimental Medicine*.
- Leslie, R., M. Atkinson, and A. Notkins (1999). Autoantigens ia-2 and gad in type 1 (insuline-dependent) diabetes. *Diabetologia* 42, 3–14.
- Lo, J. and M. J. Clare-Salzler (2006). Dendritic cell subsets and type i diabetes: Focus upon dc-based therapy. *Autoimmunity Reviews* 5.
- Ludewig, B., B. Odermatt, S. Landmann, H. Hengartner, and R. M. Zinkernagel (1998). Dendritic cells induce autoimmune diabetes and maintain disease via de novo formation of local lymphoid tissue. *Journal of Experimental Medicine* 188(8), 1493–1501.
- Lynch, S. (2004). *Dynamical Systems with Applications using Matlab*. Springer.
- Mahaffy, J. M. and L. Edelstein-Keshet (2007). Modeling cyclic waves of circulating t cells in autoimmune diabetes. *SIAM Journal of Applied Mathematics* 67(4), 915–937.
- Manuel, D. G. and S. E. Schultz (2004). Health-related quality of life and health-adjusted life expectancy of people with diabetes in ontario, canada, 1996–1997. *Diabetes Care* 27, 407–414.
- Marée, A. F., M. Komba, C. Dyck, M. Labecki, D. T. Finegood, and L. Edelstein-Keshet (2005). Quantifying macrophage defects in type 1 diabetes. *Journal of Theoretical Biology*.
- Marée, A. F. M., M. Komba, D. T. Finegood, and L. Edelstein-Keshet (2007). A quantitative comparison of rates of phagocytosis and digestion of apoptotic cells by macrophages from normal (balb/c) and diabetes-prone (nod) mice. *Journal of Applied Physiology*.
- Marée, A. F. M., R. Kublik, D. T. Finegood, and L. Edelstein-Keshet (2006). Modelling the onset of type 1 diabetes: can impaired macrophage phagocytosis make the difference between health and disease? *Philosophical Transactions of The Royal Society* 364, 1267–1282.
- Marée, A. F. M., P. Santamaria, and L. Edelstein-Keshet (2006). Modeling competition among autoreactive $cd8^+$ t cells in autoimmune diabetes: implications for antigen specific therapy. *International Immunology* 18(7), 1067–1077.
- Mathis, D., L. Vence, and C. Benoist (2001). Beta-cell death during progression to diabetes. *Nature* 414, 792–798.
- Murray, J. (2002). *Mathematical Biology: I. An Introduction* (Third ed.). Springer.
- Nauck, M. (1998). Glucagon-like peptide 1 (glp-1): a potent gut hormone with a possible therapeutic perspective. *Acta Diabetol* 35, 117–129.

- Notkins, A. L. and Åke Lernmark (2001). Autoimmune type 1 diabetes: resolved and unresolved issues. *The Journal of Clinical Investigation* 108(9), 1247–1252.
- O'Brien, B. A., Y. Huang, X. Geng, J. P. Dutz, and D. T. Finegood (2002). Phagocytosis of apoptotic cells by macrophages from nod mice is reduced. *Diabetes* 51.
- Onengut-Gumuscu, S. and P. Concannon (2006). Recent advances in the immunogenetics of human type 1 diabetes. *Current Opinion in Immunology* 18, 634–638.
- Othmer, H. G. (2006, August). Analysis of complex reaction networks in signal transduction, gene control and metabolism.
- Pociot, D. M. F. (2009). personal communication.
- Poulter, L. W. and J. L. Turk (1975). Rapid quantitation of changes in macrophage volume induced by lymphokine in vitro. *Clinical & Experimental Immunology* 19.
- Reynolds, A., J. Rubin, G. Clermont, J. Day, Y. Vodovotz, and G. B. Ermentrout (2006). A reduced mathematical model of the acute inflammatory response: I. derivation of model and analysis of anti-inflammation. *Journal of Theoretical Biology* 242.
- Roman, I. and L. Bouwens (2004). Combined gastrin and epidermal growth factor treatment induces islet regeneration and restores normoglycaemia in c57bl6/j mice treated with alloxan. *Diabetologia* 47.
- Rosenfeld, L. (2002). Insulin: Discovery and controversy. *Clinical Chemistry*, 2270–2288.
- Saisho, Y., E. Manesso, T. Gurlo, C. jiang Huang, G. M. Toffolo, C. Cobelli, and P. C. Butler (2008). Development of factors to convert frequency to rate for β -cell replication and apoptosis quantified by time-lapse video microscopy and immunohistochemistry. *American Journal of Physiology – Endocrinology and Metabolism* 296.
- Seeley, R. R., T. D. Stephens, and P. Tate (2008). *Anatomy & physiology* (8 ed.). McGraw-Hill.
- Shampine, L., I. Gladwell, and S. Thompson (2003). *Solving ODEs with MATLAB*. Cambridge University Press.
- Siegel, E. G., B. Gallwitz, G. Scharfa, R. Mentlein, C. Morys-Wortmann, U. R. Fölsch, J. Schrezenmeir, K. Drescher, and W. E. Schmidt (1999). Biological activity of gip-1-analogues with n-terminal modifications. *Regulatory Peptides* 79, 93–102.
- Skarsvik, S., M. Tiittanen, A. Lindström, R. Casas, J. Ludvigsson, and O. Vaarala (2004). Poor in vitro maturation and pro-inflammatory cytokine response of dendritic cells in children at genetic risk of type 1 diabetes. *Scandinavian Journal of Immunology* 60, 647–652.
- Souza, K. L. A., E. Gurgul-Convey, M. Elsner, and S. Lenzen (2008). Interaction between pro-inflammatory and anti-inflammatory cytokines in insulin producing cells. *Journal of Endocrinology* 197, 139–150.
- Sparre, T., M. Larsen, P. E. Heding, A. E. Karlsen, O. N. Jensen, and F. Pociot (2005). Unraveling the pathogenesis of type 1 diabetes with proteomics. *The American Society for Biochemistry and Molecular Biology*, 441–457.
- Sreenan, S., A. J. Pick, M. Levisetti, A. C. Baldwin, W. Pugh, and K. S. Polonsky (1999). Increased β -cell proliferation and reduced mass before diabetes onset in the nonobese diabetic mouse. *Diabetes* 48, 989–996.

-
- Staeva-Vieira, T., M. Peakman, and M. von Herrath (2008). Translational mini-review series on type 1 diabetes: Immune-based therapeutic approaches for type 1 diabetes. *Clinical and Experimental Immunology* 148, 17–31.
- Steer, S. A., A. L. Scarim, K. T. Chambers, and J. A. Corbett (2006). Interleukin-1 stimulates β -cell necrosis and release of the immunological adjuvant hmgbl. *PLoS Medicine* 3, 253–266.
- Stoffels, K., L. Overbergh, A. Giulietti, A. Kasran, R. Bouillon, C. Gysemans, and C. Mathieu (2004). Nod macrophages produce high levels of inflammatory cytokines upon encounter of apoptotic or necrotic cells. *Journal of autoimmunity* 23, 9–15.
- Strogatz, S. H. (2000). *Nonlinear Dynamics and Chaos - With Applications to Physics, Biology, Chemistry, and Engineering*. Perseus Books Group.
- Suarez-Pinzon, W. L., R. F. Power, Y. Yan, C. Wasserfall, M. Atkinson, and A. Rabinovitch (2008). Combination therapy with glucagon-like peptide-1 and gastrin restores normoglycemia in diabetic nod mice. *Diabetes* 57, 3281–3288.
- Szkudelskii, T. (2001). The mechanism of alloxan and streptozotocin action in b cells of the rat pancreas. *Physiological Research* 50.
- Teta, M., S. Y. Long, L. M. Wartschow, M. M. Rankin, and J. A. Kushner (2005). Very slow turnover of β -cells in aged adult mice. *Diabetes* 54.
- Trudeau, J. D., J. P. Dutz, E. Arany, D. J. Hill, W. E. Fieldus, and D. T. Finegood (2000). Neonatal beta-cell apoptosis a trigger for autoimmune diabetes? *Diabetes* 49, 1–7.
- Trudeau, J. D., C. Kelly-Smith, C. B. Verchere, J. F. Elliott, J. P. Dutz, D. T. Finegood, P. Santamaria, , and R. Tan (2003). Prediction of spontaneous autoimmune diabetes in nod mice by quantification of autoreactive t cells in peripheral blood. *The Journal of Clinical Investigation* 111, 217–223.
- Urusova, I. A., L. Farilla, H. Hui, E. D'Amico, and R. Perfetti (2004). Glp-1 inhibition of pancreatic islet cell apoptosis. *TRENDS in Endocrinology and Metabolism* 15.
- Verchere, D. B. (2009). personal communication.
- Wang, X., Z. He, and S. Ghosh (2006). Investigation of the age-at-onset heterogeneity in type 1 diabetes through mathematical modeling. *Mathematical Biosciences*, 79–99.
- Wigginton, J. E. and D. Kirschner (2001). A model to predict cell-mediated immune regulatory mechanisms during human infection with mycobacterium tuberculosis. *Journal of Immunology* 166, 1951–1967.
- Wild, S., G. Roglic, A. Green, R. Sicree, and H. King (2004). Global prevalence of diabetes – estimates for the year 2000 and projections for 2030. *Diabetes Care* 27(5), 1047–1053.
- Wong, F. S. and C. A. J. Jr. (1999). Insulin dependent diabetes mellitus and its animal models. *Current Opinion in Immunology* 11, 643–647.
- Yoon, J.-W. and H.-S. Yun (2001). Cellular and molecular pathogenic mechanisms of insulin-dependent diabetes mellitus. *Annals of the New York Academy of Sciences*, 200–211.

- Yu, J. and G. S. Eisenbarth (2006). Mechanisms underlying type 1 diabetes and islet transplantation. *Drug Discovery Today: Disease Mechanisms* 3(2), 155–162.
- Yu, P. (1997). Computation of normal forms via a perturbation technique. *Journal of Sound and Vibration* 211, 19–38.
- Zeeman, M. (1990). Hopf bifurcation in competitive three-dimensional lotka-volterra systems.

A Mathematical Appendices

This appendix is dedicated to rigoristic statements of the important theorems that have been casually stated in different sections of the thesis. Other important concepts that pertain to mathematics will also be dealt with in the following sections; e.g. the Newton-Raphson method.

A.1 Existence and Uniqueness Theorem

A very important thing to determine when working with (systems of) differential equations, is whether the solution is unique, and in what interval the solution exist. I.e. given a set of initial conditions on the DuCa model (equations 5.6-5.10), we would like to know if the solution is unique, and if it exists for all time, t . To determine this we first need to introduce the property of Lipschitz continuity

Definition 1

Given a function $\mathbf{g}(\mathbf{x})$, $\mathbf{g} : \mathbb{R}^n \rightarrow \mathbb{R}^n$, and a domain $U \subset \mathbb{R}^n$, suppose that

$$\|\mathbf{g}(\mathbf{x}_1) - \mathbf{g}(\mathbf{x}_2)\| \leq L\|\mathbf{x}_1 - \mathbf{x}_2\| \quad (\text{A.1})$$

where $\mathbf{x}_1, \mathbf{x}_2 \in U$, and L is the Lipschitz constant. Then we say that \mathbf{g} is Lipschitz

When \mathbf{g} fulfills this condition we say that \mathbf{g} is Lipschitz continuous, or that it is continuously Lipschitz.

Now for the existence and uniqueness theorem itself

Theorem A.1

Suppose that \mathbf{g} is Lipschitz continuous. Given an initial point $\mathbf{x}_0 \in U$, the autonomous differential equation

$$\dot{\mathbf{x}} = \mathbf{g}(\mathbf{x}) \quad (\text{A.2})$$

has a unique solution, $\phi_t(\mathbf{x}_0)$, that is defined on the maximal interval of existence.

Basically as long as $\mathbf{g} \in C^1(U)$, where U is a compact set, we need not be concerned about pathological behavior of the solution (Lynch, 2004, p.176). Loosely put the C^1 condition guarantees that pathological behavior will not occur.

One thing that may concern the reader is the fact that we need the differential equation to be autonomous, i.e. not explicitly dependent on time, which the DuCa model is not; cf. equation 5.8. The apoptotic wave depends explicitly on time, but we can remedy this by introducing another dimension, and an additional equation, into the system of equations, by setting t equal to, say, X . By this little trick we have made the DuCa model autonomous. In our case we have not been able to provide an analytic expression of

the compact set, but our simulations (with varying initial conditions) seem to verify that as long as we stick to choosing initial conditions in at least $\max\|(M, M_a, B_a, B_n, C)\|$ we are on the safe side (due to the crowding terms and the Michaelis-Menten function these concentrations will never exceed ∞ and the concentrations cannot be negative). By these means the solutions to the DuCa model will be unique, and the maximal interval of existence is $0 \leq t < \infty$.

A.2 The Implicit Function Theorem

The implicit function theorem¹ is the theorem at the heart of bifurcation analysis, since it provides sufficient conditions for an equilibrium to exist as a parameter is varied. Formally the theorem can be stated as

Theorem A.2

Let $r \in \mathbb{R}$ and $\mathbf{x} \in \mathbb{R}^n$, then, if $\mathbf{g}(r, \mathbf{x})$ is a C^1 function on $\mathbb{R} \times \mathbb{R}^n$ with the properties

$$\mathbf{g} : \mathbb{R} \times \mathbb{R}^n \rightarrow \mathbb{R}^n, \quad \mathbf{g}(0, \mathbf{0}) = \mathbf{0} \quad (\text{A.3})$$

and

$$\text{Det}(D_{\mathbf{x}}\mathbf{g}(0, \mathbf{0})) \neq 0 \quad (\text{A.4})$$

there exists a unique differentiable function $G(r)$, defined on a neighborhood, $U \subset \mathbb{R}$, of $r = 0$, such that

$$G : U \rightarrow \mathbb{R}^n, \quad G(0) = \mathbf{0} \quad (\text{A.5})$$

and

$$\mathbf{g}(r, G(r)) = \mathbf{0}, \quad \text{for } r \in U \quad (\text{A.6})$$

This theorem promises us that: given an equilibrium for a system of differential equations that depends on a parameter, then if the Jacobian of the system evaluated in that equilibrium is invertible, i.e. has a nonzero determinant, the equilibrium will persist (in a neighborhood of the parameter value) as the parameter is changed.

The theorem can be generalized to an m -dimensional parameter, and a general equilibrium other than $(0, \mathbf{0})$.

A.3 The Hartman-Grobman Theorem

The Hartman-Grobman theorem provides the link between the behavior of a nonlinear system and the behavior of its linearized counterpart, when the eigenvalues of the Jacobian are not purely imaginary or zero. The following formal statement of the theorem is based on Guckenheimer and Holmes (2002).

Theorem A.3

Let (r, \mathbf{x}) be as in Theorem A.2, and let $\mathbf{g}(r, \mathbf{x}) = \dot{\mathbf{x}}$ be a system of ordinary differential equations. Assume that $(0, \mathbf{0})$ is an equilibrium, then if $D_{\mathbf{x}}\mathbf{g}(0, \mathbf{0})$ has no zero or purely imaginary eigenvalues there is a homeomorphism, h , defined on some neighborhood, V ,

¹ The following is loosely based on Crawford (1991).

of $(0, \mathbf{0})$ in \mathbb{R}^n locally taking orbits of the nonlinear flow generated by the vector field \mathbf{g} to those of the linear flow

As with the implicit function theorem it can be stated for an arbitrary equilibrium, but through a change of variables we can always move the equilibrium to the origin (Crawford, 1991, p.993).

A.4 Michaelis-Menten Kinetics

This appendix² serves to introduce the idea behind the Michaelis-Menten function which Marée et al. (2006) uses in their model, to make the cytokine-induced apoptosis more realistic, i.e. saturated. It all comes from the fact that saturation is a feature inherent to all biological systems, and therefore it is important to incorporate saturation when modelling such systems – The Michaelis-Menten saturation function is one way of doing so.

To arrive at the Michaelis-Menten saturation function let us imagine that we have some kind of bacteria in a petri dish, that grows when supplied with a nutrient of sorts. In fact its growth rate depends on the availability of nutrient. How should one go about modelling such a growth rate? To begin with we could ask ourselves how the bacteria consumes the nutrient – as it turns out, the nutrient is mediated into the bacterial cell via receptors. Thus a receptor can either be occupied or it can be available for business. Sometimes the nutrient is broken down to a product and sometimes it is “set free”. If we denote an external nutrient molecule with N , an occupied receptor with R_o , an available receptor with R_a , and the product with P , we can write the reactions as



where k_1, k_{-1}, k_2 are reaction rates. This equation should be read as: an external nutrient molecule, N , comes into contact with an available receptor, R_a , thus constituting the nutrient-receptor complex, R_o . Either the nutrient is relinquished, at rate k_{-1} , or it is broken down, at rate k_2 , yielding a reaction product, P , and an available receptor. Denoting concentrations by appropriate lower-case letters we can transform this equation into the following system of nonlinear autonomous differential equations

$$\frac{dn}{dt} = k_{-1}r_o - k_1nr_a \quad (\text{A.8})$$

$$\frac{dr_a}{dt} = k_{-1}r_o - k_1nr_a + k_2r_o \quad (\text{A.9})$$

$$\frac{dr_o}{dt} = k_1nr_a - k_{-1}r_o - k_2r_o \quad (\text{A.10})$$

$$\frac{dp}{dt} = k_2r_o \quad (\text{A.11})$$

With initial conditions: $n(0) = n_0, r_a(0) = r_{a,0}, r_o(0) = 0, p(0) = 0$. The observant reader may have noticed that if we add equations A.9 and A.10 a little miracle happens,

² This appendix is based on Edelstein-Keshet (1988) and Murray (2002).

in that

$$\frac{dr_a}{dt} + \frac{dr_o}{dt} = 0 \quad (\text{A.12})$$

but before we start calling in people from the Vatican, we should note that, this tells us that the total concentration of receptors remains constant – as it should since no receptors are destroyed or created during the process. By equation A.12 we can write the sum of the receptors as a constant, which we could call r . Further noticing that equations A.8, A.9 and A.10 do not depend on A.11 we neglect this equation (we can always solve it once we have solved the others). Making the substitution $r_a = r - r_o$ leaves us with two equations

$$\frac{dn}{dt} = -k_1 r n + (k_{-1} + k_1 n) r_o \quad (\text{A.13})$$

$$\frac{dr_o}{dt} = k_1 n r - (k_{-1} + k_2 + k_1 n) r_o \quad (\text{A.14})$$

If we assume that the number of occupied receptors remains constant over the course of time we are interested in, i.e. making a quasi-steady-state assumption, we can isolate r_o in equation A.14 by which we get

$$r_o(t) = \frac{k_1 n(t) r}{k_{-1} + k_2 + k_1 n(t)} = \frac{n(t) r}{K_m + n(t)} \quad (\text{A.15})$$

Where $K_m = (k_{-1} + k_2)/k_1$ is the *Michaelis constant*. Substituting equation A.15 into equation A.13 we obtain

$$\frac{dn}{dt} = -\frac{K_{\max} n(t)}{K_m + n(t)} \quad (\text{A.16})$$

Where $K_{\max} = k_2 r$. Equation A.16 can be solved explicitly to yield an implicit in terms of $n(t)$, given by

$$n(t) = n_0 + K_m \ln \left(\frac{n_0}{n(t)} \right) \quad (\text{A.17})$$

Which obeys the initial condition on $n(t)$. However when we substitute equation A.17 into the approximated result for $r_o(t)$, and look at $t = 0$ we have

$$r_o(0) = \frac{k_1 r n_0}{k_{-1} + k_2 + k_1 n_0} \quad (\text{A.18})$$

which is obviously not in agreement with the initial conditions for $r_o(t)$. This illustrates the fact that we are dealing with an approximation, that may suffice at a transient time, when the amount of nutrient is abundant, and the number of occupied receptors can be taken to be constant. But on a longer timescale the nutrient will start to run out, and the number of occupied receptors will start to decrease.

A.5 Newton-Raphson Method

The Newton-Raphson method is a numerical method, that can be used for finding the roots of an equation or even system of equations (Shampine et al. (2003)). Having a system of differential equations, this of course means, finding the fixed points of a

system, $\dot{\mathbf{x}} = \mathbf{0}$. The method uses a simple and a fast convergent algorithm provided that the initial guess value is close to the root (Eldén et al. (2004)). When we walk through the derivation and the applications it will be evident that the method is based on differential calculus and the simple idea of linear approximation.

In order to derive it we start with the Taylor series expansion and since we applied the method on a system of differential equations the derivation will be based here on. Now let

$$\dot{\mathbf{x}} = \mathbf{f}(\mathbf{x}) \quad (\text{A.19})$$

And then let $\mathbf{f}(\mathbf{x})$ be a n-dimensional vector $\mathbf{f} = (f_1, f_2, \dots, f_n)^T$, $\mathbf{x} = (x_1, x_2, \dots, x_n)$. Then starting with the Taylor series expansion of the function $f_i(\mathbf{x})$ about the point \mathbf{x}

$$f_i(\mathbf{x} + \Delta\mathbf{x}) = f_i(\mathbf{x}) + \sum_{j=1}^n \frac{\partial f_i}{\partial x_j} \Delta x_j + O(\Delta x_j^2) \quad (\text{A.20})$$

where the “big O ” notation is an abbreviated way of writing the next terms in the series, i.e. the quadratic and higher order terms, and denotes that they are small, since Δx is expected to be small. So by ignoring them we have the linearized version of equation A.20, which we write using vector notation

$$\mathbf{f}(\mathbf{x} + \Delta\mathbf{x}) \approx \mathbf{f}(\mathbf{x}) + \mathbf{J}(\mathbf{f}(\mathbf{x}))\Delta\mathbf{x} \quad (\text{A.21})$$

here $\mathbf{J}(\mathbf{f}(\mathbf{x}))$ is the jacobian matrix. Since MATLAB is build to process calculations numerically the elements in the Jacobian can not be derived analytically. Instead we rewrite equation A.20 (again without the quadratic terms) to the form of a finite difference which then can be used as an approximation of the elements in the Jacobian

$$\frac{\partial f_i}{\partial x_j} \approx \frac{f_i(\mathbf{x} + h\hat{x}_j) - f_i(\mathbf{x})}{h} \quad (\text{A.22})$$

where \hat{x}_j is a unit vector pointing in the direction of x_j and h is the small increment of x . Now, the purpose remains to find the roots of the function $\mathbf{f}(\mathbf{x})$ and the way of doing it will be through iterative steps. Lets assume that \mathbf{x} is the initial approximation of the root \mathbf{x}^* and hence solution to $\mathbf{f}(\mathbf{x}) = \mathbf{0}$. Then let $\mathbf{x} + \Delta\mathbf{x}$ be a better approximation. To find the increment $\Delta\mathbf{x}$, and thereby the improved approximation for the root, we set $\mathbf{f}(\mathbf{x} + \Delta\mathbf{x}) = 0$ in equation A.21

$$0 = \mathbf{f}(\mathbf{x}) + \mathbf{J}(\mathbf{f}(\mathbf{x}))\Delta\mathbf{x} \quad (\text{A.23})$$

Since $\Delta\mathbf{x} = \mathbf{x}^{k+1} - \mathbf{x}^k$, where k is the number of iterations, we can rewrite equation A.23 in the following way

$$\mathbf{x}^{k+1} = \mathbf{x}^k - \mathbf{J}(\mathbf{f}(\mathbf{x}))^{-1}\mathbf{f}(\mathbf{x})^k \quad (\text{A.24})$$

the procedure now repeats itself by setting \mathbf{x}^{k+1} equal to \mathbf{x}^k until the increment $|\Delta\mathbf{x}| < \varepsilon$, where ε is a user defined error tolerance on the estimated value of \mathbf{x}^* compared to the analytical value. This is the essence in the Newton-Raphson method.

A.6 Dimensionless Form of the Intermediate Model Including Crowding Terms

In the following we nondimensionalize the three dimensional system including the crowding terms. We start out by reminding the reader how this version of the system looks

$$\frac{dM}{dt} = a + (k + b)M_a - cM - gMB_a - e_1M^2 - e_1MM_a \quad (\text{A.25})$$

$$\frac{dM_a}{dt} = gMB_a - kM_a - e_2M_a^2 - e_2MM_a \quad (\text{A.26})$$

$$\frac{dB_a}{dt} = W(t) + lM_a - f_1MB_a - f_2M_aB_a - dB_a \quad (\text{A.27})$$

We set $m\tilde{M} = M, m_a\tilde{M}_a = M_a, b_a\tilde{B}_a = B_a$, and obtain the following for the change in macrophage concentration

$$\frac{d\tilde{M}}{d\tau} = \frac{aT}{m} + \frac{(k + b)T}{m}m_a\tilde{M}_a - cT\tilde{m} - gTb_a\tilde{M}\tilde{B}_a - e_1Tm\tilde{M}^2 - e_1Tm_a\tilde{M}\tilde{M}_a \quad (\text{A.28})$$

We choose T, m, m_a, b_a in a fashion such that we obtain

$$\frac{d\tilde{M}}{d\tau} = 1 + \frac{k + b}{c}\tilde{M}_a - \tilde{M}\tilde{B}_a - \tilde{M} - \frac{e_1a}{c^2}\tilde{M}^2 - \frac{e_1a}{c^2}\tilde{M}\tilde{M}_a \quad (\text{A.29})$$

For the change in concentration of active macrophages we get

$$\frac{d\tilde{M}_a}{d\tau} = \frac{gT}{m_a}mb_a\tilde{M}\tilde{B}_a - kT\tilde{M}_a - e_2Tm_a\tilde{M}_a^2 - e_2Tm\tilde{M}_a\tilde{M} \Leftrightarrow \quad (\text{A.30})$$

$$= \tilde{M}\tilde{B}_a - \frac{k}{c}\tilde{M}_a - \frac{e_2a}{c^2}\tilde{M}_a^2 - \frac{e_2a}{c^2}\tilde{M}_a\tilde{M} \quad (\text{A.31})$$

And for the change in apoptotic β -cells

$$\frac{d\tilde{B}_a}{d\tau} = \frac{T}{b_a}W(t) + \frac{lT}{b_a}m_a\tilde{M}_a - f_1Tm\tilde{B}_a\tilde{M} - f_2Tm_a\tilde{B}_a\tilde{M}_a - dT\tilde{B}_a \Leftrightarrow \quad (\text{A.32})$$

$$= \frac{g}{c^2}W(t) + \frac{alg}{c^3}\tilde{M}_a - \frac{af_1}{c^2}\tilde{B}_a\tilde{M} - \frac{af_2}{c^2}\tilde{B}_a\tilde{M}_a - \frac{d}{c}\tilde{B}_a \quad (\text{A.33})$$

Noting that $e_1 = e_2$, and $f_1 = f_2$ for NOD mice, we define the following dimensionless groups. So the dimensionless equations become

$$\frac{d\tilde{M}}{d\tau} = 1 + \alpha\tilde{M}_a - \tilde{B}_a\tilde{M} - \tilde{M} - \beta\tilde{M}(\tilde{M} + \tilde{M}_a) \quad (\text{A.34})$$

$$\frac{d\tilde{M}_a}{d\tau} = \tilde{M}\tilde{B}_a - \gamma\tilde{M}_a - \beta\tilde{M}_a(\tilde{M} + \tilde{M}_a) \quad (\text{A.35})$$

$$\frac{d\tilde{B}_a}{d\tau} = \omega(t) + \delta\tilde{M}_a - \epsilon\tilde{B}_a(\tilde{M} + \tilde{M}_a) - \kappa\tilde{B}_a \quad (\text{A.36})$$

Letter	Dimensionless group	NOD	Balb/c
α	$\frac{k+b}{c}$	4.9	4.9
β	$\frac{ae_i}{c^2}$	0.01	0.01
γ	$\frac{k}{c}$	4	4
δ	$\frac{alg}{c^3}$	41	81
ϵ	$\frac{af_1}{c^2}$	10	20
ϕ	$\frac{af_2}{c^2}$	-	50
κ	$\frac{d}{c}$	5	5
$\omega(t)$	$\frac{g}{c^2}W(t)$	$40000 \times \exp(-((10\tau d - 9d)/(3d))^2)$	$40000 \times \exp(-((10\tau d - 9d)/(3d))^2)$

for the NOD mice, and

$$\frac{d\tilde{M}}{d\tau} = 1 + \alpha\tilde{M}_a - \tilde{B}_a\tilde{M} - \tilde{M} - \beta\tilde{M}(\tilde{M} + \tilde{M}_a) \quad (\text{A.37})$$

$$\frac{d\tilde{M}_a}{d\tau} = \tilde{M}\tilde{B}_a - \gamma\tilde{M}_a - \beta\tilde{M}_a(\tilde{M} + \tilde{M}_a) \quad (\text{A.38})$$

$$\frac{d\tilde{B}_a}{d\tau} = \omega(t)\delta\tilde{M}_a - \epsilon\tilde{B}_a\tilde{M} - \phi\tilde{B}_a\tilde{M}_a - \kappa\tilde{B}_a \quad (\text{A.39})$$

for the balb/c mice.

A.7 Fixed Point for the IM Including Crowding Terms

Looking at the healthy rest state $M_a, B_a = 0$ and solving equation 5.6 with respect to M

$$M = \frac{-c + \sqrt{c^2 + 4e_1a}}{2e_1} \quad (\text{A.40})$$

An approximated expression can be obtained, using Taylor series expansion (about $e_1 = 0$)

$$M = \frac{1}{2e_1} \left(-c + c\sqrt{1 + 4\frac{ae_1}{c^2}} \right) \quad (\text{A.41})$$

for $0 < e_1 \ll 1$ we obtain

$$\approx \frac{1}{2e_1} \left(-c + c \left(1 + 2\frac{ae_1}{c^2} \right) - 2\frac{a^2(e_1)^2}{c^3} \right) \quad (\text{A.42})$$

$$M \approx \frac{a}{c} - \frac{a^2}{c^3}e_1 = \frac{a}{c} \left(1 - \frac{ae_1}{c^2} \right) \quad (\text{A.43})$$

So provided that $e_1 \ll c^2/a$ then $M \approx a/c$ defines the healthy rest state to be

$$(M, M_a, B_a) = (a/c, 0, 0) \quad (\text{A.44})$$

B Additional Figures

In this appendix we have gathered some figures that were not presented in the text because, they were either not interesting to the analysis or because they would take up too much space compared to their relevance. The ones that were deemed “not interesting” have been gathered here for the purpose of documentation.

B.1 Eigenvalue-Plots Used to Evaluate Stability of the Fixed Points Shown in Figure 8.1

The following figures were all done with $f_2 = 1 \times 10^{-5}$. Figure B.1 shows the eigenvalues

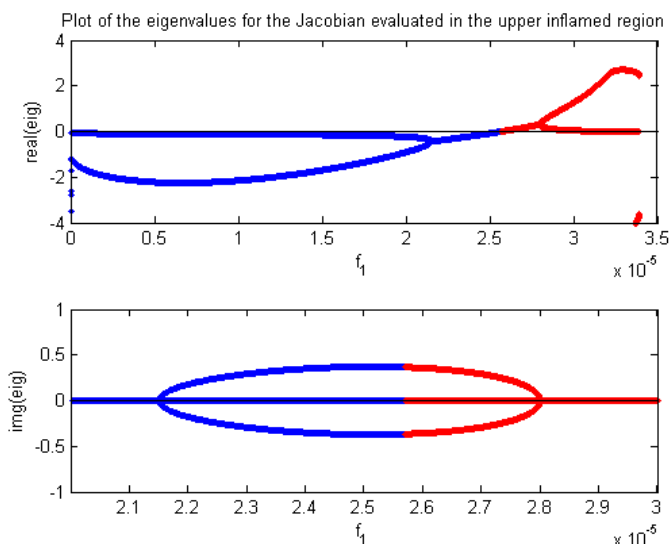


Figure B.1 Plot of the eigenvalues for the Jacobian evaluated in fixed points in the upper inflamed region.

of the Jacobian evaluated in the fixed points that correspond to a chronic inflammation, i.e. the USB. Figure B.2 shows the eigenvalues of the Jacobian evaluated in the fixed points on the LUB. The eigenvalues appear to make sudden jumps. However, this is a figment of MATLAB’s way of representing elements by magnitude, and as such does not represent a *de facto* change in the respective values of the eigenvalues. Figure B.3 shows the eigenvalues of the Jacobian evaluated in the HRS. This figure serves to document

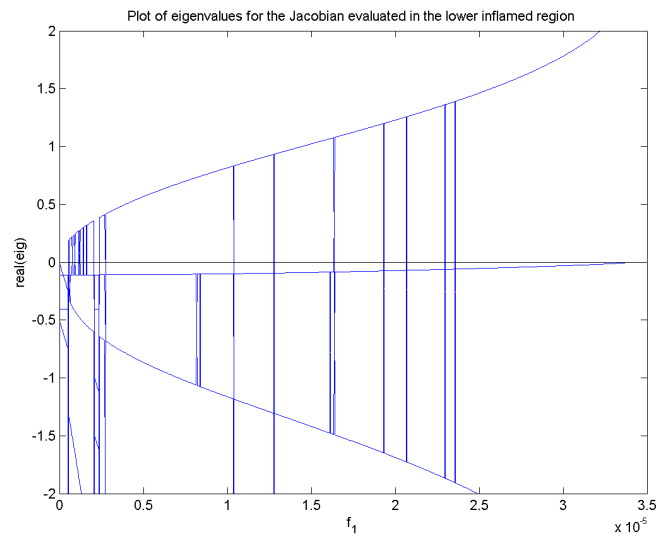


Figure B.2 Plot of the eigenvalues for the Jacobian evaluated in fixed points in the lower inflamed region.

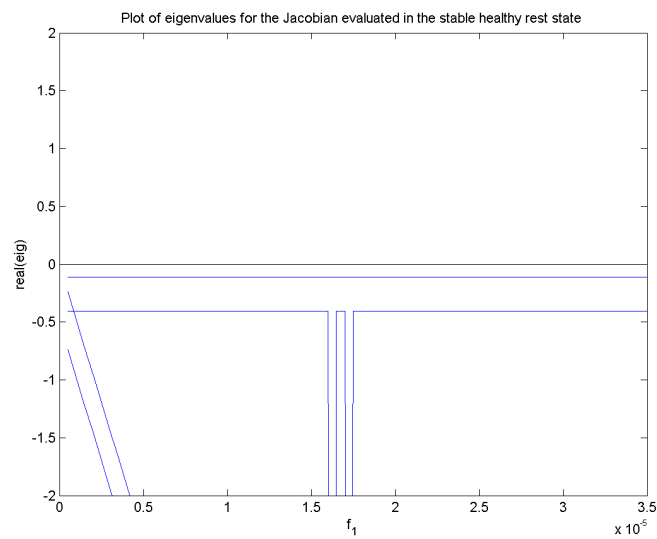


Figure B.3 Plot of the eigenvalues for the Jacobian evaluated in the healthy rest state.

that the state is in fact stable (all eigenvalues are negative) as we claimed in the analysis. Figure B.4 is a plot of the eigenvalues that become complex at $f_1 \approx 2.15 \times 10^{-5}$ in the complex plane.

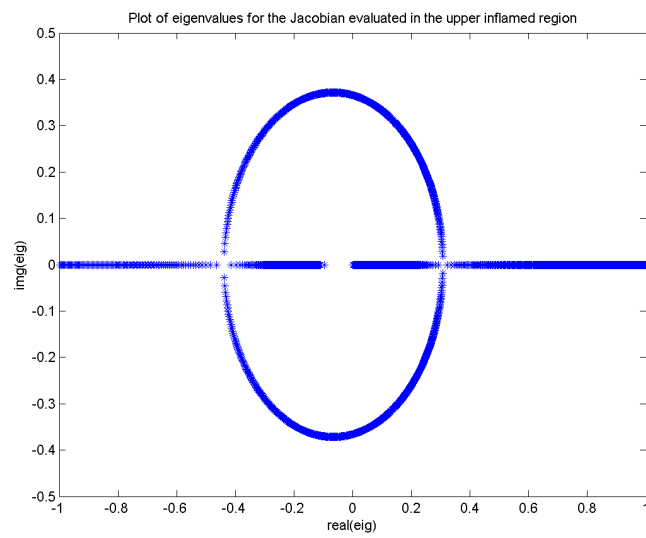


Figure B.4 A classical diagram of the imaginary part versus real part of the eigenvalues for the Jacobian evaluated in fixed points in the upper inflamed region.

B.2 Eigenvalue-Plots Used to Evaluate Stability of the Fixed Points Shown in Figure 8.11

The following figures were all done with $f_2 = 5 \times 10^{-5}$.

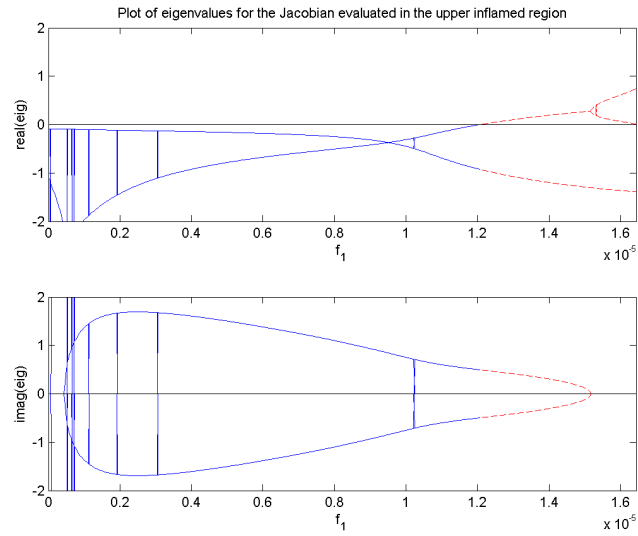


Figure B.5 Plot of the eigenvalues for the Jacobian evaluated in fixed points in the upper inflamed region.

B.2 Eigenvalue-Plots Used to Evaluate Stability of the Fixed Points Shown in Figure 8.11 143

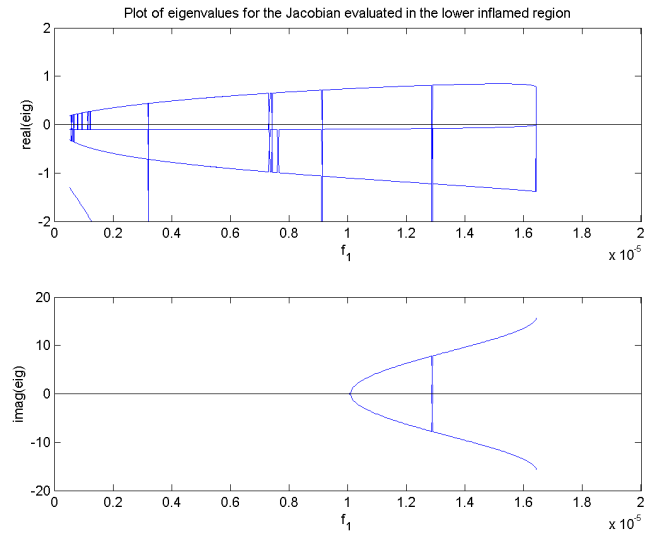


Figure B.6 Plot of the eigenvalues for the Jacobian evaluated in fixed points in the lower inflamed region.

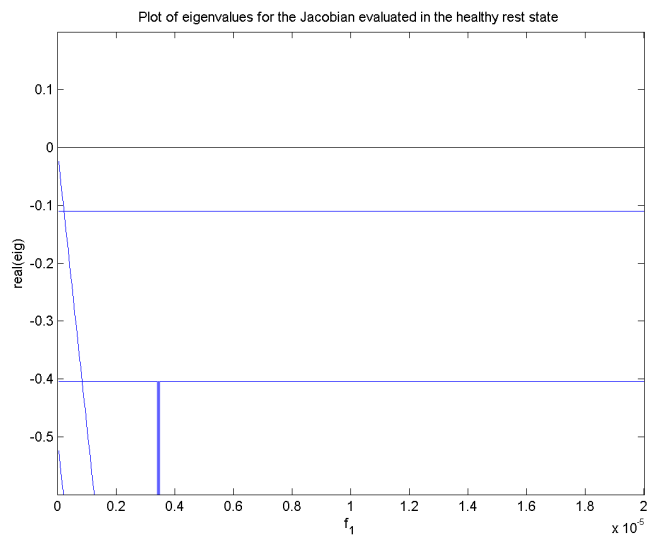


Figure B.7 Plot of the eigenvalues for the Jacobian evaluated in the healthy rest state.

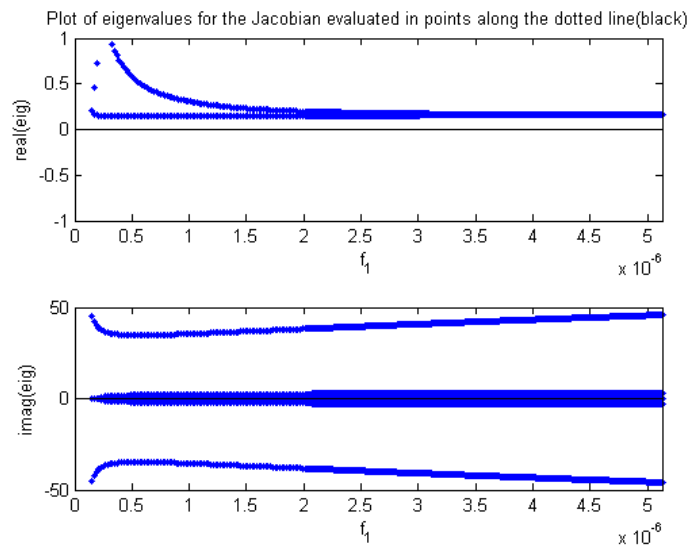


Figure B.8 Plot of the eigenvalues for the Jacobian evaluated in the fixed points along the dotted (black) line seen in figure 8.11.

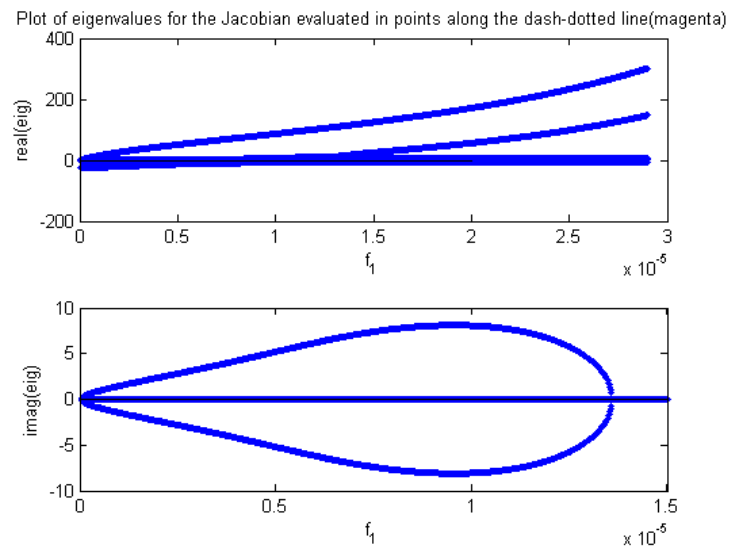


Figure B.9 Plot of the eigenvalues for the Jacobian evaluated in the fixed points along the dashed-dotted (magenta) line seen in figure 8.11.

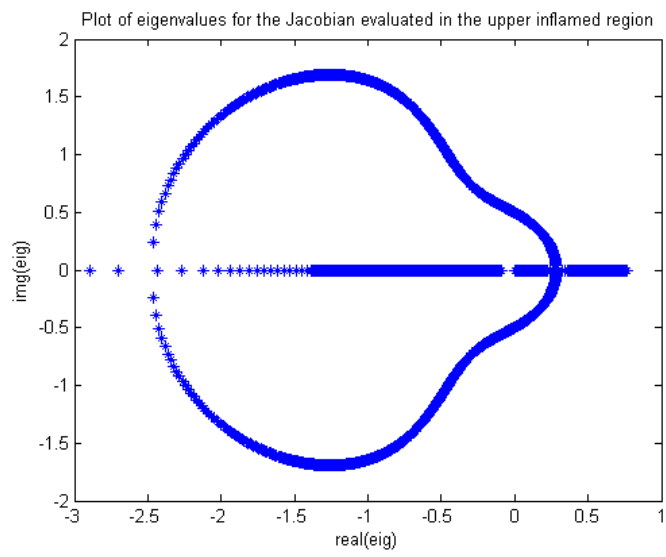


Figure B.10 A classical diagram of the imaginary part versus real part of the eigenvalues for the Jacobian evaluated in fixed points in the upper inflamed region.

B.3 Eigenvalue-Plots Used to Evaluate Stability of the Fixed Points Shown in Figure 8.12

The following figures were all done with $f_1 = 1 \times 10^{-5}$.

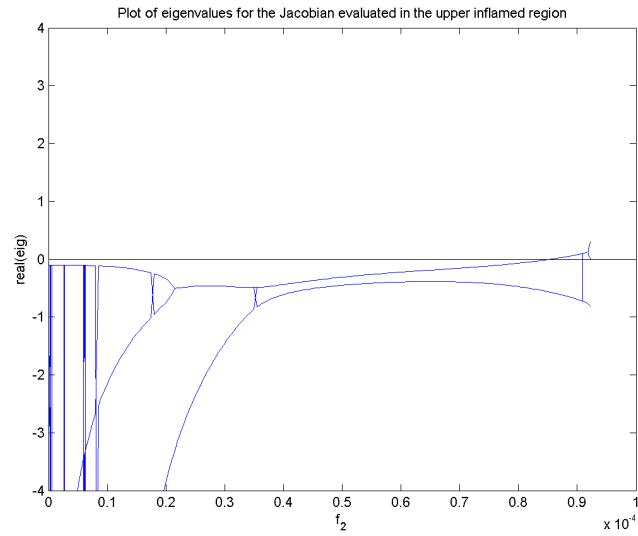


Figure B.11 Plot of the eigenvalues for the Jacobian evaluated in fixed points in the upper inflamed region.

B.3 Eigenvalue-Plots Used to Evaluate Stability of the Fixed Points Shown in Figure 8.12 147

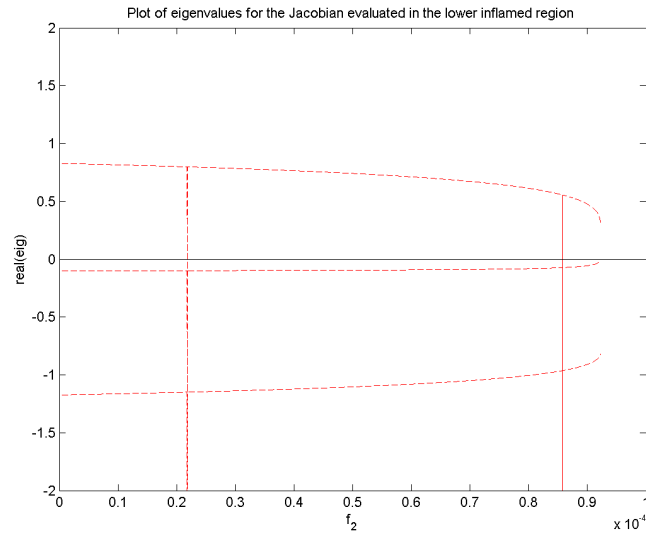


Figure B.12 Plot of the eigenvalues for the Jacobian evaluated in fixed points in the lower inflamed region.

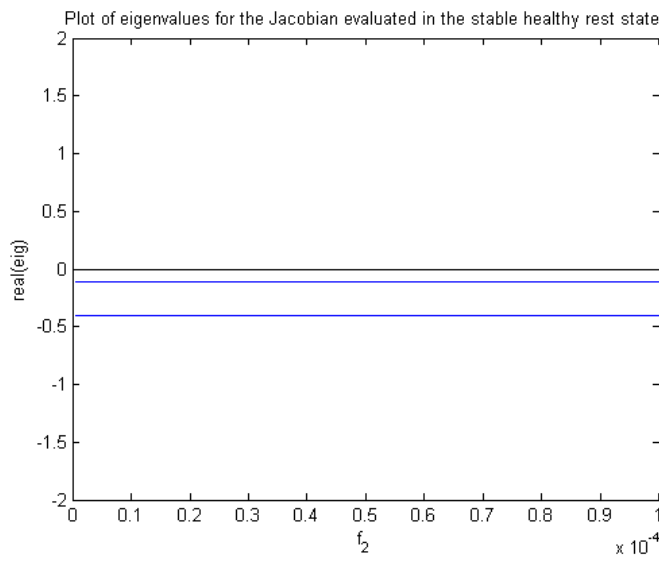


Figure B.13 Plot of the eigenvalues for the Jacobian evaluated in the healthy rest state.

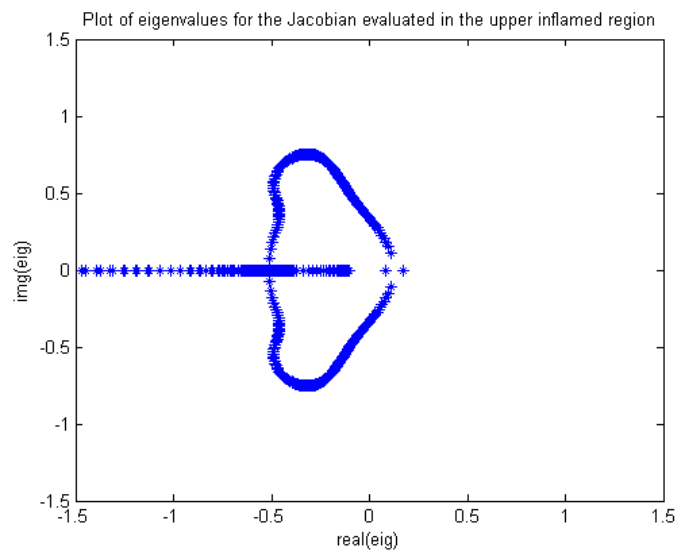


Figure B.14 A classical diagram of the imaginary part versus real part of the eigenvalues for the Jacobian evaluated in fixed points in the upper inflamed region.

B.4 Eigenvalue-Plots used to Evaluate Stability of the Fixed Points Shown in Figure 8.15

The following figures were all done with $f_1 = 2 \times 10^{-5}$.

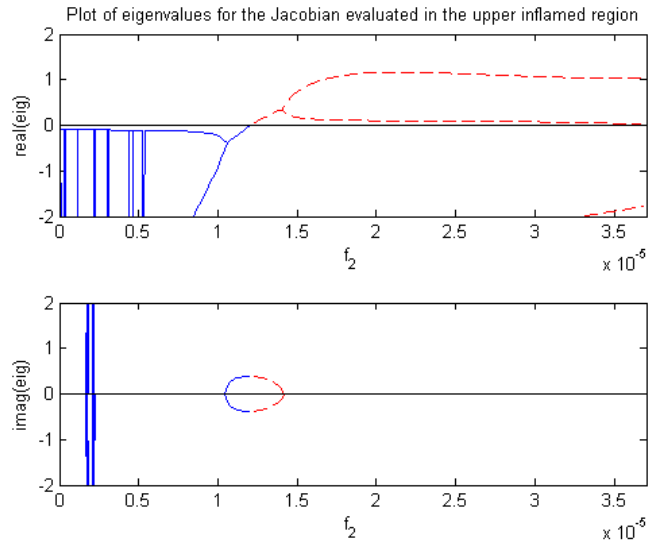


Figure B.15 Plot of the eigenvalues for the Jacobian evaluated in fixed points in the upper inflamed region.

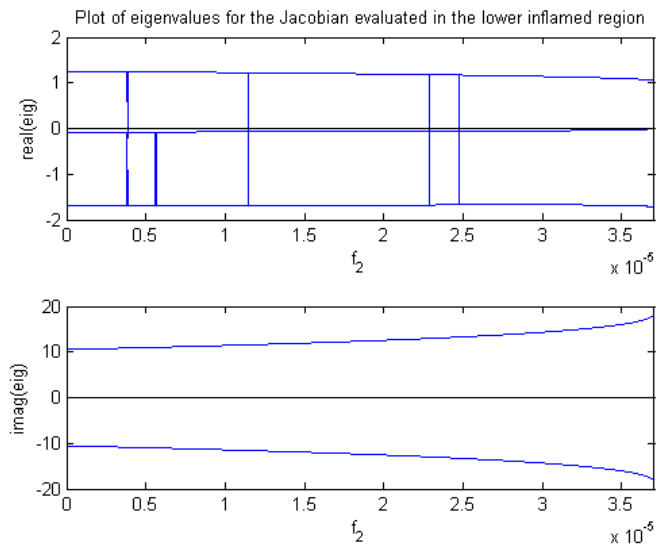


Figure B.16 Plot of the eigenvalues for the Jacobian evaluated in fixed points in the lower inflamed region.

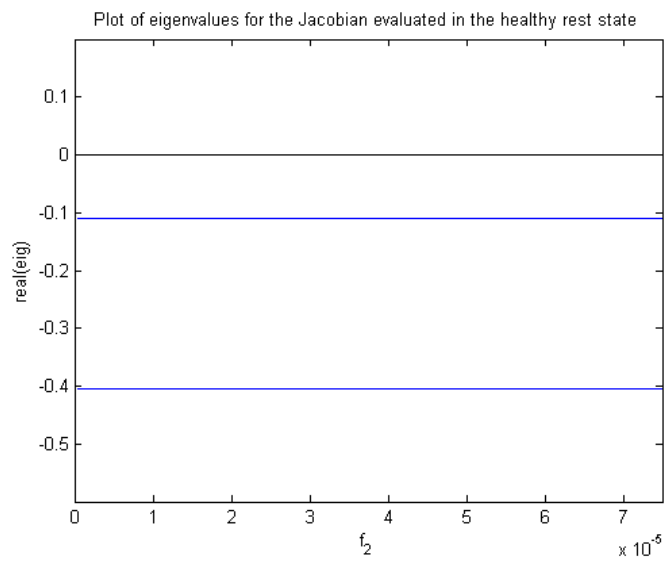


Figure B.17 Plot of the eigenvalues for the Jacobian evaluated in the healthy rest state.

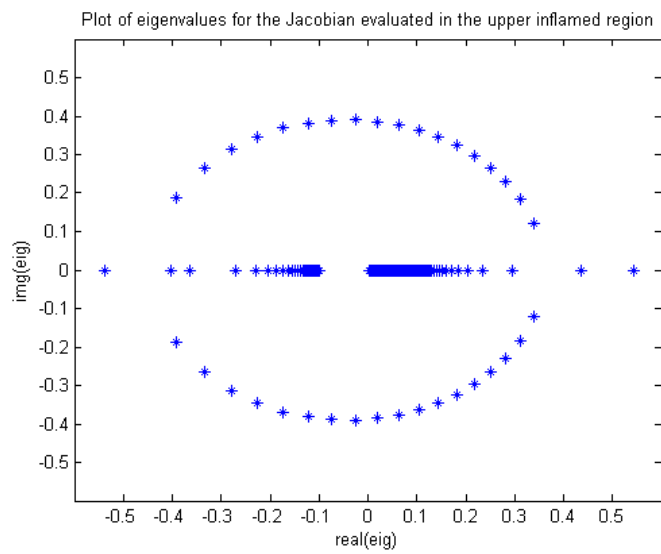


Figure B.18 A classical diagram of the imaginary part versus real part of the eigenvalues for the Jacobian evaluated in fixed points in the upper inflamed region.

B.5 Eigenvalue-plots Used to Evaluate Stability of the Fixed Points Shown in Figure 8.18

These figures pertain to figure 8.18 in section 8.4. In all of them f_2 is set to 1×10^{-5} .

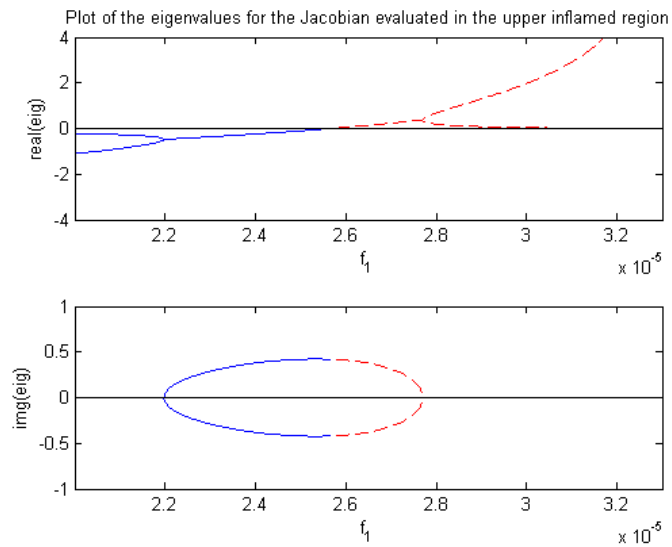


Figure B.19 Plot of the eigenvalues for the Jacobian evaluated in fixed points in the upper inflamed region.

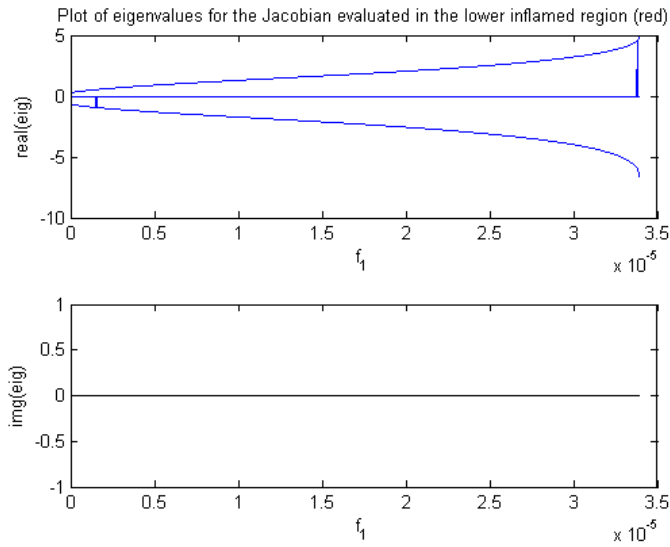


Figure B.20 Plot of the eigenvalues for the Jacobian evaluated in fixed points in the lower inflamed region.

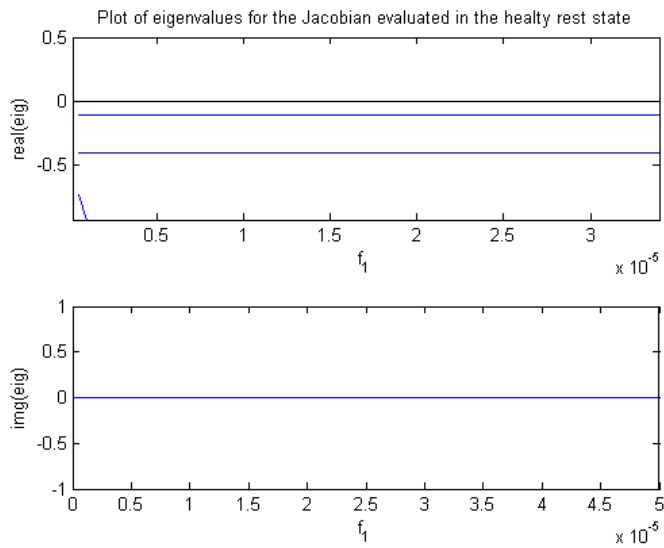


Figure B.21 Plot of the eigenvalues for the Jacobian evaluated in the healthy rest state.

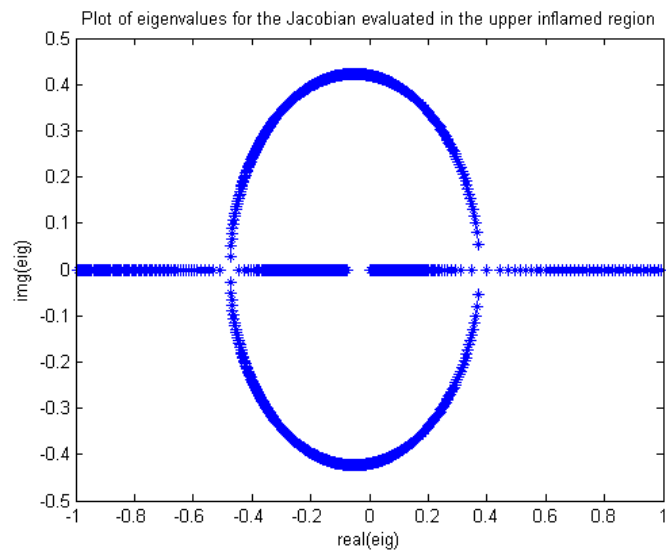


Figure B.22 A classical diagram of the imaginary part versus real part of the eigenvalues for the Jacobian evaluated in fixed points in the upper inflamed region (setting $f_2 = 1 \times 10^{-5}$).

B.6 Stable Spirals for f_1 near the Bifurcation Point

Here we present a series of phase space plots that show how the stable spiral behaves as f_1 nears the bifurcation point. f_1 grows from left to right in every figure and also as we go down through the figures. In figure B.25 f_1 changes very little from the figure on the left to the right; $f_1 = 2.5663 \times 10^{-5}$ on the left, $f_1 = 2.566305 \times 10^{-5}$ on the right. We have made such minuscule changes because this is very close to the bifurcation point. For $f_1 = 2.574 \times 10^{-5}$ the spiral has vanished, and the phase space curve tends to the healthy rest state; cf. figure 8.4.

The figures should be self-explanatory so we will not bother with a lot of repetitive caption.

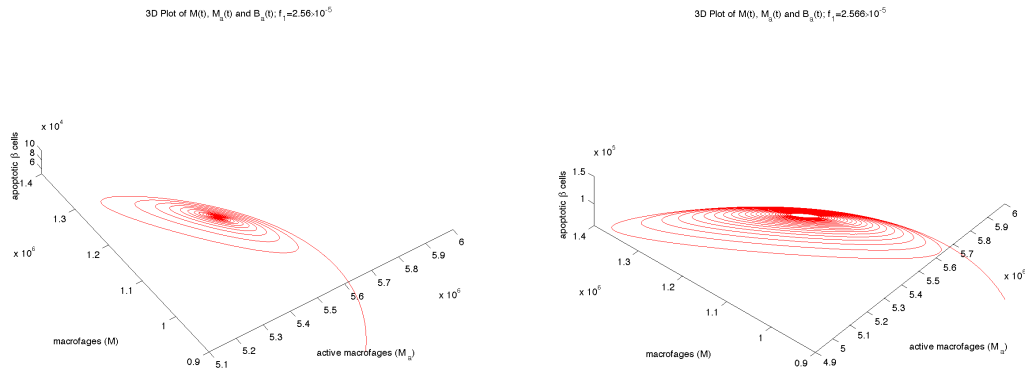


Figure B.23

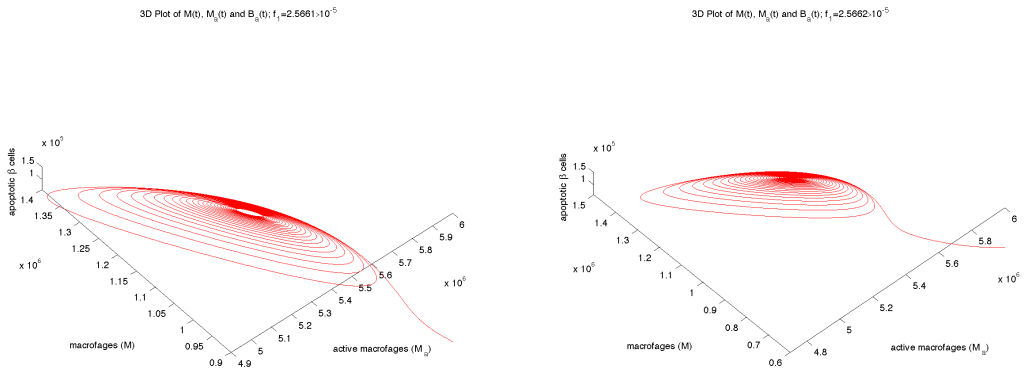


Figure B.24

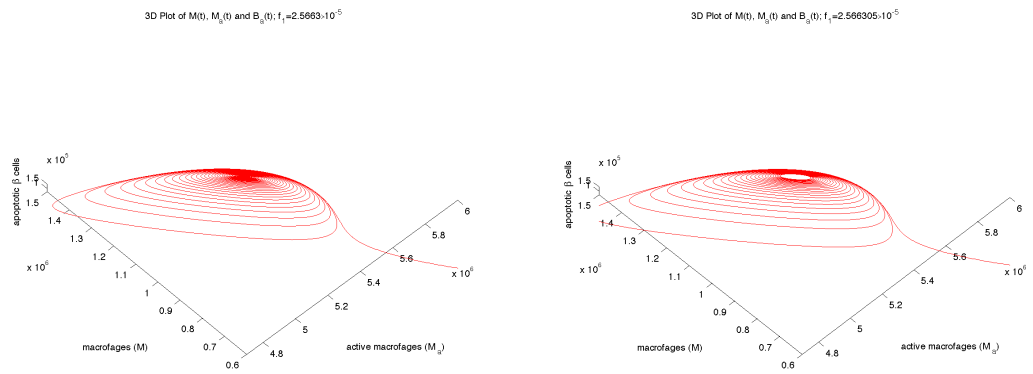


Figure B.25

C matlab Code

In the following appendix we provide the most important code that has been used in this thesis

C.1 Code for the Bifurcation Diagrams in Chapter 8

Sample-code used to produce the Hopf bifurcation. The code presented here are for Hopf bifurcation diagram shown in 8.1 and the associated eigenvalue plots seen in appendix B.1.

```
clear all
close all

format long e

global g;
global E;

%-----

%n=1283; %number of simulations
n=430;
w=0; %initial value for w
dw=0.002e-05; %step size

s=zeros(1,n);
V=zeros(n,5);
Q=zeros(n,5);
%initial values for M
ini_1 =[1.270545352258887e+006    2.176041550288973e+006...
7.441465343929523e+005    1.615186732129120e+004...
7.031245923372193e+000];

%

for r=1:n;
```

```

w(r+1)=w(r)+dw;

g=w(end);

[M]=newtonRaphson2(@eqdefT1D_full,ini_1);

M=M';

s(r)=M(end,2,:);
Q(r,:)=M(end,:);

V_1(r)=E(1);
V_2(r)=E(2);
V_3(r)=E(3);
V_4(r)=E(4);
V_5(r)=E(5);

end

w(1)=[];
%
% %-----
%
n=855;
w_2=8.6e-6;
dw_2=0.002e-05;

s_2=zeros(1,n);
Q_2=zeros(n,5);
V=zeros(n,5);

ini_2 =[1.177753840657023e+006    5.017144005834548e+006...
1.967867544648059e+005    1.588274974061828e+003...
1.593754564310941e+000]

for r=1:n;

w_2(r+1)=w_2(r)+dw_2;

g=w_2(end);

[M]=newtonRaphson2(@eqdefT1D_full,ini_2);

M=M';

Q_2(r,:)=M(end,:);

```

```

s_2(r)=M(end,2,:);

V_6(r)=E(1);
V_7(r)=E(2);
V_8(r)=E(3);
V_9(r)=E(4);
V_10(r)=E(5);

end

w_2(1)=[];

% %-----

%n=330;
n=1300;

%w_3=3.21e-5;
w_3=2.57e-5

dw_3=0.0005e-05;
Q_3=zeros(n,5);
s_3=zeros(1,n);

ini_3 =[1.116505900837692e+006    5.392570475033534e+006...
8.740562819326353e+004    5.289622803983940e+002...
5.704932751365578e-001];

%ini_3 =[1.328372622370533e+006    3.067127736673758e+006...
3.193345211780306e+004    2.177913256243388e+002...
1.335987631258712e-001];

for r=1:n;

    w_3(r+1)=w_3(r)+dw_3;

    g=w_3(end);

[M]=newtonRaphson2(@eqdefT1D_full,ini_3);

M=M';

s_3(r)=M(end,2,:);
Q_3(r,:)=M(end,:);

```

```

    V_11(r)=E(1);
    V_12(r)=E(2);
    V_13(r)=E(3);
    V_14(r)=E(4);
    V_15(r)=E(5);

end

w_3(1)=[];

% %-----

n=311;
%n=1300;

w_8=3.22e-5;
%w_8=2.57e-5;

dw_8=0.0005e-05;
Q_8=zeros(n,5);
s_8=zeros(1,n);

ini_8 =[1.328372622370533e+006    3.067127736673758e+006...
3.193345211780306e+004    2.177913256243388e+002  1.335987631258712e-001];

for r=1:n;

    w_8(r+1)=w_8(r)+dw_8;

    g=w_8(end);

[M]=newtonRaphson2(@eqdefT1D_full,ini_8);

M=M';

    s_8(r)=M(end,2,:);
    Q_8(r,:)=M(end,:);

    V_36(r)=E(1);
    V_37(r)=E(2);
    V_38(r)=E(3);
    V_39(r)=E(4);
    V_40(r)=E(5);

```

```
end

w_8(1)=[];

% %-----

n=369;
w_4=3.375e-5;

dw_4=0.00005e-05;
s_4=zeros(1,n);
Q_4=zeros(n,5);

ini_4 =[1.039297813007866e+006    1.114781993794900e+006...
1.339725328517090e+004    1.449162575570958e+002...
3.231000690655891e-002];

for r=1:n;

    w_4(r+1)=w_4(r)+dw_4;

    g=w_4(end);

[M]=newtonRaphson2(@eqdefT1D_full,ini_4);

M=M';

    s_4(r)=M(end,2,:);
    Q_4(r,:)=M(end,:);
%
    V_16(r)=E(1);
    V_17(r)=E(2);
    V_18(r)=E(3);
    V_19(r)=E(4);
    V_20(r)=E(5);

end

w_4(1)=[];

% %-----
%
```

```
n=675;
w_5=0;

dw_5=0.005e-05;
s_5=zeros(1,n);
Q_5=zeros(n,5);

ini_5 =[9.330299576072529e+005    8.242650262704889e+005...
1.087081707245666e+004    1.362102268102312e+002...
2.245466523600889e-002];

for r=1:n;

    w_5(r+1)=w_5(r)+dw_5;

    g=w_5(end);

[M]=newtonRaphson2(@eqdefT1D_full,ini_5);

M=M';

    s_5(r)=M(end,2,:);
    Q_5(r,:)=M(end,:);
%
    V_21(r)=E(1);
    V_22(r)=E(2);
    V_23(r)=E(3);
    V_24(r)=E(4);
    V_25(r)=E(5);

end

w_5(1)=[];
%
% %-----

n=923;
w_6=3.375e-5;

dw_6=0.00002e-05;
s_6=zeros(1,n);
Q_6=zeros(n,5);

ini_6 =[8.418272915816533e+005    6.159233005050864e+005
8.987431430737131e+003    1.299854844090522e+002
```

```

1.601221771499518e-002 ];

for r=1:n;

    w_6(r+1)=w_6(r)+dw_6;

    g=w_6(end);

[M]=newtonRaphson2(@eqdefT1D_full,ini_6);

M=M';

    s_6(r)=M(end,2,:);
    Q_6(r,:)=M(end,:);
%
    V_26(r)=E(1);
    V_27(r)=E(2);
    V_28(r)=E(3);
    V_29(r)=E(4);
    V_30(r)=E(5);

end

w_6(1)=[];

% %-----

n=80;
w_7=0;

dw_7=0.05e-05;
s_7=zeros(1,n);
Q_6=zeros(n,5);

ini_7 =[4.772255750458808e+005    0 5.600225683160789e-007    0 0];

for r=1:n;

    w_7(r+1)=w_7(r)+dw_7;

    g=w_7(end);

[M]=newtonRaphson2(@eqdefT1D_full,ini_7);

```

```

M=M';

    s_7(r)=M(end,2,:);
    Q_7(r,:)=M(end,:);
%
    V_31(r)=E(1);
    V_32(r)=E(2);
    V_33(r)=E(3);
    V_34(r)=E(4);
    V_35(r)=E(5);

end

w_7(1)=[];

%-----

k=w(1):0.0005e-05:w_7(end);

%-----

%-----

figure
plot(w,s,'-b',w_2,s_2,'-b',w_3,s_3,'--r',w_4,s_4,'--r',w_5,s_5,'--r',...
w_6,s_6,'--r',w_7,s_7,'-g',w_8,s_8,'--r')%

axis([0 4e-5 -0.1e6 6e6])
xlabel('f_1')
ylabel('M_a(t)*')

%ini=[ini_1;ini_2;ini_3;ini_4;ini_5;ini_6;ini_7;ini_8];

%legend([repmat('ini = ',size(ini,1),1) num2str(ini)])

Title('Numerical bifurcation diagram')
%-----
% figure
%
% subplot(2,1,1);plot(w,real(V_1),' .b',w,real(V_2),' .b',w,
real(V_3),' .b',w,real(V_4),' .b',w,real(V_5),' .b',
w_2,real(V_6),' .b',w_2,real(V_7),' .b',w_2,real(V_8),' .b',
w_2,real(V_9),' .b',w_2,real(V_10),' .b',w_3,real(V_11),
'.b',w_3,real(V_12),' .b',w_3,real(V_13),' .b',w_3,real(V_14),' .b',
w_3,real(V_15),' .b',w_4,real(V_16),' .b',w_4,real(V_17),' .b',

```

```

w_4,real(V_18),'.b',w_4,real(V_19),'.b',w_4,real(V_20),'.b',
w_8,real(V_36),'.b',w_8,real(V_37),'.b',
w_8,real(V_38),'.b',w_8,real(V_39),'.b',w_8,real(V_40),'.b',k,0,'black')
% axis([0 3.5e-5 -4 4 ])
% Title('Plot of eigenvalues for the Jacobian evaluated in the upper inflamed region')
% xlabel('f_1')
% ylabel('real(eig)')
%
% subplot(2,1,2);plot(w,imag(V_1),'.b',w,imag(V_2),'.b',
w,imag(V_3),'.b',w,imag(V_4),'.b',w,imag(V_5),'.b',
w_2,imag(V_6),'.b',w_2,imag(V_7),'.b',w_2,imag(V_8),'.b',
w_2,imag(V_9),'.b',w_2,imag(V_10),'.b',w_3,imag(V_11),'.b',
w_3,imag(V_12),'.b',w_3,imag(V_13),'.b',w_3,imag(V_14),'.b',
w_3,imag(V_15),'.b',w_4,imag(V_16),'.b',w_4,imag(V_17),'.b',
w_4,imag(V_18),'.b',w_4,imag(V_19),'.b',w_4,imag(V_20),'.b',
w_8,imag(V_36),'.b',w_8,imag(V_37),'.b',w_8,imag(V_38),'.b',
w_8,imag(V_39),'.b',w_8,imag(V_40),'.b',k,0,'black')
% xlabel('f_1')
% ylabel('imag(eig)')
%

% -----
figure

subplot(2,1,1);plot(w_5,real(V_21),'.b',w_5,real(V_22),'.b',
w_5,real(V_23),'.b',w_5,real(V_24),'.b',
w_5,real(V_25),'.b',w_6,real(V_26),'.b',w_6,real(V_27),'.b',
w_6,real(V_28),'.b',w_6,real(V_29),'.b',
w_6,real(V_30),'.b',k,0,'black')
axis([0 3.5e-5 -2 2 ])
Title('Plot of eigenvalues for the Jacobian evaluated in the lower inflamed region ')
xlabel('f_1')
ylabel('real(eig)')

subplot(2,1,2);plot(w_5,imag(V_21),'.b',w_5,imag(V_22),'.b',
w_5,imag(V_23),'.b',w_5,imag(V_24),'.b',
w_5,imag(V_25),'.b',w_6,imag(V_26),'.b',w_6,imag(V_27),'.b',
w_6,imag(V_28),'.b',w_6,imag(V_29),'.b',
w_6,imag(V_30),'.b',k,0,'black')
xlabel('f_1')
ylabel('imag(eig)')

%-----
figure

plot(w_7,V_31, '.b',w_7,V_32, '.b',w_7,V_33, '.b',

```

```

w_7,V_34,'.b',w_7,V_35,'.b',k,0,'black')
axis([0 3.5e-5 -2 2 ])
Title('Plot of eigenvalues for the Jacobian evaluated in the stable healthy rest state ')

xlabel('f_1')
ylabel('real(eig)')
%-----

figure

subplot(2,1,1); plot(w,real(V_1),'.b',w,real(V_2),'.b',
w,real(V_3),'.b',w,real(V_4),'.b',w,real(V_5),'.b',
w_2,real(V_6),'.b',w_2,real(V_7),'.b',w_2,real(V_8),'.b',
w_2,real(V_9),'.b',w_2,real(V_10),'.b',
w_3,real(V_11),'.r',w_3,real(V_12),'.r',w_3,real(V_13),'.r',
w_3,real(V_14),'.r',w_3,real(V_15),'.r',w_4,
real(V_16),'.r',w_4,real(V_17),'.r',w_4,real(V_18),'.r',
w_4,real(V_19),'.r',w_4,real(V_20),'.r',
w_8,real(V_36),'.r',w_8,real(V_37),'.r',w_8,real(V_38),'.r',
w_8,V_39,'.r',w_8,real(V_40),'.r',k,0,'black')

axis([0 3.5e-5 -4 4 ])
Title('Plot of the eigenvalues for the Jacobian evaluated in...
the upper inflamed region')

xlabel('f_1')
ylabel('real(eig)')

subplot(2,1,2); plot(w,imag(V_1),'.b',w,imag(V_2),'.b',
w,imag(V_3),'.b',w,imag(V_4),'.b',w,imag(V_5),'.b',
w_2,imag(V_6),'.b',w_2,imag(V_7),'.b',w_2,imag(V_8),'.b',
w_2,imag(V_9),'.b',w_2,imag(V_10),'.b',
,w_3,imag(V_11),'.r',w_3,imag(V_12),'.r',w_3,imag(V_13),'.r',
w_3,imag(V_14),'.r',w_3,imag(V_15),'.r',
w_4,imag(V_16),'.r',w_4,imag(V_17),'.r',w_4,imag(V_18),'.r',
w_4,imag(V_19),'.r',w_4,imag(V_20),'.r',
w_8,imag(V_36),'.r',w_8,imag(V_37),'.r',w_8,imag(V_38),'.r',
w_8,V_39,'.r',w_8,imag(V_40),'.r',k,0,'black')%
%axis([0 3.5e-5 -4 4 ])
axis([2e-5 3e-5 -1 1 ])
xlabel('f_1')
ylabel('img(eig)')

figure
%
plot(real(V_4),imag(V_4),'*b',real(V_5),imag(V_5),'*b',
real(V_9),imag(V_9),'*b', real(V_10),imag(V_10),'*b',

```

```

real(V_14),imag(V_14),'*b',real(V_15),imag(V_15),'*b',
real(V_19),imag(V_19),'*b',real(V_20),imag(V_20),'*b',
real(V_39),imag(V_39),'*b',
real(V_40),imag(V_40),'*b')%k,0,'b'...
axis([-1 1 -0.5 0.5 ])

Title('Plot of eigenvalues for the Jacobian evaluated in
the upper inflamed region')

xlabel('real(eig)')
ylabel('img(eig)')

%-----

```

C.2 Code for the Newton-Raphson Method

The code for the Newton-Raphson method. This is adapted from Shampine et al. (2003).

```

function root = newtonRaphson2(func,M,tol)
% Newton-Raphson method of finding a root of simultaneous
% equations  $f_i(x_1,x_2,\dots,x_n) = 0$ ,  $i = 1,2,\dots,n$ .
% USAGE: root = newtonRaphson2(func,x,tol)
% INPUT:
% func = handle of function that returns [f1,f2,...,fn].
% x = starting solution vector [x1,x2,...,xn].
% tol = error tolerance (default is 1.0e4*eps).
% OUTPUT:
% root = solution vector.

%define global

%global g;

Q=M;

if nargin == 2; tol = 1.0e7*eps; end %NARGIN defines the
number of input arguments that were used to call the function
(M,tol). %Tol is the error tolerance for the computation
here set to 1.0e4*eps = 2.2204e-012

%if size(M,1) == 1; M = M'; end % M must be column vector
(ctranspose - Complex conjugate transpose [''] ). if 3==1??

%for i = 1:50

```

```

M=M'; % M must be column vector

for i = 1:1e7
[jac,F0] = jacobian(func,M);
if sqrt(dot(F0,F0)/length(M)) < tol %where sqrt to scalar
product of f0 are the length of f0

root = M; return

end

dM = jac\(-F0); % mldivide - Backslash or left matrix divide
\. This is the Newton-Raphson formular  $J(x)*dx=-f(x)$ 

M = M + dM; if sqrt(dot(dM,dM)/length(M)) < tol*max(abs(M),1.0) %
For vectors, MAX(X) is the largest element in X

root = M; return
end
end
error('Too many iterations') % if the value doesnt subside the error
tolerance during the end i'th iteration and error messags is displayed

%-----

```

Code for Approximation of the Jacobian

The following code was used to approximate the Jacobian by the finite difference method. This is adapted from Shampine et al. (2003).

```

function [jac,F0] = jacobian(func,M)
% Returns the Jacobian matrix and f(x).

global E;

h = 1.0e-4;
n = length(M);
jac = zeros(n);
F0 = feval(func,M);
for i =1:n;
temp = M(i);
M(i) = temp + h;
F1 = feval(func,M);
M(i) = temp;

jac(:,i) = (F1 - F0)/h;

```

```

end
E=eig(jac);
%-----

%The code to "call" when solving the system
of differential equations by ode45.

function Mdot = eqdefT1D_full(M)

global g;

b = 0.09; %defines the parameter values
c = 0.1;
d = 0.5;
e = 1e-8;

f2=1e-5;
f1=1e-5
a = 5e4;
k = 0.4;
alpha=5e-9;
delta=25;
kc=1;
Amax = 2e7;
kb=(delta/alpha)*kc;

%DuCa model without apoptotic wave

Mdot = [a + (b + k) * M(2) - c * M(1) -
f1 * M(1) * M(3) - e * M(1) * ( M(1) + M(2) );
;f1 * M(1) * M(3) - k * M(2) - e * M(2) * ( M(1) + M(2) );
;(( Amax * M(5) )./( kc + M(5) )) - f1 * M(1) * M(3)
- f2 * M(2) * M(3) - d * M(3);
;d * M(3) - f1 * M(1) * M(4) - f2 * M(2)* M(4);
;alpha * M(4) * M(2) - delta * M(5)];
%-----

%A sample code used for solving the system of differential
%equations by ode15s

clear all
close all
% initial values
M = [4e3 10e6 2e3 2e3 2e3];
% time span
tspan = [0 200];

```

```

%options = odeset('RelTol',1e-6,'AbsTol',1e-6);

[t,M] = ode15s(@modelT1DmareeG_full,tspan,M);

figure
plot(t,M)
xlabel('t')
ylabel('M(t), Ma(t), Ba(t), Bn(t),C(t)')
legend('M(t)', 'Ma(t)', 'Ba(t)', 'Bn(t)', 'C(t)', 2)

```

C.3 The Function-File for Model C

The following is the function-file that contains Model C.

```

function Mdot = mareemodelfuld6C(t,M)
Mdot = zeros(6,1);
global A b c d e f1 f2 a k k_c l x2 x3 x4
%defines parameter values
A = 2*10^7/(1e9);
a = 5*10^4;
b = 0.09;
c = 0.1;
d = 0.5;
e = 1*10^-8;
f1 = 1*10^-5;
f2 = 1*10^-5;
h = 5*10^-9;
k = 0.4;
k_c = 1;
l = 0.41;
m = 25;
r0 = 0.04;
a0 = 0.022;
t1 = (365*log((r0-0.036)/0.036)-30*log((r0-0.0007)/0.0007))/(log((0.0007*(r0-0.036))...
/(0.036*(r0-0.0007))))
p1 = log((r0-0.036)/0.036)/(30-t1)
t2 = (365*log((a0-0.018)/0.018)-30*log((a0-0.001)/0.001))/(log((0.001*(a0-0.018))...
/(0.018*(a0-0.001))))
p2 = log((a0-0.018)/0.018)/(30-t2)
x5 = 1*10^7;
Mdot(1,1) = a + (b + k) * M(2,1) - c * M(1,1) - f1 * M(1,1) * M(3,1)...
- e * M(1,1) * (M(1,1) + M(2,1));
Mdot(2,1) = f1 * M(1) * M(3) - k * M(2) - e * M(2) * (M(1) + M(2));
Mdot(3,1) = (a0*(1+exp(-p2*t2))/(1+exp(p2*(t-t2)))+0.001)*M(6)...
+ (4*10^7 *exp(-((t-9)/3)^2)/(1e9))*M(6) + (A*M(5)/(k_c + M(5)))*M(6)...
- f1 * M(3) * M(1) - f2 * M(2) * M(3) - d * M(3);
Mdot(4,1) = d*M(3) - f1*M(1)*M(4) - f2*M(2)*M(4);

```

```

Mdot(5,1) = h*M(4)*M(2) - m*M(5);
Mdot(6,1) = -(a0*(1+exp(-p2*t2))/(1+exp(p2*(t-t2))) + 0.001)*M(6)...
- (4*10^7 *exp(-((t-9)/3)^2)/(1e9))*M(6) - (A*M(5)/(k_c + M(5)))*M(6) ...
+ r0*(1+exp(-p1*t1))/(1+exp(p1*(t-t1)))*M(6);

```

Simulation Code for Model C

The following code was used to produce the simulations of Model C.

```

clear all
close all
figure
hold on
M = [4.77e5,0,0,0,0,1e9];...
tspan = [0;5000];
options = odeset('Reltol',1e-20,'AbsTol',1e-20);
[t,M] = ode15s(@mareemodelfuld6C,tspan,M);
Mtilde=M(:,6);
Mtilde(find(Mtilde<=0))=0;
M(:,6)=Mtilde;
plot(t,M)
grid
title('Concentrations versus time for Balb/c-mice')
xlabel('Time(d)')
ylabel('Concentration')
figure
hand=plot(t,M);
set(hand, 'LineWidth', 2);
axis([0 125 0 6.5e6])
legend('Resting Macrophages','Active Macrophages','Apoptotic \beta-cells'...
,'Necrotic \beta-cells','Cytokines','\beta-cells')
%axis([0 500 0 1.65e6])
hand1=title('Concentrations versus time for NOD-mice; x_{3,0} = 0.022, r_0 = 0.04');
set(hand1,'FontSize',10)
set(hand1,'FontWeight','Bold')
hand2=xlabel('Time(d)');
set(hand2,'FontSize',10)
set(hand2,'FontWeight','Bold')
hand3=ylabel('Concentration');
set(hand3,'FontSize',10)
set(hand3,'FontWeight','Bold')
hold off

```


Index

- W^s
 - of NOD $_{f_1}$ -USB, 79
 - dimension of, 80
- W^u , 79
 - of NOD $_{f_1}$ -USB, 79
 - dimension of, 80
- β -Cell, 1, 7
 - apoptosis, 7
 - apoptotic, 25
 - necrosis, 7
 - necrotic, 25
 - neogenesis, 15
 - proliferation
 - during inflammation, 36
 - replication, 14
- MATLAB, 42, 73, 76, 77
- MATLAB, 34, 73, 88, 108

- Activated Macrophages, 82
- Activation
 - due to necrotic cells, 36
- Activation Step, 38
- Active Macrophages
 - behavior of concentration
 - and heteroclinic orbits, 83
- Akaike Information Criterion, 38
 - Akaike information criterion, **38**
- Alloxan, 15
- Andrew C. Ivy, 2, 8
- Animal Model, 7
 - Sprague Dawley rat, 120
- Antigen Presenting Cell (APC), 9
- Antigen Therapy, 16
- Apoptosis, 7
 - in healthy individuals, 33
 - maximal cytokine induced rate of,
 - 25
 - natural
 - Model A, 107
 - Model B, 110
 - Model C, 114
- Apoptotic Wave, 19, **19**, 25, 26, 73
 - and β -cell population, 107
 - and bifurcation analysis, 89
 - dependence on time, 131
- Arrow
 - fully drawn, 23
 - stippled, 23
- Autoantibodies, 8
- Autoantibody, 7
 - and risk of developing T1D, 8
- Autoantigen, 8, 15
- Autoimmune Response, 7
- Autoimmunity, 15
 - autoimmune response, 14

- B Cell, 9, 18
- Bacteria, 133
- Balb/c Mouse, 18
- Bifurcation, **65**
 - codimension of, 66
 - codimension one, 65
 - diagram, 73
 - Hopf, 77
 - local, 66
 - parameter, 66
 - pitchfork, 66
 - point, 66
 - saddle-node, 66, 95
 - transcritical, 66
 - codimension one, 73
 - codimension two, 101
 - global, 71, 83
 - pitchfork, 86
 - point, 77
 - saddle-node, 81

- value, 73
- Bifurcation Analysis, 65
- Bifurcation Parameter
 - choice of, 69
- Bifurcation Value
 - definition of, 66
- Bio-Model, 21
- Bio-model, 7
- Biological System, 133

- CD4⁺, 8
- CD8⁺, 8
- Chaos, 59
- Characteristic Polynomial, 50, 66, 94
- Closed Orbit, 66
- Codimension
 - of bifurcation, 65
- Compact Subset, 59
- Compartment Model, **21**
 - Marée et al. (2006), 23
 - arrow
 - fully drawn, 23
 - stippled, 23
 - discussion of, 28
 - apoptotic wave, 28
 - crowding terms, 28
 - Efflux, 22
 - inflow, 21
 - Influx, 22
 - Mathematical Modelling, 21
 - outflow, 22
- Competition
 - Lotka-Volterra model of, 26
 - active versus inactive macrophages, 26
 - modelling of, 26
- Continuous Deformation, 59
- Cooperativity, 35
- Copenhagen Model, 2
- CPH Model, 21, 45
 - is quantitatively incorrect, 54
- Crowding Effect, 26
- Crowding Rate, 25
- Cytokine, 10, 45
 - and necrosis, 10
 - and proliferation, 10
 - cytotoxic, 19
- Cytotoxicity, 10

- Deactivation Step, 38
- Dendritic Cell, 15, 18
- Dendritic Cell (DC), 9
- Determinant
 - expansion of, 50
- Diabetes, 1
 - etiology of, 7
 - subtype of, 11
- DuCa Model, 19, 21, 46
 - expanding the, 105
 - Model A, 106, **108**
 - Model B, 110
 - validating, 117
 - maximal interval of existence, 132
 - parameters, 27
 - uniqueness of solutions to, 132
 - with cM_a
 - limit cycle, 42
 - phase space, 42
 - solution curve of, 42

- Efflux
 - of active macrophages, 40, 41
 - of macrophages, 25
- Eigendirection, 79
- Eigenspace, 59
- Eigenvalue, 70, 94
 - complex, 66, 75, 76
- Eigenvector, 59, 67, 79, 94
- Environmental Factors, 1
- Enzyme, 35
- Error-Tolerance, 70
- Etiology, 1, 2, 13
- Euler's Formula, 67
- Existence and Uniqueness Theorem, 25, **131**

- Feedback Loop, 19
- Fixed Point, 54
 - and chronic inflammation, 97
 - definition, 48
 - nontrivial, 97
 - unstable, 97
- Flow
 - on the circle, 87

-
- Gastrin, 14, 15
 Global Bifurcation, 71, 83
 GLP-1, 121
 anti-apoptosis, 14
 Glucagon-Like Peptide 1 (GLP-1), 2, **14**
 Glutamic Acid Decarboxylase (GAD), 8
 Growth Rate, 133
- Hartman-Grobman's Theorem, 59, **132**
 Healthy β -Cells
 linear depletion of, 106
 simulation of, 108
 Healthy Rest State(HRS), 75
 Heteroclinic Orbit, 83
 figure 8.7, 83
 Hill Function, 34
 Hill function, **26**
 Homeomorphism, 59
 Homeostasis, 7
 Hopf Bifurcation, 71
 degenerate, 68
 on the USB $_{f_1}$ -NOD, 77
 point, 75
 subcritical, 87
 supercritical, 68
 value, 87
 Hopf Bifurcation Theorem, 77
 Hyperbolic, 59
 Hyperglycemia, **1**, 7
 Hypoglycemia, 2
 Hysteresis, **69**, 87
- IDDM, 1, 2
 IM
 including crowding terms
 flow equivalence to the DuCa, 81
 Immune System
 Adaptive, 15
 Implicit Function Theorem, 55, **132**
 Incretin Concept, **2**, 8
 Inflammation
 upper bound of, 81
 Influx
 of macrophages, 25
 Initial Condition, 66
 Insulin, 1
 first bolus of, 1
 Insulin Dependent Diabetes Mellitus (IDDM),
 1
 Insulinitis, 9, 106
 Interferon (IFN), 10
 Interleukin (IL)
 1, 10, 120
 2, 10
 Intermediate Model (IM), 21
 Irreversible Model
 NOD phagocytosis, 40
 phase space
 M versus M_a , 42
 Islet of Langerhans, **7**, 9
- Jacobian, 50, 59, 71
 and general solution of ODE, 66
 in Newton-Raphson, 70
- La Barre, 2
 Limit Cycle, 67, 77
 detection of, 77
 semi-stable, 43
 Linear Differential Equation
 general solution of, 67
 Lipschitz, 131
 Lipschitz Continuity, 131
 Lower Unstable Branch (LUB)
 NOD $_{f_2}$, 90
 NOD $_{f_1}$, 75
- Macrophage, 9, 18
 volume of, 99
 Manifold, 59
 stable, 94
 stable, 79
 NOD $_{f_1}$ -USB, 76
 unstable, 79
 of the NOD $_{f_1}$ -LUB, 83
 of the NOD $_{f_1}$ -USB, 83
 Mass Action Kinetics, 30
 Mathematical Model, 16
 Mathematical Modelling, **17**
 and etiology of T1D, 2
 and medical sciences, 17
 construction of, 17
 GLP-1, 15
 guidelines, 17

- of diabetes, 2
- Michaelis Constant, 25, 134
- Michaelis-Menten, 25, 26
- Michaelis-Menten Kinetics, **133**
- Miracle, 133
- Model A, 106, **108**
 - and criterion II, 109
 - system of equations, 108
- Model B, 110, **110**
- Model Criteria
 - expanded model, 105
- Multistability, 101
- Newton-Raphson, 71, **134**
 - initial guess, 70
 - iteration function, 70
 - method, 70
- Nobel Prize, 8
- NOD, 7, 18
- Nonlinear System, 59
 - flow of, 59
- Nonlinearity, 24
- Normoglycemia, 14, 15
- Nullcline, 54, 57, 60
- Nutrient, 133
- Oscillation
 - and spirals, 67
- Pancreas, **7**
- Parameter Sensitivity, 69
- Phagocytosis, **9**
 - Rate, 70
- Phase Space, 41, 67
 - stable spiral, 155
- Pitchfork Bifurcation, 66
- Poincaré-Bendixson's Theorem, 59
- Principal Minor, 53
- QSS Assumption, 74
- Quasi-Steady-State Assumption (QSS), 134
- Rate Constant, 22
- Reaction Equation, 22
 - differential equation, 22
- Reaction Rate, 133
- Receptor, 133
- Recruitment Rate, 25
- Reversible Model
 - NOD phagocytosis, 40
- Routh-Hurwitz criteria, 53, 96
- Saddle-Node
 - bifurcation, 81
- Saddle-Node Bifurcation, 66, 75, 89
- Saddle-Point, 66, 81
- Saturation, 133
- Separatrix, 63, 95
 - and the IM, 56
 - in the IM, 56
- Sound Model, **3**
- Specimen-Specific Model, 41
- Spiral, 41, 66
 - stable, 34, 41, 67, 79
 - at NOD_{f1}-USB, 76
 - unstable, 67, 77
- Sprague Dawley Rat, 120
- Spiral
 - unstable
 - at NOD_{f1}-USB, 78
- Stable Manifold
 - of the IM, 56
- Stable Manifold Theorem, 59
- Stable Spiral
 - existence of, 76
 - Fig. 8.3, 77
- Steady State
 - and nullclines, 54
- Substrate, 35
- Symptoms, 1
- T Cell, 9, 18
 - autoreactive, 7
 - immature, 9
- T1D, 1, 2, 13, 18, 46
 - and autoantibodies, 8
 - and environmental factors, 1
 - and fatality, 1
 - and genetic screening, 13
 - dendritic cell, 15
 - interspecimen difference in development, 41
 - symptoms of, 7
- T2D, 1

-
- The Intermediate Model, **45**
 - Therapy, 13
 - β -cell
 - neogenesis, 14
 - proliferation, 14
 - regeneration, 14
 - and DCs, 15
 - and progression, 13
 - antigen based, 13
 - dendritic cells, 16
 - diet, 13
 - Epidermal Growth Factor (EGF),
15
 - gastrin, 14
 - GLP-1, 14
 - immunotherapy, 14
 - Thesis Statement, 3
 - Topological Equivalence, 59
 - of flow, 65
 - Transcritical Bifurcation, 66
 - Turnover
 - of activated macrophages, 41
 - of cytokine, 26
 - Type 1 Diabetes (T1D), 1
 - Type 2 Diabetes (T2D), 1
 - Tyrosine Phosphatase (IA-2), 8

 - Unstable Manifold, 79
 - Upper Stable Branch (USB)
 - NOD_{f_1} NOD_{f_1} , 75
 - NOD_{f_2} , 90
 - Upper Unstable Branch (UUB), 85
 - UUB
 - as part of unstable limit cycle, 86
 - function of f_1 , 98

 - Vatican, 134